PNNL-14398

Pacific Northwest National Laboratory
Operated by Battelle for the U.S. Department of Energy

Transient Inverse Calibration of the Site-Wide Groundwater Flow Model (ACM-2): FY 2003 Progress Report

V. R. Vermeul
M. P. Bergeron
C. R. Cole
C. J. Murray
W. E. Nichols
T. D. Scheibe
P. D. Thorne
S. R. Waichler
Y. Xie

September 2003

Prepared for the U.S. Department of Energy
under Contract DE-AC06-76RL01830

DISCLAIMER

This report was prepared as an account of work sponsored by an agency of the United States Government. Neither the United States Government nor any agency thereof, nor Battelle Memorial Institute, nor any of their employees, makes **any warranty, express or implied, or assumes any legal liability or responsibility for the accuracy, completeness, or usefulness of any information, apparatus, product, or process disclosed, or represents that its use would not infringe privately owned rights**. Reference herein to any specific commercial product, process, or service by trade name, trademark, manufacturer, or otherwise does not necessarily constitute or imply its endorsement, recommendation, or favoring by the United States Government or any agency thereof, or Battelle Memorial Institute. The views and opinions of authors expressed herein do not necessarily state or reflect those of the United States Government or any agency thereof.

PACIFIC NORTHWEST NATIONAL LABORATORY
operated by
BATTELLE
for the
UNITED STATES DEPARTMENT OF ENERGY
under Contract DE-ACO6-76RLO183O

Printed in the United States of America

Available to DOE and DOE contractors from the
Office of Scientific and Technical Information,
P.O. Box 62, Oak Ridge, TN 37831-0062;
ph: (865) 576-8401
fax: (865) 576-5728
email: reports@adonis.osti.gov

Available to the public from the National Technical Information Service,
U.S. Department of Commerce, 5285 Port Royal Rd., Springfield, VA 22161
ph: (800) 553-6847
fax: (703) 605-6900
email: orders@ntis.fedworld.gov
online ordering: http://www.ntis.gov/ordering.htm

This document was printed on recycled paper.
(8/00)

PNNL-14398

Transient Inverse Calibration of the Site-Wide Groundwater Flow Model (ACM-2): FY 2003 Progress Report

V. R. Vermeul
M. P. Bergeron
C. R. Cole
C. J. Murray
W. E. Nichols
T. D. Scheibe
P. D. Thorne
S. R. Waichler
Y. Xie

September 2003

Prepared for the U.S. Department of Energy
Under Contract DE-AC06-76RL01830

Pacific Northwest National Laboratory
Richland, Washington 99352

Executive Summary

The U. S. Department of Energy (DOE) and Pacific Northwest National Laboratory (PNNL) have embarked upon a new initiative designed to strengthen the technical defensibility of the groundwater flow and transport model at the Hanford Site in Southeast Washington State and to develop a more robust capability to incorporate uncertainty into the model. One aspect of the initiative is developing and using a three-dimensional transient inverse modeling approach to estimate the hydraulic conductivities, specific yields, and other site-wide scale parameters that incorporates data on the transient behavior of the unconfined aquifer system resulting from Hanford Site waste management since 1943. Over the historical period of Hanford operations, the large volumes of wastewater discharged to a variety of waste facilities resulted in large water table changes over most of the Hanford Site and created significant groundwater mounds (in excess of 20 m) under waste management facilities in the central part of the site.

Since 1988, the mission of the Hanford Site has changed from producing weapons to restoring the environment. Thus wastewater discharges have declined significantly, which has caused significant water table declines.

The three-dimensional transient inverse calibration, which an external peer review panel recommended to DOE, is being performed using UCODE, a universal inverse modeling code developed jointly by the U.S. Geological Survey and the International Groundwater Modeling Center of the Colorado School of Mines. The work uses the existing consolidated site-wide groundwater model (SGM) implemented with the Coupled Fluid Energy and Solute Transport (CFEST) code, which is the forward model whose parameters are estimated by UCODE. The transient inverse calibration uses approximately 70,000 water level measurements made at the Hanford Site since the mid-1940s.

Compared with the prior model, the initial baseline transient inverse calibration effort (Cole et al. 2001a) significantly improved the ability of the baseline model to simulate historical trends in water table changes over the entire site for the 1943–1996 period of calibration. Most notably improved were the historical trends of water table changes and mound building observed near major discharge facilities in the 200 West Area. The focus of the inverse modeling initiative in the following year (Vermeul et al. 2001) was to use the developed inverse calibration methodology to test an alternative conceptual model (ACM-1) that no longer considered the underlying basalt bedrock system the no-flow base of the unconfined aquifer system as it had in the past. This alternative SGM model was used to examine and evaluate a variety of mechanisms that affect intercommunication between the Hanford Site unconfined aquifer system and the underlying upper basalt-confined aquifer system.

The focus of the ACM-2 inverse modeling initiative, as documented in this report, has been to 1) address data and model implementation limitations identified in the ACM-1 model, 2) complete the implementation and evaluation of the facies-based approach for representing the hydraulic conductivity distribution in both the Hanford and middle Ringold Formations, 3) develop the approach and implementation methodology for generating multiple ACMs of Unit 1 zonation and Ringold mud unit distribution based on geostatistical data analysis, and 4) develop an approach for inverse modeling of these stochastic ACMs. The ACM-2 transient inverse model was developed to test the SGM that incorporates conceptual model modifications that were identified for investigation based on knowledge gained during previous inverse calibration efforts. The primary modifications incorporated into ACM-2 that were not in

ACM-1 include facies-based zonation of Units 1 (Hanford) and 5 (middle Ringold); an improved approach for handling run-on recharge from upland areas (Cold Creek, Dry Creek, Rattlesnake Springs) based on watershed modeling results; an improved approach for representing artificial discharges from site operations based on the Site Assessment Capabilities (SAC) methodology; and minor changes to the geologic conceptual model.

In developing the ACM-2 parameterization, all model parameters, including those representing the hydraulic properties of all the hydrogeologic units and those representing all the specified boundary conditions (except for artificial discharges associated with Hanford operations and pumping well rates) were considered. Model boundaries associated with the Columbia and Yakima Rivers were not specifically addressed because they are treated as constant-head boundary conditions that vary in time and space, and the estimates for these spatial and temporal variations are a function of historical river flows and channel configuration, which are reasonably well documented. The intensive computational requirements of the inversing process provide motivation to limit the number of estimated parameters to those not well quantified by available hydrogeologic or operational data. Based on a detailed parameter sensitivity analysis of the ACM-2 model, the following general parameter sensitivities were indicated:

Hydraulic conductivity of conductive units: In general, the solution was sensitive to the hydraulic conductivity of the more conductive units. The only permeable units not determinable by the inverse were Ringold Units 7 and 9, which are moderately permeable and situated deeper in the profile, where fewer observational data are available.

Hydraulic conductivity of the Ringold mud units: The solution was sensitive to the hydraulic conductivity of the lower-conductivity, slightly more extensive mud unit (Unit 8) and insensitive to Unit 6. Because of the limited saturated extent of the upper Ringold mud (Unit 4), this parameter was not included in the inverse.

Vertical hydraulic conductivity of underlying basalt layer: The solution was sensitive to this parameter, which affects basalt leakage.

Features associated with increased basalt leakage: In general, hydraulic conductivity associated with head-dependent flux boundaries at the erosional window and thrust fault was insensitive. One exception was a section of fault in Cold Creek Valley upgradient of the Cold Creek flow impediment. High basalt heads upgradient of this feature are the primary reason for the solution's increased sensitivity to hydraulic conductivity, controlling leakage over this section of the thrust fault.

Specific yield of the conductive units containing the water table: The solution was generally insensitive to all tested specific-yield parameter values. The specific yield of several facies of the Hanford and Ringold formations across the 200 Area plateau, where the largest amount of groundwater mound buildup occurs, however, were marginally sensitive for a limited time during the inverse process but became insensitive as the inverse progressed.

Anisotropy ratio of all conductive hydrogeologic units: The solution was insensitive to all anisotropy parameters.

Components of surface recharge: The solution was insensitive to areally distributed surface recharge but sensitive to run-on recharge from Cold Creek, Dry Creek, and Rattlesnake Hills.

An overall comparison of simulated and measured water levels indicated that, over the entire prediction period, reasonable overall fit was realized for the ACM-2 inverse model. Residual error statistics indicate that 65.8 percent of the simulated values were within ±1 m of measured values, and 98.9 percent were within ±5 m. The overall mean residual was 0.06 m (-0.82 m for 39,264 negative residuals and 1.19 m for 30,511 positive residuals). The residual values ranged from –7.39 m to 9.38 m, and the total sum of squared residuals was 1.40×10^5 m^2. Comparing residual error statistics generally indicates an improvement in model fit for ACM-2 relative to ACM-1d. The sum of squared residuals for ACM-2 was 1.08×10^5, a 9 percent reduction from the sum of squared residuals for the ACM-1d inverse model, which was 1.19×10^5. In addition to the overall increase in the goodness of fit for ACM-2 relative to ACM-1, there are advantages associated with moving the SGM to a more technically defensible, hydrogeologically based conceptual model and eliminating reliance on a questionable transmissivity distribution developed during early two-dimensional, steady-state inverse calibration efforts. ACM-2 represents the first attempt to fully incorporate the facies-based approach for representing the hydro-geologic structure of the model, and it is expected that further refinement of this distribution and additional improvements to overall model fit will be realized during future inverse simulations of groundwater flow and transport.

In addition to development and transient inverse calibration of the ACM-2 model, preliminary work was completed toward developing an approach and implementation methodology for the generation and inverse modeling of stochastic ACMs. These geostatistical techniques were applied to develop alternative models of the Hanford Site geological structure and to assess the uncertainty in the facies-based zonation of the Hanford formation (Unit 1) and the geological structure of Ringold mud units. Due to the sequencing of the various tasks associated with this effort, the geostatistical analysis used a preliminary interpretation of the facies-based zonation and thus was not consistent with that used in ACM-2. Although the overall objective of this task is to assess uncertainty based on the most current model (i.e., ACM-2 or future revisions to the geologic structure and/or facies zonation), this preliminary work provided an effective basis for developing the approach and implementation methodology.

Also included in this effort was development of a strategy to facilitate inverse calibration analysis of the large number of stochastic ACMs generated. These stochastic ACMs represent random selections from a range of possible model structures, all of which are consistent with available observations and thus are amenable to Monte Carlo analysis. Within the inverse model framework, however, the computational requirements are further expanded by virtue of the fact that a single inverse run requires many forward flow model runs. Subsequently, full inverse analysis of the large number of combinations of stochastic alternative mud geometry and Unit 1 (and Unit 5) zonation models is not now computationally feasible. To address these limitations, a two-part approach was developed that includes 1) full inverse modeling of selected realizations based on the ranking analysis described above combined with limited forward modeling and 2) implementation of the UCODE/CFEST inverse modeling framework on the DOE Science Grid using Globus technology to enhance computational capabilities.

Glossary

CFEST	Coupled Fluid, Energy, and Solute Transport
CFEST- INV	Coupled Fluid, Energy, and Solute Transport Inverse computer code
CHARIMA	Charriages de Rivieres Mailles (computer code for simulating transport of river sediments)
DOE-RL	U.S. Department of Energy, Richland Operations Office
GIS	Geographic Information System
GEOFEST	Geological Finite Element Synthesis Tool
HEIS	Hanford Environmental Information System
HGWP	Hanford Groundwater Project
IGWMC	International Groundwater Modeling Center
MASS1	Modular Aquatic Simulation System 1D
MMT	Multicomponent Mass Transport
MRGT	Multiple Realization Generator Task
ONWI	Office of Nuclear Waste Isolation
PNNL	Pacific Northwest National Laboratory
PERL	Practical Extraction and Report Language, a freeware language designed for text manipulation
PSPL	Puget Sound Power and Light
SGM	Site-Wide Groundwater Model
TRANSS	A Simplified Model for Radioactive Transport
UCODE	Universal Inverse Modeling Code
USGS	U. S. Geological Survey
VTT	Variable Thickness Transient

Acknowledgments

Many people contributed to the development of this report. The authors wish to thank Dr. Sumant Gupta (CFEST Co.) for his technical assistance and implementation of modifications to CFEST to simplify its use with UCODE with the calibration and evaluation of the current conceptual model. The authors also thank Doug Hildebrand (DOE-RL) for his ongoing encouragement and support for our efforts and the useful review comments and suggestions he provided on the draft of the report.

Thanks and appreciation also go to other PNNL staff who provided invaluable assistance in the important areas of data processing and model data input preparation and final report preparation. Contributors include Bruce Bjornstad, Andre Coleman, Darrell Newcomer, Steve Reidel, Frank Spane, and Mark Williams. Philip Meyer provided technical peer review and Sheila Bennett provided technical editing support.

Contents

Executive Summary iii
Glossary vii
Acknowledgments ix
1.0 Introduction 1.1
1.1 SGM Modeling Initiative Objectives 1.1
1.2 Scope of the Report 1.3
2.0 Background 2.1
2.1 Groundwater Flow Model Selection and Chronology 2.2
2.1.1 Code Selection 2.2
2.1.2 Chronology of SGM Development 2.2
2.2 Inverse Methodology and Implementation 2.5
2.2.1 Inverse Methodology and Computational Codes 2.5
2.2.2 Implementation of the Transient Inverse Approach 2.6
2.2.3 Parameterization 2.6
2.2.4 Well Observation Processing and Weighting for Use in Regression 2.7
2.2.5 Measurement Error 2.8
2.2.6 Time Weighting 2.9
2.2.7 Spatial Weighting 2.10
2.2.8 Final Measurement Error Statistic 2.10
3.0 Description of the Groundwater Flow Model: ACM-2 ..... 3.1
3.1 Hydrogeologic Framework 3.1
3.2 ACM-2 Transient Inverse Model Development 3.1
3.2.1 Implementation 3.5
3.2.2 Modifications to the Geologic Conceptual Model 3.6
3.2.3 Flow System Boundaries 3.9
3.2.4 Basalt Intercommunication 3.14
3.2.5 Natural Surface Recharge 3.17
3.2.6 Artificial Recharge 3.19
3.2.7 Facies-Based Zonation of Hydraulic Properties 3.21
4.0 Results and Evaluation of the ACM-2 Transient Inverse Simulation 4.1
4.1 ACM-2 Parameterization 4.1
4.2 Transient Inverse Simulation Results 4.3
4.2.1 Spatial and Temporal Distributions of Residual Errors 4.4
4.2.2 Hydraulic Conductivities 4.7
4.2.3 Storage Properties 4.10
4.2.4 Boundary Flux Estimates 4.11
4.2.5 Natural Recharge 4.11
4.2.6 Basalt Intercommunication 4.12

4.3 Evaluation of Transient Inverse Model 4.15
4.3.1 Evaluation of Regression Measures 4.15
4.3.2 Evaluation of Model Fit 4.18
4.3.3 Evaluation of Optimized Parameter Values 4.21
5.0 Generation and Inverse Modeling of Stochastic Alternative Conceptual Models 5.1
5.1 Alternative Conceptual Model for Unit 1 Zonation 5.1
5.1.1 Geostatistical Data Analysis 5.1
5.1.2 Indicator Simulation of Unit 1 Zonation 5.7
5.1.3 Post-Processing of Zonation Simulations 5.9
5.2 Alternative Conceptual Model for Ringold Mud Units 5.15
5.2.1 Geostatistical Data Analysis 5.15
5.2.2 Indicator Simulation of Presence/Absence of Mud Units 5.18
5.2.3 Gaussian Simulations of Mud Unit Thickness 5.20
5.2.4 Merging of Presence/Absence and Thickness Simulations 5.21
5.2.5 Post-Processing of Mud Unit Simulations 5.21
5.2.6 Future Needs—Joint Simulation of Mud Units 5.26
5.3 Planned Inverse Modeling of Stochastic ACMs 5.26
5.3.1 Full Inverse Modeling of Selected Realizations 5.27
5.3.2 Globus Implementation on the DOE Science Grid 5.28
5.3.3 Optimal Parameter Zonation Studies 5.28
6.0 Summary and Conclusions 6.1
7.0 References 7.1
Appendix: Plots of Water Table Elevations and Head Residuals from Simulation of Hanford Wastewater Discharges Using ACM-2 ..... A.1

Figures

1.1 Location of the Hanford Site 1.2

2.1 Relationship Between Water Level Variability and Distance from the River 2.9

3.1 Regional Setting for the Hanford Site Unconfined Aquifer System 3.2

3.2 Structural Geologic Features of the Pasco Basin 3.3

3.3 Cross Section B-B' Hydrostratigraphic and Stratigraphic Columns Illustrating Geology of Pasco Basin and Nine Supra-Basalt Hydrostratigraphic Units of SGM 3.4

3.4 Finite-Element Grid and Boundary Conditions Used in Three-Dimensional Flow Model 3.6

3.5 Lateral Extent of Unit 3 at the Water Table 3.7

3.6 SGM Model Domain Within the Pasco Basin Illustrating the Location of the Important Flow System Boundaries for the Hanford SGM 3.10

3.7 Lower Boundary Specification for Watershed Modeling 3.11

3.8 Water Pathways in DHSVM 3.12

3.9 Contributing Areas for Recharge to Western SGM Boundary 3.13

3.10 Location of Thrust Faults and Normal Faults on the Hanford Site 3.16

3.11 Geologic Cross Section Through the Gap Between Gable Mountain and Gable Butte Indicating the Northern and Southern Boundary of the Erosional Window 3.17

3.12 Estimates of Recharge for 1979 Conditions 3.18

3.13 Artificial Discharges to the Unconfined Aquifer from 1943 to 2000 ..... 3.19

3.14 Facies-Based Zonation of Unit 1 ..... 3.22

3.15 Facies-Based Zonation of Unit 5 ..... 3.24

3.16 Distribution of Hydrogeologic Units and Facies Zones at Pre-Hanford Water Table 3.25

3.17 Distribution of Hydrogeologic Units and Facies Zones at Maximum Water Table 3.26

3.18 Cross Sections Along A-A' and B-B' Showing Distribution of Hydrogeologic Units Below Maximum Water Table 3.27

4.1 Measured Versus Predicted Heads 4.4

4.2 Predicted Head Residuals 4.5

4.3 Hydraulic Conductivity Distribution for Best-Fit ACM-2 and ACM-1d Inverse Models 4.8

4.4 Cross-Section A-A' Showing Distribution of Hydraulic Conductivity for Best-Fit ACM-2 Model 4.9

4.5 Cross-Section B-B' Showing Distribution of Hydraulic Conductivity for Best-Fit ACM-2 Model 4.9

4.6 Simulated Basalt Leakage in 1960 ..... 4.12

4.7 Simulated Basalt Leakage in 1996 ..... 4.13
4.8 Areally Distributed Basalt Leakage Flux over the Simulated Period 4.13
4.9 Relative Contribution of Each Basalt Leakage Feature to Net Leakage Flux 4.14
5.1 Location Map of the 230 Unit 1 Facies Observations 5.2
5.2 Unit 1 Zonation Based on Geological Knowledge 5.3
5.3 Declustering Weights of Data Colored in Terms of Facies Type 5.4
5.4 Experimental Variograms and Variogram Models. 5.6
5.5 Four Unit 1 Facies Realizations before and after Cleanup with MAPS 5.8
5.6 Facies Proportion Histogram of the 101 Simulated Realizations before and after Cleanup with MAPS 5.9
5.7 Most Likely Facies-Based on 101 Raw and Cleaned Realizations 5.10
5.8 Probability Maps Based on 101 Realizations for Facies 1 to Facies 5 ..... 5.10
5.9 Influence of Number of Realizations 5.12
5.10 Four Facies Realizations That Ranked Highest, Lowest, and Medium in Conductivity 5.14
5.11 Location Maps of Presence/Absence of the Three Mud Units: U4, U6, and U8. ..... 5.16
5.12 Histograms of the Mud Thickness when a Mud Unit is Present. 5.16
5.13 Experimental Variograms and Fitted Models for Presence/Absence of the Three Mud Units ... 5.17
5.14 Experimental Directional Variograms and Fitted Models of Normal Score Transformed Thickness of OU4 and OU8 ..... 5.17
5.15 Three Presence/Absence Realizations of U4, U6, and U8. ..... 5.18
5.16 Histogram of Global Presence/Absence Proportion from 51 Realizations for Mud Units U4, U6, and U8 ..... 5.19
5.17 Probability Maps of Presence of the Three Mud Units. 5.19
5.18 Realizations of Thickness Simulations for U4, U6, and U8 ..... 5.20
5.19 E-Type Thickness Maps of U4, U6, and U8 ..... 5.21
5.20 Three Merged Thickness Realizations for U4, U6, and U8 ..... 5.22
5.21 E-Type Thickness Maps Based on 100 Randomly Merged Realizations 5.22
5.22 Constructing Mud Unit Realizations for the Highest and Lowest Conductive Merged Pseudo-3D Realizations 5.24
5.23 Cross Sections of Hydrogeologic 3D Structures with the Lowest and Highest Conductivity Compared with the Base Case 5.25

Tables

3.1 Major Hydrogeologic Units Used in the Site-Wide Three-Dimensional Model 3.5

3.2 Summary of Recharge in the Four Regions..... 3.14

4.1 Summary of Residual Error Statistics of Best-Fit ACM-2 Inverse Model..... 4.5

4.2 Comparison of Residual Error Statistics for Observations Common to ACM-1d and ACM-2 Inverse Models..... 4.7

4.3 Summary of Relative Contribution from Various Boundary Fluxes Included in ACM-2 ..... 4.14

4.4 Notation for and Descriptions of the 17 Parameters Estimated in the Inverse Calibration 4.16

4.5 Parameter Estimates and Regression Measures as a Function of Parameter Estimate Iteration .. 4.17

4.6 Summary of Parameter Estimates Derived for the Inverse Model ACM-2..... 4.22

4.7 Parameter Cross-Correlation Matrix 4.23

4.8 Parameter Scaling Factor Estimates and Associated Confidence Intervals..... 4.24

5.1 Name and Number of Samples of Hanford Formation Unit 1..... 5.2

5.2 Global Proportion of the Five Facies in Hanford Unit 1 ..... 5.4

5.3 Variogram Models of Five Unit 1 Facies 5.6

5.4 Facies Proportion Reproduction Based on 101 Realizations..... 5.9

5.5 Saturated Hydraulic Conductivity of the Five Unit 1 Facies..... 5.12

5.6 Ranking of Facies Realizations 5.13

5.7 Presence/Absence and Thickness Data for the Three Mud Units..... 5.15

5.8 Models of the Indicator Variogram of the Three Mud Units..... 5.17

5.9 Rank of Merged Pseudo-3D Realizations and Realization Index of Constructing Mud Units 5.23

1.0 Introduction

In 1996, the U.S. Department of Energy Richland Operations Office (DOE-RL) initiated a project to consolidate multiple groundwater models at the Hanford Site (Figure 1.1) into a single consolidated site-wide groundwater model (SGM). From that process, RL selected a three-dimensional groundwater flow and transport model developed by the Hanford Groundwater Project (DOE 2000) as the preferred alternative for the initial phase of the consolidation. The consolidated SGM was calibrated using 1979 data and a steady-state inverse approach along with trial-and-error transient model calibration runs using estimates of artificial discharges and a limited set of representative head observations from 1979 to 1996.

In the autumn of 1998, an external peer review panel was convened to conduct a technical review of the Hanford SGM. A formal report transmitted to RL on January 14, 1999 documents the results of their review.[(a)] The panel agreed with the concept of developing a broadly applicable SGM and made several general comments and related recommendations that centered on a broad theme of uncertainty.

1.1 SGM Modeling Initiative Objectives

During the first year of this initiative (FY 2000), efforts focused on 1) characterizing major uncertainties in the then-current conceptual model that could affect model predictions and 2) developing a calibration approach and methodology that could be implemented to assist the testing and evaluation of plausible alternative conceptual models of the Hanford Site aquifer system. The initial transient inverse calibration effort (Cole et al. 2001a) was undertaken as part of the effort to address the panel's specific recommendation that the concept of uncertainty be acknowledged and embraced from the outset and that a new modeling framework be established that is stochastic rather than purely deterministic, with the expected values of head and concentration and their associated parameter uncertainty as products of any modeling effort. A companion report (*Uncertainty Analysis Framework—Hanford Site-Wide Groundwater Flow and Transport Model*) (Cole et al. 2001b) discusses the uncertainty analysis framework developed for the Hanford Site SGM that will enable the key uncertainties in model predictions of groundwater flow and transport to be quantified.

The calibration process that was developed involves transient inverse calibration of plausible alternative models of the Hanford Site unconfined groundwater system to historical observations of hydraulic and water-quality impacts to the system from Hanford Site operations beginning in the mid-1940s. From the beginning of operations in 1943, Hanford activities discharged large volumes of wastewater to a variety of facilities. These operational discharges raised the water table and created groundwater mounds. They were the source of contaminant plumes along the Columbia River and in the central part of the Site. In 1988, Hanford's mission changed from weapons production to environmental restoration.

(a) Gorelick S, C Andrews, and J Mercer. January 14, 1999. *Report of the Peer Review Panel on the Proposed Hanford Site-Wide Groundwater Model*. Letter report to U. S. Department of Energy, Richland Operations Office, Richland, WA.

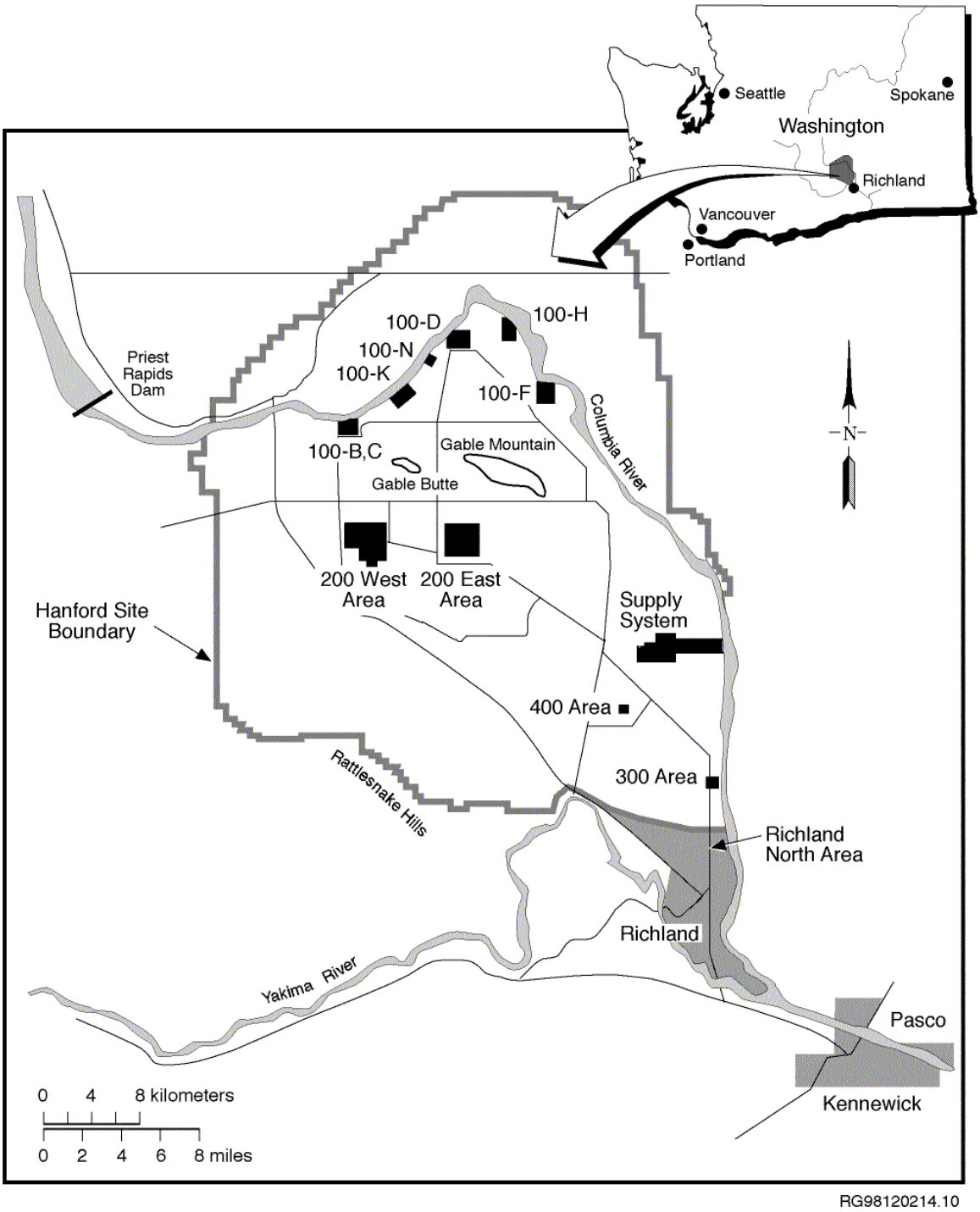

Figure 1.1. Location of the Hanford Site

The attendant reduction in wastewater discharges has resulted in significant declines in the water table over the past decade. Results from the initial inverse modeling effort identified weaknesses in the prior model that have aided in the development of plausible alternative conceptual models. The statistical information from the inverse modeling of alternative conceptual model interpretations allows this conceptual and parameter uncertainty to be factored into predictions of future groundwater flow and contaminant transport.

The focus of the inverse modeling initiative in FY 2001 was to use the developed inverse calibration methodology to test an alternative conceptual model (ACM-1) (Vermeul et al. 2001) that no longer considered the underlying basalt bedrock system as the no-flow base of the unconfined aquifer system as it had in the past. This alternative SGM was used to examine and evaluate a variety of mechanisms that affect intercommunication between the Hanford unconfined aquifer system and the underlying upper basalt-confined aquifer system. In addition, initial geologic interpretation and model implementation activities were conducted to facilitate the change from an adopted hydraulic conductivity distribution, which was based on a previous two-dimensional steady-state inverse modeling effort (Cole et al. 1997), to a facies-based approach that incorporated zonation of both the Hanford formation (Unit 1) and the middle Ringold formation (Unit 5).

The focus of the inverse modeling initiative in FY 2002 and the first quarter of 2003, as documented in this report, has been to address data and model implementation limitations identified in the ACM-1 model, complete the implementation and evaluation of the facies-based approach for representing the hydraulic conductivity distribution in both the Hanford and middle Ringold formations (ACM-2), develop the approach and implementation methodology for the generation of multiple ACMs of Unit 1 zonation and Ringold mud unit distribution based on geostatistical data analysis, and develop an approach for inverse modeling of these stochastic ACMs.

1.2 Scope of the Report

The scope of this report is to 1) provide a brief description of the technical approach and methods used to perform a three-dimensional transient inverse calibration of the Hanford SGM alternative conceptual models, 2) document model modifications and upgrades that have been incorporated into ACM-2, 3) summarize results from the ACM-2 inverse modeling effort and compare them with ACM-1 results, and 4) develop the approach and implementation methodology for generating and inverse modeling of stochastic alternative conceptual models.

Section 2 of this report provides general background information on the SGM, including the chronology of its development and selection of computer code used to implement it. This section also contains a description of the inverse methodology and implementation, including computational code selection, parameterization of the inverse model, and water-level observation processing and weighting for use in the regression. Section 3 summarizes the current understanding of the Hanford Site aquifer system (i.e., the conceptual model) and its numerical implementation. Section 4 summarizes the results from the transient inverse simulation of the ACM-2 inverse model for the 1943–2000 period and provides a cursory comparison with the results from the ACM-1 inverse model. Section 5 describes the generation and inverse modeling approach of stochastic ACMs. Section 6 summarizes the main conclusions resulting from this transient inverse calibration of ACM-2. Section 7 lists the cited references.

2.0 Background

The model developed for the calibration effort (ACM-2) reported here incorporates numerous modifications and upgrades from the previous model (ACM-1), as discussed Section 3. However, all of the models used in the inverse modeling initiative are derived from the three-dimensional numerical model for groundwater flow of the Hanford Site unconfined aquifer that was developed and enhanced as part of the Hanford Groundwater Project (HGWP) (Thorne and Chamness 1992; Thorne et al. 1993, 1994; Wurstner et al. 1995; Cole et al. 1997). This three-dimensional site-wide groundwater model (SGM) of the Hanford Site unconfined aquifer system was developed to better understand future changes in water levels and to enhance predictions of contaminant plume movement that were being monitored by the HGWP (Cole et al. 1997). Applications and developments made to the SGM are routinely reported in the annual Hanford Site groundwater monitoring report (e.g., Hartman et al. 2001). The SGM was calibrated using 1979 data and a two-dimensional steady-state inverse approach (Wurstner and Devary 1993; Jacobson and Freshley 1990) in conjunction with additional trial-and-error three-dimensional transient model calibration runs using estimates of artificial discharges and a limited set of representative head observations between 1979 and 1996 (Cole et al. 1997). The following paragraphs outline the basic reports that discuss the historic development of the SGM and, more importantly, available data on the Hanford unconfined aquifer system and the existing interpretations of those data.

The hydraulic property data used in the development of the SGM were obtained from the results of tests documented in Bierschenk (1959), Kipp and Mud (1973), Deju (1974), Lindberg and Bond (1979), Graham et al. (1981), DOE (1988), Liikala and Aaberg (1988), Thorne and Newcomer (1992), Peterson (1992), Connelly et al. (1992a, 1992b), Swanson (1992), Thorne et al. (1993), Connelly (1994), and Swanson (1994). Data were also obtained from new and previously unreported tests. Information on the subsurface geologic framework came primarily from interpreting geologic descriptions of samples acquired during well drilling. These interpretations were based on work by Lindsey et al. (1991, 1992), Lindsey (1992), Lindsey and Jaeger (1993), Lindberg (1993a, 1993b), Hartman and Lindsey (1993), and Swanson (1992) in the 100, 200, and 300 Areas of the Hanford Site, which use the lithofacies units outlined in Lindsey (1991).

Many of the wells used to define the geologic framework were drilled to basalt as part of a study for a proposed nuclear power plant (PSPL 1982). Other information used in defining the top of basalt came from wells drilled for the Basalt Waste Isolation Project (DOE 1988), which studied the basalts underlying the Hanford Site for disposal of high-level nuclear waste. Approximately 550 wells were used to define the three-dimensional hydrogeologic structure of the unconfined aquifer system. Many of these wells were used to determine the elevation of the top of basalt, and not all have been interpreted over their entire depth. Information on the southern part of the Hanford Site and the Richland area came from studies conducted by the U.S. Geological Survey (Ebbert et al. 1993), from Liikala (1994), and private well logs filed with the State of Washington Department of Ecology (Ecology). Information on the construction of Hanford Site wells was obtained from Chamness and Merz (1993) and the Hanford Environmental Information System (HEIS) database.

2.1 Groundwater Flow Model Selection and Chronology

The three-dimensional groundwater flow and transport model developed for the HGWP, as well as subsequent transient inverse calibration efforts (Cole et al. 2001a; Vermeul et al. 2001) and the inverse model described in this report, are implemented numerically using the Coupled Fluid, Energy, and Solute Transport (CFEST) code (Gupta et al. 1987; Cole et al. 1988; Gupta 1997). The CFEST code was originally designed to support the radioactive waste repository investigations under DOE's Civilian Radioactive Waste Management Program (Gupta et al. 1987). The chemical waste-management community has also used it effectively for conducting exposure assessments, evaluating remediation alternatives, and designing extraction and control systems for aquifers.

2.1.1 Code Selection

Evans et al. (1988) and Wurstner et al. (1995) described the capabilities and approach used in the CFEST code and its selection for the HGWP. CFEST is an approved code for working on Hanford Federal Facility Agreement and Consent Order (Tri-Party Agreement) (Ecology 1989) milestones related to risk assessment (DOE 1991). The CFEST software library was tested extensively and brought under strict software quality assurance/quality control procedures by the DOE Office of Nuclear Waste Isolation (ONWI) when it was developed for the Civilian Radioactive Waste Management Program. The supercomputer version (CFEST-SC) developed to run on all major UNIX workstations (Cole et al. 1988) was used for all flow and transport modeling before FY 1997. In FY 1997, refinement of the site-wide three-dimensional model continued with its application to contaminant transport of selected contaminant plumes (Cole et al. 1997). An updated version of the CFEST code called CFEST96 (Gupta 1997) was used in this effort. This version of the code runs in a PC or UNIX environment. The direct solver was replaced with an iterative solver, and the disk storage requirements were reduced from the previous version of CFEST.

Results from CFEST are displayed graphically using the ARC/INFO®[(a)] geographic information system (GIS) and Tecplot®.[(b)] The ARC/INFO GIS package is also used to store fundamental hydro-geologic data and information used to represent the three-dimensional conceptual model and construct the three-dimensional numerical model. The three-dimensional visualization software package known as EarthVision®[(c)] is used to manipulate hydrogeologic data for the conceptual model.

2.1.2 Chronology of SGM Development

Summarizing from the chronology discussed in Wurstner et al. (1995) and Kincaid et al. (1998), a site-wide flow and transport model has been under continuous development by PNNL since the early 1960s as part of PNNL's continuing involvement in Hanford's groundwater monitoring efforts. The capabilities of the model are refined and updated as additional information is gathered and as conditions and application needs change at Hanford. PNNL's Hanford Site unconfined aquifer model consists of a conceptual model and database that define current system understanding.

(a) ARC/INFO is a registered trademark of Environmental Systems Research Institute Inc., Redlands CA.
(b) Tecplot is a registered trademark of Amtec Engineering Inc., Bellevue, WA.
(c) EarthVision is a registered trademark of Dynamic Graphics Inc., Alameda, CA.

Early flow models were two-dimensional (e.g., the Variable Thickness Transient [VTT] code) (Kipp et al. 1972), and transport modeling, depending on application, was of the advective type (e.g., Hanford Pathline Calculation code) (Friedrichs et al. 1977), the quasi-three-dimensional particle tracking type (e.g., the Multicomponent Mass Transport [MMT] code) (Alhstrom et al. 1977), or the multiple streamtube type (e.g., the TRANSS code) (Simmons et al. 1986). Early flow models were calibrated with a streamtube approach that used available field measurements of transmissivity, river stage, disposal rate to ground, and head in an iterative approach to determine the Hanford unconfined aquifer transmissivity distribution (Transmissivity Iterative Calculation Routine) (Cearlock et al. 1975). Freshley and Graham (1988) describe applications of the VTT, MMT, and TRANSS codes at the Hanford Site.

In the mid 1980s, the CFEST code was selected for upgrading PNNL's two-dimensional modeling capability. CFEST has been used to model Hanford and a number of other sites in both two and three dimensions (Dove et al. 1982; Cole et al. 1984; Gale et al. 1987; Foley et al. 1995). Evans et al. (1988), in a 1987 Hanford Site groundwater monitoring report, discuss the CFEST code for modeling flow and transport in the Hanford Site's unconfined aquifer.

Initial flow modeling with the CFEST code was two-dimensional as it had been with the VTT code. New data were used to recalibrate the CFEST two-dimensional groundwater flow model of the Hanford Site unconfined aquifer. A steady-state, finite-element, inverse calibration method developed by Neuman and Yakowitz (1979) and modified by Jacobson (1985) was used in this effort. All available information on aquifer hydraulic properties (e.g., transmissivities), hydraulic heads, boundary conditions, and discharges to and withdrawals from the aquifer were included. Evans et al. (1988) described inverse calibration efforts, Jacobson and Freshley (1990) described final calibration results, and Wurstner and Devary (1993) described the calibrated two-dimensional model of the unconfined aquifer.

Two-dimensional flow models used extensively at the Hanford Site before disposal operations ceased were generally adequate for predicting aquifer head changes and directions of groundwater flow because groundwater levels were somewhat stable through time across the Hanford Site. However, in the early 1990s, it was recognized that a three-dimensional model was needed to accurately calculate future aquifer head changes, directions of groundwater flow, mass transport, and predictions of contaminant concentrations. The three-dimensional model was needed because there is significant vertical heterogeneity in the unconfined aquifer, and the water table was dropping over most of the Hanford Site in response to cessation of large liquid disposals to the ground. Development of a three-dimensional model began in 1992 (Thorne and Chamness 1992) and was completed in 1995 (Wurstner et al. 1995). Thorne et al. (1994) interpreted the hydrogeology of the Hanford Site unconfined aquifer as an alternating series of transmissive units that are separated from each other in most places by less-transmissive, or mud units. Accounting for this vertical heterogeneity is particularly important for unconfined aquifer predictions at the Hanford Site as future water table changes result in the dewatering of hydrogeologic layers. The water table is near the contact between the Hanford formation and the underlying and much less-permeable Ringold Formation over a large part of the Hanford Site. Water level declines due to decreased discharge at disposal facilities is causing, and will continue to cause, dewatering of the highly permeable Hanford formation sediments in some areas (Wurstner and Freshley 1994). This may result in aquifer transmissivity changes of an order of magnitude or more that would not be properly accounted for by two-dimensional flow and transport models that average vertical properties at each spatial location. As a result, a two-dimensional model cannot accurately simulate changes in groundwater levels and flow

direction and contaminant transport because it cannot properly account for the three-dimensional routing of groundwater flow and contaminant mass resulting from the vertical heterogeneity.

The initial three-dimensional model of the Hanford Site unconfined aquifer (Wurstner et al. 1995) was calibrated in a two-step process. In the first step, the two-dimensional model was recalibrated with a steady-state, statistical inverse method implemented with the CFEST-INV computer code (Devary 1987). The two-dimensional transmissivity distribution from this inverse modeling was preserved during the calibration of the three-dimensional model described in Wurstner et al. (1995).

The SGM was improved further during FY 1996 and FY 1997 as part of the HGWP. The purpose of this effort was to assist the HGWP in interpreting monitoring data, to investigate contaminant mass transport issues and evaluate the future movement of existing contaminant plumes, and to identify and quantify potential groundwater quality problems for onsite and offsite use. The report on this effort (Cole et al. 1997) describes the improvements to the three-dimensional model, the model recalibration, and the application of the model to predict the future transport of existing contaminant plumes in the unconfined aquifer. Cole et al. (1997) present predicted changes in transient-flow conditions in the unconfined aquifer to the year 4000.

In FY 2000, the initial transient inverse calibration effort (Cole et al. 2001a) was undertaken as part of the effort to address the external peer review panel's specific recommendation[(a)] that the concept of uncertainty be acknowledged and embraced and that a new modeling framework be established that is stochastic rather than purely deterministic, with both the expected values of head and concentration and their associated parameter uncertainties the products of any modeling effort. As discussed in Section 1, the focus during the first year of this effort was on 1) characterizing major uncertainties that could affect model predictions in the adopted conceptual model (Cole et al. 2001b) and 2) developing a calibration approach and methodology that could be implemented to assist testing and evaluation of plausible alternative conceptual models of the Hanford Site unconfined and underlying confined aquifer system as necessary. The focus during the second year of this effort was to use the developed inverse calibration methodology to test an alternative conceptual model (ACM-1) (Vermeul et al. 2001) that no longer considered the underlying basalt bedrock system as the no-flow boundary (i.e., accounted for intercommunication between the Hanford Site unconfined aquifer system and the underlying upper basalt-confined aquifer system). The focus during the third year of this effort, which is the subject of this report, was to implement the facies-based approach for representing the hydraulic conductivity distribution in both the Hanford and middle Ringold Formations and to develop the approach and implementation methodology for generating and inverse modeling of stochastic alternative conceptual models.

(a) Gorelick S, C Andrews, and J Mercer. January 14, 1999. *Report of the Peer Review Panel on the Proposed Hanford Site-Wide Groundwater Model*. Letter report to U. S. Department of Energy, Richland Operations Office, Richland, WA.

2.2 Inverse Methodology and Implementation

This section discusses the basic concepts used in the universal inverse modeling code UCODE (Poeter and Hill 1998), which was selected for application to the Hanford SGM. More detailed information is presented in Cole et al. (2001a), including discussions of the objective function and the modified Gauss-Newton method used in UCODE to perform the nonlinear regression, operational aspects of UCODE, and recent enhancements to UCODE and CFEST to increase the efficiency of inverse parameter estimation. Also discussed in this section is the approach used to set up the transient inverse calibration of the SGM for the historical period of Hanford operations (1943–2000). A detailed discussion of the numerical implementation and evaluation approach, which was based on the *Guidelines for Effective Model Calibration* (Hill 1998), is contained in Cole et al. (2001a).

2.2.1 Inverse Methodology and Computational Codes

UCODE (Poeter and Hill 1998) performs universal inverse modeling using an indirect approach in which the unknown parameters for the problem being solved are considered to be the dependent variables (Peck et al. 1988). In the indirect approach, normal model equations (referred to as forward equations) are solved and parameter estimates are sought that minimize a set of residuals (e.g., differences between observed and model predicted quantities). The UCODE concept of universal comes from the fact that UCODE solves the inverse problem through an indirect approach that is not directly linked or tied to any particular forward model or implementing computer code. Hill (1998) provides a full discussion of all other aspects of UCODE and MODFLOW inverse model implementation. Much of the basic regression theory implemented is discussed in Cooley and Naff (1990). Other programs used by UCODE to test weighted residuals and calculate linear confidence and prediction intervals are discussed in Hill (1994).

The inverse problem of groundwater flow consists of estimating the vector of flow parameters being determined based on field observations of dependent variables (e.g., hydraulic head and flux to streams) and independent information about the parameters themselves (i.e., prior information). If concentration and travel time observations and estimates as well as information on prior estimates for additional transport parameters (e.g., dispersivity) are also available, they can be added as additional observations and prior information, and a coupled inverse problem involving both flow and transport can be posed.

An objective function is a measure of the fit between simulated values and the observations that are being matched by the regression. The purpose of the regression is to calculate values for the poorly known parameters that minimize the objective function. The resulting values are said to be "optimal," "optimized," or "estimated by regression." In UCODE, the objective function used in the nonlinear regression to determine the vector of unknown parameters being estimated is a weighted least-squares function (e.g., the sum of the weighted square of differences between simulated and observed values). The regression consists of calculating the vector of the unknown parameter values that minimize the objective function.

In UCODE, an estimated parameter can be any quantity that appears in the input files of the application model(s) or can be used in conjunction with user-defined functions to calculate a quantity that appears in the input files. Observations to be matched in the nonlinear regression performed by UCODE can be any quantity for which a simulated equivalent value can be produced. Simulated equivalent values

are calculated using values that appear in the application model output files and a set of additive and multiplicative functions. Also in UCODE, prior or direct information on estimated parameters can be included in the regression.

UCODE provides a variety of printed results (at each iteration if desired) and files to allow for graphical analysis and for the user to analyze the regression results. Parameter statistics reported inform the user of optimal parameter values for evaluating the quality of the calibration. Parameter statistics include scaled sensitivities, composite-scaled sensitivities, parameter covariance matrix, parameter values, standard deviations, coefficients of variation, 95% linear individual confidence intervals, and correlation coefficients. Regression performance measures reported include Marquardt (1963) parameter, the parameter that changed the most, and the amount of change.

2.2.2 Implementation of the Transient Inverse Approach

The SGM was selected for the initial inverse calibration effort instead of developing a new model because this allowed technical emphasis to be placed on developing and testing the inverse approach and not on model building. It also allowed multiple activities, all of which were identified for further investigation during various reviews of the Hanford SGM (DOE 2000), to be developed and proceed in parallel. These activities include development and evaluation of the effects of basalt leakage (ACM-1, Vermeul et al. 2001), development of facies-based zonation of hydraulic conductivity and specific yield for the Hanford and middle Ringold formations (ACM-2), and generation of stochastic alternative conceptual models (e.g., multiple realizations of Hanford formation zonation and the areal extent and thickness of the Ringold mud units).

The rationale for the selected period of calibration (1943–2000), even though little observational data are available early in the time period, is that the groundwater system prior to this time period was not affected by artificial recharge associated with Hanford Site operations and thus was in a state of approximate equilibrium with natural recharge and mean river flow conditions. This means that when performing a forward model run for a new set of parameters as part of the transient inverse, initial conditions for each new forward model run could be calculated from a steady-state model run that considered only natural recharge and mean annual river flow stage for river boundary conditions. Preparing to simulate this extended calibration period required developing 1) a complete set of head observations for the entire period from 1943 to 2000, 2) estimates of river stage variations for the entire extended period, and 3) estimates of the artificial discharges resulting from Hanford Site operations prior to 1979 and after 1996 to supplement the existing 1979–1996 data set prepared for the prior model (Cole et al. 1997).

2.2.3 Parameterization

In developing the parameterization, all model parameters, including 1) those that represent the hydraulic properties of all the hydrogeologic units and 2) those that represent all the specified boundary conditions except artificial discharges associated with Hanford Site operations and pumping well rates were considered for inclusion in keeping with Guideline 3 of *Guidelines for Effective Model Calibration* (Hill 1998). Artificial discharges and pumping were excluded because better records are available that quantify these model inputs relative to the uncertainties associated with other inputs. Uncertainty in these artificial discharge estimates is the subject of an ongoing effort that will be factored into subsequent

inverse analyses. Model boundaries associated with the Columbia and Yakima Rivers were not specifically addressed because they are treated as constant-head boundary conditions that vary in time and space, and the estimates for these spatial and temporal variations are a function of historical river flows and channel configuration and are reasonably well documented. The intensive computational requirements of the inversing process provide additional motivation to limit the number of estimated parameters to only those not well quantified by available hydrogeologic or operational data.

The final model parameters that were initially evaluated in the inversing process by performing a UCODE phase 22 analysis to examine parameter correlations and sensitivity coefficients was limited to:

- hydraulic conductivity of conductive units: Hanford formation (Unit 1, facies-based zonation), pre-Missoula gravels (Unit 3), and Ringold Formation (Unit 5 with facies-based zonation, Unit 7, and Unit 9)
- hydraulic conductivity of the Ringold mud units (Units 6 and 8)
- vertical hydraulic conductivity of underlying basalt layer (estimation of basalt leakage)
- hydraulic conductivity associated with head-dependent flux boundaries at the erosional window, Gable Mountain fault, and the Yakima Ridge fault (estimation of increased basalt leakage)
- specific yield of the conductive units containing the water table: Hanford formation (Unit 1, facies-based zonation), Cold Creek gravels (Unit 3), and Ringold Formation (Unit 5, facies-based zonation)
- anisotropy ratio of all conductive hydrogeologic units
- components of surface recharge.

Parameter sensitivity analysis results provided information to determine whether some parameters should be omitted from early phases of the regression to maintain a well-posed regression problem (see Section 4.1 for a discussion of sensitivity analysis). Because parameter sensitivity coefficients change throughout the regression process as a result of nonlinearities, the sensitivities need to be reinvestigated as the regression proceeds and parameters move away from their starting values.

2.2.4 Well Observation Processing and Weighting for Use in Regression

As many different kinds of observational data as possible need to be included in the regression to provide the variety of constraints needed to break intrinsic correlations (e.g., recharge and hydraulic conductivity). Inclusion of flow observations (e.g., base streamflow contributed by the groundwater system) generally provides more information about the hydrologic system for groundwater flow model calibration. Although previous studies of groundwater-river interactions on the Hanford Site provide estimates of groundwater discharge to the Columbia River at discrete locations, the incremental river fluxes related to groundwater system contributions cannot be directly measured and are not well characterized over the entire model boundary. In addition, observational flux measurements are not available for wastewater disposal activities associated with Hanford Site operations, although the quantity of water discharged is relatively well documented. Subsequently, the only observations included in the regression were measurements of hydraulic head in wells completed in the unconfined aquifer.

During the FY 2002 inverse calibration efforts, a water-level monitoring plan previously developed by the HGWP (McDonald et al. 1999) was adopted as the guiding document for determining which wells would be used for observations of hydraulic head. Based on the information provided in this plan, a database query was developed that provided the best available spatial distribution and density of data while avoiding head observations where well completion, elevation survey control, and/or data quality flag issues were identified. For the period between 1943 and 2000, a total of 69,775 individual measurements were selected for use, with the initial measurements becoming available in 1948. These observations were used by UCODE during the parameter estimation process to define the objective function for the period of model simulation.

For the inversing process, each measurement of head had the following quantities specified: measured head value, well location, the principal contributing model unit represented by the measurement, and a statistical measure that would be representative of the potential measurement error in the observation. UCODE guidance was followed in assigning measurement errors; however, additional weighting following standard statistical approaches from Isaaks and Srivastava (1989) was also developed to remove sampling bias in the measurements related to the large variations in the spatial and temporal distributions of observation well measurements. Without proper weighting, the final calculation of the sum of squared residuals and the associated estimates of model parameters would be incorrectly influenced by measurements that are close in space and time.

2.2.5 Measurement Error

At the Hanford Site, nearly all wells under consideration have been carefully surveyed and measured using a steel tape or other precise measuring device. Thus, the measurement error associated with each of the observations was assumed to be relatively small for most wells. This would generally hold true for all measurements made in wells outside of the influence of the effects of transient river-stage fluctuations of the Columbia River. The measurement error, which incorporated potential sources of error such as direct measurement error, well casing declination from vertical, external effects (e.g., barometric effects), and the timing of water level measurements and its impact on how representative the measurement was of average conditions over the modeled time step, was assumed to be a constant value of 0.03 m (0.1 ft).

For other wells located near and influenced by the Columbia River, a different specification of measurement error was developed to deal with the temporal effects not accounted for in the Hanford SGM. Because of the time-stepping used in the inversing process, simulated heads at these wells are more representative of the semi-annual averages of head predicted near the river, and the Hanford SGM is not capable of predicting the large fluctuations in head in wells near the river that respond to the highly transient behavior in river-stage fluctuation at time scales not simulated. To account for this effect, an approach for assigning measurement error for near-river observations was developed based on the distance of the observation from the river.

In an effort to quantify the variability in observed hydraulic heads in the vicinity of the time-varying head river boundary condition, hydrographs from wells in this area were inspected to determine whether sufficient data were available to develop a relationship between variability and distance from the river. Results from this data search identified six wells with a continuous water-level monitoring data record of sufficient length, at different distances from the river, that could be used to develop this relationship (199-D4-38, 199-K-32A, 199-D5-38, 199-D4-20, 199-N-50, and 199-D5-43). Although these data are

limited to the 100 D, 100 K, and 100 N Areas of the Site, and the degree of variability in this relationship along the length of the river was not investigated, they were sufficient to provide a generalized approximation of hydraulic head variability in near-river wells. A summary of these data are shown in Figure 2.1. Data in this plot represent the average standard deviation in hydraulic head for each six-month time period (i.e., equivalent to the model time step) throughout the available data record at various distances from the river. Based on UCODE guidelines, measurement error for each well along the river corridor was set based on its expected variability (two standard deviations in water level response for a well located that distance from the river). This approach resulted in wells near the river being assigned measurement errors as high as 0.74 m. Subsequently, wells near the river that were assigned a larger measurement error were given relatively less weight in developing the objective function than wells away from the river.

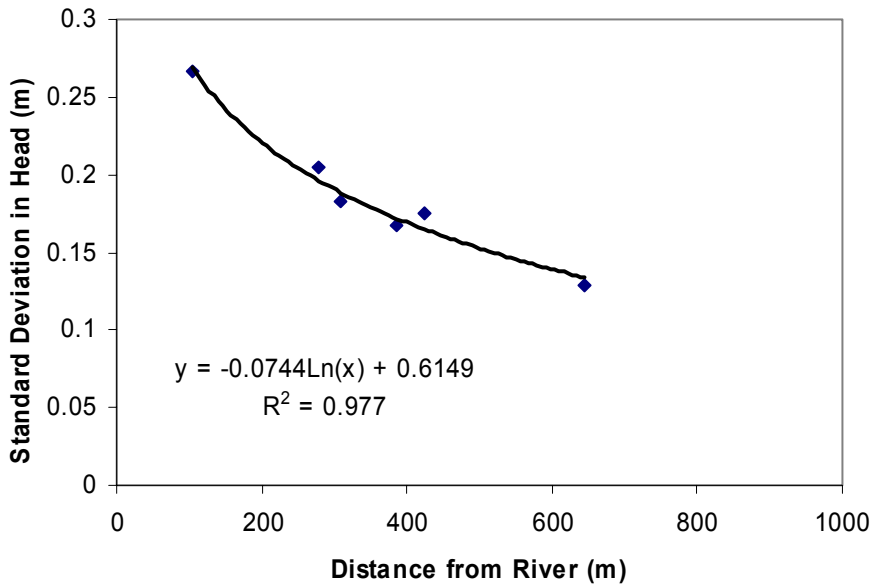

Figure 2.1. Relationship Between Water Level Variability and Distance from the River

2.2.6 Time Weighting

For time declustering, an approach was used that assigned a weight to each observation that was proportional to the period of time it represents within a given model time step. The period represented by each observation *i* made at time *t* is

$$\Delta t = \frac{(t_{i+1} - t_i) + (t_i - t_{i-1})}{2} \tag{2.1}$$

except for first and last observations within a time step, where the corresponding portion of the numerator is not divided by two. Consequently, the weight for observation *i* is

$$w_i = \frac{\Delta t}{T} \tag{2.2}$$

where T is the total time step.

A computer code was developed to read head observations, observation times, and well data from many data files that contain this information (a file for each well). Weights for all observations are calculated, and the times and dates are converted to model time.

2.2.7 Spatial Weighting

In some cases, more than one observation was within the same time step and within the same element of the finite element grid used for the inverse calibration. This produced a need for weighting the observations based on their location, that is, declustering based on spatial distribution. In this inversing effort, the method used for spatial declustering was a simple weighting calculation based on the number of observations within an element during each time step. Observations falling singly within an element were assigned a weight of 1.0. If more than one observation fell within the same time step and element, the weight assigned to the observation was equal to 1.0 divided by the number of well observations.

Other applicable spatial declustering methods that implement similar global spatial declustering techniques described in Isaaks and Srivastava (1989) will be identified and investigated for use in future inversing efforts.

2.2.8 Final Measurement Error Statistic

For this analysis, the resulting statistic used was the standard deviation calculated from the combination of the measurement error and the space and time weights using the following equation:

$$\sigma = \sqrt{ME^2 / (1.96^2 * SW * TW)} \tag{2.3}$$

where

σ	is the standard deviation
ME	is the measurement error
SW	is the space weight
TW	is the time weight.

3.0 Description of the Groundwater Flow Model: ACM-2

This section provides a description of the conceptual and numerical basis for the consolidated SGM of the Hanford Site unconfined aquifer system that was used in this transient inverse calibration effort—ACM-2. The conceptual model was developed from information on the hydrogeologic structure of the aquifer, spatial distributions of hydraulic and transport properties, aquifer boundary conditions, and distribution and movement of contaminants. Development of the basic aspects of this three-dimensional conceptual model of the Hanford Site unconfined aquifer system is documented in Thorne and Chamness (1992), Thorne et al. (1993, 1994), and Wurstner et al. (1995). Uncertainties associated with the SGM are fully discussed in Cole et al. (2001b).

3.1 Hydrogeologic Framework

The Hanford Site lies within the Pasco Basin, a structural depression that has accumulated a relatively thick sequence of fluvial, lacustrine, and glaciofluvial sediments (Figure 3.1). The geology and hydrology of the Hanford Site have been studied extensively for more than 50 years and are summarized in a number of documents (Wurstner et al. 1995 and references therein). The Pasco Basin and nearby anticlines and synclines initially developed in the underlying Columbia River Basalt Group, a sequence of continental flood basalts covering more than 160,000 km^2 (Figures 3.1 and 3.2). Overlying the basalt within the Pasco Basin are fluvial and lacustrine sediments of the Ringold Formation and the glaciofluvial Hanford formation and pre-Missoula gravels. Together, these sedimentary deposits compose the Hanford Site unconfined aquifer system, which consists of nine hydrostratigraphic units. The saturated thickness of this unconfined aquifer system is greater than 61 m in some areas but pinches out along the flanks of the basalt ridges, as illustrated by the B-B' cross section of Figure 3.3 (a). The corresponding hydrostratigraphic (left) and stratigraphic (right) columns illustrating the geohydrology of the Pasco Basin along with the relationship to the nine supra-basalt hydrostratigraphic units of the SGM are shown in Figure 3.3 (b). The Hanford and Ringold formations can be defined as several distinct hydrogeologic units. Data from wells on the site were used to define these hydrogeologic units based on textural composition. A brief summary of each of these units is provided in Table 3.1 based on descriptions in Wurstner et al. (1995). Depth to the groundwater ranges from less than 0.3 m near the Columbia River to more than 100 m near the 200 Areas. Groundwater in this unconfined aquifer system generally flows from recharge areas in the west to the Columbia River in the east.

3.2 ACM-2 Transient Inverse Model Development

The ACM-2 transient inverse model was developed to test an alternative conceptual model of the SGM that incorporates modifications that were identified based on knowledge gained during previous inverse calibration efforts. The primary modifications incorporated into ACM-2 include 1) facies-based zonation of Units 1 (Hanford) and 5 (middle Ringold), 2) an improved approach for handling run-on recharge from upland areas (Cold Creek, Dry Creek, Rattlesnake Springs) based on watershed modeling results, 3) an improved approach for representing artificial discharges from site operations based on the Site Assessment Capabilities (SAC) methodology, and 4) minor modifications to the geologic conceptual model.

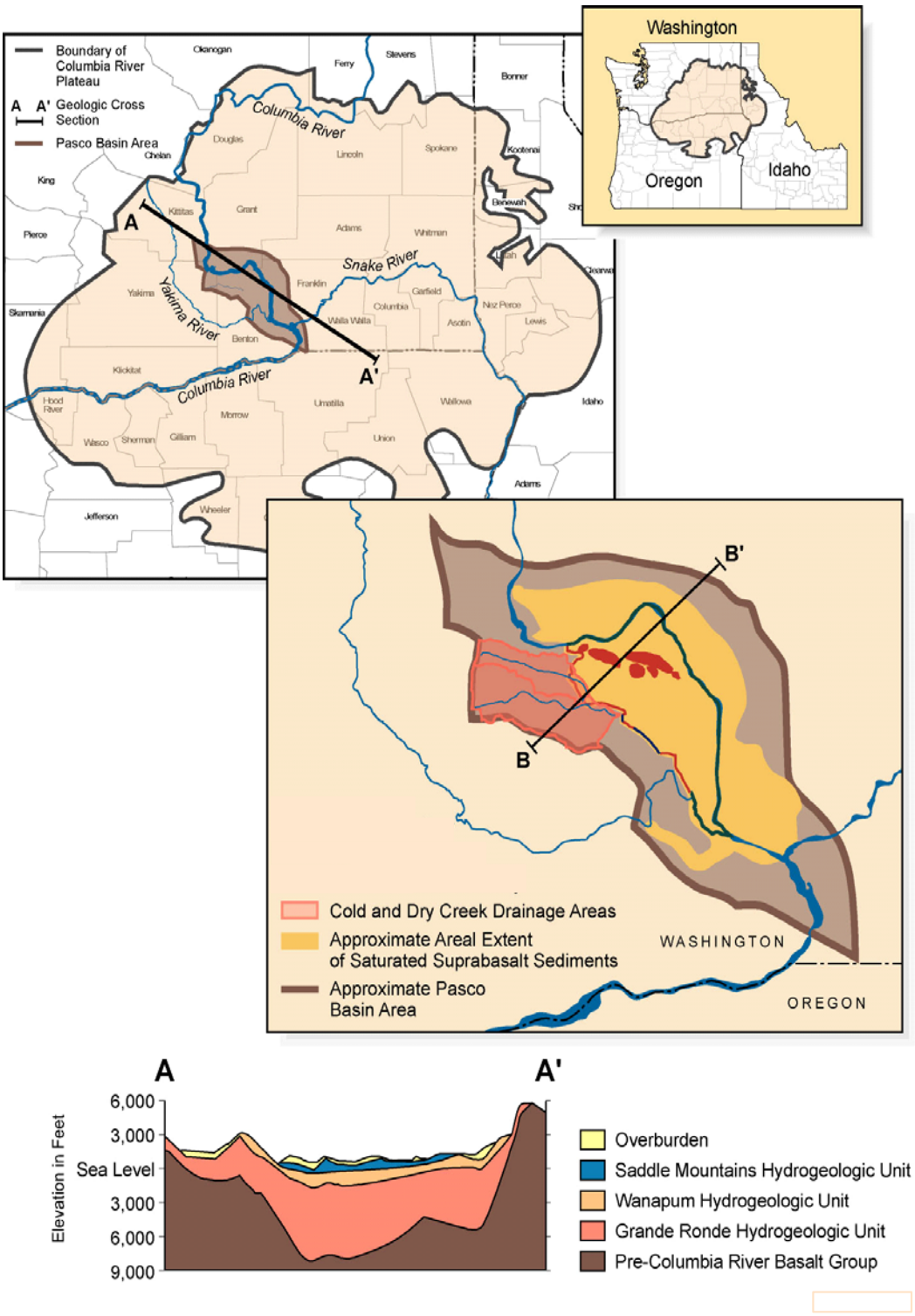

Figure 3.1. Regional Setting for the Hanford Site Unconfined Aquifer System (part of the saturated supra-basalt sediments) within the Pasco Basin and the Regional Columbia Plateau Aquifer System that Covers Most of Eastern Washington and Parts of Idaho and Oregon (cross section B-B' shown in Figure 3.3)

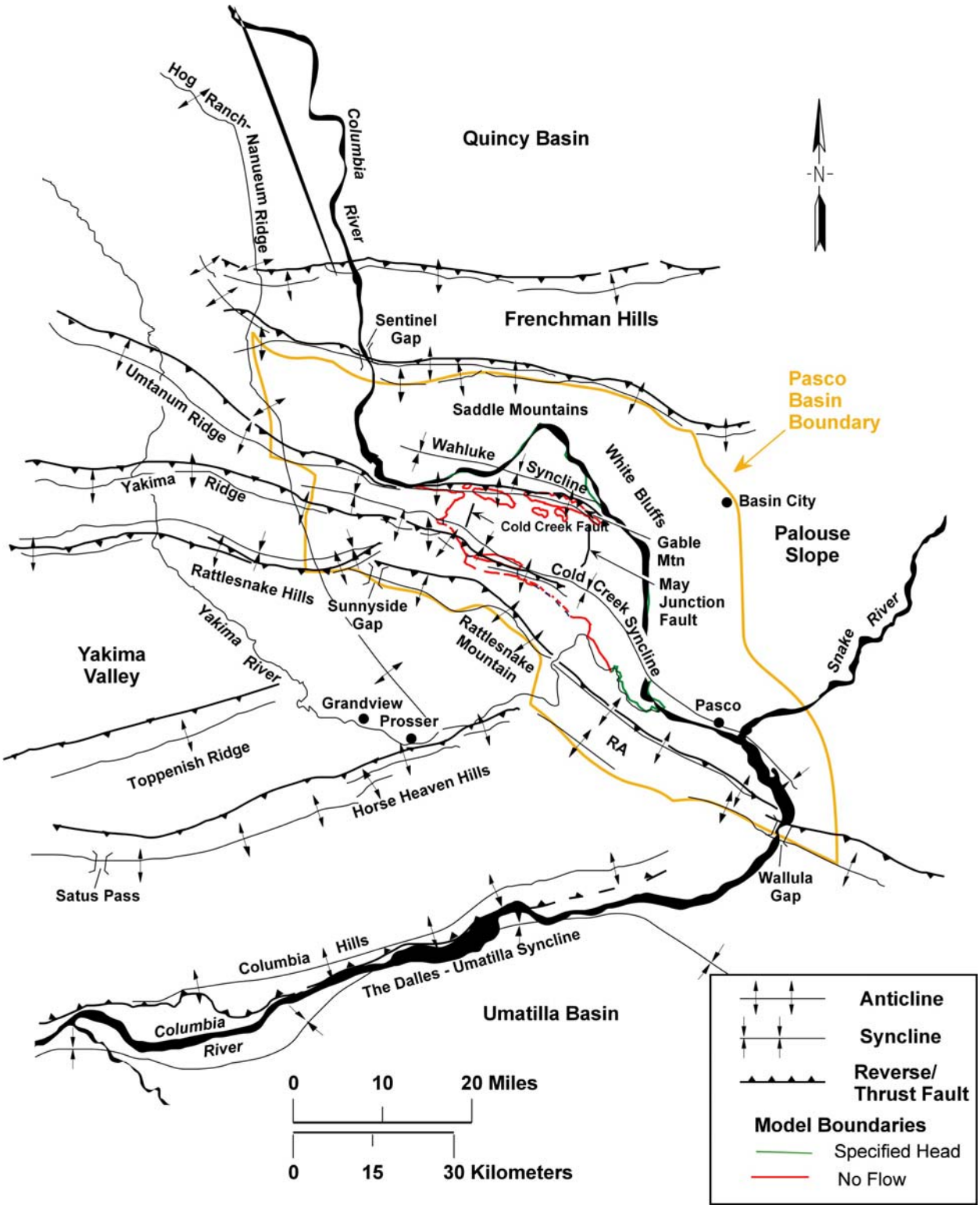

Figure 3.2. Structural Geologic Features of the Pasco Basin

a)

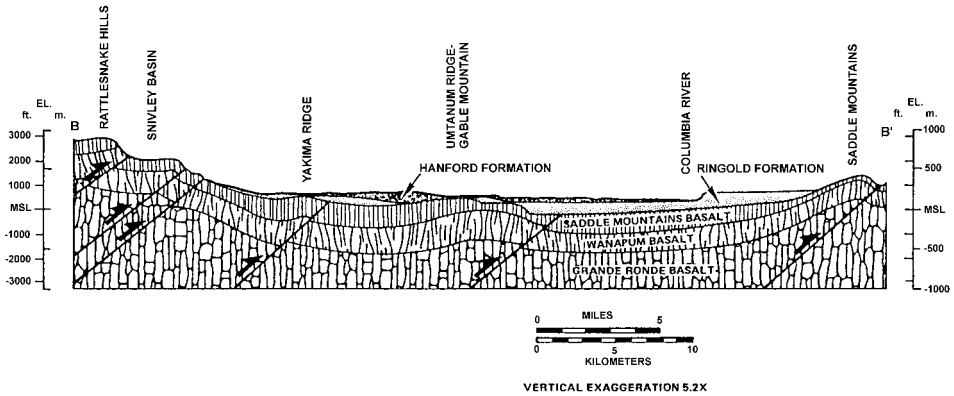

b)

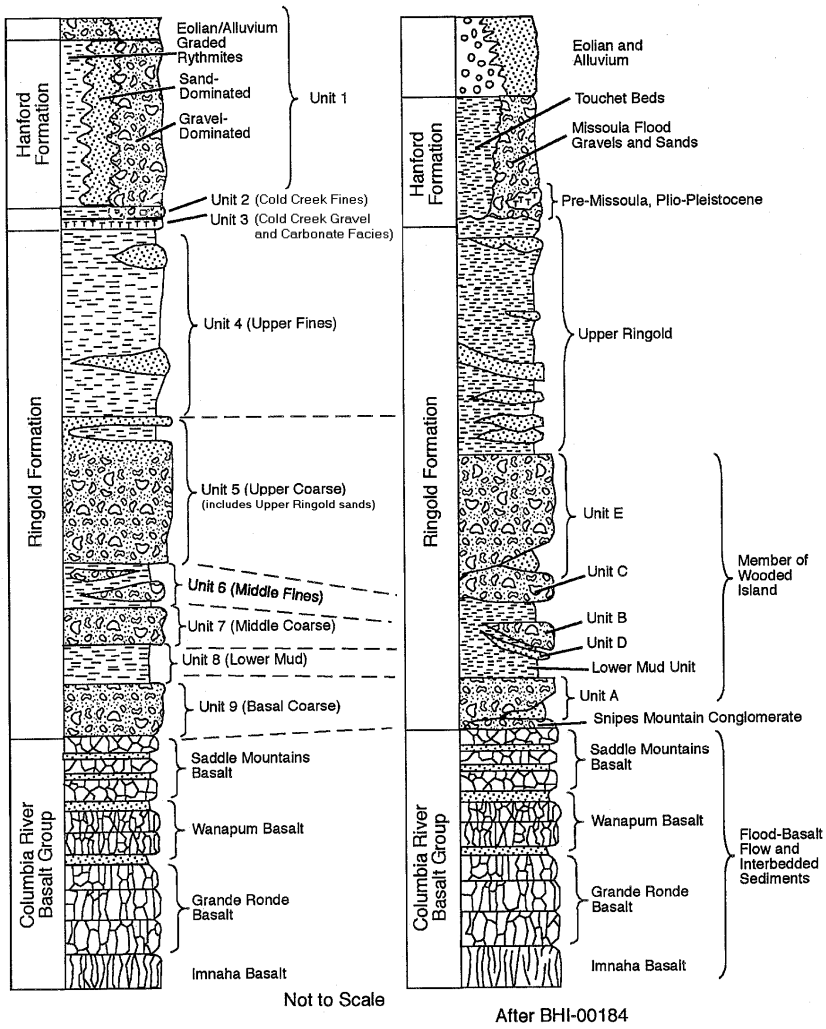

Figure 3.3. (a) Cross Section B-B' (Figure 3.1), (b) Hydrostratigraphic (left) and Stratigraphic (right) Columns Illustrating the Geology of the Pasco Basin and the Nine Supra-Basalt Hydrostratigraphic Units of the SGM

Table 3.1. Major Hydrogeologic Units Used in the Site-Wide Three-Dimensional Model

Unit Number	Hydrogeologic Unit	Lithologic Description
1	Hanford Formation	Fluvial gravels and coarse sands
2	Cold Creek Unit (fines)	Fine-grained sediments and eolian silts
3	Cold Creek Unit (coarse and carbonate rich)	Buried soil horizon containing caliche, side-stream gravel and Pre-Missoula gravel deposits
4	Upper Ringold Formation	Fine-grained fluvial/lacustrine sediments
5	Middle Ringold (Unit E)	Semi-indurated coarse-grained fluvial sediments
6	Middle Ringold (Unit C)	Fine-grained sediments with some interbedded coarse-grained sediments
7	Middle Ringold (Units B and D)	Coarse-grained sediments
8	Lower Mud Sequence (Lower Ringold and part of Basal Ringold)	Lower blue or green clay or mud sequence
9	Basal Ringold (Unit A)	Fluvial sand and gravel
10	Columbia River Basalt	Basalt

3.2.1 Implementation

The lateral extent and relationships between the nine hydrogeologic units, including the subunits of the Ringold and Hanford formations, were defined by determining geologic contacts between these layers at as many wells as possible. These interpreted distributions and thicknesses were input to EarthVision®, which was used to construct a database for formulating the three-dimensional Hanford Site conceptual model. The resulting numerical model contains nine hydrogeologic units above the top of the underlying basalt aquifer system. The Geological Finite Element Synthesis Tool (GEOFEST) described in Foley et al. (1995) was used to transfer the interpreted water table and the extent and thickness of major hydrogeologic layers to the correct format for input to CFEST to develop the regional numerical model of the Hanford Site. Bottom elevations of layers and elevation of the water table were input to GEOFEST.

Figure 3.4 is a plan view of the finite-element grid and boundary conditions used in the ACM-2 three-dimensional flow model. Most of the interior surface elements are regular elements that measure 750 m on a side. The total number of surface elements in the three-dimensional model is 2245, and the total number of surface nodes is 2478. The three-dimensional model based on this surface grid comprises 12295 elements and 14336 nodes. This finite-element grid was a modified version of the one used in previous transient inverse efforts. Primary modifications included extension of the grid to include portions of the unconfined aquifer that extend westward into the Cold Creek and Dry creek Valleys and an area located along the Columbia River in the far northwest corner of the model domain. In addition, small modifications were made to improve the alignment of the grid to boundary features and an optimization was performed to improve the computational efficiency of the finite-element mesh.

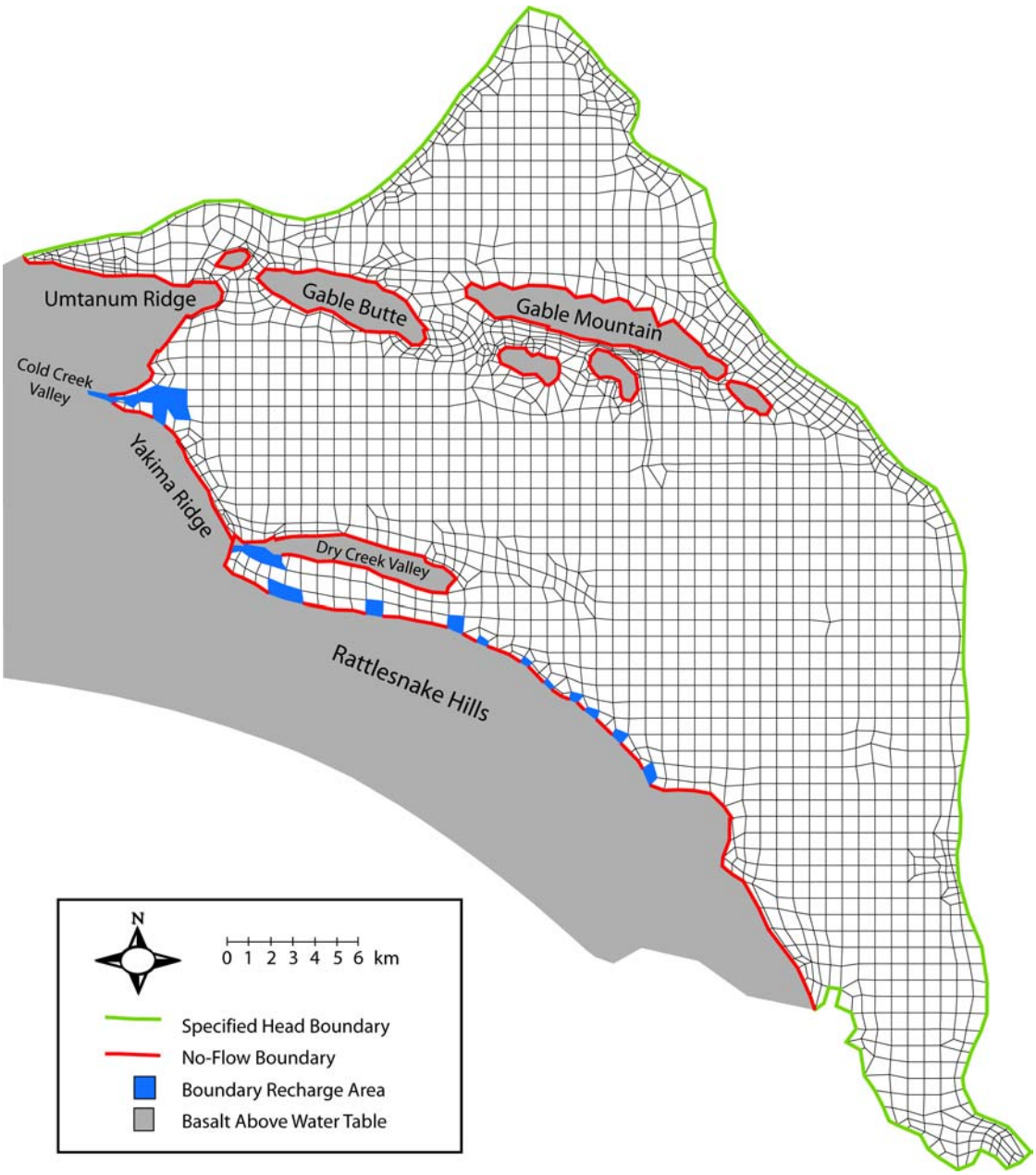

Figure 3.4. Finite-Element Grid and Boundary Conditions Used in the Three-Dimensional Flow Model

3.2.2 Modifications to the Geologic Conceptual Model

The gravel facies of the Cold Creek unit (previously called the "pre-Missoula gravel unit) exists at the water table in the region between 200 East Area and the Columbia River (Figure 3.5). These sediments had previously been combined with the Hanford formation to form model Unit 1. However, the hydraulic conductivity of the Cold Creek gravels is significantly lower than that of the Hanford formation gravels that lay over them. In the previous model, the difference in conductivity was addressed by designating a separate two-dimensional facies zone where the Cold Creek gravels existed below the water table and the

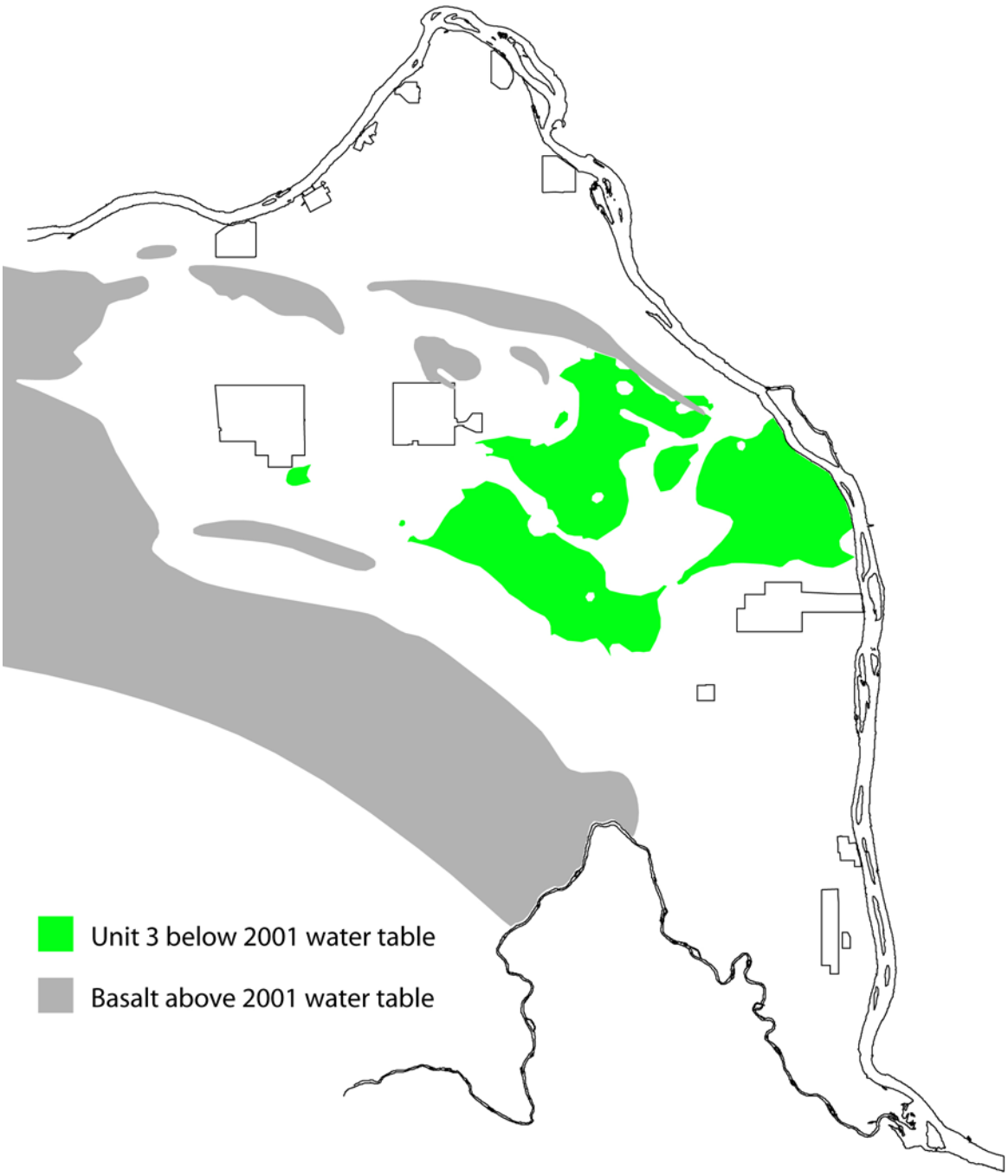

Figure 3.5. Lateral Extent of Unit 3 at the Water Table

Hanford formation was above the water table. However, this strategy did not represent the three-dimensional contact between these units and did not allow the extent of the Cold Creek zone to change with changes in water table elevation. To better represent groundwater flow and transport between the 200 East Area and the Columbia River, the Cold Creek unit gravels were redefined as part of model Unit 3. Unit 3 had previously represented the Cold Creek unit only in the vicinity of 200 West Area,

where it generally has much lower hydraulic conductivity. Combining these sediments in Unit 3 does not cause a problem in the model because the lower-conductivity Cold Creek sediments around 200 West Area are above the water table. Only the gravel-dominated facies exists below the water table and is included in the saturated zone model. In the prior model, baseline model, and ACM-1 the Cold Creek gravel unit was included with the Hanford formation as part of Unit 1.

Examination of head responses predicted by the revised model in the region between 200 East Area and the Columbia River indicated that hydraulic conductivities were too low. Groundwater could not move rapidly enough across this region. It was also known that the tritium plume from the 200 East Area PUREX cribs had moved to wells near the central landfill relatively quickly and without creating a large groundwater mound. This indicated that tritium had moved through saturated Unit 1 (Hanford formation) sediments between these points. However, in the existing conceptual model, the water table was below Unit 1 and in either Unit 3 (gravel facies of the Cold Creek unit) or 5 (Ringold gravel). Therefore, the geologic model was revised based on both historical observations of plume movement and additional geologic data from wells. Examination of well data showed that some sediments previously identified as Unit 3 or Unit 5 in the area around the central landfill were described in well logs as coarse-grained cobble and gravel deposits with little or no fine-grained material. This material appears to be Unit 1 or reworked Ringold gravel with hydraulic properties similar to Unit 1. Thus the bottom of Unit 1 was revised based on this new interpretation of the well data, creating a pathway in the Hanford formation (Unit 1) between the 200 East Area and the central landfill that is more consistent with historical tritium transport and water level data.

Some additional model unit surfaces were also refined to eliminate highs and lows that resulted from extrapolating the surfaces by the mathematical gridding routine used in Earth Vision. This affected the contact between Units 1 and 5 in the region northwest of the gap between Gable Mountain and Gable Butte. The top of Unit 8 near the mouth of the Cold Creek Valley and the top of Unit 3 in the area down-gradient from Dry Creek valley were revised to be consistent with well logs. Revisions were also made after extracting information from the model showing the model units corresponding to screened intervals at each monitoring well location. Geologic well logs were examined for monitoring wells that did not have screened intervals intersecting permeable units of the model. The model unit contacts were modified in some places to honor data from these observation wells. A minor change was also made in the top of basalt surface near the May Junction fault to represent it more accurately. Additional modifications were made to the Ringold Mud Units north of the Gable Mountain anticline to better represent the contact between these units and faults that influence flow between the basalt-confined and unconfined aquifer systems.

Another significant change to the geologic framework of the model involved the basalt subcrop on the north side of the Dry Creek Valley formed by the extension of the Yakima Ridge. In the previous version of the model there was a connection between the upper Dry Creek Valley and the area to the north. However, the large head difference between theses areas indicated that there was little or no hydraulic connection. Examination of well and geophysical data indicated uncertainty in the elevation of the top of this basalt surface. If the basalt surface is below the water table, there may be a mud unit that eliminates any hydraulic connection through this area. Therefore, the model was modified to eliminate the connection between the upper Dry Creek Valley and the area to the north (see Figure 3.4).

3.2.3 Flow System Boundaries

The conceptual model for ACM-2 contains several important flow-system boundaries illustrated in Figure 3.6. The flow system is bounded by the Columbia River on the north and east and by the Yakima River and basalt ridges on the south and west, respectively. The Columbia River is assumed to represent a point of regional discharge for the unconfined aquifer system. The amount of groundwater discharging to the river is a function of the local hydraulic gradient between the groundwater elevation adjacent to the river and the river-stage elevation. This hydraulic gradient is highly variable because the river stage is affected by releases from upstream dams. To approximate the long-term effect of the Columbia River on the unconfined aquifer system in the SGM, water-surface elevation boundary conditions for the Hanford Reach of the Columbia River and the lower reach of the Yakima River were generated using the Modular Aquatic Simulation System 1D (MASS1) (Cole et al. 2001a). Results of the MASS1 modeling provided the historical Columbia and Yakima River stages that were averaged into six-month time steps to represent the gross annual and seasonal changes in river stage during the period.

One of the primary modifications to ACM-2 was implementing run-on recharge from upland areas along the western model boundary. As mentioned in Section 3.2.1, the finite element grid in previous models did not extend to the head of the Dry Creek and Cold Creek valleys where the water table intersects the basalt surface. The flux entering this truncated boundary was approximated using results from a previous steady-state calibration of the SGM that used a prescribed-head boundary condition to estimate boundary fluxes entering the aquifer system from the Cold Creek and Dry Creek valleys as well as along Rattlesnake Springs. To reduce the uncertainty associated with these boundary conditions, ACM-2 incorporated a process-based, distributed-parameter hydrologic model to estimate run-on recharge. Three main sources of natural recharge with respect to the groundwater model exist. The first, direct infiltration of rainfall and snowmelt inside the model domain, is discussed in Section 3.2.5. The other two sources, which are discussed below, include infiltration from stream flow that originates outside the domain and flows into the model domain and lateral subsurface flow from outside the model domain.

The Distributed Hydrology Soil Vegetation Model (DHSVM) was modified for application in an arid setting and used to simulate the surface and subsurface water balance in the greater Cold Creek watershed. This area along the western boundary of the groundwater model includes Cold and Dry Creek valleys and the northeastern face of Rattlesnake Mountain (Figure 3.7). DHSVM was used to calculate stream flow and water that infiltrates below the soil zone in these watershed basins. This run-on recharge was applied to selected elements in the SGM near the western boundary, as shown in Figure 3.4. For this initial implementation, run-on recharge estimated with DHSVM was applied uniformly across the recharge areas shown in the figure by scaling up the natural surface recharge values by a factor that resulted in a total representing both surface and run-on recharge. Although this approach does not account for the spatial variability of run-on recharge as it is applied to the recharge areas within the model domain (i.e., stream flow would be distributed farther into the model domain than lateral subsurface flow, which would be applied at the boundary), it does provide a reasonable approximation allowing the inverse calibration efforts to proceed while the DHSVM modeling efforts are refined to provide the spatial distribution of run-on recharge within the model domain.

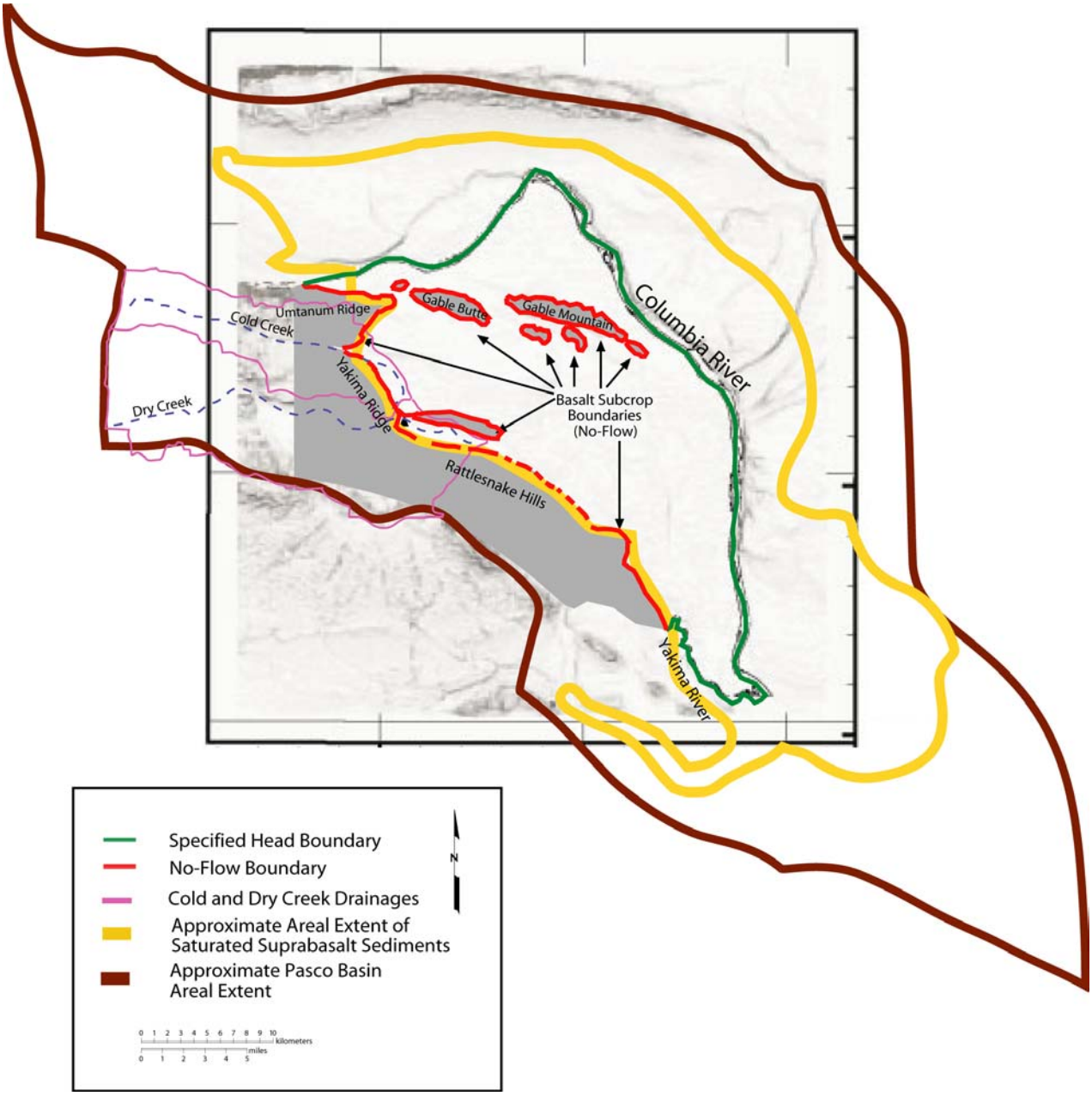

Figure 3.6. SGM Model Domain Within the Pasco Basin Illustrating the Location of the Important Flow System Boundaries for the Hanford Site Groundwater Model

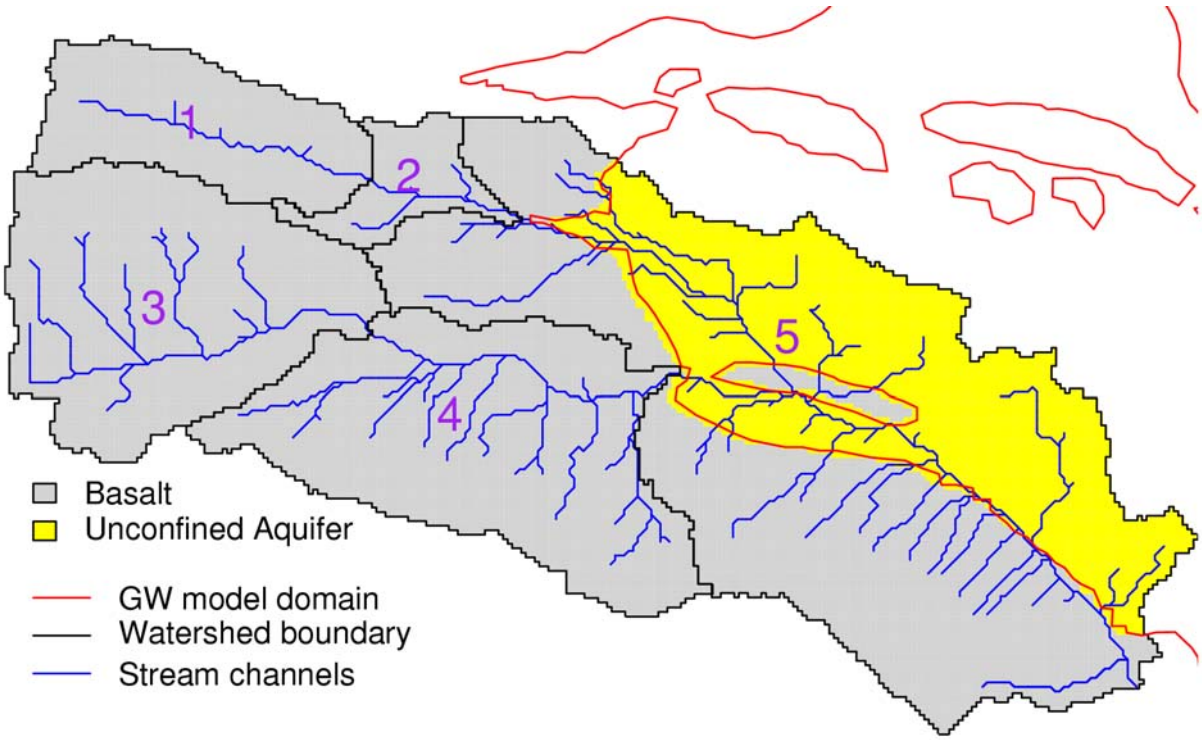

Figure 3.7. Lower Boundary Specification for Watershed Modeling

DHSVM is a process-based, distributed-parameter hydrologic model that is able to simulate runoff processes in environments with highly variable terrain (Wigmosta et al. 1994, 2002). A particular strength of DHSVM is its grid-based representation of the watershed, which allows specification of climate, vegetation, and soil at the resolution of the digital elevation model (DEM). Topographic controls on precipitation, air temperature, and down-slope water movement in DHSVM are important to the distributed water balance and stream flow generation. A conceptual diagram of DHSVM is shown in Figure 3.8. Overland flow, if any, is subject to infiltration in lower grid cells and interception by stream channels. Subsurface flow moves in an upper ("shallow") layer and a lower ("deep") layer. If the shallow water table is below the streambed, the stream may lose water to the shallow water table.

Travel time from the streambed to the water table is neglected and the infiltrated water is added immediately to the shallow water table. Similarly, water percolates through the upper groundwater layer as Darcian flow, but vertical travel time within the lower layer is neglected, and recharge from the upper layer is added immediately to the lower layer. For the recharge estimates used in ACM-2, hydraulic conductivity of the basalt was set to zero, forcing all deep groundwater to follow a lateral flow-path until a cell defined as unconfined aquifer is encountered. A relatively large hydraulic conductivity for recharge is defined for the unconfined aquifer, resulting in recharge of all groundwater in the lower layer entering an unconfined aquifer cell at the SGM boundary. In this application, the flow-path map for the deep groundwater was set equal to the surface and shallow flow-path map, but the model allows separate definition, as depicted in Figure 3.8.

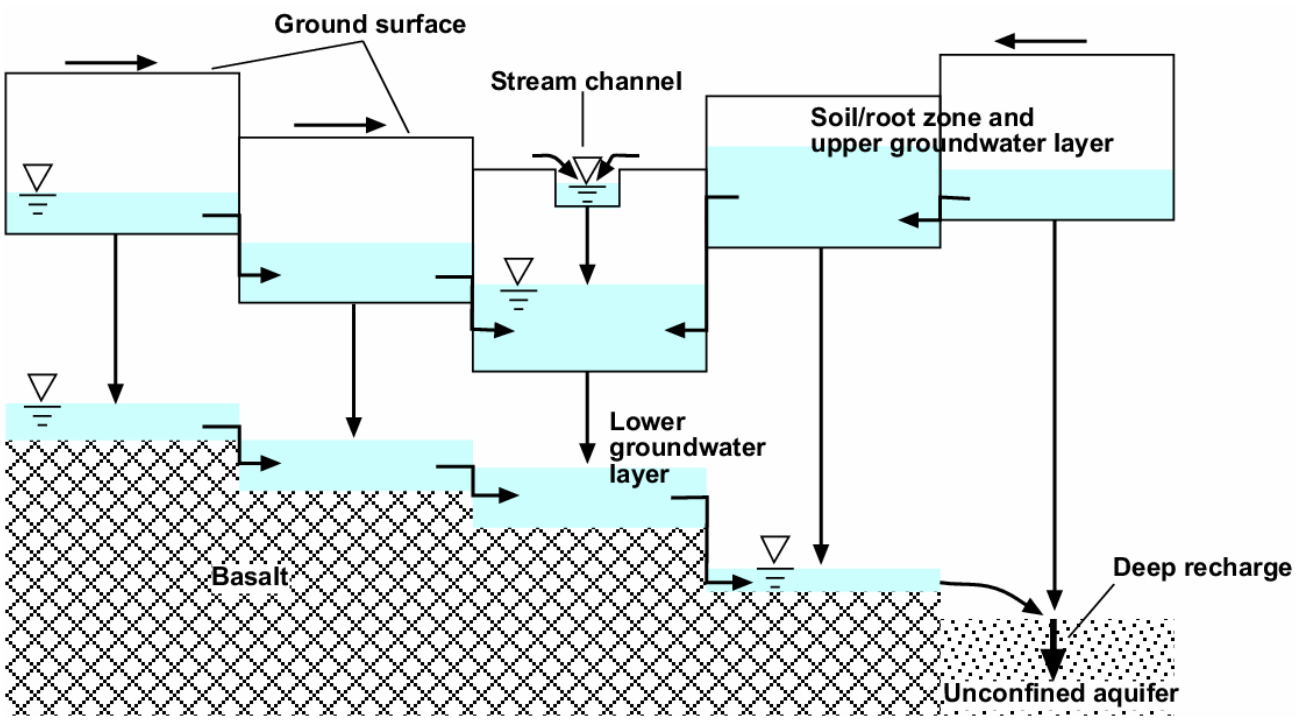

Figure 3.8. Water Pathways in DHSVM

DHSVM was modified in several important ways to make it more suitable for the arid setting of Hanford. The deep groundwater layer was added to facilitate movement below the root zone and provide for slower lateral groundwater movement. Flow routing in stream channels was modified to include infiltration into the channel bed and the simulation of "losing" streams. The infiltration capacity of the soil was limited by freezing temperatures and high soil moisture to simulate the ephemeral runoff-generating conditions at Hanford. Overland flow routing was modified to allow faster movement of runoff down the hillslope to simulate the ephemeral flash floods of Cold and Dry creeks. Along with these changes to model functions, new variables were added to DHSVM to permit mapping of channel infiltration, recharge from upper to lower groundwater layers, and deep recharge from the lower groundwater layer.

DHSVM input grids were prepared at 200 m resolution and include digital elevation models (DEMs), soil type maps, vegetation type maps, and flow direction maps. Two soil types were specified, one with an impermeable lower boundary to represent areas where basalt lies above the water table and one with essentially unlimited permeability to represent areas where the water table is the lower boundary (Figure 3.7). All other properties of the two soil types were defined alike. Vegetation consisted of one type, sagebrush-steppe, with 50% coverage of the ground surface.

DHSVM requires each of the following meteorologic variables for each time step: air temperature, wind speed, relative humidity, solar radiation, long-wave radiation, soil temperature, and precipitation. Meteorology input to the model was developed from hourly data from the Hanford Meteorological Station (HMS) and daily precipitation data from three National Weather Service (NWS) cooperative stations, Moxie City 10 E, Priest Rapids Dam, and Sunnyside. HMS hourly data start on January 1, 1955, so

meteorological input for water years 1956–2001 (WY56-01) was created. Complete details of meteorology input creation for DHSVM are described in a report that will be published by PNNL early next year.[(a)]

Calibration of DHSVM has focused on two objectives: 1) simulation of evapo-transpiration at lower elevations to constrain the vertical water balance over an average water year and 2) generating streamflow during January 1995 when ephemeral streamflow was observed in Cold and Dry Creeks. Work on this task is ongoing, and recharge estimates provided here should be considered preliminary. The second objective has been especially difficult to meet because meteorological conditions in the upper basins must be inferred from distant stations, and therefore the soil and snow conditions modeled from them are highly uncertain. Also, only a small fraction (13 percent in Basin 1) of inferred precipitation was observed as stream flow during that month, indicating that runoff is generated only under special meteorology, soil moisture, and snowpack conditions.

The recharge estimates used for ACM-2 were obtained by applying the model in its current calibration to WY56-65. Three contributing areas were delineated: Cold Creek (Basins 1 and 2, Figure 3.7); Dry Creek (Basins 3 and 4); and Rattlesnake Springs, the portion of Basin 5 west of groundwater model domain (Figure 3.9). For Cold and Dry creeks, the annual average recharge rate was computed by summing the total recharge to the lower groundwater layer in DHSVM and ephemeral stream flow at the lower gauging station locations. Perennial base flow in Dry Creek was assumed to be accounted for adequately in the groundwater recharge simulated for that watershed. For the Rattlesnake Springs contributing area, stream

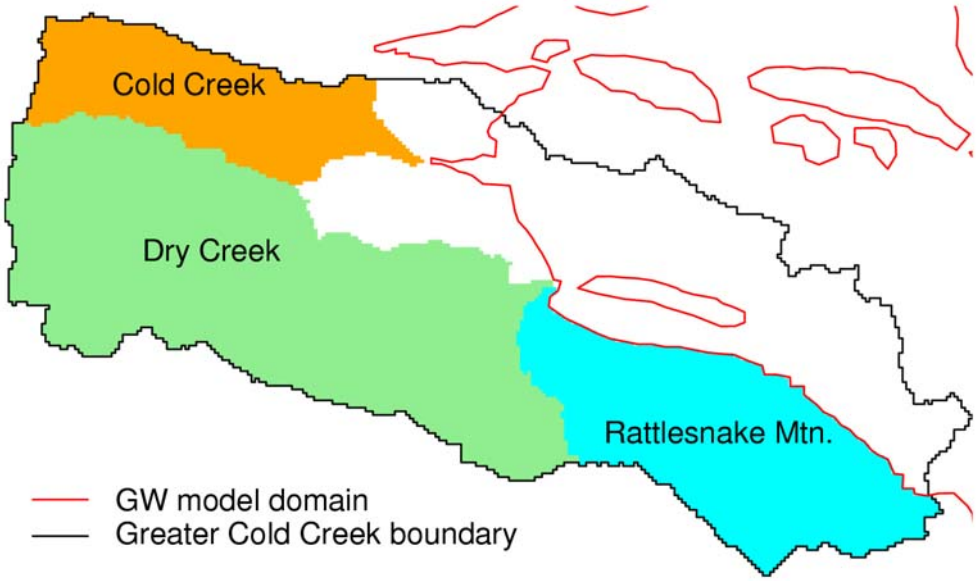

Figure 3.9. Contributing Areas for Recharge to Western SGM Boundary

(a) Waichler SR, MS Wigmosta, and A Coleman. "Groundwater Recharge to the Hanford Site from Greater Cold Creek." Draft report, Pacific Northwest National Laboratory, Richland, WA.

flow was not tracked in the model output because of logistical problems with the large number of channels that terminate on the groundwater model boundary. Instead, the runoff fraction (total recharge/ precipitation) was computed in Dry Creek and applied to the precipitation along the eastern front of Rattlesnake Mountain. The estimates of recharge (Table 3.2) were then applied to the active recharge cells in the groundwater model (Figure 3.4). As indicated, total run-on recharge from the upland areas is estimated to be of the same order of magnitude as the total surface recharge estimate for the Hanford site. The run-on recharge estimates are increased by a factor of approximately 3 for Cold Creek Valley and Rattlesnake Springs and a factor of approximately 13 for Dry Creek Valley relative to the values used in previous inverse calibration efforts. However, because earlier estimates were based on a less technically defensible approach, more confidence is placed in the magnitude of recharge estimated by the improved approach that incorporates DHSVM.

Table 3.2. Summary of Recharge in the Four Regions

Cold Creek Valley	8.13×10^3 m^3/d
Dry Creek Valley	1.57×10^4 m^3/d
Rattlesnake Springs	7.83×10^3 m^3/d
Natural Surface Recharge	2.35×10^4 m^3/d

To date, all of the necessary DHSVM modifications, model input, and post-processing tools to simulate and analyze the hydrologic extremes that prevail at Hanford have been completed. Calibration of the model to simulate the critical aspects of this hydrologic setting is ongoing and is expected to be completed by the end of FY 2003. The calibration will attempt to address the relatively rare events of runoff production at higher elevations during winter, streamflow that reaches the valley floor during such events, and a loss of most soil moisture on an annual basis as ET, particularly at low elevations. During FY 2004 we will also begin a field measurement program with installation of a streamflow and meteorology station in upper Cold Creek. Ongoing data collection will help define the critical runoff-generating conditions in Hanford watersheds and improve the distribution of meteorologic information. Data collected at this location will help parameterize existing methods like DHSVM and will likely influence our choice of methods in the future to estimate natural recharge in the greater Cold Creek watershed.

3.2.4 Basalt Intercommunication

During the initial baseline inverse calibration efforts, the uppermost units of basalt underlying the unconfined aquifer were assumed to represent the lower boundary for the Hanford Site unconfined aquifer system. The potential for interflow (recharge and discharge) between the basalt-confined aquifer system and the unconfined aquifer system was largely unquantified but postulated to be very small relative to the other flow components estimated for the unconfined aquifer during the operational period. Therefore, the underlying basalt units were not included in these models, and the bottom of the unconfined aquifer was treated as a no-flow boundary. During the ACM-1 inverse calibration effort, interactions between the unconfined aquifer system and the uppermost confined aquifer of the Columbia River Basalts were considered and a methodology was developed to incorporate the effects of basalt leakage into the SGM (Vermeul et al. 2001). During this calibration effort, an approach was developed that, with the exception of unrealistically high leakage flux along two segments of the Gable Mountain fault, provided a reason-

able representation of the primary components of basalt leakage including 1) head-dependent, areally distributed leakage, 2) increased leakage at an erosional window in the basalt near Gable Mountain/Gable Butte, and 3) increased leakage along fault zones. Minor modifications to this approach were implemented during the ACM-2 transient inverse calibration effort and are discussed below.

As discussed above, unrealistically high leakage flux was simulated along two segments of the Gable Mountain fault, one to the northeast of Gable Butte and the other to the southwest of Gable Mountain. Upon further inspection of the geology in these areas, it was determined that the location of the Gable Mountain fault, as implemented in the SGM, was not being represented correctly and that this location error was the cause of the unrealistically high fluxes. In ACM-1, the string representing the Gable Mountain fault was erroneously located a substantial distance up the side of the anticlinal structure instead of at the base of the anticline, where curvature of the rock is at its highest and subsequently where the fault is most likely to occur. Due to this error, which put the fault in direct contact with the high-conductivity Hanford formation sediments, and because these fault segments were close to the Columbia River discharge boundary, the unrealistically high basalt leakage rates did not result in a corresponding head increase in the unconfined aquifer, and the model was able to maintain these unrealistically high rates. However, by moving the fault to the correct location along the base of the anticline, which placed the fault below a laterally continuous mud unit that pinches out against Gable Mountain farther up the anticline, this problem was eliminated. The updated location of the Gable Mountain thrust faults, as represented in ACM-2, is shown in Figure 3.10.

One additional ACM-2 fault leakage modification was a change from the element-based approach used in ACM-1 to a nodal head dependent flux boundary condition in the new model. This modification allowed for improved representation of fault leakage that was not based on scaling the basalt permeability of an entire element according to the relative permeability and size of the fault in relation to the element size. This improvement resulted in a more localized flux input that more closely represents the conceptual model of fault leakage. Based on limited information regarding enhanced vertical permeability induced by basalt fracturing, as discussed in Vermeul et al. (2001), fault thickness was set to 2 m and the initial fault conductivity to 5 m/d (the midpoint of the expected range).

During investigation of the unrealistically high fault leakage discussed above, a related problem associated with increased leakage at the erosional window near Gable Mountain/Gable Butte was identified. In ACM-1, leakage at the erosional window was implemented using a head-dependent flux boundary at both the northern and southern boundary of the erosional window. However, close inspection of the mud units on the north side of the erosional window indicated that this portion of the erosional window boundary was sealed off by a relatively thick mud unit (Figure 3.11). Based on this new conceptual model of the erosional window, nodes on the northern boundary were removed from the head dependent flux calculation and leakage from this feature was estimated based on flux calculations for the southern boundary nodes, which are in direct contact with the Hanford formation.

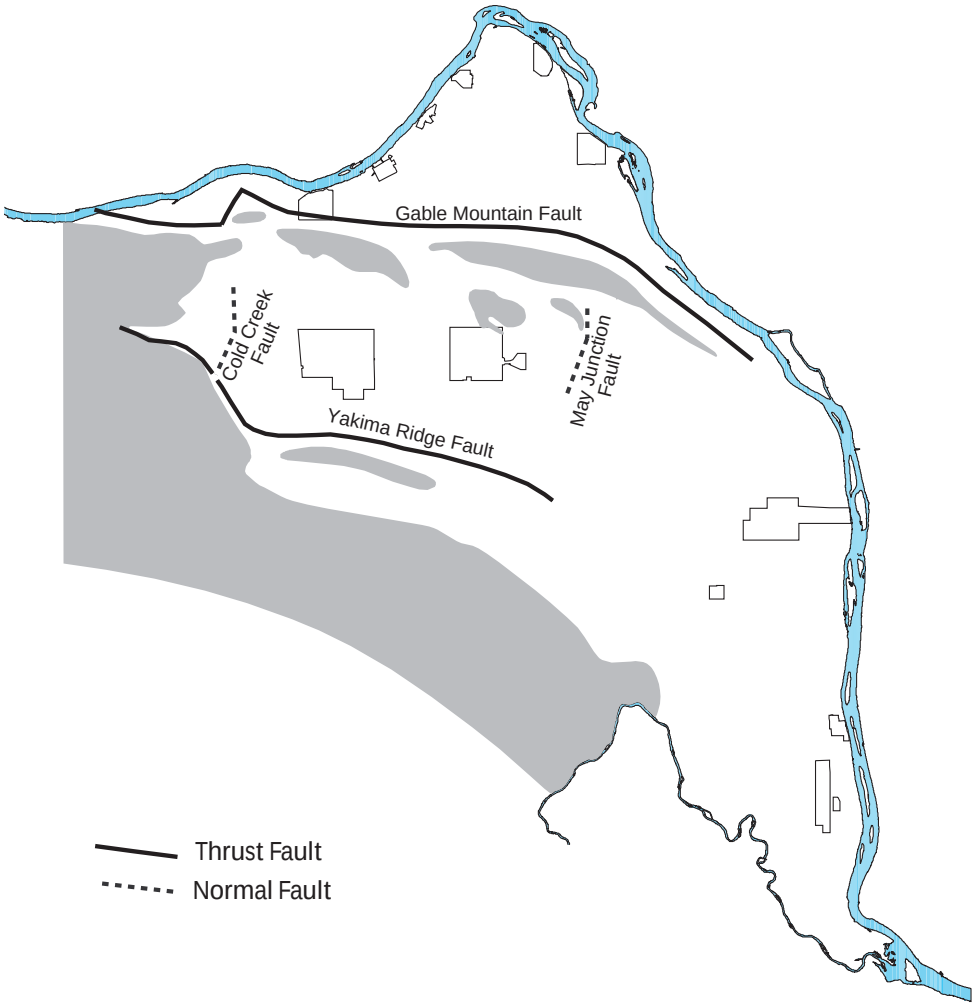

Figure 3.10. Location of Thrust Faults and Normal Faults on the Hanford Site

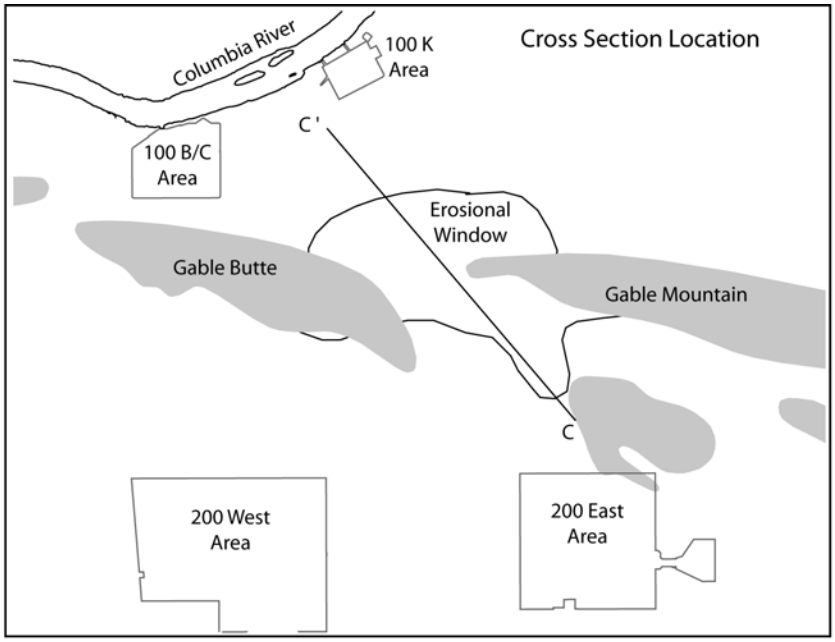

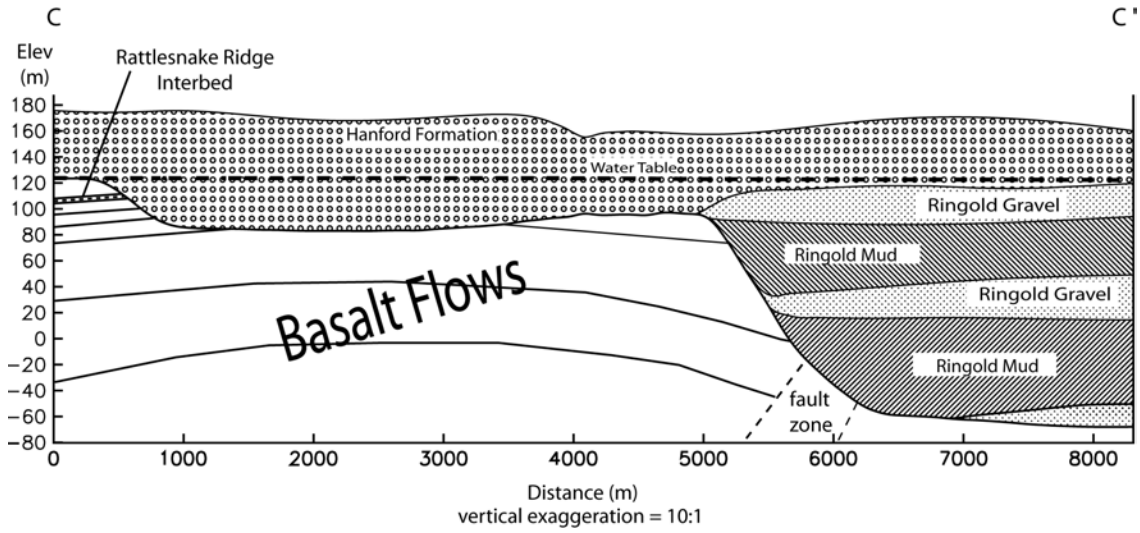

Figure 3.11. Geologic Cross Section Through the Gap Between Gable Mountain and Gable Butte Indicating the Northern and Southern Boundary of the Erosional Window

3.2.5 Natural Surface Recharge

Natural recharge from precipitation falling on the Hanford Site is highly variable both spatially and temporally, ranging from near zero to more than 100 mm/yr depending on climate, vegetation, and soil texture (Gee et al. 1992; Fayer and Walters 1995). Areas with shrubs and fine-textured soils like silt loams tend to have low recharge rates, while areas with little vegetation and coarse-textured soils, such as dune sands, tend to have high recharge rates. Recharge is also generally higher near the basalt ridges because of greater precipitation and runoff. Past estimates of recharge have been summarized in status

reports (Thorne and Chamness 1992; Thorne et al. 1993). Fayer and Walters (1995) developed a natural recharge map (Figure 3.12) for 1979 conditions to support the SGM. Distributions of soil and vegetation types were mapped first. A recharge rate was then assigned to each combination on the basis of data from lysimeters, tracer studies, neutron probe measurements, and computer modeling. Estimated recharge rates for 1992 were found to range from 2.6 to 127 mm/yr, and the total volume of natural recharge from precipitation over the Hanford Site was estimated to be 2.35 x 10^4 m^3/d. This value is of the same order of magnitude as the artificial recharge to the 200-Area waste disposal facilities during 1992 and approximately six times less than peak discharges to these facilities during the 1960s (Figure 3.13).

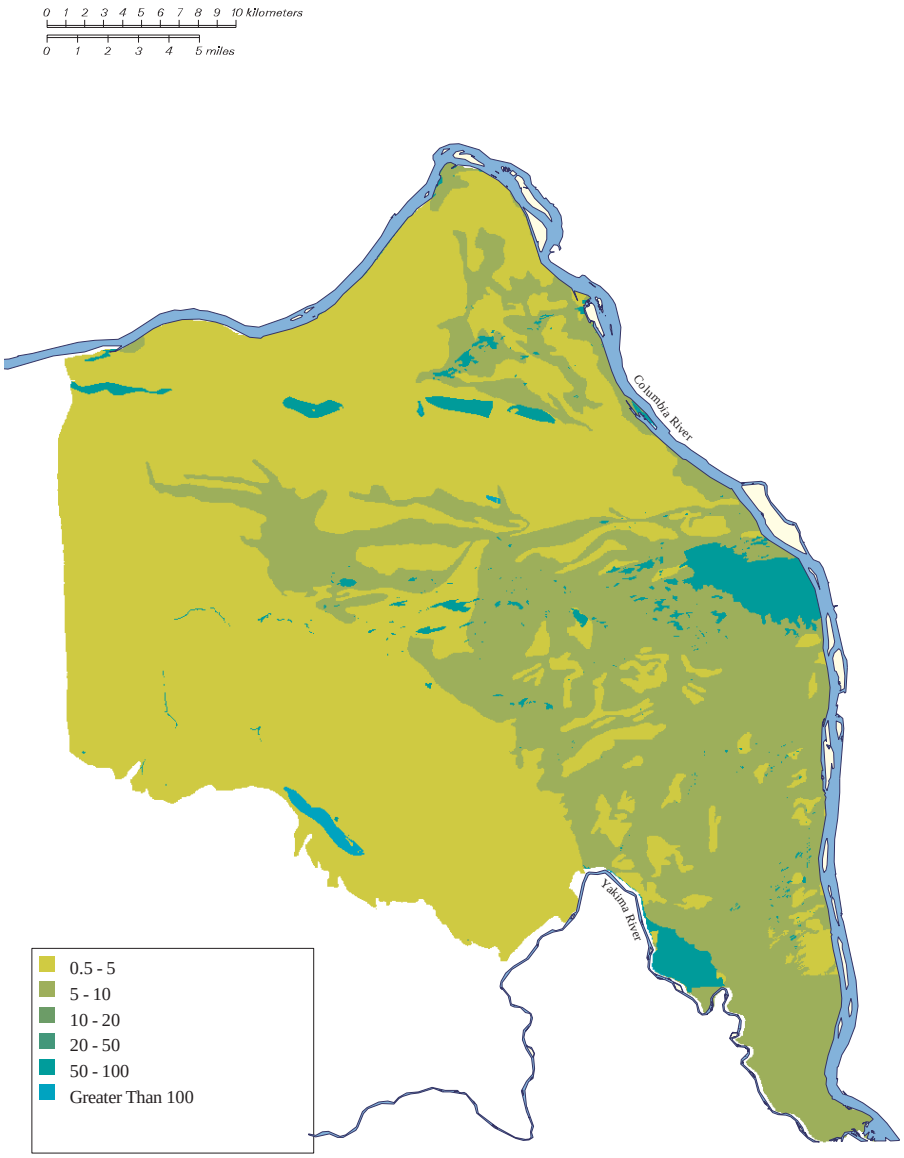

Figure 3.12. Estimates of Recharge for 1979 Conditions (Fayer and Walters 1995)

Figure 3.13. Artificial Discharges to the Unconfined Aquifer from 1943 to 2000

3.2.6 Artificial Recharge

As discussed above, another source of recharge to the unconfined aquifer is artificial recharge from wastewater disposal. Over the past 59 years, the large volume of wastewater discharged to disposal facilities at the Hanford Site has significantly affected groundwater flow and contaminant transport in the unconfined aquifer (Figure 3.13). The volume of artificial recharge has decreased significantly during the past 10 years and continues to decrease. Wurstner et al. (1995) summarized the major discharge facilities incorporated in the SGM. Cole et al. (1997) summarized the major wastewater discharges from both past and future sources. Significant uncertainties are associated with the artificial discharges related to the spatial location and timing of their arrival at the water table. As discussed below, ACM-2 implemented a new application of artificial discharges to account for the lag time associated with movement of the initial wetting front through the vadose zone. Investigation and verification of the spatial locations of the various discharge locations, and their change over time, is ongoing.

Previous versions of the SGM have been calibrated and used with records of artificial liquid discharges specified as inputs to the saturated flow system without regard to the vadose zone. In effect, the vadose zone was ignored and disposals of liquid to ground were considered to instantly reach the unconfined aquifer at the time of disposal. Consideration of vadose zone effects coupled with the SGM has been problematic until recently.

The System Assessment Capability (SAC) is a new tool developed to provide the first-ever total systems modeling of all waste disposal locations at the Hanford Site. It accounts for inventory distribution, release, environmental transport, and impacts to human, ecological, economic, and cultural resources. The software framework of the SAC necessarily included a coupling of many vadose zone site-specific models to the SGM. Because the SAC already includes a vadose zone model for all the Hanford waste disposal locations with full coupling to the SGM, it was recognized that, with relatively minor adaptations to the SAC framework and data, the SAC could be used to account for the vadose zone's effects on liquid disposal arrival at the unconfined aquifer.

In SAC, vadose zone sites are modeled using the STOMP (Subsurface Transport over Multiple Phases) simulator. A separate STOMP model is used for each individual waste disposal site, as identified in the Waste Information Data System (WIDS).[(a)] Releases at all of these sites (hundreds) are accumulated in time and space by the VZDROP (Vadose Zone Data Restructure for Other Programs) code and used to prepare a single "L3I" input file for CFEST.

The focus of the SAC is on analyte mass moving from the vadose zone to groundwater and beyond. To support improved treatment of fluid movement from the vadose zone to groundwater, some improvements were added to the SAC modification set of the STOMP code and to the VZDROP code. STOMP was modified to produce a record of fluid discharge to groundwater from the vadose zone in excess of the natural recharge rate declared as an upper boundary flux (that is, a Neumann-type boundary condition). Because artificial recharge is represented in SAC STOMP modeling as a nodal source, and natural recharge is represented as a boundary flux, the difference between the lower and upper boundary fluxes were taken to represent the arrival of artificial recharge at the water table. The natural recharge rate in SAC simulations is not constant; it changes in time to represent changes to the surface conditions. Hence, the difference between fluxes at the upper and lower boundaries is measured relative to the current time to preclude misclassifying variations in natural recharge as the artificial recharge signal. VZDROP was modified to have a runtime option that redirected its focus from the standard handling of analyte mass to handle liquid fluxes instead. Using this new option, VZDROP collects the STOMP-recorded values of liquid flux to the water table in excess of natural recharge at the vadose zone model's upper boundary for all sites, and uses it to modify a CFEST L3I file's nodal fluid sources. The final product is a CFEST input set that represents artificial recharge sources to the unconfined aquifer from a vadose zone model, rather than directly from the discharge record.

One consideration in applying the SAC database and software was that "clean" water sources were not included in the SAC site list. The SAC site list includes all sites that potentially received certain radioactive or chemical wastes. But other sources of artificial discharge, such as septic disposal systems, still exist on the Hanford Site. These additional water source locations were identified and added to the SAC site list for this special "fluid" application of SAC.

Recent corrections to specification of infiltration rates for input to the STOMP model in the SAC framework were incorporated in this special "fluid" application run of SAC. Additionally, a correction was introduced for the B-Pond complex. In the SAC database, all discharges to the B-Pond complex are represented as discharging at B-Pond itself (WIDS Site ID 216-B-3). Conditions during the period 1983–1995 involved considerable discharge to ditches 216-B-3A, 216-B-3B, and 216-B-3C as well. To account for this, the release predicted in the SAC simulation for site 216-B-3 was divided into four equal releases and each reassigned to 216-B-3, 216-B-3A, 216-B-3B, and 216-B-3C before using the VZDROP code to distribute STOMP fluid releases at the water table.

(a) WIDS is the computerized database operated by Fluor Hanford to track all Hanford Site solid waste management units, as required by the Tri-Party Agreement.

3.2.7 Facies-Based Zonation of Hydraulic Properties

Hydraulic properties of most importance to the conceptual model include both horizontal and vertical conductivities and specific yield. Hydraulic properties have been measured for the unconfined aquifer (considered a simple hydrogeologic unit) mainly during aquifer pumping tests and from laboratory permeability tests. The results of these tests have been documented over the past 50 years and recently summarized (DOE 1988; Thorne and Newcomer 1992). As indicated in these documents, the quality of results from aquifer tests at the Site varies widely and is affected by both aquifer conditions and analysis procedures. Thorne and Newcomer (1992) and Wurstner et al. (1995) reanalyzed the aquifer tests, many of which were single-well pumping tests.

Hydraulic properties of sediments within each of the units defined for the model vary spatially. To account for at least the larger scale variations, which are reflected in the observed hydraulic-head data used for model calibration, two-dimensional facies-based zones were defined within model Units 1 and 5. These are the units existing at the water table over most of the site and are the most significant units in contaminant transport.

Geologic and hydrologic information had been used previously to make preliminary maps of zones with relatively similar hydraulic properties within the saturated Hanford formation (Unit 1) and the upper Ringold Formation gravel and sand unit (Unit 5) (Vermeul et al. 2001). Data used to develop this facies-based zonation included borehole records, aquifer test data, water table gradient, and the current understanding of the geologic depositional environment that existed when these sediments were deposited.

Cataclysmic flood deposits of the Hanford formation are divided into six facies zones, as shown in Figure 3.14. They include four different gravel-dominated zones, a sand-dominated zone, and a silt-dominated zone. Textural information provided on Lindsey's (1995) cross sections was used to determine the predominant facies type (silt, sand, or gravel). In general, the texture of the Hanford formation becomes finer-grained away from the center of the basin (i.e., the Gable Butte-Gable Mountain axis). The gravel facies are dominant over most of the area where Hanford formation sediments lie below the water table, primarily in the northern and southeastern parts of the Site. The sand facies (HS) is present below the water table along the Columbia River on the northeastern boundary of the model. Sand (HS) and silt (HL) facies zones along the southwestern boundary are generally above the water table. The gravel-dominated facies (zones HG1 through HG4 in Figure 3.14) were delineated based on depositional environment, aquifer test results, and hydraulic head gradients. The water table is very flat where the highly conductive facies HG2 and HG3 are present below the water table. The highest conductivity zone, HG2, encompasses the 200 East Area and the area to the southeast. The next most conductive zone, HG3, lies north of the 200 East Area to the Columbia River. Zones HG2 and HG3 were in an area of very high energy during the cataclysmic floods because floodwaters were channeled through the gap between Gable Mountain and Gable Butte. The BPOND zone (HG4) covers only a small area around B-Pond and reflects the lower conductivity of Hanford formation sediments in this area, which was likely in the lee of basalt outcrops during the Missoula floods.

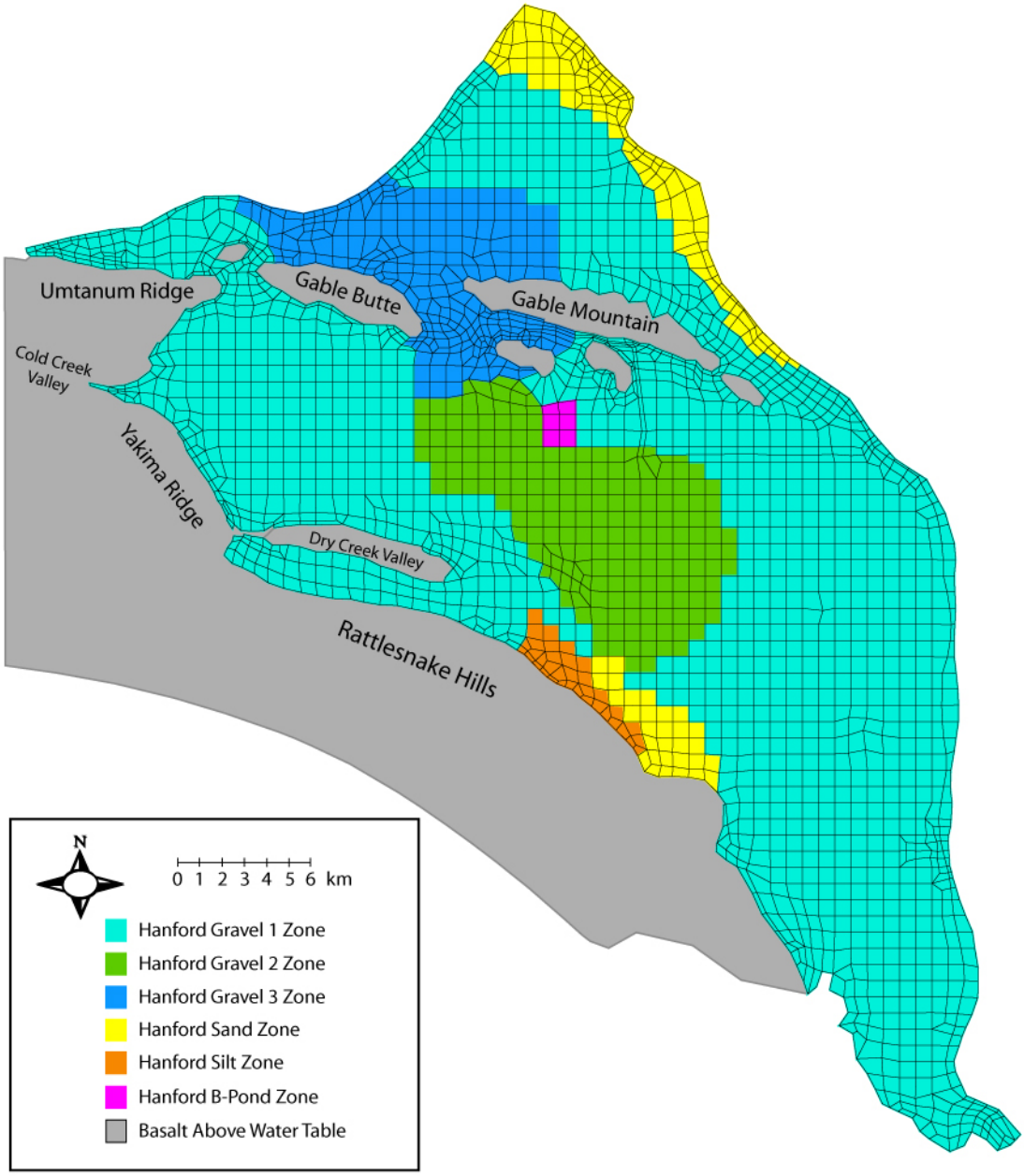

Figure 3.14. Facies-Based Zonation of Unit 1

Geologic information and aquifer test data indicate that the Ringold gravels and sands that compose model Unit 5 display smaller textural features, and thus smaller-scale heterogeneity in hydraulic properties, than the post-Ringold sediments. This is consistent with the fact that these sediments were deposited by the ancestral Columbia River system as it moved back and forth across the Pasco Basin. Over most of the Hanford Site, there are not enough data to delineate areas with consistently high or low hydraulic properties within this unit. However, in the vicinity of the 200 West Area, the distribution of wells completed in this unit is relatively dense, and aquifer tests have recently been completed in about 20 of these wells. Based on these data and test results from several wells in the 100 Areas, a zone of relatively high hydraulic conductivity was delineated around the southern part of the 200 West Area and near the Columbia River along the northern site boundary (Figure 3.15).

During preliminary inverse calibration efforts associated with the development of ACM-2, it was also recognized that Ringold sediments along the western edge of the Pasco Basin are likely more dominated by alluvial fan deposits and are expected to have generally higher conductivity. The conductivity of these sediments is also important in controlling flow from recharge areas on the western boundary. Therefore, separate facies zones were defined for the area at the bottom of the Cold Creek and Dry Creek valleys (Figure 3.15). In earlier calibration attempts, a separate facies zone was established along the Yakima Ridge between the Cold Creek and Dry Creek zones. However, this zone was later merged with the relatively high-conductivity zone encompassing the southern part of the 200 West Area. Hydraulic head data from wells in the Dry Creek Valley indicate a change in aquifer transmissivity along the length of the valley. Equal potential lines (water table elevation contours) are much closer together in the lower part of the valley than in the upper part. This could be caused by either a difference in conductivity of the Ringold gravel units or a change in thickness. Geologic data does indicate that the Ringold gravels are thinner and the Ringold mud unit is thicker in the lower area. To account for these various hydrogeologic conditions, three separate facies zones were created in the dry creek valley to help the inverse modeling process to control flow in this important recharge area.

As the water table elevation has risen and fallen over time, the distribution of hydrogeologic units and facies at the water table has also changed. Figure 3.16 shows the distribution of hydrogeologic units/ facies that existed at the water table before Hanford operations began. Figure 3.17 shows the distribution of hydrogeologic units/facies that existed at the maximum water table measured since Hanford operations began. Figure 3.18 shows the vertical distributions of the major hydrogeologic units defined in the three-dimensional model along the A-A' and B-B' transects indicated in Figure 3.17.

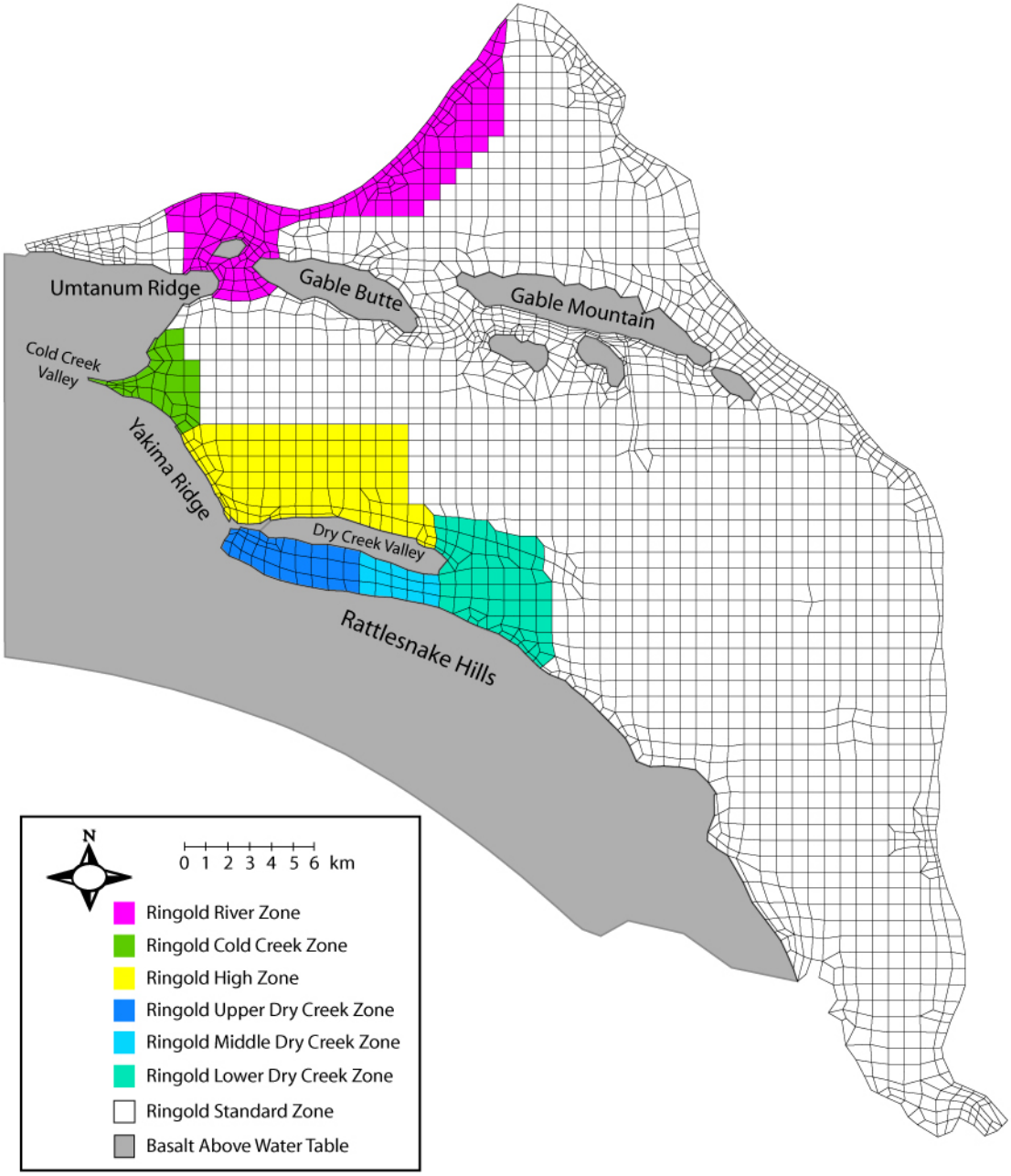

Figure 3.15. Facies-Based Zonation of Unit 5

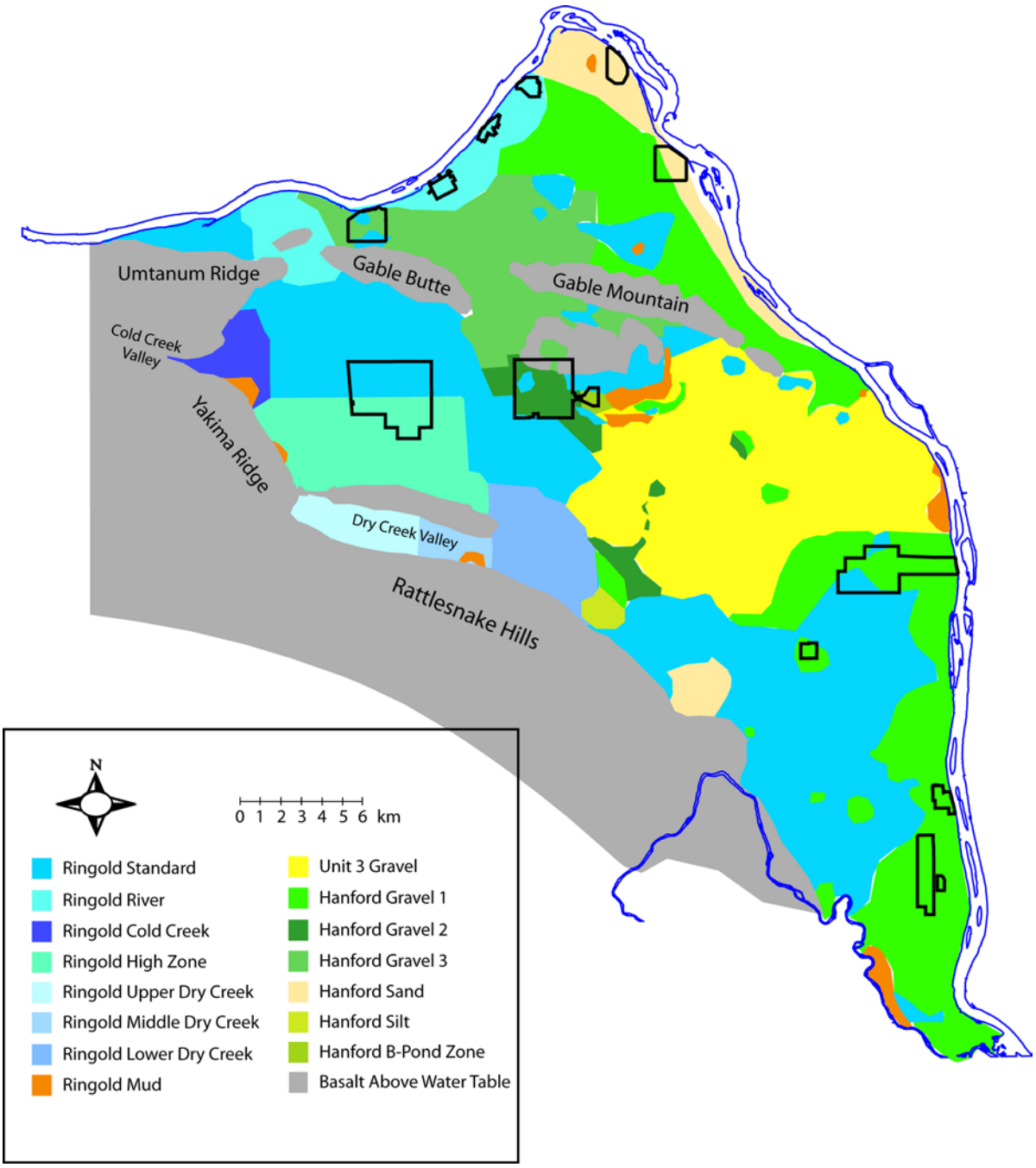

Figure 3.16. Distribution of Hydrogeologic Units and Facies Zones at the Pre-Hanford Water Table

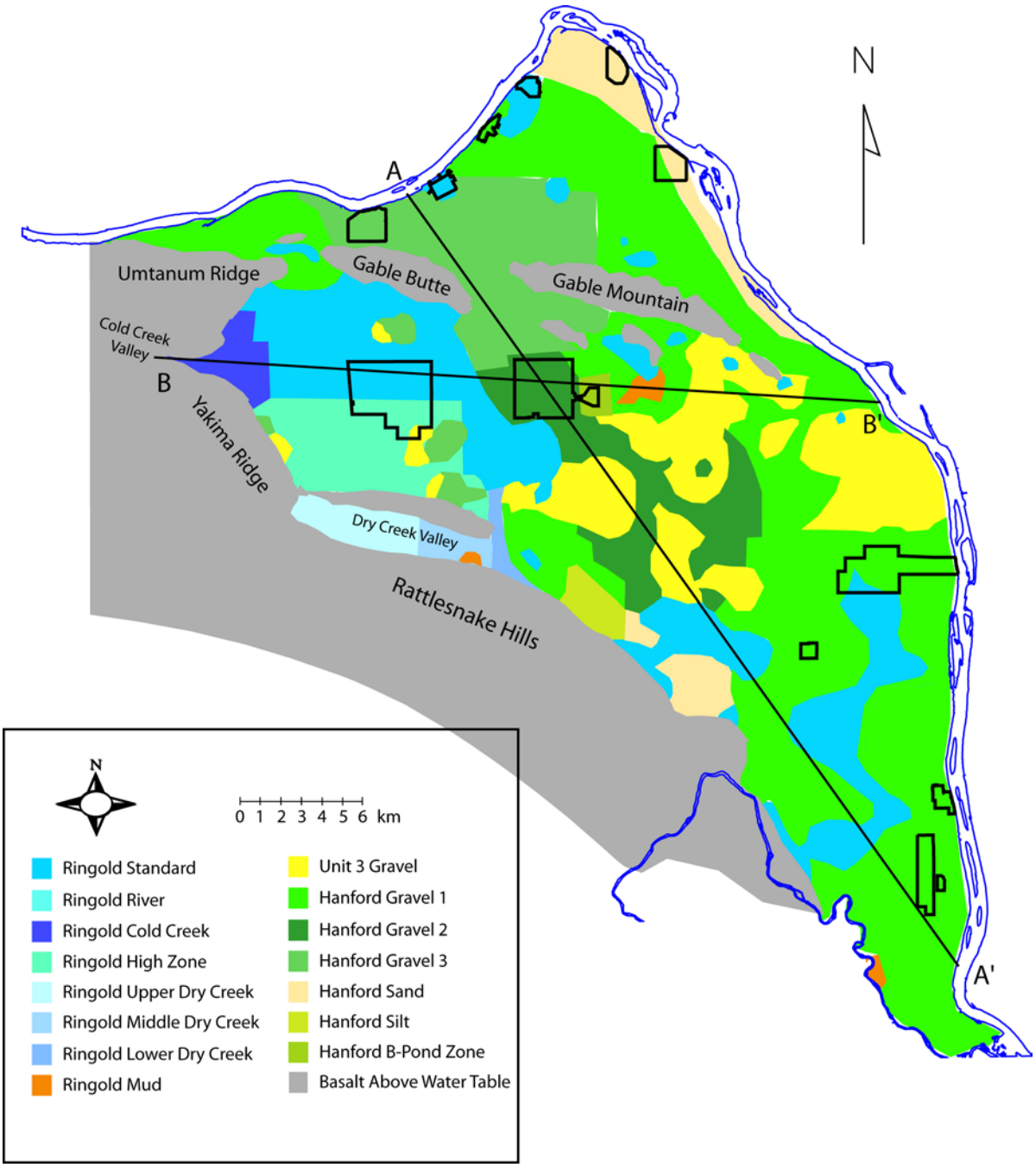

Figure 3.17. Distribution of Hydrogeologic Units and Facies Zones at the Maximum Water Table

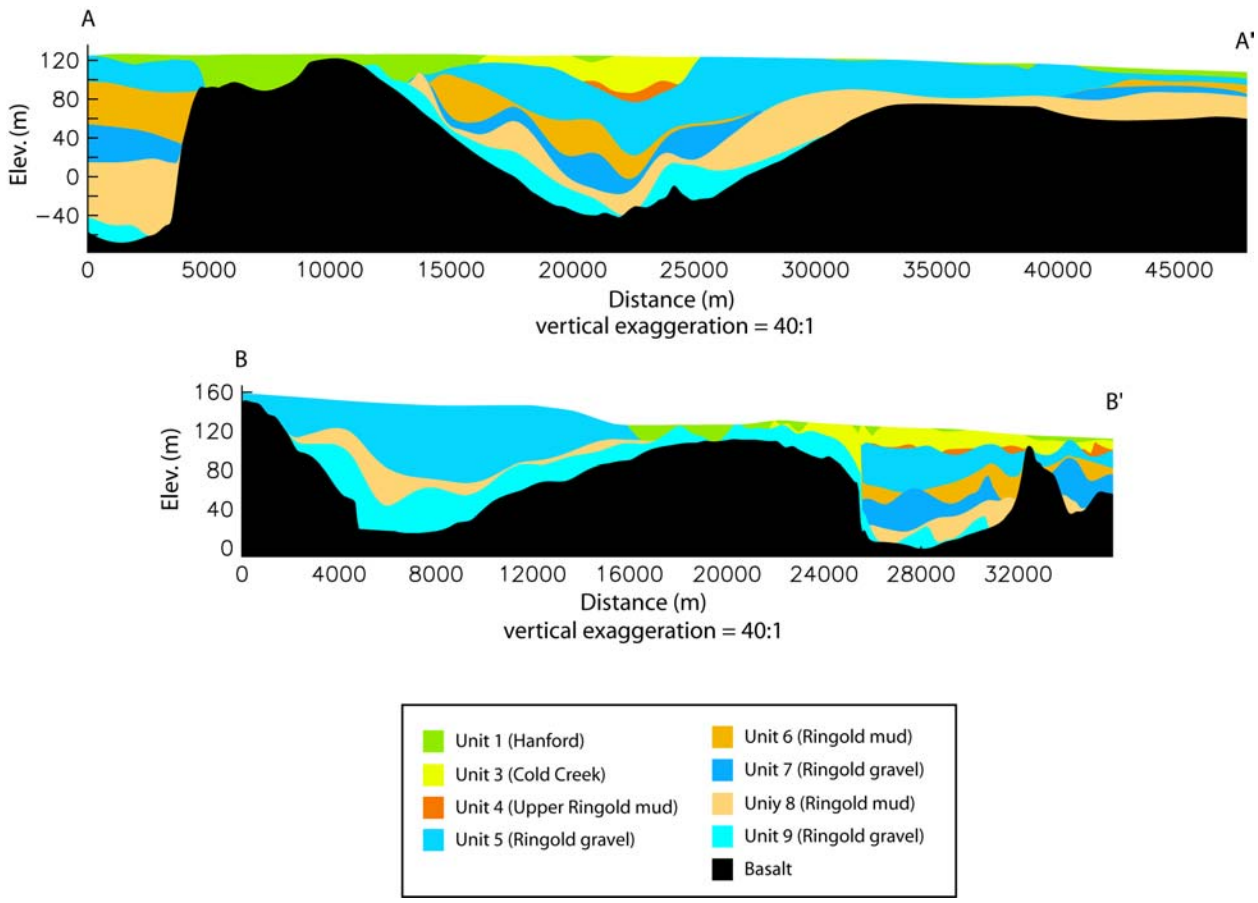

Figure 3.18. Cross Sections Along A-A' and B-B' Showing Distribution of Hydrogeologic Units Below the Maximum Water Table (see Figure 3.17 for transect locations)

4.0 Results and Evaluation of the ACM-2 Transient Inverse Simulation

A brief discussion of the step-wise investigation and determination of the ACM-2 transient inverse model parameterization that provided the best model fit is contained in Section 4.1. Detailed results from the ACM-2 transient inverse calibration for the historical period of Hanford Site operations (1943–2000) are discussed in Section 4.2. Discussions in Section 4.3 evaluate the regression results by following the "Guidelines for Effective Model Calibration" (Hill 1998; Cole et al. 2001a).

4.1 ACM-2 Parameterization

Prior to initiation of parameter estimation using the transient inverse approach, parameter sensitivities were examined to ensure that the regression started as a well-posed problem. A fairly extensive parameter set was included in this initial analysis to determine which parameters could be estimated. Parameters examined in this initial sensitivity analysis (i.e., UCODE phase 22) included:

- hydraulic conductivity of conductive units: Hanford formation (Unit 1, facies-based zonation), Cold Creek gravels (Unit 3), and Ringold Formation (Unit 5 with facies-based zonation, Units 7 and 9)
- hydraulic conductivity of the Ringold mud units (Units 6 and 8); due to its limited saturated extent, the upper Ringold mud (Unit 4) was not included in the inverse
- vertical hydraulic conductivity of underlying basalt layer (estimation of basalt leakage)
- hydraulic conductivity associated with head dependent flux boundaries at the erosional window and fault locations (estimation of increased basalt leakage)
- specific yield of the conductive units containing the water table: Hanford formation (Unit 1, facies-based zonation), Cold Creek gravels (Unit 3), and Ringold Formation (Unit 5, facies-based zonation)
- anisotropy ratio of all conductive hydrogeologic units
- components of surface recharge.

This initial sensitivity analysis, which evaluates the composite scaled sensitivity coefficients for all parameters being considered, was used to identify which parameters could be estimated. The sensitivity coefficient for each parameter is calculated by evaluating the change in each simulated value (i.e., corresponding to a given observation) caused by a small perturbation in each of the parameters evaluated. These sensitivities are made dimensionless by scaling the sensitivity by the parameter value and by the square root of the weight. The results are summarized in a composite scaled sensitivity coefficient for each parameter that is formed by summing up the squared dimensionless sensitivity coefficients for all observations, dividing this quantity by the total number of observations, and taking the square root of this value (Hill, 1998). These results were used to identify parameters to which the solution was insensitive and provided the basis for selecting the parameters to move forward within the inverse calibration effort.

Following the initial sensitivity analysis, a series of inverse simulations were conducted to identify additional parameters of marginal sensitivity that became insensitive as the solution moved through parameter space. Each time a new parameter was identified as being too insensitive to allow estimation, the inverse had to be aborted, the offending parameter removed from the list of estimated parameters and held at its pre-inverse assumed value (i.e., book value), and the inverse simulation restarted. In several instances, the specified "book value" for a parameter was adjusted based on intermediate parameter sensitivity and estimation results (i.e., prior to conducting an inverse simulation based on the final ACM-2 parameterization) and/or inspection of head solution residuals obtained from a forward run using these intermediate results. Specific adjustments to parameter book values, which were used as the starting parameter values in the inverse, included a reduction in the hydraulic conductivity controlling fault leakage (previously assumed values resulted in excessive leakage and subsequent insensitivity in other recharge parameters), a decrease in the vertical hydraulic conductivity of the basalts (Unit 10), and a slight modification to the specific yield of several facies of the Hanford and Ringold formations present across the 200 Area plateau, where most of the groundwater mound buildup occurs.

This manual calibration approach was required due to the current configuration of UCODE, which relies solely on the phase-22 sensitivity analysis to ensure that only sensitive parameters are included in the inverse and that the regression is started as and remains a well-posed problem. However, because parameter sensitivity coefficients change throughout the regression process as a result of nonlinearities, it would be advantageous and far less labor intensive to develop a UCODE formulation that continuously calculates the sensitivity of all parameters at each location in parameter space and determines whether it is sensitive enough to estimate and include or exclude it from the inverse accordingly. Development of this alternative UCODE formulation is being investigated.

Because the alternative UCODE formulation was not available in time for this calibration effort, many of the parameters had to be removed from the inverse to determine the best estimates for all sensitive parameters. Once an acceptable solution was obtained, all previously insensitive parameters were reinvestigated to confirm that they were still insensitive at the final solution's location in parameter space. Although the results of this final sensitivity analysis were generally consistent with previously observed parameter sensitivities, several parameters were identified as having marginally significant sensitivity metrics and thus requiring further investigation.

Once the inverse calibration effort had converged on an acceptable solution and parameter sensitivities had been reinvestigated to ensure that all sensitive parameters were included, the solution's uniqueness was tested by perturbing the system and verifying that the inverse calibration would move the parameter estimates back to the same solution. This final test of solution uniqueness was conducted by setting all parameter values back to their pre-inverse assumed values and restarting the inverse. It should be noted that there were several cases where, as discussed above, starting/fixed values were modified relative to pre-inverse assumed values based on results of the various inverse simulations that were conducted during the step-wise development of the best fit model. Results from this final inverse calibration (Sections 4.2 and 4.3) indicated that, within the parameter space domain between the pre-inverse assumed values and the estimated best fit parameter values, a unique solution did exist (i.e., the parameter values moved back to the same solution). Exhaustive testing to determine how much best-fit model parameter values would need to be perturbed for the inverse calibration to move toward a different solution was not within the scope of this effort but may be investigated during future inverse efforts.

The following is a brief summary of each tested parameter's sensitivity and subsequent determinability based on the results of the above inverse calibration analyses. Additional detail regarding the sensitivity of all estimated parameters is contained in the following sections.

Hydraulic conductivity of conductive units: In general, the solution was sensitive to the hydraulic conductivity of the more conductive units. The only permeable units not determinable by the inverse were Ringold Units 7 and 9, which are of relatively moderate permeability and located deeper in the profile where fewer observational data are available.

Hydraulic conductivity of the Ringold mud units: The solution was sensitive to the hydraulic conductivity of the lower conductivity, slightly more extensive mud unit (Unit 8) and insensitive to Unit 6.

Vertical hydraulic conductivity of underlying basalt layer: The solution was sensitive to this parameter, which affects basalt leakage.

Features associated with increased basalt leakage: In general, the solution was insensitive to hydraulic conductivity associated with head-dependent flux boundaries at the erosional window and thrust fault locations. One exception was a section of fault in the Cold Creek Valley upgradient of the Cold Creek flow impediment. High basalt heads upgradient of this feature is the primary reason for the solution's increased sensitivity to the hydraulic conductivity value controlling leakage over this section of the thrust fault.

Specific yield of the conductive units containing the water table: The solution was generally insensitive to all tested specific yield parameter values. However, the specific yield of several facies of the Hanford and Ringold formations present across the 200 Area plateau where the largest magnitude of groundwater mound buildup occurs were marginally sensitive for a limited time during the inverse process but became insensitive as the inverse progressed.

Anisotropy ratio of all conductive hydrogeologic units: The solution was insensitive to all anisotropy parameters

Components of surface recharge: The solution was insensitive to areally distributed surface recharge but sensitive to run-on recharge from Cold Creek, Dry Creek, and Rattlesnake Springs.

4.2 Transient Inverse Simulation Results

Results from the ACM-2 transient inverse model, which is the first attempt at incorporating facies-based geologic information into the model structure, indicate that the proposed approach is feasible and can provide a model that adequately fits head observational data for the site while providing a more technically defensible geologic structure. This facies-based approach was developed to replace the hydraulic conductivity distribution used in previous inverse calibration efforts. The previous approach was based on a transmissivity distribution developed during initial steady-state, two-dimensional calibration efforts. Comparisons, measures, and discussions in this section parallel those summarized for the baseline and ACM-1 transient inverse simulation results presented in Cole et al. (2001a) and Vermeul et al. (2001) to provide a consistent basis for comparison. The discussions in this section include spatial and temporal distribution of residual errors and residual error statistics.

4.2.1 Spatial and Temporal Distributions of Residual Errors

An overall comparison of simulated and measured water levels for the entire calibration period (1943–2000) for ACM-2, with the first observations starting in 1948, is shown in Figure 4.1 as a scattergram plot of simulated head from the inverse model plotted versus the measured head. The scattergram also contrasts the scatter of residual error points with a 45-degree line that represents a perfect match between model and data, with the individual plotted points color-coded to indicate the magnitude of the residual error. Figure 4.2 shows a residual frequency histogram for ACM-2 over this same calibration time period that plots the number of residuals in each residual category from -12 m to +12 m in 1-m increments. The associated residual summary statistics are given in Table 4.1.

The graphical comparisons and summary statistics illustrate that, over the entire prediction period, acceptable overall model fit was realized for the ACM-2 inverse model. Residual error statistics indicate that 65.8 percent of the simulated values were within ±1 m of measured values, and 98.9 percent were within ±5 m. The overall mean residual was 0.06 m (-0.82 m for 39,264 negative residuals and 1.19 m for 30,511 positive residuals). The residual values ranged from –7.39 m to 9.38 m, and the total sum of squared residuals was 1.40 x 10^5 m^2.

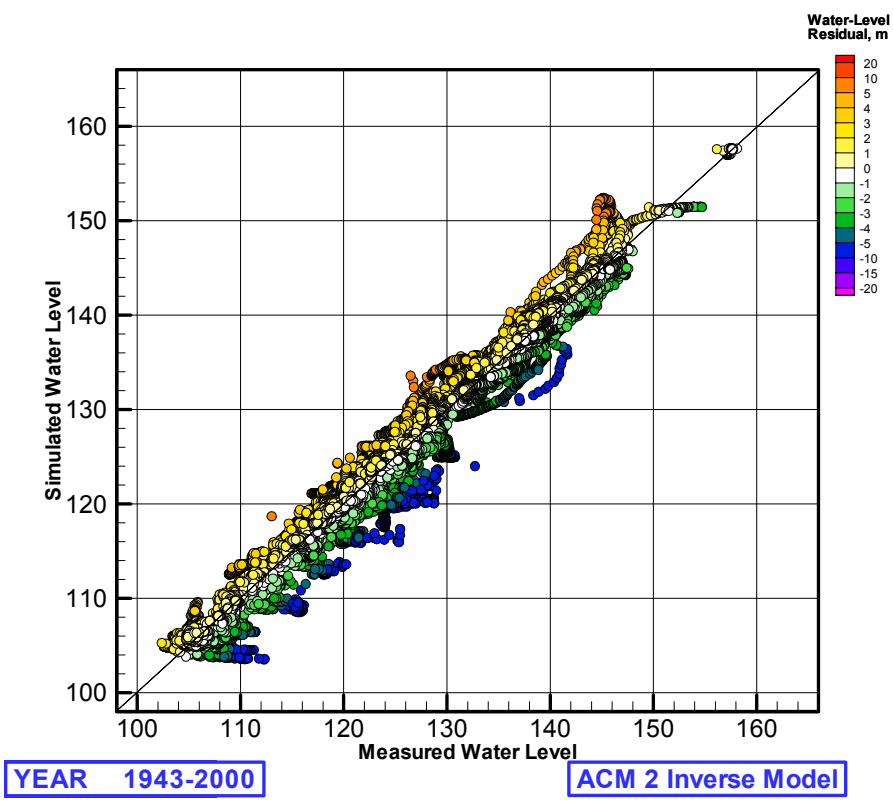

Figure 4.1. Measured Versus Predicted Heads (45-degree plot); all Observations for Best-Fit ACM-2 Inverse Model

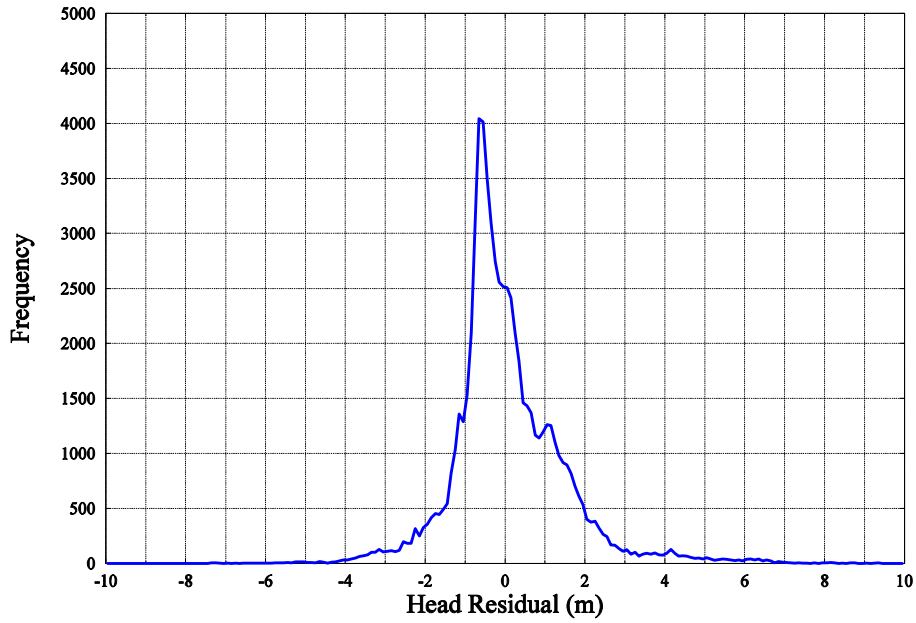

Figure 4.2. Predicted Head Residuals; All Observations for Best-Fit ACM-2 Inverse Model

Table 4.1. Summary of Residual Error Statistics of Best-Fit ACM-2 Inverse Model

Residual Statistic	Value	No. of Observations
Positive Residuals		
Mean (m)	1.19	30511
Standard Deviation (m)	1.21	
Min (m)	0.00	
Max (m)	9.38	
Negative Residuals		
Mean (m)	-0.82	39264
Standard Deviation (m)	0.74	
Max (m)	-7.39	
Min (m)	0.00	
Overall Residuals		
Overall Mean (m)	0.06	69775
Standard Deviation (m)	1.39	
Median (m)	-0.17	
Mean Absolute Error (m)	0.98	
Sum of Squared Residuals (m^2)	1.40E+05	
Residual Range	*Percent of Total*	
Between 1 and -1 m	65.8	
Between 2 and -2 m	88.6	
Between 3 and -3 m	95.4	
Between 4 and -4 m	97.7	
Between 5 and -5 m	98.9	
Greater than 5 or less than -5 m	1.1	

Because the head observations used in the ACM-2 inverse calibration contained significant revisions from those used in ACM-1d[(a)] (see discussion in Section 2.2.4), a direct comparison of UCODE-generated residual error statistics for the ACM-2 inverse relative to previous inverse efforts was not possible. However, differences in model performance in the two ACMs were evaluated by computing statistics on residuals for only those 54,694 observations that were common to both ACM-2 and ACM-1d. Table 4.2 provides a tabular comparison of summary residual statistics. Summary statistics generally indicate an improvement in model fit for ACM-2 relative to ACM-1d. The sum of squared residuals for ACM-2 was 1.08×10^5, a 9-percent reduction from the sum of squared residuals for the ACM-1d inverse model, which was 1.19×10^5.

In addition to the overall increase in the goodness of fit for ACM-2 relative to ACM-1, there are inherent advantages associated with moving the Hanford groundwater model to a more technically defensible, hydrogeologically-based conceptual model and eliminating the past reliance on a questionable transmissivity distribution developed during early two-dimensional, steady-state inverse calibration efforts. The ACM-2 model represents the first attempt to fully incorporate the facies-based approach for representing the hydrogeologic structure of the model, and it is expected that further refinement of this distribution and additional improvements to overall model fit will be realized during future inverse simulations of groundwater flow and transport.

The predicted water table elevation contours for ACM-2 is presented for 1943 and in five-year increments from 1950 to 2000 in a series of plots found in the appendix (Figures A.1a through A.1l). The appendix also contains color-coded plots illustrating how the spatial distribution of measurements, their location, and the associated head residuals vary in 5-year increments from 1950 to 2000 (Figures A.2a through A.2k). Negative residuals indicate locations where the model under-predicted head, while positive residuals indicate locations where the model over-predicted head. In addition, the appendix shows scattergrams of simulated versus measured heads for the same times for which water table elevation contours and spatial distributions of residuals are shown (Figures A.3a through A.3l). It should be noted that the first plot (A.3a) contains results from the entire simulation period (i.e., 1943 through 2000). The scattergrams contrast the scatter of residual error points with a 45-degree line that would represent a perfect match between model and data. The individual plotted points are also color-coded to indicate the magnitude of the residual error.

Although some residual groupings are apparent in the residual distribution plots at the various times presented (Figures A.2a through A.2k), there are no clear spatial trends over the full length of the simulation period that would indicate that a better fit should be attainable using the current conceptual model. In most cases, the largest residual errors occur near the river and in the vicinity of the 200 Area disposal sites where the groundwater mound was created and where the largest changes in head were subsequently observed over the simulated period. These residual distributions will be used to guide additional modifications to the geologic structure and facies based zonation and development of alternative conceptual models during future inverse calibration efforts.

(a) ACM-1 was the generic term for the previous inverse effort. During that effort, several different variations of the model were investigated that were referred to by the a-e designators. The final best-estimate case was ACM-1d.

Table 4.2. Comparison of Residual Error Statistics for Observations Common to ACM-1d and ACM-2 Inverse Models

Residual Statistic	ACM-1d	ACM-2
Positive Residuals		
Mean (m)	1.18	1.23
Standard Deviation (m)	1.31	1.21
Min (m)	0	0
Max (m)	10.21	9.37
Negative Residuals		
Mean (m)	-0.89	-0.79
Standard Deviation (m)	0.79	0.73
Min (m)	0	0
Max (m)	-5.51	-7.4
Overall Residuals		
Mean (m)	0.03	-0.12
Standard Deviation (m)	1.47	1.4
Median (m)	-0.13	-0.12
Mean Absolute Error (m)	1.02	0.99
Sum of Squared Residuals (m2)	1.19E+05	1.08E+05
Residual Range	*Percent of Total*	*Percent of Total*
Between 1 and -1 m	64.65	65.39
Between 2 and -2 m	86.95	88.52
Between 3 and -3 m	94.38	95.47
Between 4 and -4 m	97.27	97.62
Between 5 and -5 m	99.07	98.92
Greater than 5 or less than -5 m	0.93	1.08

In general, the ability of the ACM-2 model to match head observations across the Hanford Site for the full calibration period from 1943 to 2000 (i.e., during Hanford Site operations) was similar to or better than that for the ACM-1d inverse model. However, as discussed, the most noteworthy improvements in the ACM-2 transient inverse calibrated model are not associated with overall model fit but with the incorporation of a more complex conceptual model that uses facies-based hydrogeologic zonation of the most significant permeable units (Units 1 and 5) to build the model structure and provide a more technically defensible model.

4.2.2 Hydraulic Conductivities

The hydraulic conductivity distribution from ACM-2 is presented in Figure 4.3a, along with the hydraulic conductivity distribution from ACM-1d (Figure 4.3b), to illustrate the changes in properties resulting from the ACM-2 transient inverse calibration. The presented hydraulic conductivity distributions are based on the conductivity of materials present at the water table for the maximum water table elevation observed across the site over the full calibration period. Cross-sectional plots of the ACM-2 model based on the transects indicated in Figure 4.3 are shown in Figure 4.4 and 4.5 for the A and B

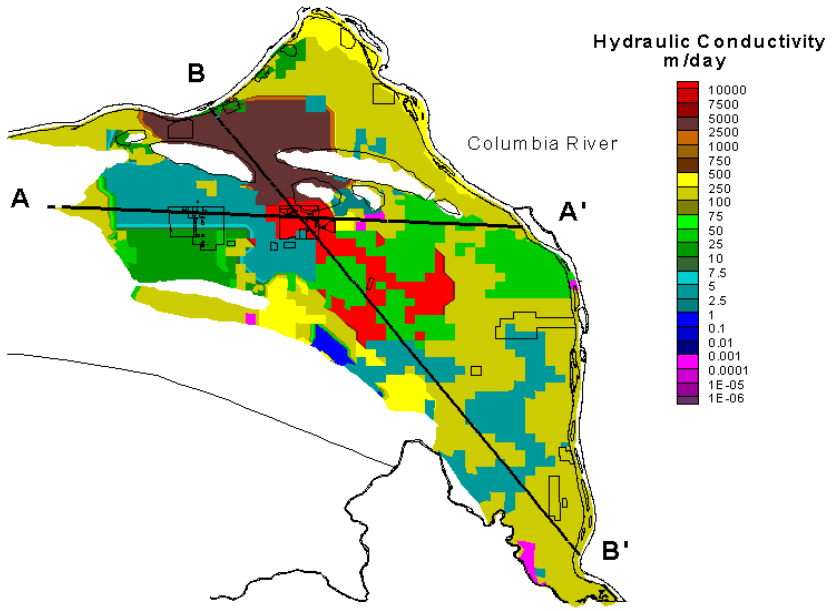

(a)

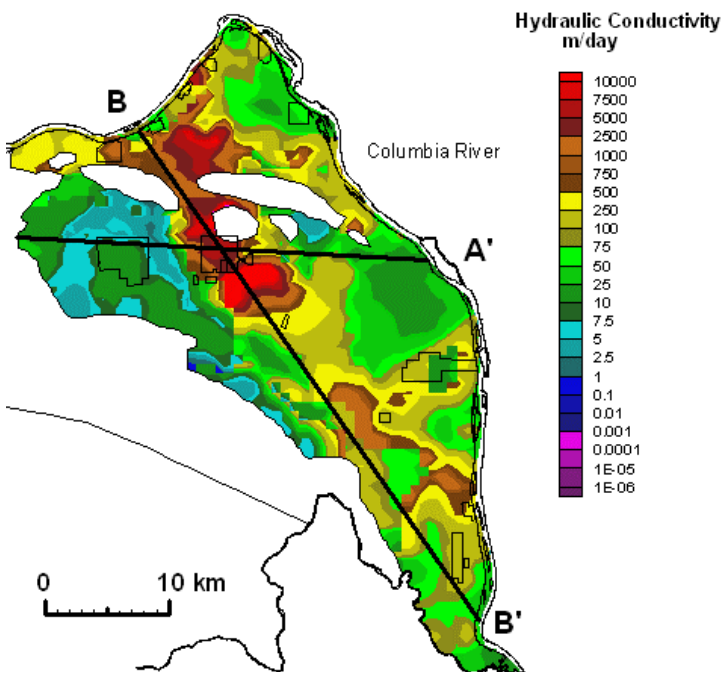

(b)

Figure 4.3. Hydraulic Conductivity Distribution for Best-Fit ACM-2 (a) and ACM-1d (b) Inverse Models

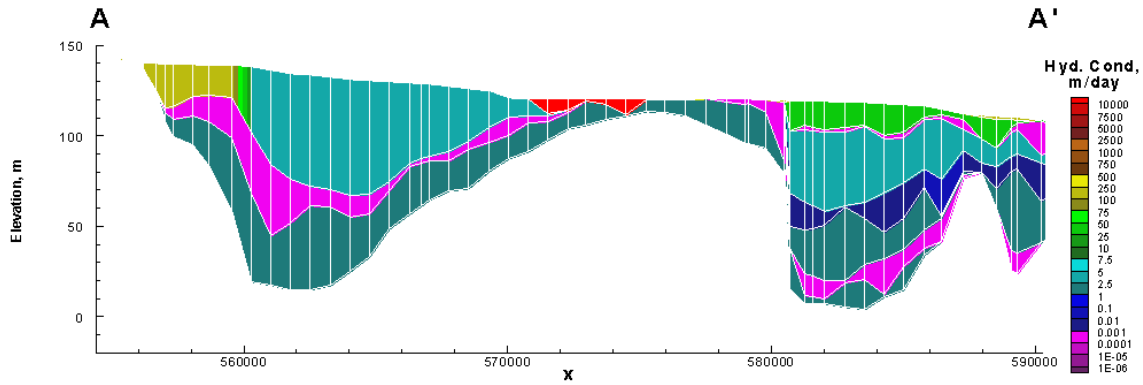

Figure 4.4. Cross-Section A-A' Showing Distribution of Hydraulic Conductivity for Best-Fit ACM-2 Model

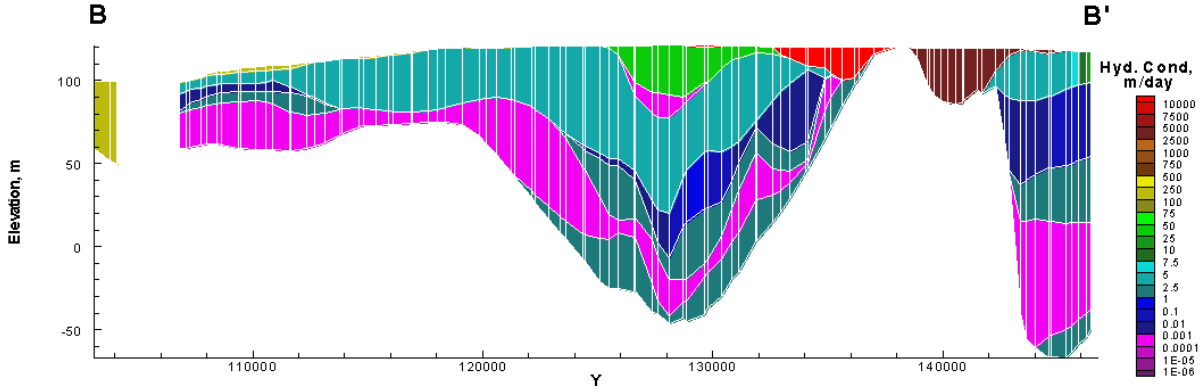

Figure 4.5. Cross-Section B-B' Showing Distribution of Hydraulic Conductivity for Best-Fit ACM-2 Model

transects, respectively. The most notable changes from the ACM-1d to the ACM-2 inverse model are associated with the incorporation of facies-based zonation of hydraulic conductivity for the Hanford and Ringold formations (see Section 3.2.6). The smoother conductivity distribution indicated for the ACM-1d model is related to the smoothed transmissivity distribution that was developed during early two-dimensional inverse calibration efforts.

The best-fit estimates for the hydraulic conductivity of the various facies-based zones composing the Hanford formation (Unit 1) were in general well within the reasonable range of previous estimates. Previous work summarized in Thorne and Newcomer (1992) and Wurstner et al. (1995) indicate that the hydraulic conductivity of Unit 1 generally ranges from about 1 to 1,000,000 m/d and is much higher than any of the other units that make up the unconfined aquifer system. Aquifer tests indicate that the minimum estimated hydraulic conductivity is about 1 m/d (Thorne et al. 1993), and the maximum estimated value is about 10,000 m/d (Thorne and Newcomer 1992; DOE 1988). However, the maximum hydraulic conductivity that can be estimated by an aquifer test is limited by the well efficiency and the flow rate that can be pumped with available equipment. Past calibration efforts by Wurstner et al. (1995) and Cole et al. (1997) have estimated that an upper limit of hydraulic conductivity for coarse-gravel flood deposits found in the central part of the Hanford Site is on the order of several tens of thousands of m/d.

Hydraulic conductivity estimates for the various Hanford formation zones obtained from the ACM-2 inverse calibration effort were consistent with results from these past calibration efforts. The highest-conductivity materials were within the coarse-grained sediments present in the eastern portion of the 200 East Area and in the gap between Gable Mountain and Gable Butte. The hydraulic conductivity of these materials was estimated to range from 4,400 to 37,000 m/d. The estimated value of hydraulic conductivity for the predominant gravel facies of the Hanford formation was 190 m/d, while the estimated value of hydraulic conductivity for the less extensive clean sand facies of the Hanford formation was 260 m/d. The estimated value of hydraulic conductivity for the Cold Creek gravels (Unit 3) was 32 m/d.

The best-fit estimates for the hydraulic conductivity of the various facies-based zones composing the Ringold Formation (Unit 5 only) were in general well within the reasonable range of previous estimates for this unit. The Ringold Formation consists of sand to muddy sandy gravel with varying degrees of consolidation or cementation. Unit 5 is the most widespread unit within the unconfined aquifer and is found below the water table across most of the model region. According to Wurstner et al. (1995), hydraulic conductivities of Units 5, 7, and 9 determined from aquifer tests vary within the range of about 0.1 to 200 m/d. Hydraulic conductivity estimates for the various Unit 5 zones obtained from the ACM-2 inverse calibration effort were generally consistent with results from past calibration efforts. The estimated value of hydraulic conductivity for the predominant facies of Ringold Unit 5, which is present across much of the 200 Area plateau, was 3.0 m/d. The estimated value of hydraulic conductivity for a more permeable facies present in the southwest portion of the 200 Area plateau and throughout the 100 Areas was 10 m/d. The highest-conductivity materials within the Ringold formation were associated with facies dominated by alluvial fan deposits along the western edge of the Pasco Basin, within the Cold Creek and Dry Creek recharge areas. The estimated value of hydraulic conductivity for these facies ranged from 110 to 390 m/d.

4.2.3 Storage Properties

According to Wurstner et al. (1995) and Thorne and Newcomer (1992), specific yield for the Hanford formation (Unit 1) is estimated to range from about 0.1 to 0.3 and is expected to be higher for coarse, well-sorted gravel than for poorly sorted mixtures of sand and gravel. From previous work (Wurstner et al. 1995; Thorne and Newcomer 1992), specific yields of the poorly sorted sediments of the Ringold Formation are estimated to range from 0.05 to 0.2. Based on these estimated ranges, the specific yield values used in the ACM-2 inverse were initially set to 0.10 for the Ringold Unit 5 and Cold Creek gravel formations and 0.25 for the Hanford Formation.

As indicated in Section 4.1, the ACM-2 inverse was generally insensitive to all tested specific yield parameter values. Initially, the specific yield of all conductive units containing the water table (Units 1, 3, and 5), and the facies-based zones contained within these units, were tested to determine whether they could be estimated. This analysis indicated that the sensitivity of the head solution to the various specific yield values ranged from highly insensitive to marginally sensitive. The cases of marginal sensitivity occurred in several facies of the Hanford and Ringold formations across the 200 Area plateau, where the effects of the groundwater mound predominate. These parameters were marginally sensitive for a limited time during the inverse process but became insensitive as the inverse progressed. Although the adjustments made to these parameter values based on results from the first few iterations of the inverse were relatively small (i.e., <10%), they were used to adjust the assumed values for these parameters and, in

keeping with the previously discussed approach for handling insensitive parameters, these parameters were held at the adjusted values during subsequent inverse simulations.

4.2.4 Boundary Flux Estimates

The ACM-2 transient inverse model contains several important flow-system boundaries illustrated in Figure 3.6. The flow system is bounded by the Columbia River on the north and east and by the Yakima River and basalt ridges on the south and west, respectively. The Columbia River is assumed to represent a point of regional discharge for the unconfined aquifer system. In addition to this discharge boundary, ACM-2 incorporates several other flux boundaries, the majority of which are recharge boundaries but in some cases also included small components of discharge. Other sources of flux included basalt leakage (both areally distributed and increased leakage at faults and erosional features), natural surface recharge, run-on recharge from upland areas along the western model boundary, and artificial recharge associated with wastewater disposal activities from Hanford operations. Following is a discussion of the various boundary fluxes that were estimated during the ACM-2 inverse calibration effort.

4.2.5 Natural Recharge

As indicated in Section 4.1, the head solution based on ACM-2 was insensitive to areally distributed surface recharge so this parameter could not be estimated. In keeping with the previously discussed approach for handling insensitive parameters, surface recharge was set to the pre-inverse assumed value (see distribution in Figure 3.13) and removed from the list of parameters to be estimated. Although the head solution was insensitive to surface recharge, the parameter sensitivity analysis indicated that run-on recharge from Cold Creek, Dry Creek, and Rattlesnake Springs could be estimated.

One of the primary modifications made to ACM-2 relative to previous inverse calibration efforts was implementing run-on recharge from upland areas along the western model boundary. This initial implementation of run-on recharge at the Cold Creek and Dry Creek valleys and at the base of Rattlesnake Hills was based on a distributed-parameter hydrologic model (i.e., a watershed model). Results from this analysis, which are summarized in Table 3.2, were used as initial conditions for the ACM-2 inverse. Although preliminary, these results were expected to provide an order-of-magnitude estimate for recharge at these locations. A sensitivity analysis of these run-on recharge parameters indicated that the head solution was sensitive to adjustment of these parameters and subsequently that the inverse could estimate the parameters and provide an independently calculated value that then could be compared with results from the watershed model. Based on results from the ACM-2 inverse calibration, the estimated value of recharge flux at Cold Creek Valley was 32,100 m^3/d, which is a factor of 3.9 higher than the initial estimate. The estimated value of recharge flux at Dry Creek Valley was 19,500 m^3/d, which is a factor of 1.2 higher than the initial estimate, and the estimated recharge flux for Rattlesnake Springs was 2,800 m^3/d, which is a factor of 2.8 lower than the initial estimate. The total run-on recharge is estimated to be 54,400 m^3/d, which is approximately 2.3 times the total surface recharge (23,500 m^3/d). These run-on recharge estimates obtained from the ACM-2 transient inverse calibration effort will be used to improve and refine implementation of the watershed model. Task activities are ongoing.

4.2.6 Basalt Intercommunication

As discussed in Section 3.2.4, there were several components of basalt leakage that were considered in the full implementation of ACM-2, including areally distributed leakage and increased leakage at the erosional window between Gable Mountain and Gable Butte and along fault zones. Figures 4.6 and 4.7 show the simulated distribution of areally distributed basalt leakage over the model domain in 1960 and 1996, respectively. The basalt leakage distributions shown provide an example of representative leakage fluxes for the range of groundwater mounding conditions observed over the simulated period. The observed leakage distribution across the site was consistent with the expected response, with downward leakage occurring throughout the area affected by the groundwater mound from 200 Area wastewater disposal activities and upward leakage occurring throughout the eastern portion of the site.

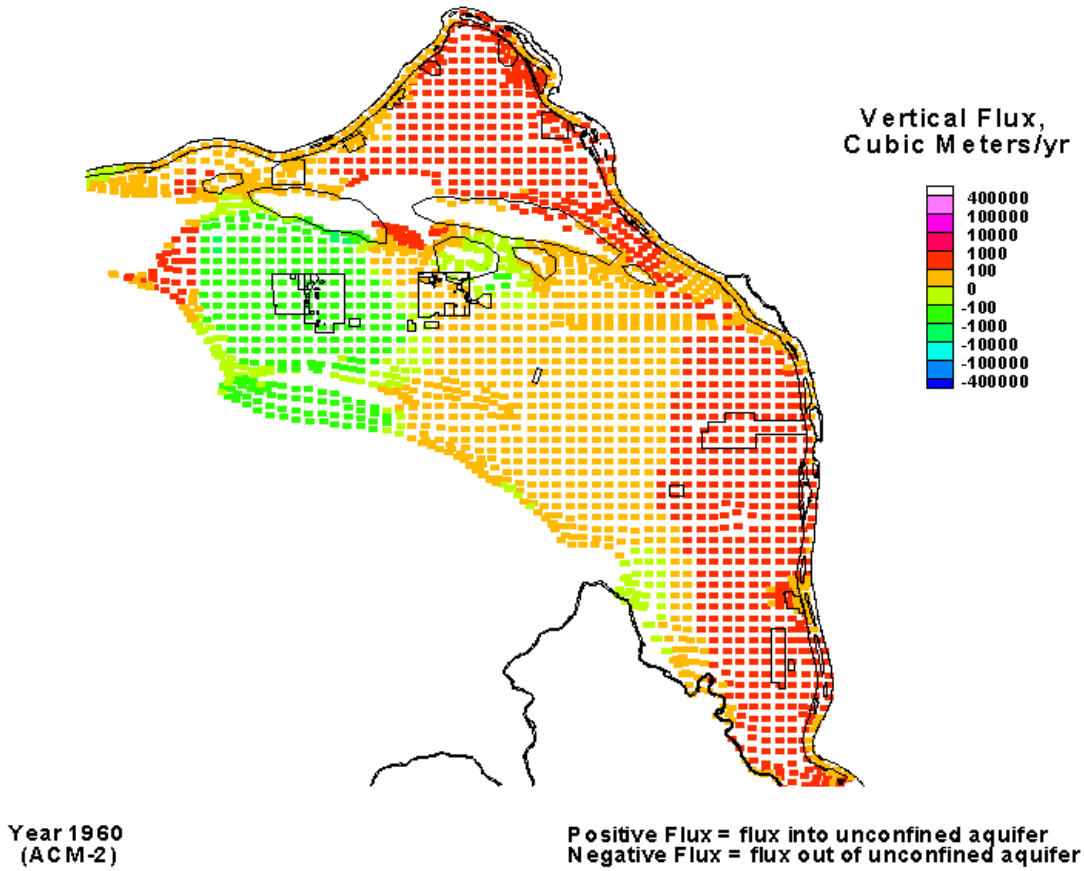

Figure 4.6. Simulated Basalt Leakage in 1960

Although Figures 4.6 and 4.7 do show the general distribution of basalt leakage across the Site, a closer inspection of flux results is needed to show the relative contribution of flux from each feature affecting basalt leakage that was considered in ACM-2. Figure 4.8 shows the areally distributed upward leakage, downward leakage, and net leakage flux over the period of simulation. Areally distributed leakage flux is calculated as the summation of flux across the basalt confining layer at all nodal locations outside the

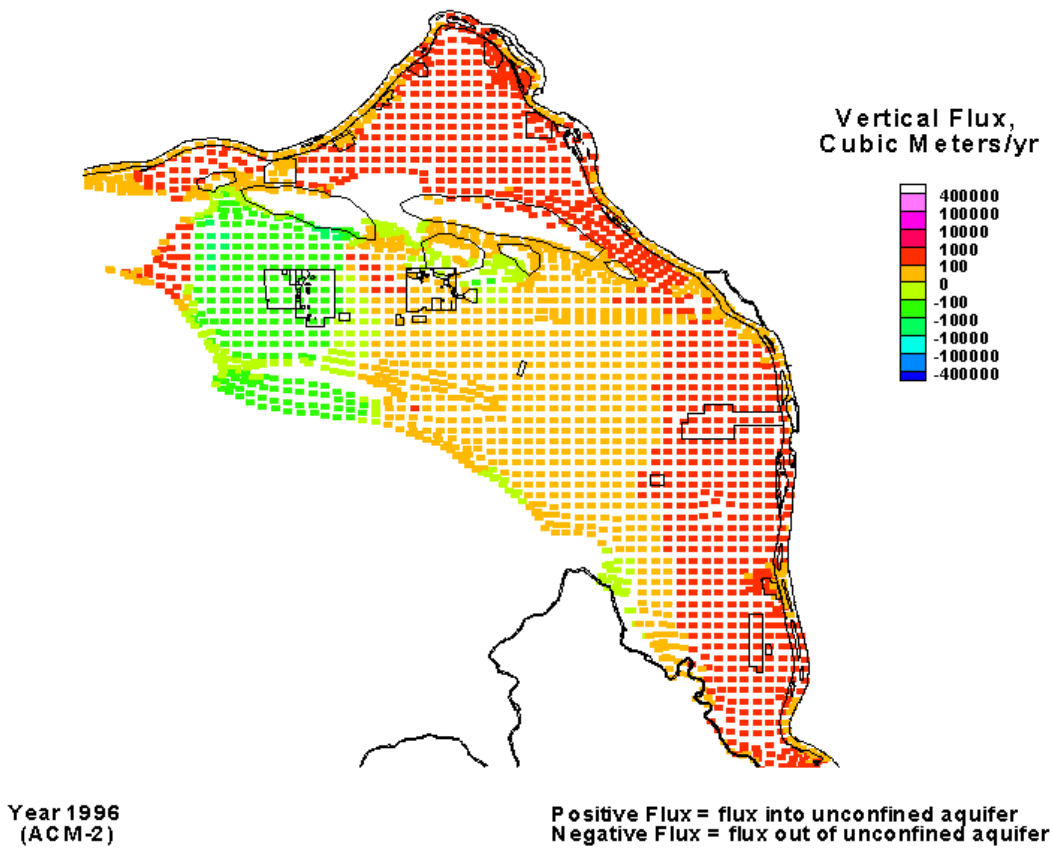

Figure 4.7. Simulated Basalt Leakage in 1996

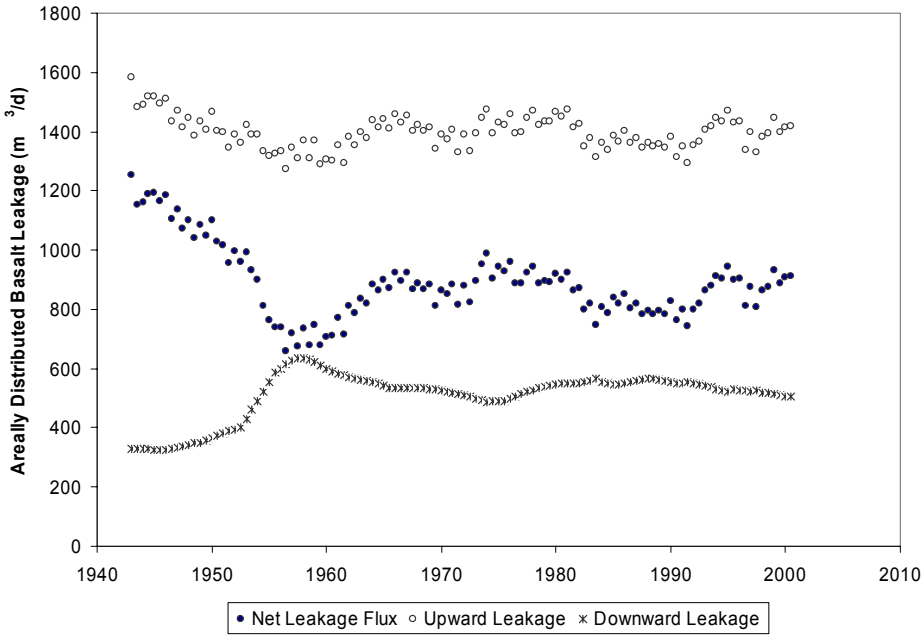

Figure 4.8. Areally Distributed Basalt Leakage Flux over the Simulated Period

zones of increased leakage associated with faults and erosional features. As indicated, both the upward and downward leakage curves contain temporal variability that is primarily associated with wastewater disposal activities in the 200 Areas. The temporal variability of the net leakage flux (upward minus downward leakage) is increased because it contains the variability in both data sets.

Figure 4.9 shows the relative contribution to net leakage flux for each of the basalt features considered in ACM-2, including areally distributed leakage and increased localized leakage at the erosional window and the Yakima Ridge, Gable Mountain, and Cold Creek thrust faults. Leakage flux estimates for ACM-2 are presented in this figure and summarized in Table 4.3. They indicate that areally distributed leakage is the dominant mechanism (890 m^3/d), with leakage flux from the Cold Creek and

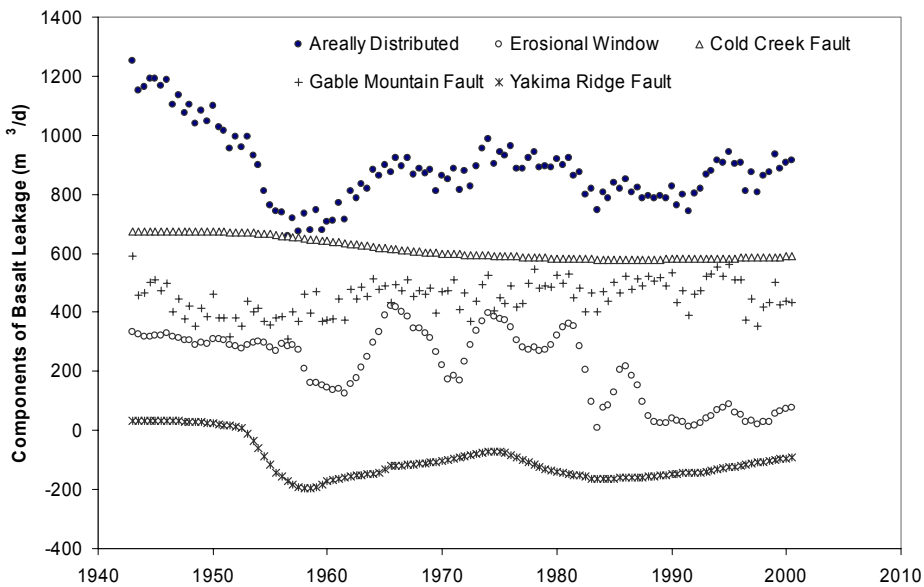

Figure 4.9. Relative Contribution of Each Basalt Leakage Feature to Net Leakage Flux

Table 4.3. Summary of Relative Contribution from Various Boundary Fluxes Included in ACM-2. Reported values represent the time-weighted average over the simulated period.

Model Boundary	Boundary Flux (m^3/d)
Discharge boundaries:	
Columbia River	86,600
Recharge Boundaries:	
Areally Distributed Basalt Leakage	890
Leakage at Erosional Window	220
Leakage at Thrust Faults	970
Natural Surface Recharge	23,500
Run-on Recharge from Upland Areas	54,400
Artificial Recharge	64,600

Gable Mountain faults contributing to a lesser extent (610 m^3/d and 450 m^3/d, respectively) and the erosional window contributing even less (220 m^3/d). Figure 4.9 also shows that, once the effect of the rising groundwater mound in the 200 Area reaches the Yakima Ridge fault in the early 1950s, the fault section acts as a discharge boundary, allowing relatively small amounts of localized downward leakage (100 m^3/d). Based on these data, the time-weighted average total basalt leakage flux contributing to recharge of the unconfined aquifer is 2,080 m^3/d, or approximately 9 percent of the flux associated with natural surface recharge. Table 4.3 shows the time-weighted average artificial recharge from Hanford operations for comparison.

The simulated leakage reversal at the erosional window that was observed in the ACM-1 inverse model and predicted based on model design analysis (Vermeul et al. 2001) was not simulated using the ACM-2 model. This difference is likely associated with the high hydraulic conductivity estimates obtained by the ACM-2 inverse for the coarse-grained sediments near the erosional window. This relatively high value of hydraulic conductivity may not allow heads to build up in the unconfined aquifer even during peak discharge times, and a subsequent leakage reversal would not be observed. The observed change in leakage response may indicate that the current conceptual model does not represent actual conditions through the gap and that further refinement of the model in this area is required.

4.3 Evaluation of Transient Inverse Model

This section provides an evaluation of the transient inverse calibration of ACM-2 using data for the historical period of Hanford operations (1943–2000). In this section the regression results, model fit, and optimized parameter values are evaluated by examining various regression and statistical performance measures provided by UCODE (Poeter and Hill 1998). This evaluation will follow the guidelines for effective model calibration (Hill 1998) and the checklist provided as part of the UCODE distribution documentation. This section includes discussions of 1) regression measures, 2) evaluation of model fit, and 3) evaluation of optimized parameter values.

The description of and abbreviated notation used for the 17 parameters investigated during this inverse calibration effort are listed in Table 4.4. In the following text and tables, a reference to a composite scaled sensitivity coefficient for a parameter will be written as *Css(parameter)*, e.g., *Css(K-HS)*.

4.3.1 Evaluation of Regression Measures

In addition to the obvious failure-to-converge measure, UCODE provides information to evaluate whether the regression is well posed. This includes

- The *Marquardt Parameter*, which is nonzero when the regression problem is ill-conditioned.
- The *Parameter That Changed the Most*, because the parameter for which the maximum fractional change occurs is likely to be at least a contributing problem when the regression does not converge.
- The *Amount of Change*, the magnitude of change.

Another measure is when the number of "parameter estimate iterations" needed to converge exceeds the "on average" estimate given in Hill (1998) as approximately equal to twice the number of parameters (NP) being estimated (i.e., 2 NP).

Based on the sensitivity analysis of the 43 parameters investigated for the full implementation of ACM-2, scaled sensitivity coefficient results indicated that 17 of the parameters were determinable. Convergence was generally well behaved, and all the regression measures for the transient inverse calibration of ACM-2 indicated that it was generally a well-posed problem. The eight iterations for convergence were significantly less than the "on average" estimate of 34 (i.e., 2*NP where NP=17), and the Marquardt parameter was zero for every iteration in the regression. Table 4.5 illustrates the numerical values for the parameter estimates and regression measures as a function of parameter estimate iteration (i). The composite scaled sensitivity coefficient ratio for the parameter with the smallest composite scaled sensitivity coefficient (Max/Min Composite Scaled Sensitivity Ratio) is also shown in Table 4.5 and calculated as Css(Maximum)/Css(Minimum). This ratio should always be less than ~100 for all the parameters estimated, and for the ACM-2 inverse run reached a maximum value of only 27.5, demonstrating that all estimated parameters retained sufficient sensitivity through all iterations.

Table 4.4. Notation for and Descriptions of the 17 Parameters Estimated in the Inverse Calibration

Parameter Number	Abbreviated Notation	Parameter Description
1	K-HG1	Hydraulic conductivity – Hanford Gravel Zone 1
2	K-HBP	Hydraulic conductivity – Hanford B-Pond Zone
3	K-HG2	Hydraulic conductivity – Hanford Gravel Zone 2
4	K-HG3	Hydraulic conductivity – Hanford Gravel Zone 3
5	K-HS	Hydraulic conductivity – Hanford Sand Zone
6	K-RE	Hydraulic conductivity – Middle Ringold Unit E
7	K-RRH	Hydraulic conductivity – Ringold River Zone / Ringold High Zone
8	K-RCC	Hydraulic conductivity – Ringold Cold Creek / Upper Dry Creek Zones
9	K-RMD	Hydraulic conductivity – Ringold Middle Dry Creek Zone
10	K-RLD	Hydraulic conductivity – Ringold Lower Dry Creek Zone
11	K-CCU	Hydraulic conductivity – Cold Creek Unit
12	K-RLM	Hydraulic conductivity – Ringold Lower Mud Sequence
13	K-BAS	Hydraulic conductivity – Columbia River Basalt
14	F-CCF	Cold Creek Fault Flux
15	R-RH	Run-On Recharge – Rattlesnake Springs
16	R-CC	Run-On Recharge – Cold Creek
17	R-DC	Run-On Recharge – Dry Creek

Table 4.5. Parameter Estimates and Regression Measures as a Function of Parameter Estimate Iteration (i). For an explanation of variable abbreviations, see Table 4.4.

i	K-HG1 (m/d)	K-HBP (m/d)	K-HG2 (m/d)	K-HG3 (m/d)	K-HS (m/d)	K-RE (m/d)	K-RRH (m/d)	K-RCC (m/d)	K-RMD (m/d)	K-RLD (m/d)	K-CCU (m/d)	K-RLM (m/d)	K-BAS (m/d)	F-CCF[(a)]	R-RH[(a)]	R-CC[(a)]	R-DC[(a)]	Sum Sq. Wt. Residuals	Max/Min CSS Ratio
0	500	500	8000	4000	500	2	8	100	100	100	350	1.0E-04	1.0E-05	0.50	269	24	915	3.32E+08	--
1	475	494	8060	3910	444	2.1	8.2	104	107	112	328	1.0E-04	1.3E-05	0.41	271	46	957	2.99E+08	25.8
2	289	555	7950	3770	556	2.52	8.77	117	133	158	302	1.2E-04	2.0E-05	0.24	263	87	1100	2.01E+08	25.3
3	151	410	11300	5970	351	3.26	13.8	49.3	73.7	163	50.4	1.6E-04	2.2E-05	0.06	120	130	495	8.93E+07	27.5
4	185	442	13800	3730	193	2.96	11.1	63.7	96.6	271	31.0	1.8E-04	2.6E-05	0.04	145	110	629	6.66E+07	20.6
5	155	471	16900	4210	302	2.96	10.8	77.9	118	365	29.1	2.5E-04	1.5E-05	0.06	107	86	803	6.57E+07	15.9
6	184	471	27800	3980	283	3.01	10.5	92.5	144	332	34.4	2.0E-04	2.0E-05	0.05	107	96	962	6.55E+07	21.4
7	167	466	19500	4910	320	2.96	10.7	100	148	479	27.2	2.3E-04	1.6E-05	0.06	82.8	88	1040	6.56E+07	21.2
8	192	462	37100	4400	256	2.97	10.4	109	167	391	32.3	2.0E-04	1.4E-05	0.05	98.3	90	1130	6.50E+07	14.3

*Scaling Factor.

4.3.2 Evaluation of Model Fit

Section 4.2.1 indicates that in general the regression was well-posed and converged. This solution is thus the best fit for the problem posed. However, the quality of the model fit (e.g., how well it matches observations) must still be evaluated. In the rest of this section, the various statistical measures for evaluating model fit and residual statistics provided as part of the UCODE distribution are presented and discussed to evaluate the results of the regression. The following are statistics on the residuals from the converged regression printed by UCODE:

Statistics on Residuals:

Sum of Squared Weighted Residuals	0.65228E+08		
Sum of Squared Weighted Residuals (with prior)	0.65228E+08		
Maximum Weighted Residual:	0.558E+03	Obs#	9109 H09109
Minimum Weighted Residual:	-0.364E+03	Obs#	38095 H38095
Average Weighted Residual:	0.111E+00		
# Residuals > = 0:	30511.0		
# Residuals < 0:	39264.0		
Number of Runs:	9850.0 in 69,775 observations.		

Interpreting the calculated runs statistic value of -188.0
Note: The following applies only if
Residuals >= 0. is >10
Residuals < 0. is >10
The negative value may indicate too few runs:
If the value is <-1.28, there is <10% chance the values are random
If the value is <-1.645, there is <5% chance the values are random
If the value is <-1.96, there is <2.5% chance the values are random.

With nearly 70,000 observations, it is impractical to present tables of observations, simulated values, residuals (calculated as the observations minus the simulated values), and weighted residuals. The maximum and minimum weighted residual indicates where the worst fit occurs relative to the expected fit and often reveals gross errors that can be identified and corrected. An average weighted residual near zero is needed for an unbiased model fit (usually satisfied if regression converges). The average weighted residual of 0.111 for ACM-2 was an improvement over ACM-1d, which had an average weighted residual of 0.197. Hill (1998) indicates that, if weights reflect the measurement errors, weighted residuals larger than 1.0 on average indicate that the model is worse than would be expected given anticipated measurement error, and values smaller than 1.0 indicate that the model fits better than expected given anticipated measurement error. However, because in this case additional weighting factors were applied to account for spatial and temporal clustering of data, the average weighted residual value (here being significantly less than 1.0) is not easily interpreted.

The number of positive and negative residuals indicates whether the model fit is consistently low or high. Preferably, the two values are about equal. The numbers, 39,264 negative and 30,511 positive, are fairly evenly balanced but slightly biased toward negative residuals, as better illustrated in the histogram in Figure 4.2. This figure provides more information about the distribution of residuals and indicates that

the mode of the distribution is approximately –0.7, a slight negative bias. The tails of the distribution are skewed on the positive side and thus not normally distributed. The number of test runs provides a statistic to help identify trends in spatially distributed weighted residuals because identifying trends (lack of non-randomness) by visual inspection is not always reliable. Too few or too many runs could indicate model bias. The number of runs, the runs' statistical value, and the means to interpret are printed by UCODE (see above). For this regression the run statistic indicates too few runs, and the calculated statistic indicates that there is a very small (much less than 2.5 percent) chance the values are random. This suggests that there may be some systematic spatial and/or temporal pattern in the residuals that reflects possible model error. However, personal communication with Eileen Poeter indicates there may be a problem with this statistic related to the way the observations are ordered in our input file, because in UCODE the weighted residuals are analyzed using the sequence in which the observations are listed in the input file. Hill (1998) goes on to say that the runs test is included because it takes the order of the residuals into account, which is ignored in all the other summary statistics. If observations are grouped by location in transient simulations, too few runs commonly indicate positive serial correlation between residuals at individual locations. The effect of input observation ordering on the runs test will need to be investigated. The following statistical information from UCODE provides additional data about the model fit:

Least-squares objective function	
(dependent variable only)	0.65228E+08
(w/parameters)	0.65228E+08
Calculated error variance	935.07
Standard error of the regression	30.579
Correlation coefficient	0.99991
Correlation coefficient (w/parameters)	0.99991
Maximum likelihood objective function	0.65172E+08
AIC statistic	0.65172E+08
BIC statistic	0.65172E+08
Hannan statistic (Hannan 1980)	0.65172E+08

The weighted least-squares objective function value of 0.65228×10^8 is the same with and without parameters because no prior information was used. Given randomly distributed residuals and the same observations and weight matrix, a lower value of the least-squares objective function indicates a closer model fit to the data. This value is smaller than the baseline inverse model's weighted least squares objective function value of 0.71381e+08 but larger than that of ACM-1d (0.57724e+08). However, because of differences in weightings and observations between ACM-1d and ACM-2, the results are not directly comparable. As shown in Table 4.2, when comparing the same set of residuals, the sum of squared residuals is smaller for ACM-2 than for ACM-1d, indicating better overall fit.

Smaller values of the calculated error variance for randomly distributed residuals are desirable. Normally, values less than 1.0 indicate that the model fits the data better than the variances used to weight the observations and prior information; values greater than 1.0 indicate that the fit is worse. However, a non-standard weighting was used to account for spatial and temporal clustering of data, so the calculated error variance cannot be interpreted directly. The standard error of the regression is the square root of the calculated error variance, and the same comments apply. The correlation coefficient with and without prior information is the correlation between weighted observed or prior information and simulated values. Correlation coefficient values below ~0.9 indicate poor model fit. The value of 0.99991 for the current

regression indicates a very good fit and is similar to the corresponding statistic for ACM-1d. The maximum likelihood objective function, the AIC, and BIC statistics for randomly distributed residuals can be used to compare one model with another where a lower absolute value indicates a better fitting model. The AIC (Akaike Information Criterion) (Akaike 1974) and BIC (Bayesian Information Criterion (Schwartz 1978) are information-based measures of model goodness-of-fit that incorporate measures of model parsimony. Simpler models (with fewer parameters relative to the number of data) are favored over more complex models given comparable residual statistics.

Another measure of model fit provided by UCODE uses ordered weighted residuals, which are the weighted residuals ordered smallest to largest. UCODE provides the correlation between ordered weighted residuals and normal order statistics. $R_N^{\ 2}$ values above the critical value printed by UCODE below indicate independent, normal weighted residuals. The value of 0.612 for this regression indicates the residuals are not independent normal weighted residuals:

Correlation Between Ordered Weighted Residuals and Normal Order Statistics = 612 [calculated using Eq. 38 of Hill (1992) or Eq. 23 of Hill (1998)]

Comments on Interpretation of the Correlation Between Weighted Residuals and Normal Order Statistics:

Generally, if the reported correlation is greater than the critical value, at the selected significance level (usually 5 or 10%), the hypothesis that the weighted residuals are independent and normally distributed would be accepted. However, in this case, conditions are outside the range of published critical values, as discussed below.

The sum of the number of observations and prior information items is 69,775, which is greater than 200, the maximum value for which critical values are published. Therefore, the critical values for the 5 and 10% significance levels are greater than 0.987 and 0.989, respectively. Correlations greater than these critical values suggest that probably the weighted residuals are independent and normally distributed. Correlations less than these critical values clearly indicate that we can reject the hypothesis. The Kolmogorov-Smirnov test can be used to further evaluate the residuals.

The validity of confidence and prediction intervals estimated for model outputs depends upon the assumption that weighted residuals are independent and normally distributed as well as upon the representativeness and linearity of the model (Poeter and Hill 1998). The non-normality of the weighted residuals suggests that confidence and prediction intervals computed using the ACM-2 model must be used with caution. Non-normality may be related to the temporal and spatial declustering scheme incorporated into the observation weights in this application, and/or could represent the effects of more fundamental error (e.g., systematic bias) in the underlying model, as is also suggested by the run length statistics (see description above). The effect of declustering weights on normality of weighted residuals requires further investigation.

In general, comparing the model fit statistics of ACM-1d and ACM-2 indicates a modest improvement in model fit for the latter. The average weighted residual statistic of 0.111 and the correlation coefficient statistic of 0.99991 indicate a good overall model fit. However, the other measures looking for patterns and trends in the residuals indicate the model fit is poor, as shown by the value of the calculated error variance; the 0.612 value for the correlation between ordered weighted residuals and normal order statistics that indicates the residuals are not independent, normal weighted residuals; and the runs test statistic that indicates trends are present in the spatially distributed weighted residuals. For a good model the residuals should be random. These measures, as shown, continue to build on the baseline set of values for future reference as different conceptual models or conceptual model components are examined.

4.3.3 Evaluation of Optimized Parameter Values

Model error or fit may also be evaluated by examining the optimized parameter values to determine whether they are unrealistic and the confidence intervals on the optimized values include reasonable values. This section evaluates the optimized parameter values through discussions of estimated model parameters, parameter-correlation coefficients, and estimated confidence intervals in parameter estimates.

4.3.3.1 Estimated Model Parameter Values

The optimal values of the parameters considered in the inverse calibration were calculated based on how well they reproduced the historical measurements of water levels during the period between 1943 and 2000. The objective function evaluated by the inverse calibration for the 1943 to 2000 period is the sum of the squared weighted residuals between simulated water levels and the 69,775 water level measurements made over the calibration period. The intent of the inverse-calibration procedure is to find the optimal combinations of parameters that minimize the objective function and to examine the various statistical measures that represent the quality of the regression.

Changes in the objective function during the calibration process (Table 4.5) resulted in the optimal combination of parameters presented in Table 4.6. The baseline inverse calibration of the selected model to the 1943–1996 period resulted in an overall reduction of the objective function (the sum of the squared residuals) by about an order of magnitude from the prior model. The ACM-1 transient inverse calibration resulted in another 19 percent reduction in the objective function. The ACM-2 transient inverse calibration resulted in a further 9 percent reduction in the sum of squared residuals (based on comparison of unweighted residuals for common observation sets). The hydraulic parameters that changed most relative to the book values were the hydraulic conductivities of the Hanford gravel zone 2 (K-HG2) and the Cold Creek Unit (K-CCU). K-HG2 increased by nearly a factor of 5 from the book value of 8000 to the estimated 37,100 m/d, while K-CCU decreased by about an order of magnitude from 350 to 32.3 m/d. The Cold Creek Fault Flux scaling factor (F-CCF) decreased by one order of magnitude from its book value, but all three recharge estimates differed by less than a factor of 3 or 4 from their respective book values.

Table 4.6. Summary of Parameter Estimates Derived for the Inverse Model ACM-2

Parameter Description	Parameter Estimates
Hydraulic Conductivity Distributions Within	
Hanford Gravel Zone 1	192 m/d
Hanford B-Pond Zone	462 m/d
Hanford Gravel Zone 2	37100 m/d
Hanford Gravel Zone 3	4400 m/d
Hanford Sand Zone	256 m/d
Middle Ringold Unit E	2.97 m/d
Ringold River / Ringold High Zones	10.4 m/d
Ringold Cold Creek / Upper Dry Creek	109 m/d
Ringold Middle Dry Creek Zone	167 m/d
Ringold Lower Dry Creek Zone	391 m/d
Cold Creek Unit	32.3 m/d
Ringold Lower Mud Sequence	2.0E-4 m/d
Columbia River Basalt	1.4E-05 m/d
Basalt Leakage	
Cold Creek Fault Flux	0.05[(a)]
Boundary Flux	
Rattlesnake Springs	98.3[(a)]
Cold Creek Valley	90[(a)]
Dry Creek Valley	1130[(a)]
(a) Scaling factor. See Section 4.2.2 for actual flux values.	

4.3.3.2 Parameter-Correlation Coefficients

Part of the output of the inversing process implemented in UCODE is the correlation coefficient of each parameter estimated in the process. In UCODE, correlation coefficients are defined as the co-variance between two parameters divided by the product of their standard deviations (Hill 1998). According to Hill, correlation coefficients range from -1.0 to 1.0, with values very close to -1.0 and 1.0 indicative of parameter values that cannot be uniquely estimated with the observations used in the regression. As a diagnostic output for evaluating potential significant correlation coefficients, UCODE identifies parameter pairings with correlation coefficients between 0.85 and 0.9; 0.9 and 0.95; and greater than 0.95. Guidance in training materials for UCODE (Hill et al. 1999) and in previous work described in Hill et al. (1998) has suggested that parameter correlations in these ranges, particularly those in excess of 0.95, may be indicative of problematically strong correlations between parameter pairs. Strong correlations between two or more parameter values would bring into question the optimized estimates for the parameters in question. These parameter values would require some additional testing to assess the uniqueness of the optimized values estimated.

The correlation-coefficient matrix corresponding to the parameters estimated in the baseline transient inverse calibration is summarized in Table 4.7. This summary indicates that no strong correlation was found among the parameter values estimated in the inversing process.

Table 4.7. Parameter Cross-Correlation Matrix (ACM-2)

	K-HG1	K-HBP	K-HG2	K-HG3	K-HS	K-RE	K-RRH	K-RCC	K-RMD	K-RLD	K-CCU	K-RLM	K-BAS	F-CCF	R-RH	R-CC	R-DC
K-HG1	1	-0.03	0.24	-0.29	-0.11	0.06	-0.20	0.33	0.39	0.14	0.13	-0.08	-0.03	-0.14	0.20	0.21	0.37
K-HBP	-0.03	1	-0.02	-0.07	0.01	0.01	0.00	-0.05	-0.05	0.00	-0.02	0.08	0.00	0.03	-0.01	-0.01	-0.05
K-HG2	0.24	-0.02	1	0.10	-0.01	0.02	-0.02	0.24	0.36	-0.31	-0.07	-0.05	-0.07	-0.01	0.07	0.03	0.29
K-HG3	-0.29	-0.07	0.10	1	0.06	-0.07	0.12	0.28	0.29	0.21	-0.43	0.00	-0.05	0.11	-0.17	-0.13	0.33
K-HS	-0.11	0.01	-0.01	0.06	1	0.05	0.01	0.02	0.01	0.03	-0.09	0.01	0.09	-0.02	-0.06	0.03	0.02
K-RE	0.06	0.01	0.02	-0.07	0.05	1	-0.31	0.00	0.06	-0.17	0.03	-0.01	0.20	-0.19	0.17	0.38	0.00
K-RRH	-0.20	0.00	-0.02	0.12	0.01	-0.31	1	-0.15	-0.20	-0.01	-0.17	-0.08	0.03	-0.29	-0.07	0.37	-0.18
K-RCC	0.33	-0.05	0.24	0.28	0.02	0.00	-0.15	1	0.69	0.45	0.38	-0.03	-0.13	0.13	-0.34	-0.09	0.85
K-RMD	0.39	-0.05	0.36	0.29	0.01	0.06	-0.20	0.69	1	0.25	0.41	-0.01	-0.15	0.12	-0.28	-0.10	0.91
K-RLD	0.14	0.00	-0.31	0.21	0.03	-0.17	-0.01	0.45	0.25	1	0.20	0.05	-0.09	0.06	-0.26	-0.04	0.47
K-CCU	0.13	-0.02	-0.07	-0.43	-0.09	0.03	-0.17	0.38	0.41	0.20	1	0.02	-0.04	0.05	-0.11	-0.02	0.44
K-RLM	-0.08	0.08	-0.05	0.00	0.01	-0.01	-0.08	-0.03	-0.01	0.05	0.02	1	-0.02	0.31	-0.02	-0.06	-0.02
K-BAS	-0.03	0.00	-0.07	-0.05	0.09	0.20	0.03	-0.13	-0.15	-0.09	-0.04	-0.02	1	-0.54	-0.03	0.69	-0.13
F-CCF	-0.14	0.03	-0.01	0.11	-0.02	-0.19	-0.29	0.13	0.12	0.06	0.05	0.31	-0.54	1	-0.08	-0.84	0.12
R-RH	0.20	-0.01	0.07	-0.17	-0.06	0.17	-0.07	-0.34	-0.28	-0.26	-0.11	-0.02	-0.03	-0.08	1	0.09	-0.45
R-CC	0.21	-0.01	0.03	-0.13	0.03	0.38	0.37	-0.09	-0.10	-0.04	-0.02	-0.06	0.69	-0.84	0	1	-0.09
R-DC	0.37	-0.05	0.29	0.33	0.02	0.00	-0.18	0.85	0.91	0.47	0.44	-0.02	-0.13	0.12	0	-0.09	1

4.3.3.3 Confidence Intervals on Estimated Parameters

Another important output of the inversing process using UCODE is the calculation of confidence intervals around final parameter estimates. Technically, the confidence interval around a parameter estimate is a range that has a stated probability of containing the true value of the parameter. Narrow confidence intervals around a parameter estimate are a general indication or measure of precision in the parameter estimate, given the types of observations used in the regression analysis. Narrow intervals imply greater precision; large intervals indicate less confidence in the optimized parameter value. A summary of 95 percent confidence intervals and the estimated value for each parameter considered in the inverse analysis is summarized in Table 4.8. Calculated confidence intervals around all of the parameters exhibited a relatively narrow range, suggesting a good level of precision in the final parameter estimates.

Table 4.8. Parameter Scaling Factor Estimates and Associated Confidence Intervals (ACM-2)

Parameter	Lower 95% CI	Best Estimate	Upper 95% CI
K-HG1	187	192	198
K-HBP	448	462	477
K-HG2	34000	37100	40400
K-HG3	4290	4400	4510
K-HS	233	256	282
K-RE	2.94	2.97	3.01
K-RRH	10.20	10.40	10.60
K-RCC	104.0	109.0	113.0
K-RMD	161.0	167.0	174.0
K-RLD	369.0	391.0	414.0
K-CCU	30.3	32.3	34.4
K-RLM	0.000175	0.000197	0.000223
K-BAS	1.11E-05	1.35E-05	1.64E-05
F-CCF	0.050	0.054	0.058
R-RH	90.3	98.3	107.0
R-CC	86.6	90.1	93.7
R-DC	1090.0	1130.0	1180.0

5.0 Generation and Inverse Modeling of Stochastic Alternative Conceptual Models

Geostatistical techniques were applied to develop alternative models of the Hanford Site geological structure. As described in previous sections, the Hanford Site geological structure consists of unconsolidated to consolidated sediment overlying the Columbia Plateau basalt. The spatial distribution of aquifer/aquitard units within the sediments is not homogeneous, and a great amount of spatial variability exists. Also, hydrogeological parameters vary spatially within aquifer units. Generally, zones with similar hydrogeological parameters can be distinguished. Geostatistical methods were developed to assess the uncertainty in the facies zonation of the Hanford formation (Unit 1) and the geological structure of Ringold mud units. The aquifer Unit 1 is characterized by the existence of five zones or facies: Hanford formation gravel type 1, Hanford formation gravel type 2, Hanford formation gravel type 3, Hanford formation sand, and Hanford formation silt. These five facies represent zones with different hydrogeological parameters. The three Ringold mud units, upper Ringold mud (U4), middle Ringold mud (U6), and lower Ringold mud (U8), alternate with sand and gravel units within the Ringold Formation. The low conductivity of the mud units significantly influences the direction of water flow.

The zonation of the five Hanford formation facies represents a multiclass classification problem. A sequential indicator simulation technique was used to derive the spatial zonation model and evaluate the uncertainty of the zonation model through multiple realizations. To develop alternative geological structures of Ringold mud units, a two-step method was used. The presence or absence of the mud units at each spatial location was first simulated as a binary variable via sequential indicator simulation. This was followed by a simulation of mud layer thickness via sequential Gaussian simulation for the estimated mud unit locations. The uncertainty in the presence/absence of mud units and the thickness of mud units was assessed in a probabilistic way through analysis of multiple equally probable realizations Each realization of a given mud unit honored exactly the presence/absence and thickness data and the model of spatial continuity, yet allowed differences in locations away from data control. This reflected the uncertainties of the simulated model caused by incomplete knowledge about the mud units. The geostatistical analysis of the alternative conceptual models was a joint effort between scientists in the Russian Academy of Science (RAS) and the staff at Pacific Northwest National Laboratory (PNNL).

5.1 Alternative Conceptual Model for Unit 1 Zonation

5.1.1 Geostatistical Data Analysis

5.1.1.1 Data Declustering

The geostatistical data analysis was based on interpretations of the Hanford formation sediment facies type using core data. Two-hundred-thirty locations were available for which the five facies types of the Hanford formation (Unit 1) were determined. Table 5.1 lists the number of observations for each of the

Table 5.1. Name and Number of Samples of Hanford Formation Unit 1

Facies Code	Facies Name	Number of Observations
F1	Hanford Formation Gravel Type 1	165
F2	Hanford Formation Gravel Type 2	6
F3	Hanford Formation Gravel Type 3	43
F4	Hanford Formation Sand	15
F5	Hanford Formation Silt	1
Total Number of Observations:		230

five facies, and Figure 5.1 shows the spatial location of these observations within the Hanford Site boundary. Figure 5.2 is a preliminary interpreted zonation map of the facies based on expert geological knowledge from site hydrogeologists. It presents a reasonable interpretation of the hydrogeology of Unit1 but does not asses the uncertainty of the map.

Geostatistical simulation generates realizations honoring the global data distribution and spatial correlation structure of the data. Therefore, a representative global distribution and correct description of spatial correlation are important. The global distribution of a variable is often inferred from raw data, but data are rarely collected for statistical representativeness. From Table 5.1 and Figure 5.1 it can be seen that the facies observations are spatially clustered, and the occurrence frequency of the facies in the raw data may not be a good representation of the underlying data distribution. The data proportions need to be adjusted to reflect a more representative facies distribution.

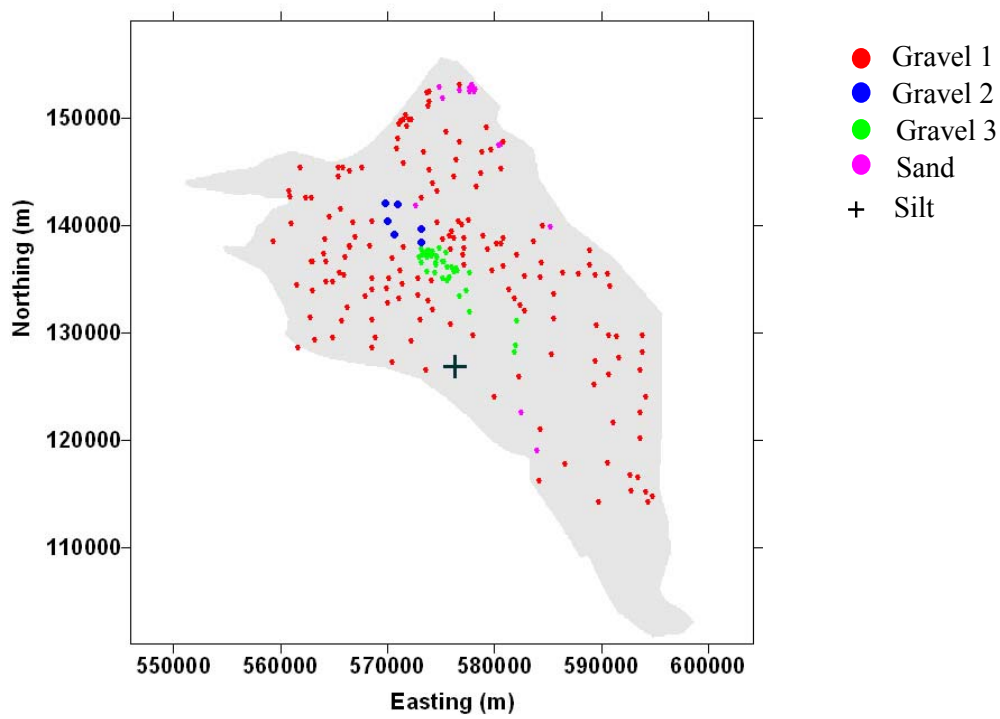

Figure 5.1. Location Map of the 230 Unit 1 Facies Observations

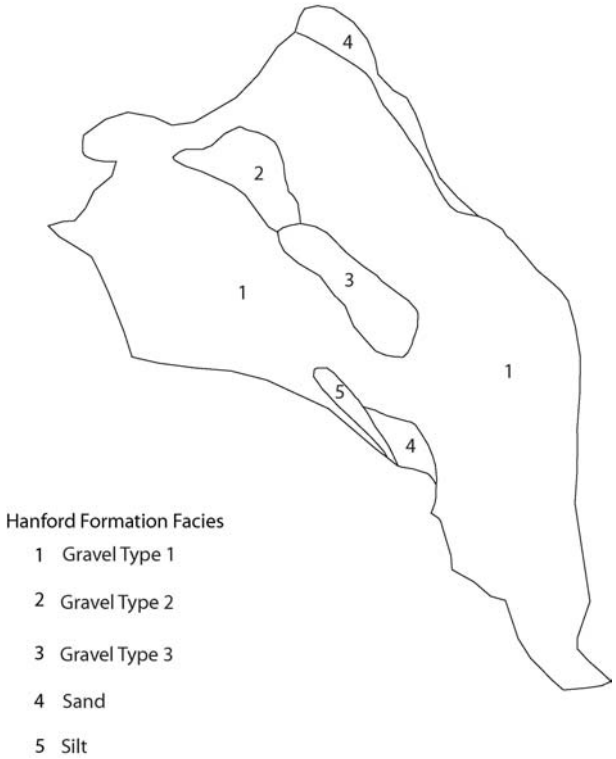

Figure 5.2. Unit 1 Zonation Based on Geological Interpretation

Different methods exist to decluster spatially clustered data to obtain more representative statistics of a data distribution. The technique of *cell declustering* (Journel 1983; Deutsch 1989) was used in this study. The approach divides the study domain into grid cells. Then the number of occupied cells containing data and the number of data points in each occupied cell are counted. Each data point is then given a weight. The weights are constrained between 0 and 1 and must add up to 1; the weights are inversely proportional to the number of data points in the occupied cells. The weights depend on how the domain is divided into grid cells. Thus the cell size needs to be changed and an optimal cell size chosen. The *declus* program in GSLIB (Deutsch and Journel 1998) was used for declustering the Unit 1 facies data. Figure 5.3 shows the optimal declustering weights each data value received based on an optimal declustering cell size of around 2000 meters. This figure shows that most of the facies 3 data points received the smallest weights, illustrating that facies 3 observations are clustered in a relatively small area (Figure 5.1).

The optimal declustering weights shown in Figure 5.3 were used to calculate the declustered facies proportions tabulated in Table 5.2. In addition, the facies proportions that were digitized from the geological map were computed and are listed in Table 5.2 along with the raw data proportions. The proportions from the geological map were similar to those derived from the declustering weights. Final global proportions were determined by compromising between the proportions from the declustering weights and the geological map used in the simulations of the Unit 1 distribution. The final global proportions are influenced more by the proportions derived from the geologic map because of the extremely small number of observations available for facies 2 and 5, which made the declustered proportions less reliable than they might normally be.

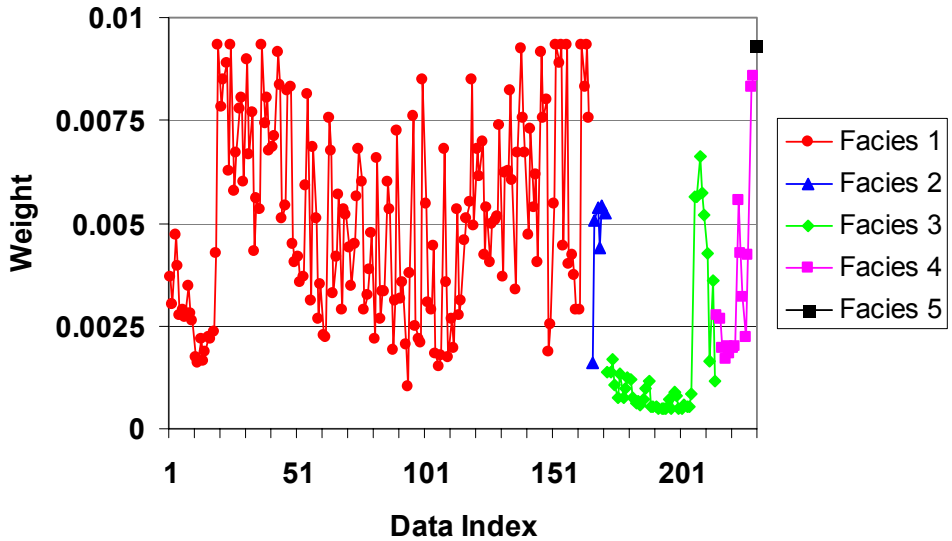

Figure 5.3. Declustering Weights of Data Colored in Terms of Facies Type

Table 5.2. Global Proportion of the Five Facies in Hanford Unit 1

Facies Name	No. Data Points	Proportion (%) from			Proportion to Be Used (%)
		Data	Declustering	Geological Map	
F1 (Gravel type 1)	165	71.74	84.38	85.71	**85.00**
F2 (Gravel type 2)	6	2.61	2.71	4.01	**4.00**
F3 (Gravel type 3)	43	18.70	6.67	4.51	**5.00**
F4 (Sand)	15	6.52	5.31	4.51	**4.75**
F5 (Silt)	1	0.43	0.94	1.25	**1.25**

5.1.1.2 Variogram

An essential aspect of geostatistical modeling is establishing quantitative measures of spatial correlation of regionalized variables for subsequent estimation and simulation. The variogram is the most commonly used measure of spatial correlation. In probabilistic notation, the variogram $\gamma(\boldsymbol{h})$ is defined as the expected value of the squared difference of the values of a regionalized variable $Z(\boldsymbol{u})$, separated a lag distance $\boldsymbol{h}$ in space:

$$\gamma(h) = \frac{E\left\{\left[Z(u) - Z(u+h)\right]^2\right\}}{2}$$

Experimentally, the variogram for lag distance $\boldsymbol{h}$ is defined as the average squared difference of values separated approximately by $\boldsymbol{h}$:

$$\gamma(h) = \frac{1}{2N(h)} \sum_{N(h)} \left[Z(u) - Z(u+h) \right]^2$$

where $N(\boldsymbol{h})$ is the number of data pairs for lag $\boldsymbol{h}$.

Usually, for simulating categorical variables like the presence or absence of Unit 1 facies and Ringold mud units, sequential indicator simulation is used, and an indicator variogram is needed. For this purpose, an indicator transform is performed on the data as follows:

$$I(u_\alpha; z_k) = \Pr ob\{facies\, k\, being\ present\} = \begin{cases} 1, & if\ \ facies\, k\, is\ present\, at\, location\ \ u_\alpha \\ 0, & otherwise \end{cases}$$

Indicator experimental variograms of the first four facies were calculated and variogram models fit to them. The anisotropy was checked by calculating directional variograms at a number of azimuth angles. Programs in GSLIB were used to calculate experimental variograms and fit variogram models. For better comparison, all variograms are normalized to a sill of one. Figure 5.4 shows the experimental variograms and the variogram models fit to them. Detailed directional variogram calculations revealed that the maximum and minimum continuity directions are -35/55 for facies 1 and -40/50 for facies 3. Although there are only 15 positive observations of facies 4, there are a total of 230 observations, so the positive data constitute almost 7% of the total data, and a directional indicator variogram could be calculated. Detailed directional variograms of facies 4 were modeled with an anisotropic variogram model with continuity directions of -40/50, which agrees with the general orientation of facies 4 on the geologic map (Figure 5.2). Insufficient data were available for reliable directional modeling of facies 2, and no clear direction of anisotropy was evident on the geologic map, so an isotropic variogram model was chosen for facies 2. Even though the experimental variogram for facies 2 is based on only six positive observations from the 230 samples, a reasonably well-behaved experimental variogram was calculated from the data and then fit by an isotropic spherical variogram model with a range of 3,750 m. For facies 5, which only had a single observation, the variogram was assumed to have the same anisotropic directions as facies 3 and 4 but a shorter range based on the geological map (Figure 5.2). The detailed parameters of the variogram models are listed in Table 5.3. The variograms in Table 5.3 were fit using spherical variogram models (Isaaks and Srivastava 1989):

$$\gamma(h) = \begin{cases} 1.5\dfrac{h}{a} - 0.5\left(\dfrac{h}{a}\right)^3 & \text{if } h \le a \\ 1 & \text{otherwise} \end{cases}$$

where h is the vector lag distance and a is the range.

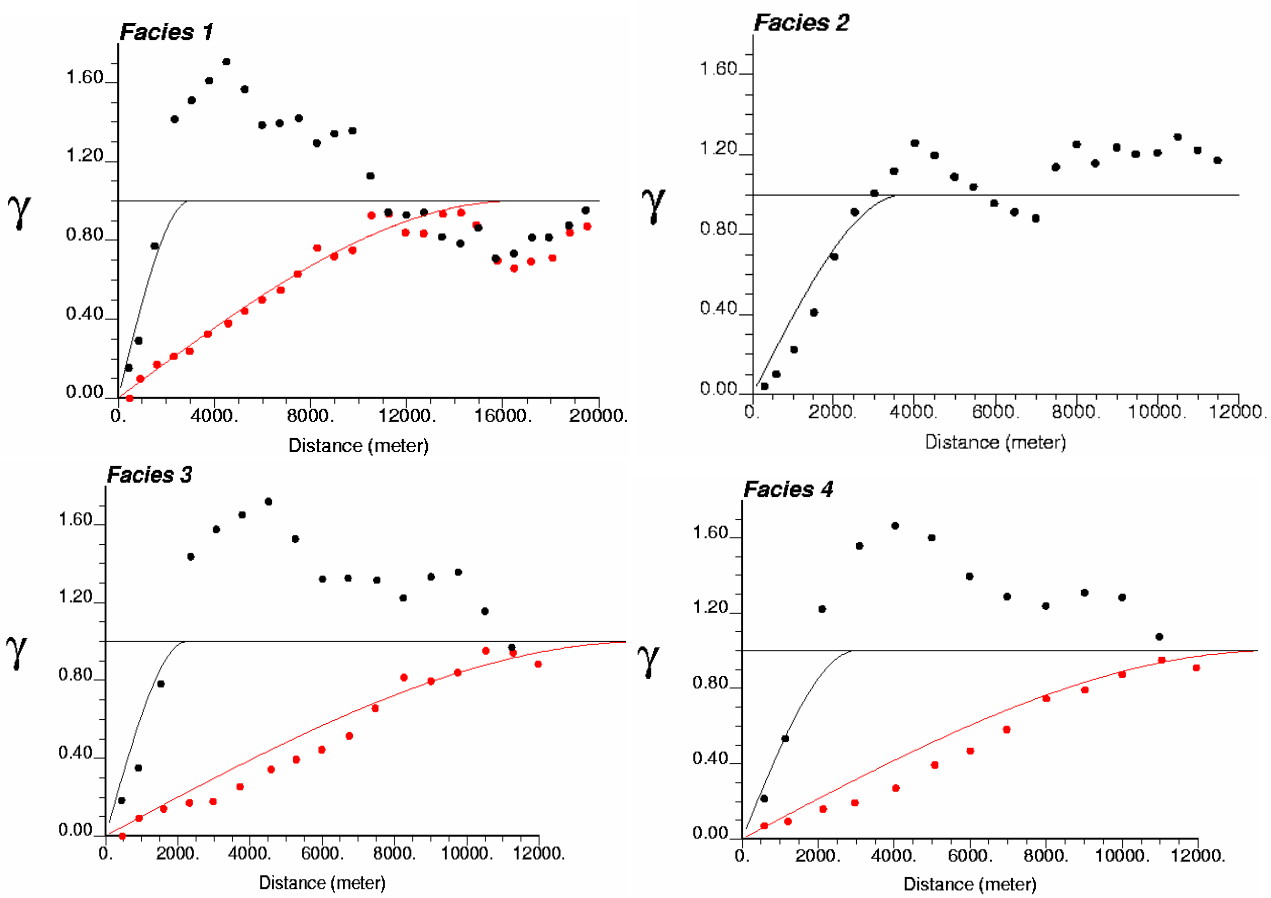

Figure 5.4. Experimental Variograms (dotted line) and Variogram Models (solid line). The red line represents the major direction of continuity; the black line denotes minor anisotropic direction.

Table 5.3. Variogram Models of Five Unit 1 Facies

Facies Type	Anisotropy	Range	Variogram Model Fitted
Gravel 1	NW 35	16500	$\gamma = 0.001 + 0.999 Sph \begin{pmatrix} -35 & 55 \\ 16500 & 3000 \end{pmatrix}$
Gravel 2	Isotropic	3750	$\gamma = 0.001 + 0.999 Sph \begin{pmatrix} 0 & 90 \\ 3750 & 3750 \end{pmatrix}$
Gravel 3	NW 40	15000	$\gamma = 0.001 + 0.999 Sph \begin{pmatrix} -40 & 50 \\ 15000 & 2250 \end{pmatrix}$
Sand	NW 40	14000	$\gamma = 0.001 + 0.999 Sph \begin{pmatrix} -40 & 50 \\ 14000 & 3000 \end{pmatrix}$
Silt	NW 40	5000	$\gamma = 0.001 + 0.999 Sph \begin{pmatrix} -40 & 50 \\ 5000 & 2250 \end{pmatrix}$

5.1.2 Indicator Simulation of Unit 1 Zonation

Sequential indicator simulation was used to simulate Unit 1 zonation. For each spatial location u_α, indicator kriging was used to derive the probability of each facies (k=1,…,K), conditional to the data and previously simulated facies types at nearby locations:

$$\text{Prob}\ \{I(u_\alpha;\ k)=1\,|\,(n)\} = p(k) + \sum_{\alpha=1}^{n} \lambda_{\alpha(k)} \left[I(u_\alpha;k) - p(k) \right],\ \ k = 1,\ldots,K$$

where $p(k) = E\{\mathrm{I}(u_\alpha;k\} \in [0,1]$ is the *a priori* probability of facies k inferred, *e.g.*, from the declustered proportion. The weights $\lambda_{\alpha(k)}$ are given by simple indicator kriging equations using indicator variograms of corresponding classes. Such conditional distributions reflect the uncertainty of the facies type at the spatial location to be estimated. A realization is derived by drawing a simulated value from the distribution of uncertainty at each of the spatial locations in the domain. The process proceeds sequentially by supplementing the original data with the simulated indicator value for subsequent locations along the random path. The sequential simulation approach ensures the modeled spatial covariance structure is reproduced, on average, for the ensemble of simulations (Deutsch and Journel 1998).

The implementation of sequential indicator simulation in GSLIB (i.e., *sisim*) was used to generate facies realizations based on the 230 original facies observations, the adjusted global facies proportions, and the established variogram models. The simulations were generated on a 389 by 437 grid with an origin at (546,000m/101,000m) and 150-meter grid spacing with square grid cells. The Hanford Site boundary was used to truncate the cells that fell outside the boundary. The left column of Figure 5.5 presents four realizations.

With the use of sequential indicator simulation it is usually unavoidable that some facies realizations have short-scale, geologically unrealistic variations. In some situations, such short-scale variations would affect simulation of flow and transport. In addition, due to the necessity of order-relation corrections in indicator simulation to ensure all K separately kriged facies probabilities are non-negative and sum to 1.0, the simulated facies proportions of a realization might depart from the target proportions, especially for facies with relatively small proportions. Thus, the facies realizations need to be post-processed to remove the undesirable short-scale variations and to honor the target global proportions (Deutsch 1998a). The maximum a-posterior selection (MAPS) technique is one of the most common post-processing methods. MAPS was implemented in GSLIB (Deutsch 1998a) and used to clean up the Hanford Unit 1 realizations. The four realizations before and after cleanup with MAPS are shown in Figure 5.5, which shows that some short-scale features in the uncleaned realizations disappear after cleaning.

Figure 5.6 shows the histogram of reproduced proportion of the five facies before and after executing the post-cleaning process based on 101 realizations. The blue vertical bars in the plots are the target global proportions. The average facies proportions reproduced from the 101 realizations are listed in Table 5.4. The facies proportions are reproduced quite well, and the post-processing cleaning generally brings the facies proportion closer to the target proportions (see Table 5.4)

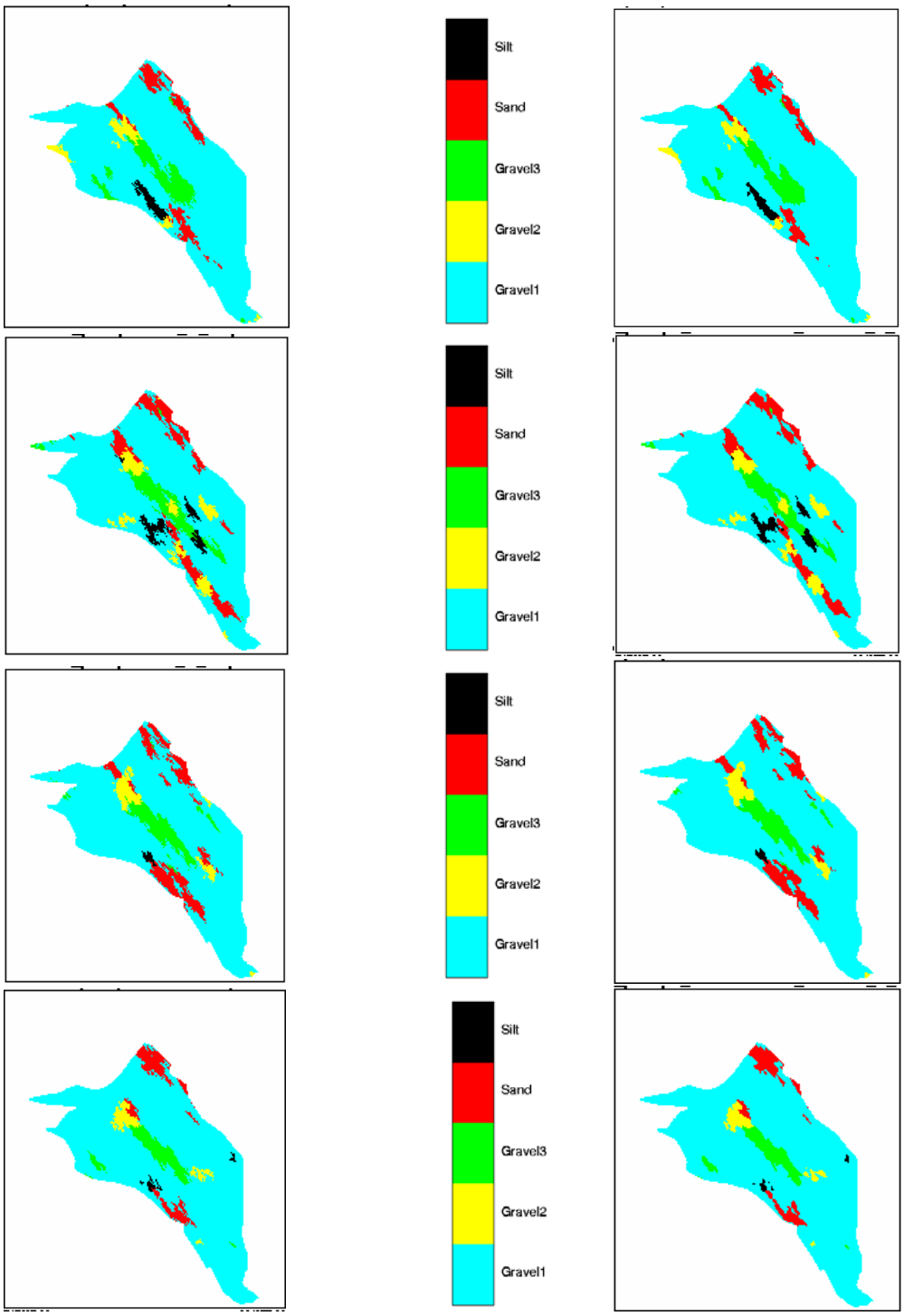

Figure 5.5. Four Unit 1 Facies Realizations before (left) and after (right) Cleanup with MAPS

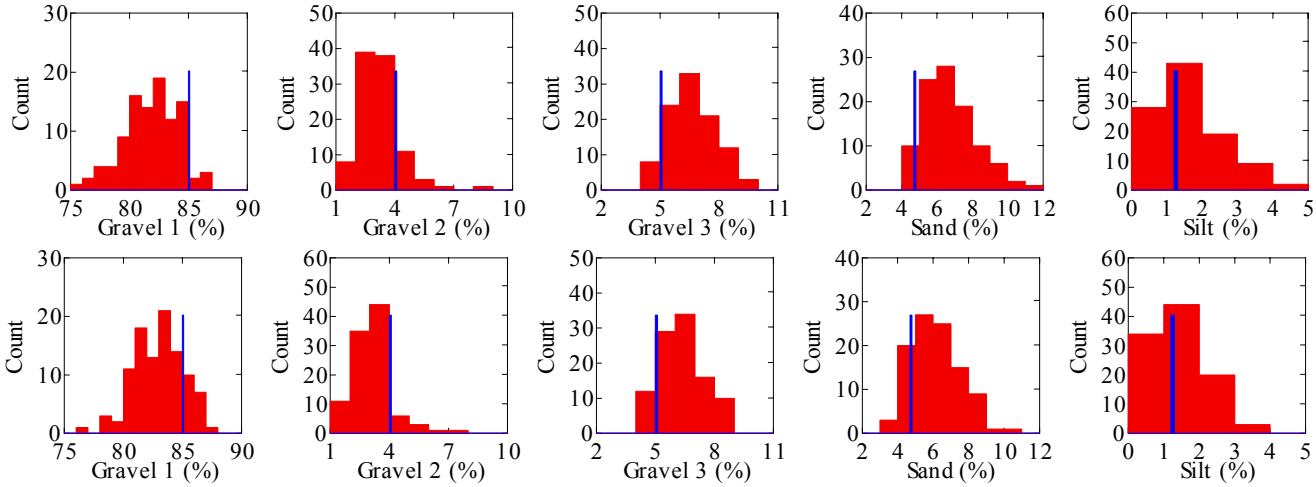

Figure 5.6. Facies Proportion Histogram of the 101 Simulated Realizations (blue vertical bar indicates the target proportion) before (top) and after (bottom) Cleanup with MAPS

Table 5.4. Facies Proportion Reproduction Based on 101 Realizations

Proportion (%)	Gravel 1	Gravel 2	Gravel 3	Sand	Silt
Target	85.00	4.00	5.00	4.75	1.25
Raw Realization	81.82	3.21	6.61	6.75	1.60
Cleaned Realization	82.93	3.14	6.35	6.17	1.41

5.1.3 Post-Processing of Zonation Simulations

5.1.3.1 Probability Maps

The purpose of generating multiple realizations through stochastic simulation is to assess the uncertainty of the models. The spatial variations of the facies zonation embedded in multiple realizations can be summarized in different ways. A likely facies map has the most frequently simulated facies in each spatial location of the domain assigned to the facies type for that location. Figure 5.7 shows the most likely facies map based on 101 raw and cleaned realizations. Compared with the map in Figure 5.2, the major features of the geological map are retained in the simulation, but some features such as the conjunction of facies 4 and 5 shown in the geological map are not reproduced. The inability to honor facies association is one of the drawbacks of the indicator simulation techniques. For that reason, future work on the zonation of Unit 1 will examine the use of the transition probability approach developed by Carle et al. (1998). The set of multiple realizations produced by indicator simulation (or other simulation methods) can also be summarized in the form of probability maps of each facies type. At each spatial location, the probability of a facies type can be calculated as the occurrence frequency of such a facies type through all simulated realizations. A map of such probabilities of all spatial locations in the domain is shown in Figure 5.8. Although the post-cleaning process affects the individual realization (Figure 5.5), no obvious effect can be seen on the probability maps (Figures 5.8 and 5.9).

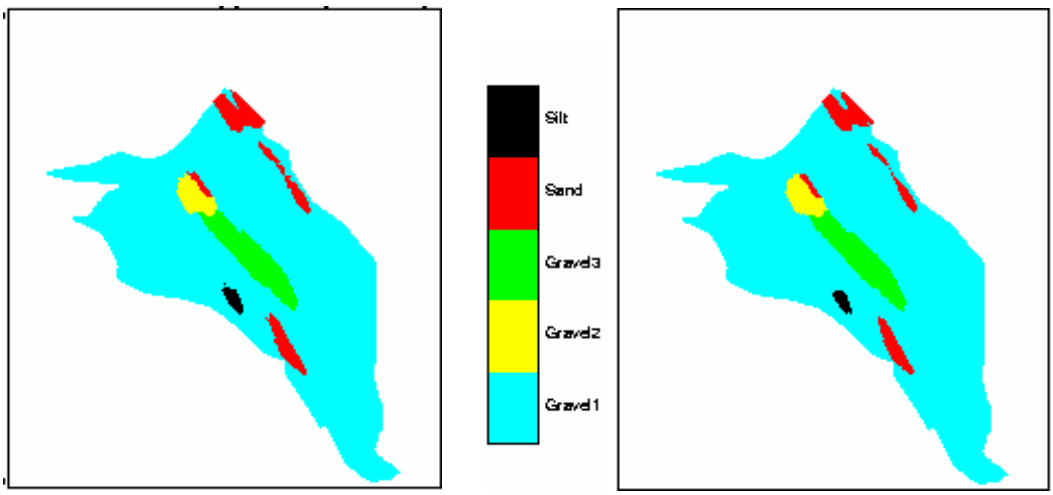

Figure 5.7. Most Likely Facies-Based on 101 Raw (left) and Cleaned (right) Realizations

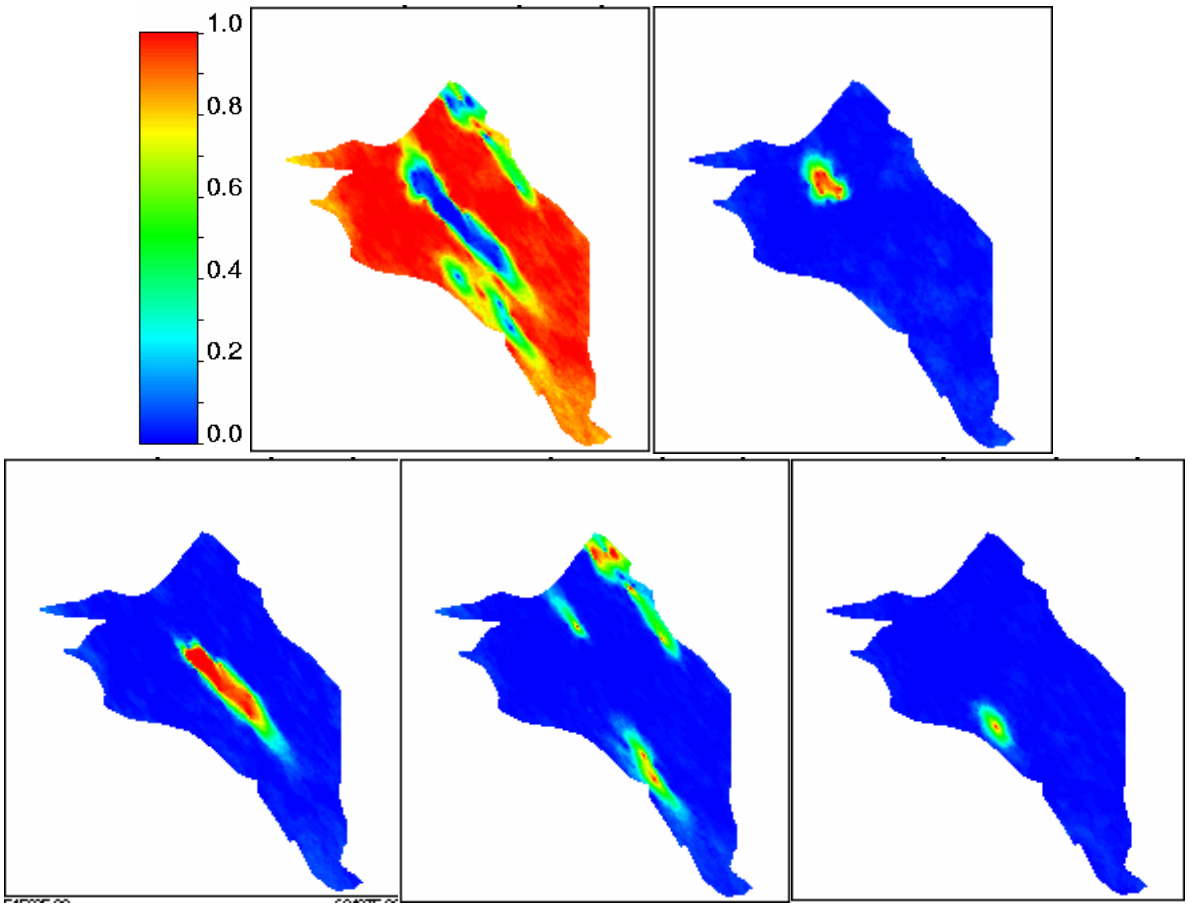

Figure 5.8. Probability Maps Based on 101 Realizations for Facies 1 to Facies 5 (in order)

5.1.3.2 How Many Realizations?

The spatial uncertainty is assessed through multiple realizations, but the number of realizations that should be generated to sufficiently model the spatial uncertainty addressed is not a trivial question. The answer depends on how uncertainty is measured. The evaluation of facies realizations provides a sense of uncertainty about the geological models created under current data and knowledge. Rigorous uncertainty evaluation should be considered at the flow and transport level. However, it is usually impractical to process a large number of facies realizations in the flow simulator to evaluate the uncertainty. Here, we just evaluate the spatial variation changes in the facies model based on the number of realizations generated. For this purpose, simulations were conducted on a series of realization numbers with distinct initial random number seeds. The random number seed defines the random path of the grid cell in the sequential simulation process. The numbers of realizations specified in the simulations are 5, 25, 50, 75, 100, 150, 200, 400, 600, and 1000, respectively. The mean, median, and standard deviation of the proportion of each facies are calculated for each set of simulations. Also, the probability maps of each facies are calculated for each set of simulations with a varying number of realizations. The sum of absolute differences between the probability maps from two sets of simulations with consecutive realization numbers is plotted against the number of realizations in Figure 5.9. It can be seen that a big drop occurs in the sum difference of probability maps, and the facies proportions level out around 200 realizations, but over 600 realizations may be needed to make things converge. This will be considered in future work generating sets of realizations.

5.1.3.3 Ranking of Simulations

Each facies realization is one possible scenario of the unknown unique geological reality of Hanford Unit 1. All realizations from the stochastic simulation algorithm honor the original data and the spatial correlations derived from the data, and all realizations are considered equally probable. However, each realization has a different spatial distribution of facies, and that will result in a different flow and transport response when the realization is used as input to a flow simulator. It is usually impractical to evaluate the flow and transport behavior of all the facies realizations by feeding them through the flow simulator because of the extensive CPU times involved, so methods of ranking realizations have been developed (Deutsch 1998b). The methods attempt to rank the realizations in terms of their continuity. For example, fluid flow will tend to be higher in facies realizations with a high volume of connected, highly conductive facies and lower in realizations with a low volume of connected, highly conductive facies. The ranking approach allows a small subset of the realizations to be run through the simulator while still capturing the range of flow and transport variability. In the Hanford Unit 1 facies simulation, the five facies have quite different hydraulic conductivities, as shown in Table 5.5. The simple ranking approach proposed by Deutsch (1998b) was used for ranking the Unit 1 facies realizations.

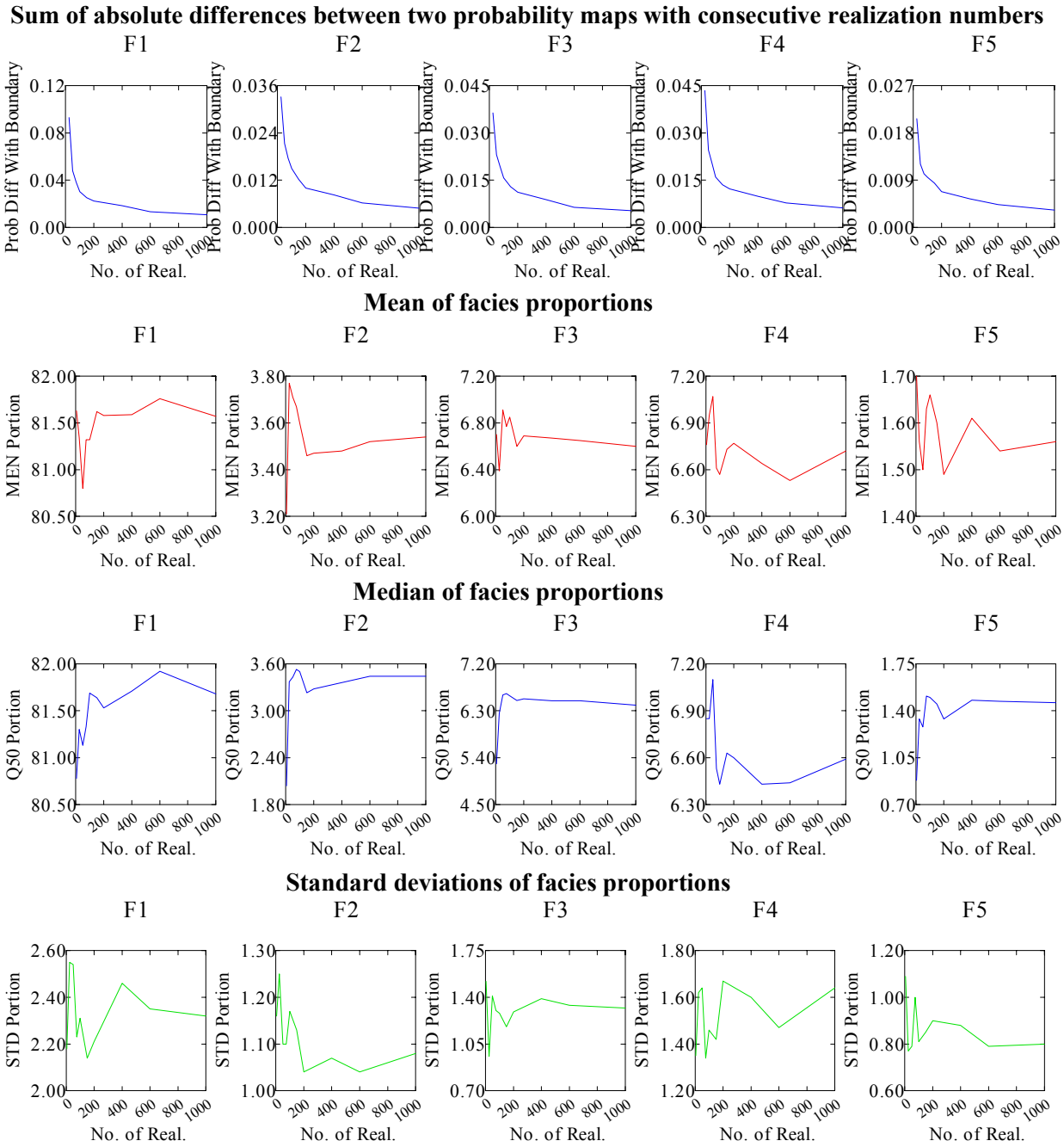

Figure 5.9. Influence of Number of Realizations

Table 5.5. Saturated Hydraulic Conductivity of the Five Unit 1 Facies

Facies	F1 (Gravel Type 1)	F2 (Gravel Type 2)	F3 (gravel type 3)	F4 (Sand)	F5 (Silt)
Mean conductivity (m/d)	1312	610	1964	401	0.5

In the approach proposed by Deutsch (1998b), each grid cell is defined as a *net* or a *non-net* cell based on certain criteria. A *net* cell is one that belongs to a connected geological body (an aggregate of connected cells) from the viewpoint of the flow and transport. In our case, two facies, i.e., gravel 1 and 3, with the highest hydraulic conductivities are regarded as the most influential media for flow and transport. Any cell with facies estimated as one of these two types is regarded as being in the flow and transport network, i.e., a net cell. An additional factor considered here is the water table. Only connected, highly conductive media below the water table influence flow and transport in the aquifer. Therefore, a map of the water table was applied to truncate the facies realizations before calculating the geological bodies. All cells above the water table are categorized into a new facies type, *aboveWT*, no matter which of the five facies was originally simulated at that location. Connected *net* cells below the water table form geological bodies for flow and transport. The more net cells aggregated in the geological bodies and the less tortuous the body, the higher the conductivity of the geological body. Therefore, the volume and the tortuosity of the geological bodies formed can be used as the criteria for ranking the realizations as "high conductive" versus "low conductive." The volume will be the total number of cells in the geological body, and the measure of tortuosity is evaluated by the ratio of surface area and volume of a geological body, which is the ratio of the number of cells on the surface to the number of cells in the geological body. Various numbers of geological bodies can be formed in different facies realizations, and the number of geological bodies formed for the 101 Unit 1 facies realizations ranged from 28 to 44 with a mode of 36. However, the first two to five largest geological bodies contained the majority of total net cells for most realizations. Therefore, it was decided to rank the Unit 1 facies realizations based on just a few of the largest geological bodies. In the ranking, the total number of net cells and the tortuosity of the geological objects were calculated and the realizations sorted according to the two criteria, respectively. Two ranks were thus obtained. Because of the lack of knowledge as to which criterion was more important, the average of the two ranks was computed and the final rank obtained by sorting the average rank, which is the default for the ranking program developed by Deutsch (1998b).

Table 5.6 lists the selected ranking results based on 2 to 15 geological bodies. Only the four realizations with the highest conductivity, four with the lowest conductivity, and five with medium conductivity realizations are listed. Some realizations were common in the ranks derived using the different numbers of geological objects. Figure 5.10 shows the facies maps of those common realizations. Although it is

Table 5.6. Ranking of Facies Realizations

No. Geological Bodies		**Realization Index of High, Low, and Medium Conductivity**				
2	High	**90**	*51*	67	27	
5		67	**90**	*51*	40	
10		**90**	40	*51*	46	
15		**90**	40	*51*	46	
2	Medium	**48**	96	**18**	14	45
5		**48**	89	*31*	8	98
10		*3*	19	82	**18**	*31*
15		41	5	**18**	*3*	64
2	Low	24	*30*	**81**	28	
5		101	23	**81**	*30*	
10		**81**	23	*30*	43	
15		50	23	*30*	43	

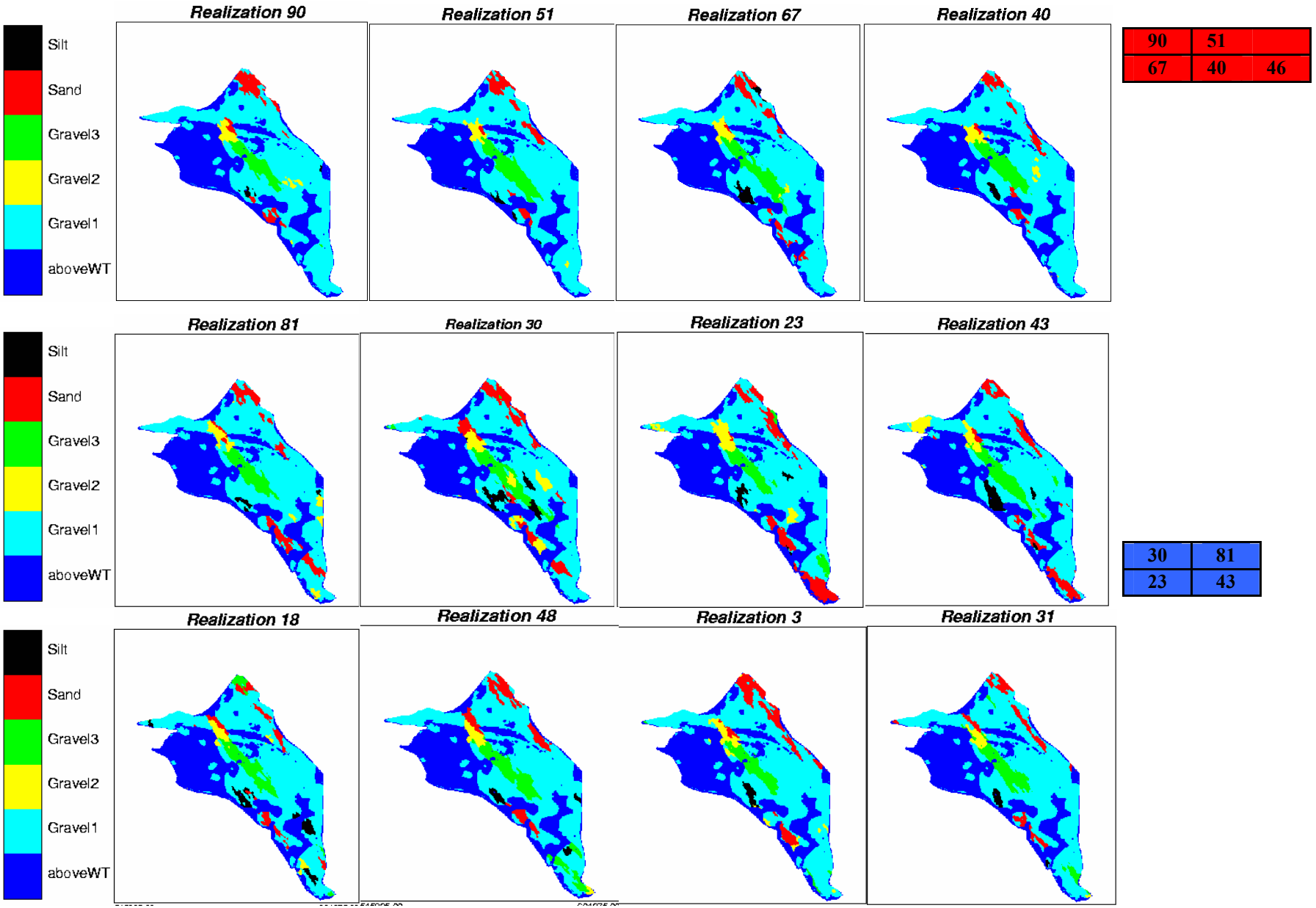

Figure 5.10. Four Facies Realizations That Ranked Highest (top), Lowest (middle) and Medium (bottom) in Conductivity

unlikely that it will ever be possible to evaluate all realizations using the inverse approach, we hope to be able to evaluate large numbers (e.g., hundreds or thousands) of them using forward modeling. This will allow us to compare important transport measures such as the predicted breakthrough to the river from forward modeling of a realization with the ranking developed using the approach described above. The comparison will be used to test, and if necessary modify, the procedures used to rank the realizations.

5.2 Alternative Conceptual Model for Ringold Mud Units

5.2.1 Geostatistical Data Analysis

5.2.1.1 Data Description

The hydrogeological structure of the Hanford Site is layered. Three Ringold Formation mud units, the upper Ringold mud (U4), middle Ringold mud (U6), and lower Ringold mud (U8), are characterized by low conductivity and alternate with highly conductive sand and gravel units. These mud units have a significant influence on the direction of water flow and contaminant transport, especially vertical transport within the unconfined aquifer. Therefore, the spatial distributions of these three mud units and the uncertainties in their distribution need to be understood. The available data for the spatial modeling of the three mud units include the elevations of the top and bottom of each mud unit for 396 monitoring wells at the Hanford Site. The presence/absence and the thickness of the mud units are unambiguous for most of the wells. However, uncertainty exists in the data set, including no mud unit information and insufficient depth for some wells. Table 5.7 tabulates the presence/absence and thickness data of the three mud units. Figure 5.11 shows the spatial maps of the presence/absence of the mud units, and Figure 5.12 shows the thickness histograms when mud units are present.

Table 5.7. Presence/Absence and Thickness Data for the Three Mud Units

	U4	**U6**	**U8**
Number of Samples			
Presence	128	151	182
Absence	248	124	54
Uncertain	20	121	160
Proportion (%)			
Presence	34	55	77
Absence	66	45	23
Number of Thickness Samples			
Thickness	119	106	172

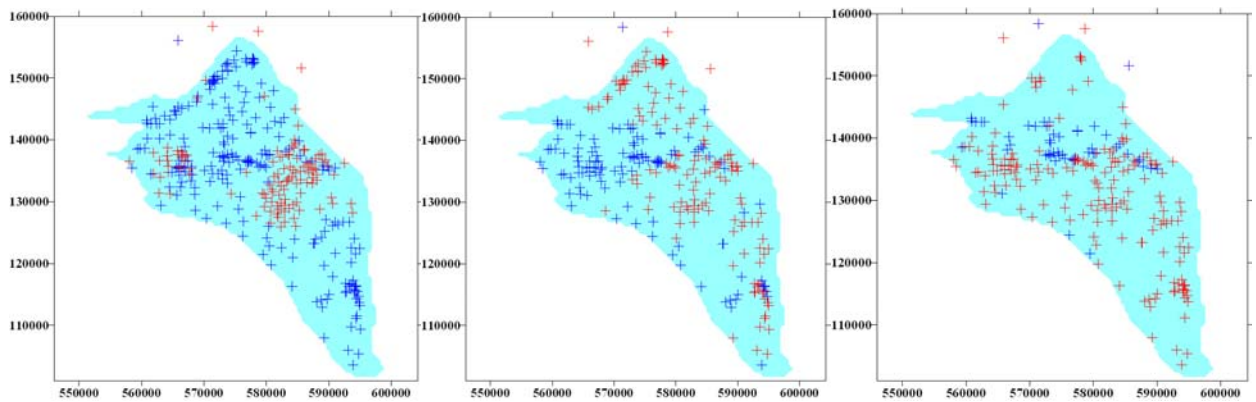

Figure 5.11. Location Maps of the Presence (red)/Absence (blue) of the Three Mud Units: U4 (left), U6 (middle), and U8 (right).

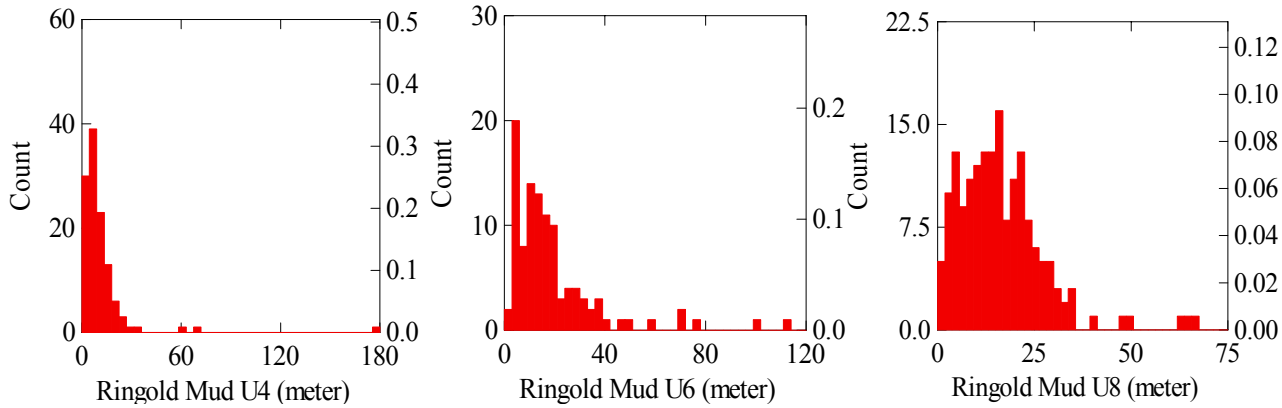

Figure 5.12. Histograms of the Mud Thickness when a Mud Unit is Present. Vertical axes indicate the counts and relative frequency for each mud unit thickness.

5.2.1.2 Variogram

As discussed previously, a two-step approach was used to simulate the structure of the Ringold mud units. The presence/absence of the mud unit was simulated first using sequential indicator simulation techniques. The thickness of the mud units was then simulated using the Sequential Gaussian Simulation technique. The presence/absence and thickness realizations were combined to form the final realizations of the mud units. The spatial heterogeneities of the presence/absence and thickness distribution were evaluated through variography. The indicator variograms of the presence/absence were calculated and modeled based on the raw presence/absence data. The thickness data were transformed to normal scores, and the variogram analyses of thickness were conducted on the transformed normal score data.

Figure 5.13 shows the calculated directional variograms and the fitted variogram models for the presence/absence of the three mud units, and Table 5.8 tabulates the fitted variogram models. The experimental variograms have all been normalized to a sill of 1.0. Figures 5.14a and b show the experimental variograms and fitted variogram models of the normal score thickness of mud units U4 and U8.

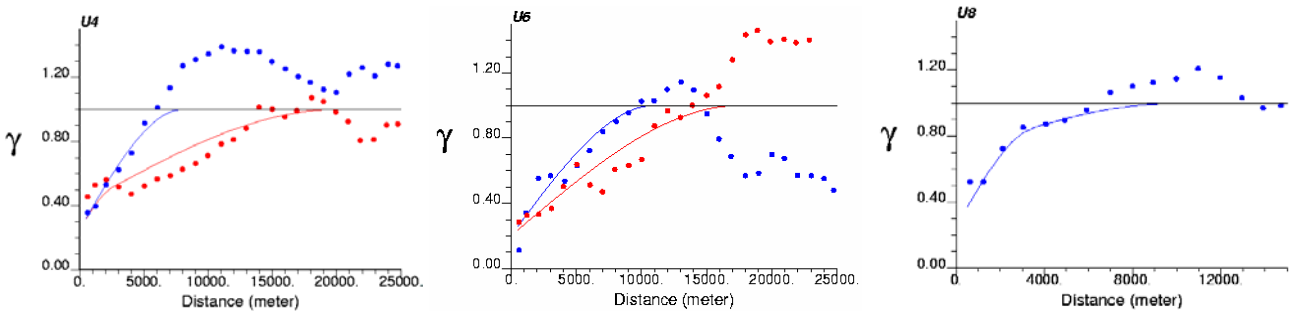

Figure 5.13. Experimental Variograms (dotted) and Fitted Models (solid) for Presence/Absence of the 3 Mud Units; red = major direction of continuity, blue = minor anisotropic direction.

Table 5.8. Models of the Indicator Variogram of the Three Mud Units

Mud Units	Fitted Variogram Models
U4	$\gamma = 0.25 + 0.15Sph\begin{pmatrix} 30 & 120 \\ 2500 & 8000 \end{pmatrix} + 0.60Sph\begin{pmatrix} 30 & 120 \\ 20000 & 8000 \end{pmatrix}$
U6	$\gamma = 0.20 + 0.80Sph\begin{pmatrix} 70 & -20 \\ 17500 & 11000 \end{pmatrix}$
U8	$\gamma = 0.25 + 0.45Sph(3500) + 0.30Sph(10{,}000)$

a

b

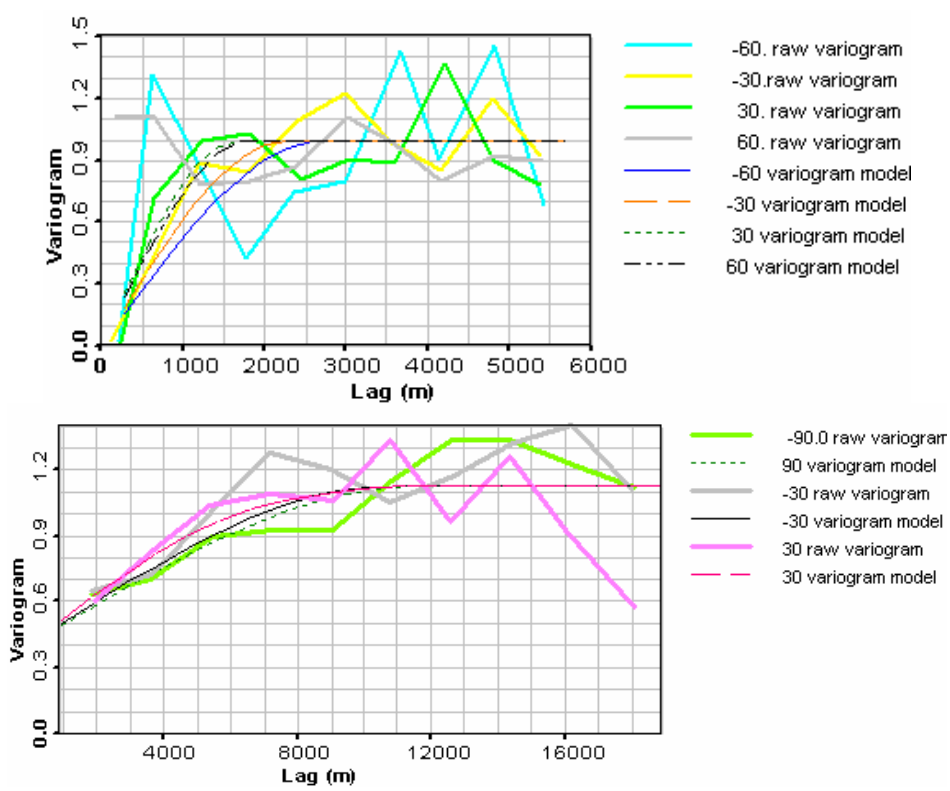

Figure 5.14. Experimental Directional Variograms and Fitted Models of Normal Score Transformed Thickness of (a) U4 and (b) U8

5.2.2 Indicator Simulation of Presence/Absence of Mud Units

The *Sisim* program from GSLIB was used for simulation of the presence and absence of the three mud units. Although simple kriging is theoretically preferred for constructing the local conditional cumulative distribution function for each spatial location, the option of ordinary kriging was used in the simulation because of the local variability in the proportions, as suggested in Deutsch and Journel (1998). The ordinary kriging option handles local variability and trends in the data better than simple kriging. The ordinary kriging option is feasible in this case because of the large number of data available. Fifty-one realizations were generated for each of the three mud units; Figure 5.15 shows three realizations for each one. The Hanford boundary used in truncating the mud unit realizations was slightly different from the one shown in Section 5.1.

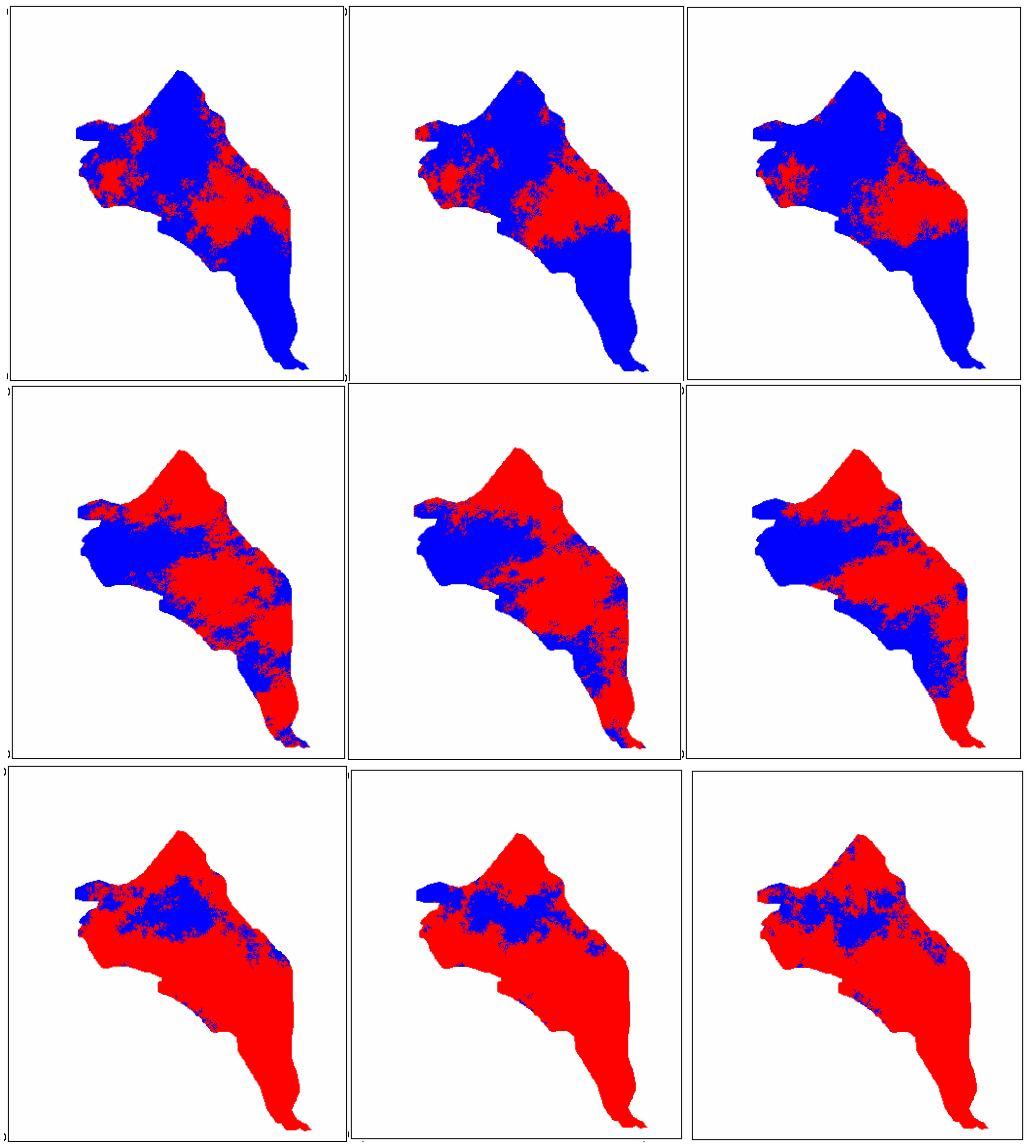

Figure 5.15. Three Presence/Absence Realizations of U4 (top), U6 (middle), and U8 (bottom); red indicates presence and blue is absence.

The distributions of the presence/absence proportions of the mud units based on the 51 realizations are shown on the histograms plotted in Figure 5.16. The proportion of U8 presence seems to be over-estimated and that of U4 underestimated. This discrepancy may be partially attributed to the truncation with the Hanford boundary. Because the simulation is conducted on a rectangular grid, and the cells outside the Hanford Site boundary are truncated after the simulation, these cells do not have data control. The cells have a greater chance to be estimated than the type with relative high proportion such as the presence of U8 and absence of U4. Based on the 51 realizations, corresponding probability maps of the mud units were calculated and are shown in Figure 5.17, superimposed with the original data.

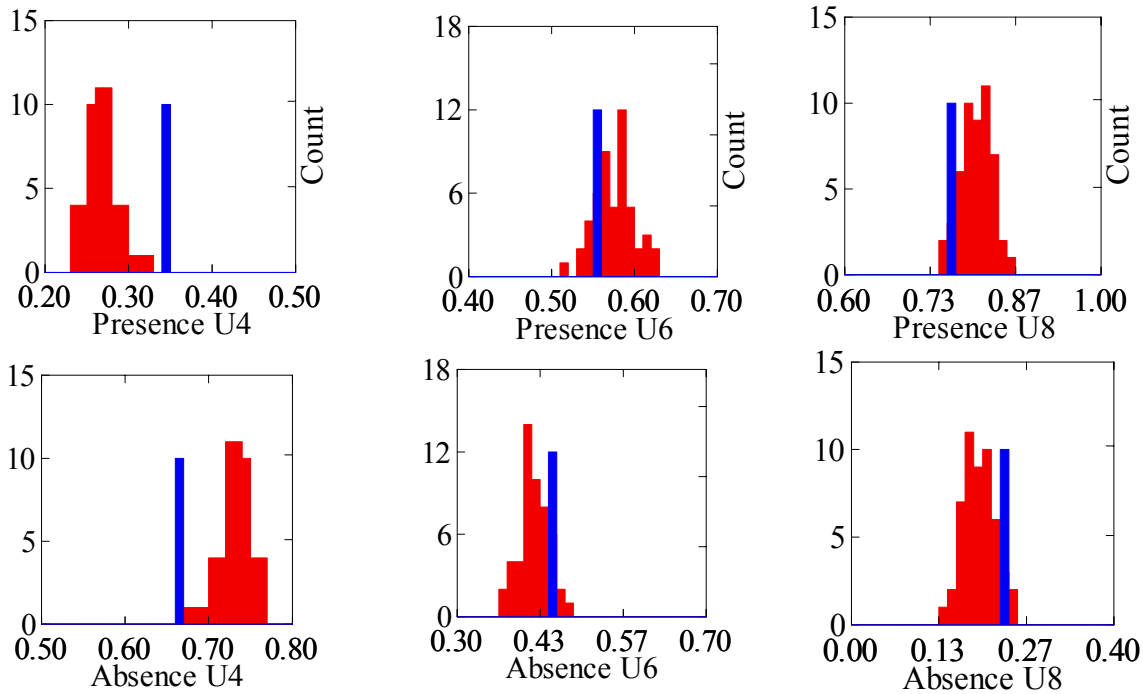

Figure 5.16. Histogram of Global Presence (top)/Absence (bottom) Proportion from 51 Realizations for Mud Units U4, U6, and U8. Blue bars represent input proportions used in the simulation

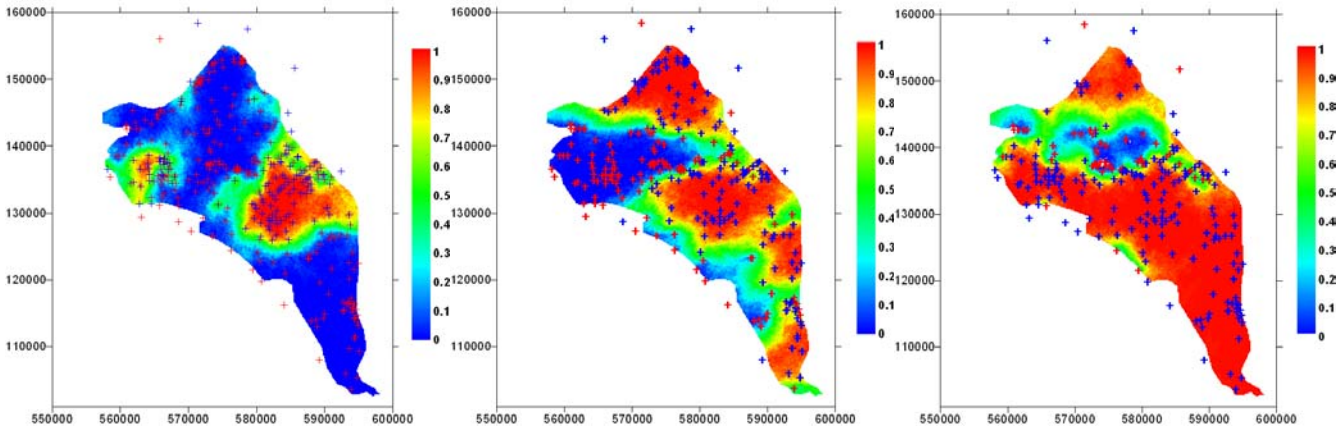

Figure 5.17. Probability Maps of Presence of Three Mud Units: U4 (*left*), U6 (*middle*), and U8 (*right*). Plus symbols represent the presence (blue) and absence (red) at well locations. To enhance contrast, the color scheme for plus symbols is reversed from previous figures.

5.2.3 Gaussian Simulations of Mud Unit Thickness

Before performing variogram analysis, the thickness data of the mud units were transformed into Gaussian distributions using a normal score transform. This transform, discussed in detail in Goovaerts (1997), is a graphical data transformation that can be used on data that initially have any univariate distribution. After the normal score transform, they have a standard Gaussian distribution with a mean of zero and variance of one. The transformation was performed using the *Nscore* program from GSLIB (Deutsch and Journel 1998). In multiGaussian kriging or simulation, the normal score data resulting from the transform are then used for the variogram analysis and simulation with a final step that back-transforms the data to its original distribution. The sequential Gaussian simulation algorithm implemented at the Russian Academy of Science with a simple kriging option was used for simulating mud unit thickness and performed by Academy researchers. Fifty-one thickness realizations were generated for each mud unit; three are shown in Figure 5.18. The realizations are summarized in *E*-type maps consisting of expected values of simulated thickness for all the grid cells from the 51 realizations shown in Figure 5.19.

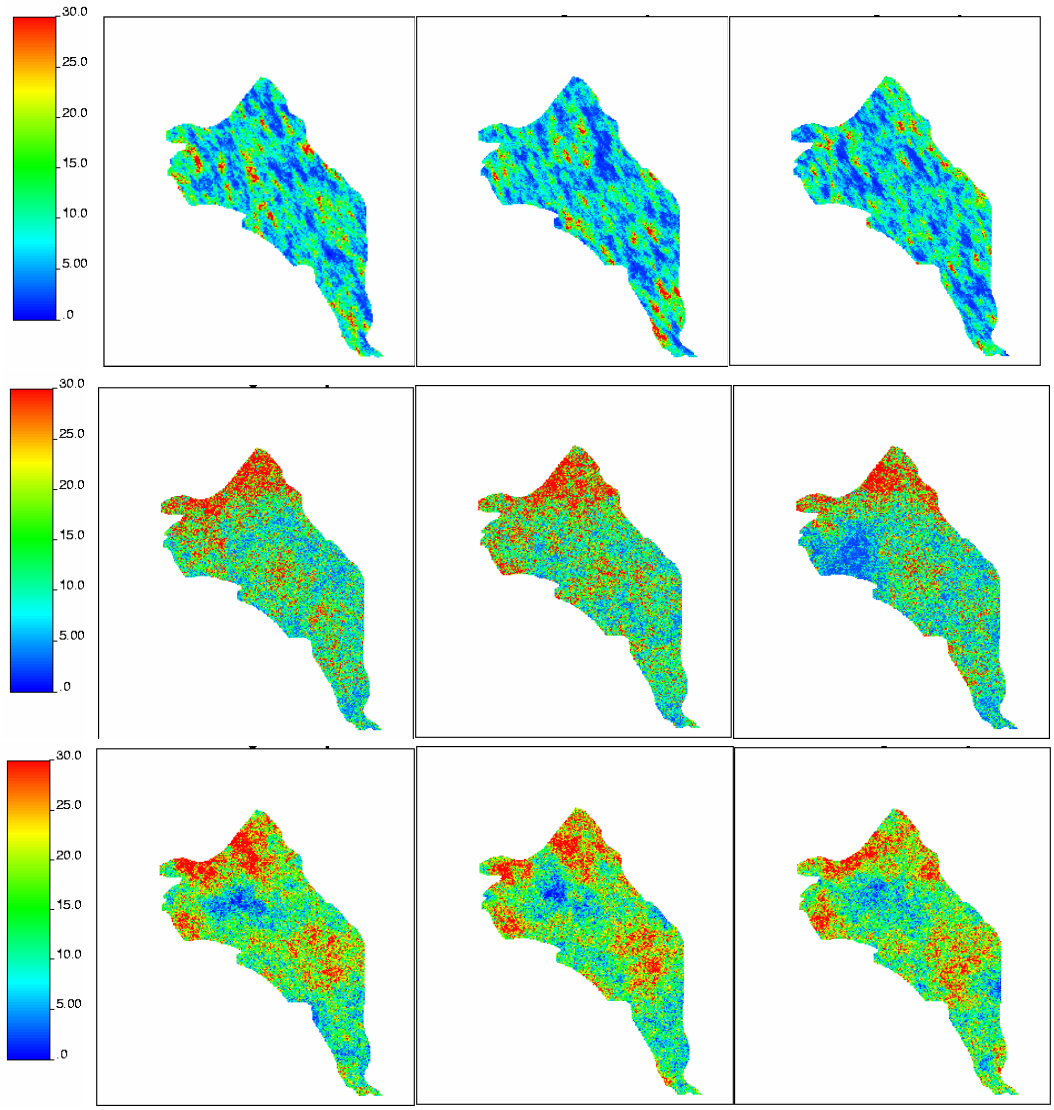

Figure 5.18. Realizations of Thickness Simulations (meters) for U4 (top), U6 (middle), and U8 (bottom)

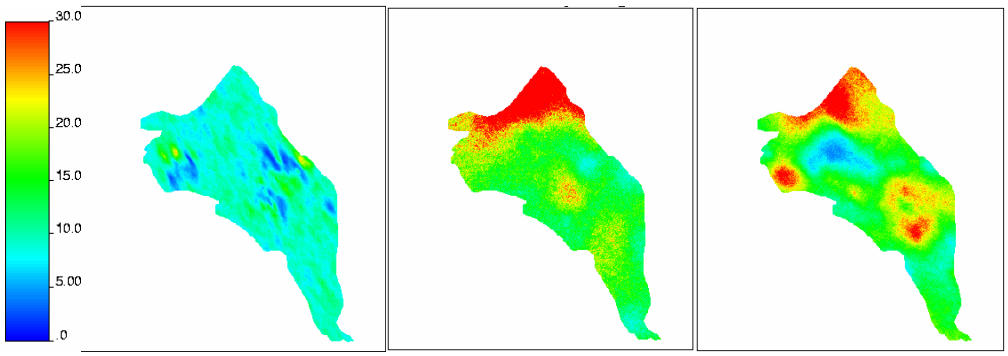

Figure 5.19. E-Type Thickness Maps (meters) of U4 (left), U6 (middle), and U8 (right)

5.2.4 Merging of Presence/Absence and Thickness Simulations

To obtain the complete structure of the Ringold mud units, the realizations of the binary presence/absence of the mud units and the continuous thickness realizations need to be combined. Because the presence/absence and thickness were simulated independently, their combination presents a valid mud unit structure realization. The combination is performed by truncating the thickness values of the cells in the thickness realization to zeros wherever the mud unit was simulated as absent and keeping thickness values in the rest of the thickness realization intact. Figure 5.20 presents three merged realizations for each mud unit.

5.2.5 Post-Processing of Mud Unit Simulations

5.2.5.1 Thickness Maps of the Merged Mud Models

As discussed, the combination of each of the presence/absence realizations and each of the thickness realizations leads to a possible realization of the complete structure of each of the three mud units as a result of the independent simulation of the presence/absence and thickness. To evaluate the uncertainty of the merged realizations for each mud unit, 100 combined realizations were generated by merging presence/absence and thickness realizations chosen randomly with replacement. The *E*-type thickness maps of the 100 merged realizations are shown in Figure 5.21.

5.2.5.2 Ranking of Realizations

The overall uncertainty evaluation of the Hanford Site geological structure should be based on three-dimensional (3D) structural models with the three mud units simulated above and the sand and gravel units in between. During the current stage of the research, the focus has been on the three Ringold mud units. Because of the lack of thickness distribution data on the sand/gravel units between the mud units, a simplified way to evaluate the geological structure was developed using just the presence/absence simulations of the three mud units.

A pseudo-3D geological model was constructed considering that 1) all mud absence cells are occupied by sand/gravel, 2) all mud units have constant thickness, and 3) a constant thickness of sand and gravel exists between two consecutive mud units. A realization of such a pseudo-3D model is constructed by superimposing the realization from one of the three mud units on the realization from another mud unit

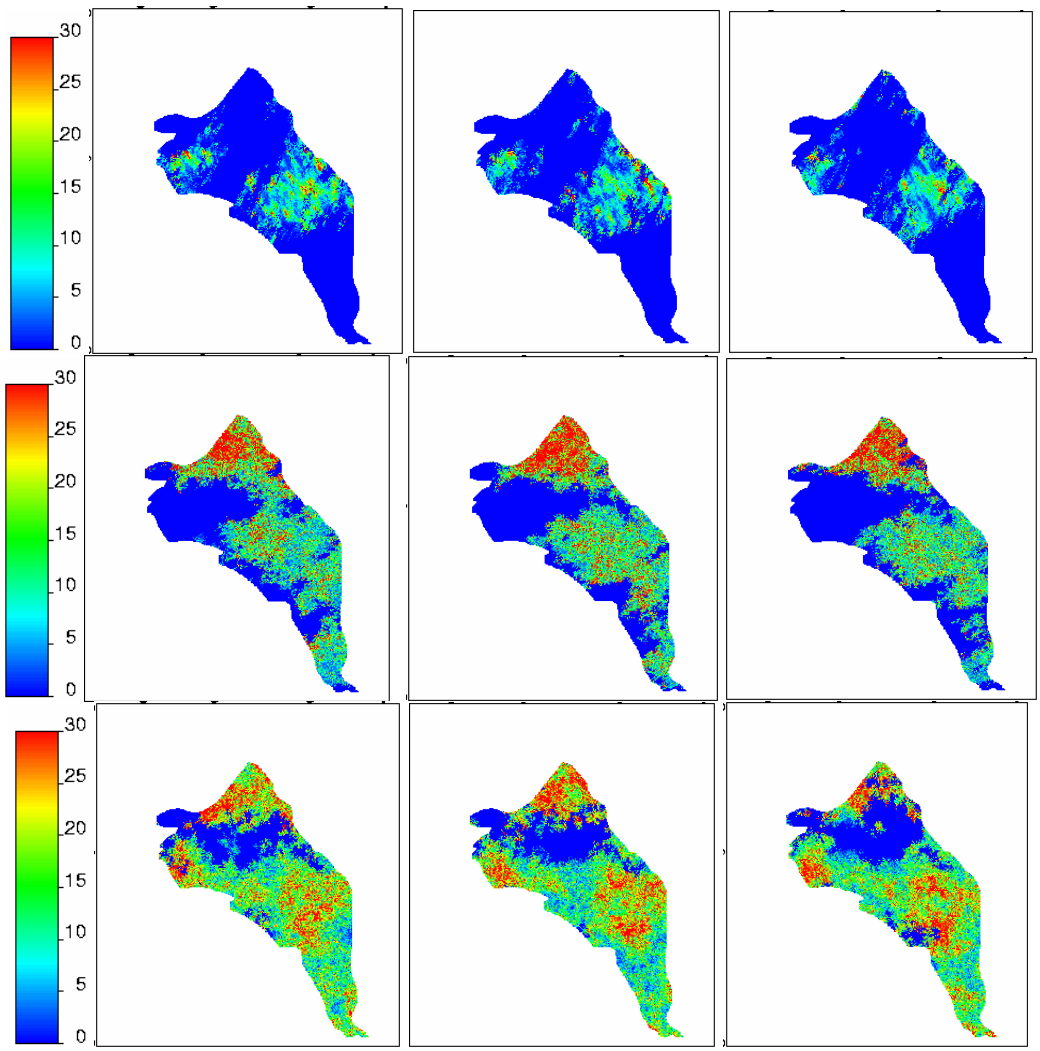

Figure 5.20. Three Merged Thickness Realizations (meters) for U4 (top), U6 (middle), and U8 (bottom)

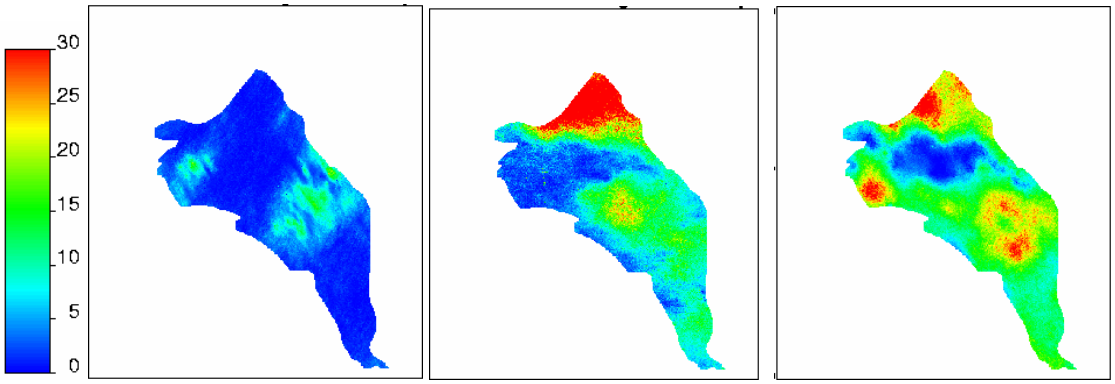

Figure 5.21. E-Type Thickness Maps (meters) Based on 100 Randomly Merged Realizations for U4 (left), U6 (middle), and U8 (right)

and separating the two consecutive mud layers (realizations) with a constant sand layer in between. Thus, a pseudo-3D geological structure consists of five layers; three are mud layers and two are separating sand/gravel layers. Because of the presence of a uniform sand layer between each mud layer, there is only a single connected sand/gravel body for each merged pseudo-3D realization. There are 132,651 (51 by 51 by 51) possible merged realizations based on the 51 realizations of each of the mud units. The merged pseudo-3D realizations have different amounts of total sand volume and varying tortuosity of the connected sand/gravel body, depending on the amount and interconnection of mud in the three layers. Again, the total net cell volume and the tortuosity of the geological body are the criteria used for ranking the merged pseudo-3D realizations.

It is possible to apply Deutsch's program for evaluating and ranking geological bodies, but it takes considerable time to accomplish, so modifications were made to Deutsch's program. The major modifications included using the net cell volume and tortuosity calculated on the two-dimensional (2D) presence/absence realizations of each of the three mud units to infer the net cell volume and tortuosity in the pseudo-3D models. Such modifications make the computation much faster yet lead to the same results calculated on the pseudo-3D models.

Table 5.9 lists the three highest, three lowest, and five medium conductive merged pseudo-3D realizations based on the average ranking of the total sand volume and the tortuosity of the connected sand body. The realization indexes of the three constructing mud units for the selected merged pseudo-3D realizations are also tabulated in Table 5.9. In Figure 5.22, the constructing mud unit realizations for the extreme merged realizations are plotted. The simplified 3D conceptual hydrogeologic models for the highest and the lowest conductive cases are constructed by merging the highest and lowest presence/absence mud realizations with the thickness of these three mud units and the other sand/gravel units taken from the basic hydrogeologic model. To retain the overall thickness of the sedimentary layer, the thickness of neighboring layers is slightly modified. The results of this procedure for a single east-west cross section are presented in Figure 5.23. The difference in obtained structures is visible.

Table 5.9. Rank of Merged Pseudo-3D Realizations and Realization Index of Constructing Mud Units

#Rank	#Realization of U4	#Realization of U6	#Realization of U8
1	12	44	27
2	12	49	9
3	42	49	31
66324	36	4	51
66325	29	26	6
66326	39	39	11
66327	51	46	49
66328	50	30	10
132649	3	51	26
132650	3	51	19
132651	3	35	19

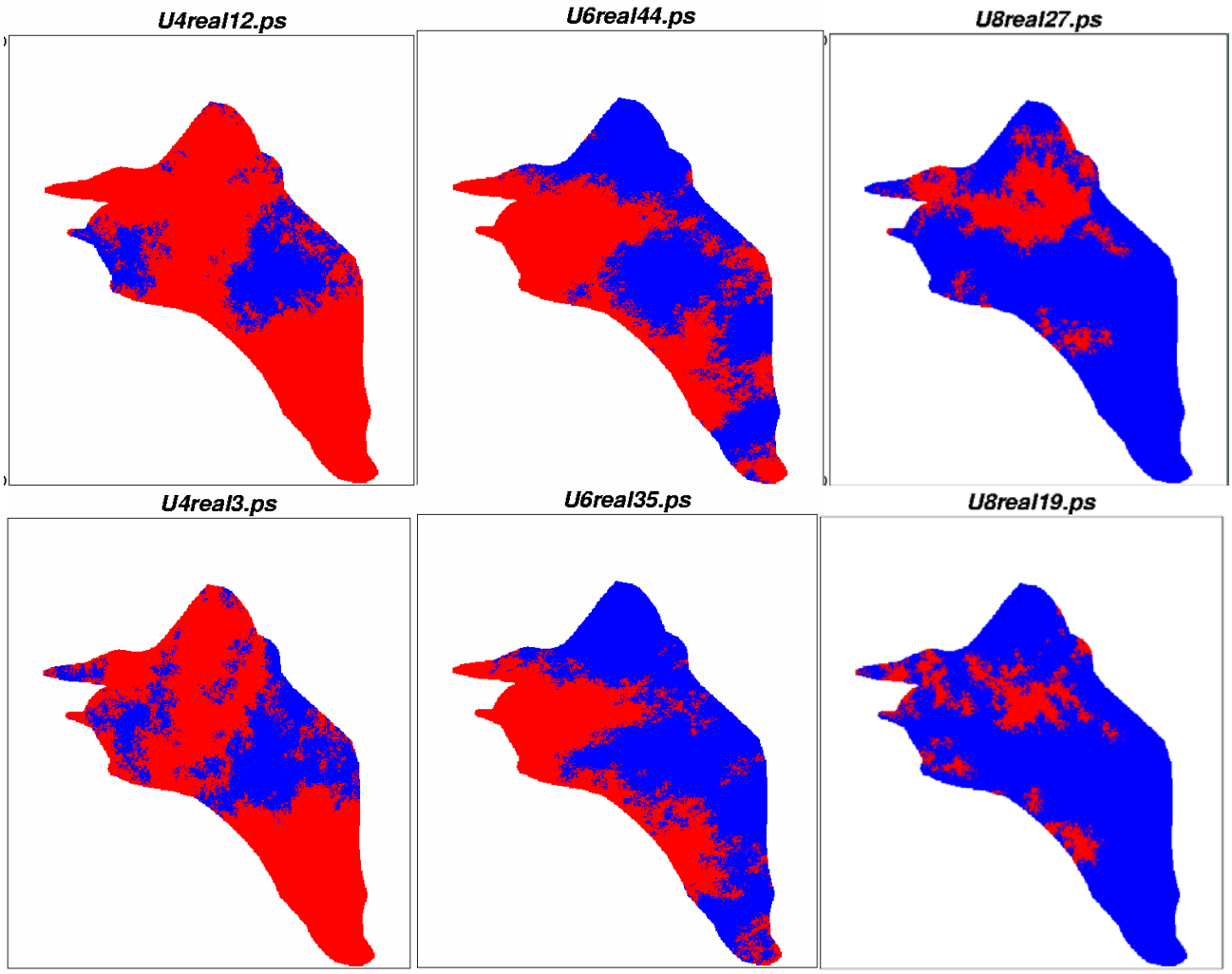

Figure 5.22. Constructing Mud Unit Realizations for the Highest (top) and Lowest (bottom) Conductive Merged Pseudo-3D Realizations

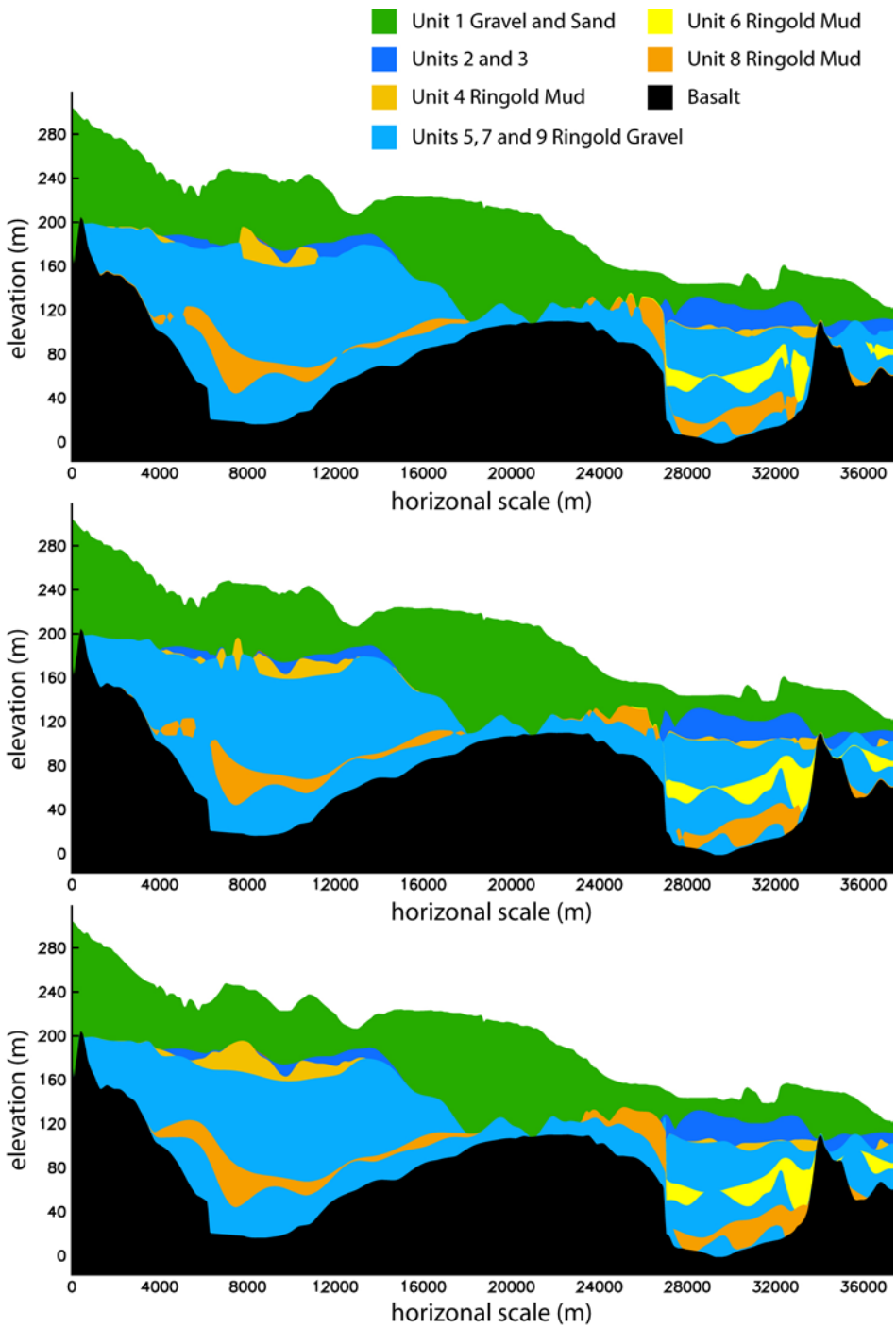

Figure 5.23. Cross Sections of Hydrogeologic 3D Structures with the Lowest (top) and the Highest (middle) Conductivity Compared with the Base Case (bottom) (cross section location is B-B' on Figure 3.17)

5.2.6 Future Needs—Joint Simulation of Mud Units

In this work, the following approach was applied to the simulation of the mud units:

- create a binary presence/absence model and a thickness model for each of the mud units independently
- merge the binary presence/absence model and the thickness model of each mud unit to get the complete model for each mud unit
- combine all three mud units with the sand/gravel units to get the final 3D geological structure models.

Although this is a relatively simple way to construct an alternative conceptual geological model of the mud unit distribution for the Hanford Site, there is room for improvement in evaluating the geological structure uncertainties. The current approach simulates the presence/absence and thickness of each mud unit independently, which has several drawbacks. For example, combining binary presence/absence and thickness models of a mud unit may show an unrealistically steep change or discontinuity in mud unit thickness. The combination of three independently simulated mud units may result in inconsistencies between the overall simulated thickness and the total thickness constrained by the top and bottom of the total Ringold thickness. Although post-processing could be developed to adjust the unit thickness to retain the overall thickness of the sedimentary layer, there is no accepted reasoning to support this. Usually geological dependence exists between the geological units and joint simulation approaches, allowing this dependency to be integrated and 3D models directly generated, should lead to better models of geological structure. Future studies will investigate methods for developing dependent simulations of the mud unit thicknesses.

5.3 Planned Inverse Modeling of Stochastic ACMs

Inverse model runs to date have developed estimates of flow parameters given a predetermined model structure (the geometries of model layers and parameter zones within layers). The inverse model framework allows characterization of the predictive uncertainty associated with uncertain parameter estimates but does not address directly the uncertainty associated with potential errors in the assumed model structure (Cole et al. 2002). It is increasingly recognized that errors in model conceptualization can be large relative to parameter uncertainty and that attention should be given to their quantification (e.g., Gaganis and Smith 2001; Dagan 2002).

Two primary methods have been used in stochastic analyses of model uncertainty (e.g., Dagan 2002), Monte Carlo simulation and first-order approximation in log-conductivity variance. Monte Carlo simulation is more general (not limited to multi-Gaussian models with weak heterogeneity) and is well suited to situations in which multiple alternative realizations of a model and its parameters can be generated. However, it is computationally intensive, requiring the numerical solution of a large number of alternative flow (and perhaps transport) models to obtain probabilistic distributions of model predictions. The stochastic ACMs described above represent random selections from a range of possible model structures that are consistent with available observations and therefore are amenable to Monte Carlo analysis. Within the inverse model framework, however, the computational requirements are further expanded because a single inverse run requires many forward flow model runs. The number of runs required is given by

$$N_{runs} = (N_p+1)(N_i+1)$$

where N_p is the number of parameters being estimated (usually 10 to 15) and N_i is the number of iterations required to converge to a solution in the inverse model process (generally on the order of 10). Each forward run takes approximately three hours of computer time, so even using multiple networked PCs a single inverse model run takes on the order of 30 hours to complete. Therefore, full inverse analysis of the large number of combinations of stochastic alternative mud geometry and layer-one zonation models is not computationally feasible. Therefore, the planned inverse analysis of the stochastic ACMs will follow a strategy consisting of two parts:

- Full inverse modeling of selected realizations based on the ranking analysis described above combined with limited forward modeling.
- Implementation of the UCODE/CFEST inverse modeling framework on the DOE Science Grid using Globus technology to enhance computational capabilities.

These planned efforts are described in the following sections.

5.3.1 Full Inverse Modeling of Selected Realizations

Because it is computationally infeasible to perform full inverse model evaluation of a large number of stochastic ACMs, it is desirable to identify a selected number of ACMs that represent the potential range in flow model predictions (and accordingly, the potential range of model parameters estimated by the inverse process). A process used to rank the stochastic ACMs according to the connectedness of sand bodies in the various realizations has already been described above. A two-step process will be applied to those ranked realizations to identify a limited number (less than 10) of candidates for full inverse analysis.

The first step is to test the validity of the current ranking in terms of actual flow predictions. In this step, a somewhat larger number of realizations (perhaps 20) will be selected that span the range of rankings (i.e., some low ranking, some medium ranking, and some high ranking). Each of these will be used as the basis for a single forward prediction of flow, and the predicted transient heads compared with the observation set to quantify goodness of fit. Because each of the realizations represents only the model structure (not the actual parameters) and we are not performing full inverse analysis at this stage, we will use the best-estimate parameters from the ACM-3 inverse results to parameterize each forward run. The rankings of the selected realizations, in terms of the weighted sum-of-squared-errors metric, will be compared with the previous rankings of the same realizations according to sand-body connectedness. If a correlation is evident between the two rankings, the initial rankings can be assumed to be representative of the realization ordering in terms of flow and transport behavior. If not, greater weight will be ascribed to the ranking according to flow and transport prediction. In either case, a smaller number of realizations (initially three, then more if computational facilities allow) will be selected for full inverse analysis: two extremes (high and low rank) and one central (median rank).

Once the subject realizations have been selected, a full inverse analysis will be performed for each to identify optimal parameter sets. This will allow us to assess the sensitivity of estimated model parameters to assumed model geometry. Any issues that arise during the course of the inverse analyses (e.g., parameters that become insensitive or unreasonable estimates) will be documented and thoroughly explored. Initially, three realizations will be subjected to full inverse analysis; if computational time allows, additional analyses will be performed using realizations with intermediate rankings.

5.3.2 Globus Implementation on the DOE Science Grid

The computational challenges of large-scale inverse analysis remain formidable despite significant increases in computational power gained through the implementation of the local PC cluster. An alternative approach that offers promise is the development of virtual clusters of computational nodes using grid technologies such as those being developed under DOE initiative (http://doesciencegrid.org/). These technologies offer the capability to efficiently access large- and small-scale computing systems distributed across organizations.

Through collaboration with EMSL researchers and developers, we have begun implementing the CFEST/UCODE inverse modeling framework on the DOE Science Grid using the Globus Toolkit. Globus provides the software tools that support grid-based applications, and the Globus Toolkit was recently named as one of the top 100 technologies of 2002 by R&D magazine. The grid implementation of CFEST/UCODE is designed so the user can specify whether to run the inverse on the local cluster or on the Science Grid using a keyword line in the "fn.uni" file (the primary input file controlling UCODE execution). If execution on the Science Grid is specified, additional lines provide grid access information (account authentication) and specify the resource on which the run is to be performed.

To date, limited CFEST/UCODE runs have been successfully run on a multiprocessor computer system at PNNL, and full runs are being tested in preparation for testing on remote systems at NERSC (National Energy Research Scientific Computing Center at Lawrence Berkeley Laboratory).

Upon completion of development and testing, the potential for execution of CFEST/UCODE inverse runs on the Science Grid provides the computational basis for a much larger number of inverse runs (e.g., full inverse analysis of additional stochastic ACMs) as well as inverse runs with larger numbers of estimated parameters (e.g., refined zonations).

5.3.3 Optimal Parameter Zonation Studies

The approach described above is based on Monte Carlo simulation of alternative realizations of the model structure (layer and zonal geometries), which are then subsequently subjected to inverse analysis. A preferable approach would be to directly incorporate the model structure into the inverse process such that optimal parameter zonations and layer geometries could be identified. This is a complex undertaking and is the subject of current research (e.g., Sun et al. 1998; 2002). One of the key issues is how to parameterize and constrain the model geometry.

We are planning to undertake some numerical experiments to address this issue during FY 2003. These will be based on the premise that the spatial pattern of model residuals (differences between predicted and observed heads) reflects information about the underlying geometry of geologic units and facies that can be used to guide selection of parameter zonations.

For these studies, we will use the final inverse parameterization and model geometry of the ACM-3 inverse results as the "true" parameter distribution. A forward simulation will be performed using that model, and "observed" heads at selected locations and times will be stored. Then we will undertake an inverse modeling exercise with the goal of identifying the proper zonation of Unit 1 (Hanford Fm). Steps in this exercise will be as follows:

Start with the entire Unit 1 as a single zone (with single values of relevant model parameters, e.g., hydraulic conductivity, specific yield).

1. Perform an inverse run to identify optimal parameters given the assumed zonation.
2. Examine the resulting spatial pattern of residuals, in conjunction with the known "true" zonation, to identify rules for sequential refinement of the parameter zones.
3. Refine the parameter zones according to the identified rules.
4. Repeat steps 2-4 until improvement in the objective function is small.
5. Compare final estimated zonation with the "true" zonation to determine the effectiveness of the procedure.

Once reliable rules have been established for a single case, these rules will be tested using other assumed parameter distributions and geometries, to evaluate the generality of the rules so obtained. Upon successful completion of this task, the systematic refinement of zonation will be applied to the actual field data (real head observations) to identify optimal zonation of Unit 1 for the Hanford SGM.

6.0 Summary and Conclusions

The primary objective of this inverse modeling effort was to document model modifications and upgrades that have been incorporated into ACM-2, summarize results from the ACM-2 inverse modeling effort, provide a comparison with ACM-1 results, and develop the approach and implementation methodology for the generation and inverse modeling of stochastic alternative conceptual models.

The ACM-2 transient inverse model was developed to test an alternative conceptual model of the SGM that incorporates modifications that were identified for investigation based on knowledge gained during previous inverse calibration efforts. Primary modifications that were made to ACM-2, include 1) facies-based zonation of Units 1 (Hanford) and 5 (middle Ringold), 2) implementation of an improved approach for handling run-on recharge from upland areas (Cold Creek, Dry Creek, Rattlesnake Springs) based on watershed modeling results, 3) adoption of an improved approach for representing artificial discharges from site operations based on the Site Assessment Capabilities (SAC) methodology, and 4) minor modifications to the geologic conceptual model.

An overall comparison of simulated and measured water levels indicated that, over the entire prediction period, reasonable overall model fit was realized for ACM-2 inverse model. Residual error statistics indicate that 65.8 percent of the simulated values were within ±1 m of measured values and 98.9 percent were within ±5 m. The overall mean residual was 0.06 m (-0.82 m for 39,264 negative residuals and 1.19 m for 30,511 positive residuals). The residual values ranged from –7.39 m to 9.38 m, and the total sum of squared residuals was 1.40×10^5 m^2. Comparison of residual error statistics generally indicates an improvement in model fit for ACM-2 relative to ACM-1d. The sum of squared residuals for ACM-2 was 1.08×10^5, a 9% reduction from the sum of squared residuals for the ACM-1d inverse model, which was 1.19×10^5. In addition to the overall increase in the goodness of fit for ACM-2, there are advantages associated with moving the Hanford groundwater model to a more technically defensible, hydrogeologically based conceptual model and eliminating past reliance on a questionable transmissivity distribution developed during early two dimensional steady state inverse calibration efforts.

The best-fit estimates for hydraulic conductivity of the various facies-based zones composing the Hanford (Unit 1) and Ringold formations (Unit 5 only) were in general well within the reasonable range of previous estimates. For the Hanford formation, the highest-conductivity materials were in the coarse-grained sediments in the eastern portion of the 200 East Area and in the gap between Gable Mountain and Gable Butte. The hydraulic conductivity of these materials was estimated to be 4,400 to 37,000 m/d. The estimated hydraulic conductivity for the predominant gravel facies of the Hanford formation was 190 m/d and for the less extensive clean sand facies of the Hanford formation 260 m/d. The estimated hydraulic conductivity for the pre-Missoula gravels (Unit 3) was 32 m/d. For the Ringold Formation, hydraulic conductivity for the predominant facies of Unit 5, which is present across much of the 200 Area plateau, was 3.0 m/d. The estimated hydraulic conductivity for a more permeable facies in the southwest portion of the 200 Area plateau and throughout the 100 Areas was 10 m/d. The highest-conductivity materials within the Ringold Formation were associated with facies dominated by alluvial fan deposits along the western edge of the Pasco Basin, within the Cold Creek and Dry Creek recharge areas. The estimated hydraulic conductivity for these facies ranged from 110 to 390 m/d.

Based on previous work, the specific yield for the Hanford formation (Unit 1) is estimated to range from about 0.1 to 0.3 and is expected to be higher for coarse, well-sorted gravel than for poorly sorted mixtures of sand and gravel. Specific yields of the poorly sorted sediments of the Ringold Formation are estimated to range from 0.05 to 0.2. Based on these estimated ranges, the specific yield values used in the ACM-2 inverse were initially set to 0.10 for the Ringold Unit 5 and pre-Missoula gravel formations and 0.25 for the Hanford formation. The ACM-2 inverse was generally insensitive to all tested specific yield parameter values and thus only relatively small (i.e., <10%) adjustments were made to these parameters.

The ACM-2 transient inverse model provided reasonable estimates of flux at the various flow-system boundaries. The flow system is bounded by the Columbia River on the north and east and by the Yakima River and basalt ridges on the south and west, respectively. The Columbia River, which represents a point of regional discharge for the unconfined aquifer system, was estimated to receive a time-weighted average discharge of 86,600 m^3/d. In addition to this discharge boundary, ACM-2 incorporates several other flux boundaries, the majority of which are recharge boundaries but in some cases also included small components of discharge. The time-weighted average recharge flux supplied by each of these boundaries is 890 m^3/d for areally distributed basalt leakage, 220 m^3/d for increased leakage at the erosional window, 970 m^3/d for increased leakage at thrust faults, 23,500 m^3/d for natural surface recharge, 54,400 m^3/d for run-on recharge from upland areas along the western model boundary, and 6,460 m^3/d for artificial recharge associated with wastewater disposal activities from Hanford operations.

Geostatistical modeling of the Unit 1 zonation was performed using categorical indicator simulation methods, which appear to work quite well. The map of the most probable facies produced from the full suite of simulations is similar to hand-drawn geologic maps of the Unit 1 zonation produced by Site hydrogeologists. However, the realizations provide a wealth of information that cannot be provided by the hand-drawn maps; e.g., the probability that a facies is present can be estimated by the relative frequency with which a facies is simulated at a given location. In addition, the individual realizations were ranked using measures of the connectivity of high-conductivity facies. Once the ranking method has been verified by performing forward simulations for a subset of the simulations, the ranking will be used to identify a suite of simulations that provide a sampling of the variability in transport properties caused by spatial uncertainty in the Unit 1 zonation. That suite of simulations, which will include realizations with extremely rapid and slow transport rates, will then be examined further using inverse methods to determine the effect of spatial uncertainty in the Unit 1 zonation on parameter uncertainty.

The geostatistical studies also produced simulations of the presence/absence and thickness of mud units 4, 6, and 8 in the Ringold Formation. The mud units are expected to exert a major influence on transport, especially vertical transport. The presence/absence simulations provide valuable information on the possible presence of "holes" in the mud units that might allow vertical movement of contaminants into lower portions of the unconfined and confined aquifers at the Site. Rankings of the merged presence/absence simulations for the three mud units together provide preliminary estimates of the continuity of aquifer sand and gravel in the Ringold Formation at the Site. The mud thickness simulations also provide valuable information on the spatial variability of the mud units. However, additional work is needed to identify methods that can be used to generate dependent simulations of the thickness of the three mud units.

The ACM-2 model is the first attempt to fully incorporate the facies-based approach for representing the hydrogeologic structure of the model and it is expected that further refinement of this distribution and

additional improvements to overall model fit will be realized during future inverse simulations of groundwater flow and transport. These future efforts will be based in large part on the geostatistical methods discussed above which can be used to provide sets of realizations that quantify the spatial uncertainty in the hydrogeological structure.

7.0 References

Ahlstrom SW, HP Foote, RC Arnett, CR Cole, and RJ Serne. 1977. *Multicomponent Mass Transport Model: Theory and Numerical Implementation* (Discrete-Parcel-Random-Walk Version). BNWL-2127, Battelle Northwest, Richland, WA.

Akaike H. 1974. "A New Look at Statistical Model Identification." *IEEE Trans. Automat. Contr*. AC-19, 716-722.

Akaike H. 1977. *On Entropy Maximization Principle, in Applications of Statistic.* PR Krishnaiah, ed. North-Holland, Amsterdam, pp-27-41.

Anderman ER, MC Hill, and EP Poeter. 1996. "Two-dimensional advective transport in groundwater flow parameter estimation." *Ground Water*, 34(6):1001–1009.

Beck JV and KJ Arnold. 1977. *Parameter Estimation in Engineering and Science*. John Wiley & Sons, New York.

Bierschenk WH. 1959. *Aquifer Characteristics and Ground-Water Movement at Hanford.* HW-60601, General Electric Company, Hanford Atomic Products Operation, Richland, WA

Brown RE and HG Ruppert. 1950. *The Underground Disposal of Liquid Waste at the Hanford Works, Washington*. HW-17088, General Electric Hanford Company, Richland, WA.

Carle, SF, EM Labolle, GS Weissman, D. Van Brocklin, and GE Fogg. 1998. "Conditional simulation of hydrofacies architecture: A transition probability/Markov approach." *Uses of Sedimentologic and Stratigraphic Information in Predicting Reservoir Heterogeneity,* GS Fraser and JM Davis, eds., Tulsa, OK. SEPM (Society for Sedimentary Geology), pp. 147-170.

Carrera J and SP Neuman. 1986a. "Estimation of aquifer parameters under transient and steady-state conditions." *Water Resources Research*, 22(2):199–242.

Carrera J and SP Neuman. 1986b. "Estimation of aquifer parameter under transient and steady state conditions: 1. Maximum likelihood method incorporating prior information." *Water Resources Research*, 22(2):199-210.

Cearlock DB, KL Kipp, and DR Friedrichs. 1975. *The Transmissivity Iterative Calculation Routine - Theory and Numerical Implementation.* BNWL-1706, Battelle Northwest, Richland, WA.

Chamness MA and JK Merz. 1993. *Hanford Wells.* PNL-8800, Pacific Northwest Laboratory, Richland, WA.

Cole CR, FW Bond, SM Brown, and GW Dawson. 1984. *Demonstration/Application of Ground-Water Modeling Technology for Evaluation of Remedial Action Alternatives.* Contract 68-03-3116, Municipal Environmental Research Laboratory, U. S. Environmental Protection Agency, Cincinnati.

Cole CR, SB Yabusaki, and CT Kincaid. 1988. *CFEST-SC, Coupled Fluid, Energy, and Solute Transport Code, SuperComputer Version, Documentation and User's Manual.* Battelle, Pacific Northwest Laboratories, Richland, WA.

Cole CR, SK Wurstner, MP Bergeron, MD Williams, and PD Thorne. 1997. *Three-Dimensional Analysis of Future Groundwater Flow Conditions and Contaminant Plume Transport in the Hanford Site Unconfined Aquifer System: FY 1996 and 1997 Status Report.* PNNL-11801, Pacific Northwest National Laboratory, Richland, WA.

Cole CR, MP Bergeron, SK Wurstner, PD Thorne, S Orr, and MI McKinley. 2001a. *Transient Inverse Calibration of Hanford Site-Wide Groundwater Model to Hanford Operational Impacts—1943 to 1996*. PNNL-13447, Pacific Northwest National Laboratory, Richland, WA.

Cole CR, MP Bergeron, CJ Murray, PD Thorne, SK Wurstner, and PM Rogers. 2001b. *Uncertainty Analysis Framework - Hanford Site-Wide Groundwater Flow and Transport Model*. PNNL-13641, Pacific Northwest National Laboratory, Richland, WA.

Cole CR, TD Scheibe, VR Vermeul, SK Wurstner, PD Thorne, VL Freedman, CJ Murray, and MP Bergeron. 2002. "Identification of Errors in the Hanford Site-Wide Groundwater Flow Model by Inverse Modeling of Alternative Conceptual Models." *Eos Trans. AGU*, 83(47), *Fall Meet. Suppl*. Poster presented by T Scheibe at 2002 AGU Fall Meeting, San Francisco.

Connelly MP. 1994. *Capture Zone Analyses for the 200-ZP-1 and 200-UP-1 Pilot Scale Pump-and-Treat Tests.* WHC-SD-EN-TI-252, Westinghouse Hanford Company, Richland, WA.

Connelly MP, BH Ford, and JV Borghese. 1992a. *Hydrogeologic Model for the 200 West Groundwater Aggregate Area.* WHC-SD-EN-TI-014, Westinghouse Hanford Company, Richland, WA.

Connelly MP, BH Ford, and JW Lindberg. 1992b. *Hydrogeologic Model for the 200 East Groundwater Aggregate Area.* WHC-SD-EN-TI-019, Westinghouse Hanford Company, Richland, Washington.

Cooley RL. 1977. "A method of estimating parameters and assessing reliability for models of steady-state groundwater flow, 1, Theory and numerical properties." *Water Resources Research*, 13(2):318–324.

Cooley RL. 1993. "Regression modeling of ground-water flow." Supplement 1 – *Modifications to the computer code for nonlinear regression solution of steady-state ground-water flow problems.* U.S Geological Survey Techniques of Water Resources Investigations, Book 3, Ch. B4, Supp. 1, p.8.

Cooley RL and RL Naff. 1990. *Regression modeling of groundwater flow.* U.S. Geological Survey Techniques in Water Resources Investigations, Book 3, Ch. B4, p. 232.

Crowley WH and RK Ledgerwood. 1988. *Borehole status chart and location maps*. SD-BWI-DP-044 Rev. 0, Westinghouse Hanford Company, Richland, WA.

Dagan G. 2002. "An overview of stochastic modeling of groundwater flow and transport: From theory to applications." *EOS Trans*. AGU, 83(53):621-625.

D' Agnese FA, CC Faunt, AK Turner, and MC Hill. 1998. *Hydrogeologic evaluation and numerical simulation of the Death Valley regional groundwater flow system, Nevada and California*. U.S. Geological Survey Water-Resource Investigation Report 96-4300, Water Resource Division, Denver.

Deju RA. 1974. *The Hanford Field Testing Program.* ARHC-00004-201, Atlantic Richfield Hanford Company, Richland, WA.

Deutsch CV. May 1989. "DECLUS: A FORTRAN 77 Program to Determine Optimum Spatial Declustering Weights." *Computers and Geosciences*, 15(3):325-332.

Deutsch CV. 1998a. "Cleaning Categorical Variable (Lithofacies) Realizations with Maximum A-Posteriori Selection." *Computers & Geosciences*, 24(6):551-562.

Deutsch CV. 1998b. "FORTRAN Programs for Calculating Connectivity of 3-D Numerical Models and for Ranking Multiple Realizations." *Computers & Geosciences*, 24(1):69-76.

Deutsch CV and AG Journel. 1998. *GSLIB: Geostatistical Software Library and User's Guide*. Oxford University Press, New York.

Devary JL. 1987. *The CFEST-INV Stochastic Hydrology Code: Mathematical Formulation, Application, and User's Manual.* ICF Northwest, Richland, WA.

DOE (see U.S. Department of Energy)

Doherty J. 1994. *PEST: Corinda, Australia*. Watermark Computing, p. 122.

Dove FH, CR Cole, MG Foley, FW Bond, RE Brown, WJ Deutsch, MD Freshley, SK Gupta, PJ Gutknecht, WL Kuhn, JW Lindberg, WA Rice, R Schalla, JF Washburn, and JT Zellmer. 1982. *AEGIS Technology Demonstration for a Nuclear Waste Repository in Basalt.* PNL-3632, Pacific Northwest Laboratory, Richland, WA.

Drost BW, SE Cox, and KM Schurr. 1997. *Changes in Groundwater Levels and Groundwater Budgets, from Predevelopment to 1986, in Parts of the Pasco Basin, Washington*. Water Resources Investigations Report 96-4086, U.S. Geological Survey in cooperation with the Washington State Department of Ecology, Tacoma.

Early TO, SH Hall, and VG Johnson. February 1988. "Tritium, carbon-14, and iodine-129 as indicators for localized vertical recharge along an anticline in the Columbia River basalts using a decay-corrected mixing model." *Proceedings of the Groundwater Geochemistry Conference*, pp. 597-620. National Water Well Association, Denver.

Ebbert JC, SE Cox, BW Drost, and KM Shurr. 1993. Distribution and Sources of Nitrates, and Presence of Fluoride and Pesticides, in Parts of the Pasco Basin, Washington, 1986-88. Water Resources Investigations Report 93-4197, U.S. Geological Survey, Tacoma, WA.

Evans JC, DI Dennison, RW Bryce, PJ Mitchell, DR Sherwood, KM Krupka, NW Hinman, EA Jacobson, and MD Freshley. 1988. *Hanford Site Groundwater Monitoring for July Through December 1987.* PNL-6315-2, Pacific Northwest Laboratory, Richland, WA.

Fayer MJ and TB Walters. 1995. *Estimated Recharge Rates at the Hanford Site.* PNL-10285, Pacific Northwest Laboratory, Richland, WA.

Foley MG, DJ Bradley, CR Cole, JP Hanson, KA Hoover, WA Perkins, and MD Williams. 1995. *Hydrogeology of the West Siberian Basin and Tomsk Region.* PNL-10585, Pacific Northwest Laboratory, Richland, WA.

Forsythe GE and EG Strauss. 1955. "On best conditioned matrices*." Proceedings of American Mathematical Society,* 10(3):340–345.

Freshley MD and MJ Graham. 1988. Estimation of Groundwater Travel Time at the Hanford Site: Description, Past Work, and Future Needs. PNL-6328, Pacific Northwest Laboratory, Richland, WA.

Friedrichs DR, CR Cole, and RC Arnett. 1977. *Hanford Pathline Calculational Program—Theory, Error Analysis and Applications.* ARH-ST-149, Atlantic Richfield Hanford Company, Richland, WA.

Gaganis P and L Smith. 2001. "A Bayesian approach to the quantification of the effect of model error on the predictions of groundwater models." *Water Resources Research*, 37(9): 2309-2322.

Gale J, R Macleod, J Welhan, CR Cole, and LW Vail. 1987. *Hydrogeological Characterization of the Stripa Site.* Technical Report 87-15, SKB, Stockholm, Sweden.

Gee GW, MJ Fayer, ML Rockhold, and MD Campbell. 1992. "Variations in Recharge at the Hanford Site." *NW Sci.* Vol. 66, pp. 237–250.

Goovaerts, P. 1997. *Geostatistics for Natural Resources Evaluation:* Oxford University Press, New York.

Graham MJ, MD Hall, SR Strait, and WR Brown. 1981. *Hydrology of the Separations Area.* RHO-ST-42, Rockwell Hanford Operations, Richland, WA.

Graham MJ, GV Last, and KR Fecht. 1984. *An Assessment of Aquifer Intercommunication in the B Pond-Gable Mountain Pond Area of the Hanford Site*. RHO-RE-ST-12 P, Rockwell Hanford Operations, Richland, WA.

Gupta SK. 1997. Draft User's Manual, CFEST-96 Flow and Solute Transport, Constant/Variable Density, Computationally Efficient, and Low Disk PC/Unix Version. Consultant for Environmental System Technologies, Irvine, CA.

Gupta SK, CR Cole, CT Kincaid, and AM Monti. 1987. *Coupled Fluid, Energy, and Solute Transport (CFEST) Model: Formulation and User's Manual.* BMI/ONWI-660, Battelle Memorial Institute, Columbus, OH.

Hannan ES. 1980. "The Estimation of the Order of an ARMA Process." *Ann. Stat*. 8, pp. 1071-1081.

Hartman MJ and KA Lindsey. 1993. *Hydrogeology of the 100-N Area, Hanford Site, Washington.* WHC-SD-EN-EV-027, Westinghouse Hanford Company, Richland, WA.

Hartman MJ, LF Morasch, and WD Webber. 2001. *Hanford Site Groundwater Monitoring for Fiscal Year 2000.* PNNL-13404, Pacific Northwest National Laboratory, Richland, WA.

Hill MC. 1992. *A computer program (MODFLOWP) for estimating parameters of a transient, three-dimensional, groundwater flow model using nonlinear regression.* U.S. Geological Survey Open-File Report 91-48, p. 358.

Hill MC. 1994. *Five Computer Programs for Testing Weighted Residuals and Calculating Linear Confidence and Prediction Intervals on Results from the Groundwater Computer Program MODFLOWP.* U.S. Geological Survey Open-File Report 93-481, p. 81.

Hill MC. 1998. "Methods and Guidelines for Effective Model Calibration." *Water Resource Investigations*. Report 98-4005, U. S. Geological Survey, Water Resources Division, Denver.

Hill MC, RL Cooley, and DW Pollack. 1998. "A Controlled Experiment in Ground-water Flow Model Calibration." *Groundwater* 36(3):520-535.

Hill MC, RL Cooley, E Poeter, and C Teideman. 1999. *Ground-Modeling Short Courses: Calibration and Uncertainty in Groundwater Models.* International Groundwater Modeling Center, Colorado School of Mines, Golden.

Isaaks EH and RM Srivastava. 1989. *An Introduction to Applied Geostatistics.* Oxford University Press, New York.

Jacobson EA. 1985. *A Statistical Parameter Estimation Method Using Singular Value Decomposition with Application to Avra Valley Aquifer in Southern Arizona.* Dissertation, Department of Hydrology and Water Resources, University of Arizona, Tucson.

Jacobson EA and MD Freshley. 1990. *An Initial Inverse Calibration of the Groundwater Model for the Hanford Unconfined Aquifer.* PNL-7144, Pacific Northwest Laboratory, Richland, WA.

Jensen EJ. 1987. An Evaluation of Aquifer Intercommunication Between the Unconfined and Rattlesnake Ridge Aquifers on the Hanford Site. PNL-6313, Pacific Northwest Laboratory, Richland, WA.

Journel AG. 1983. "Nonparametric estimation of spatial distributions." *Mathematical Geology,* 15(3):445-468.

Kincaid CT, MP Bergeron, CR Cole, MD Freshley, N Hassig, VG Johnson, DI Kaplan, RJ Serne, GP Streile, DL Strenge, PD Thorne, LW Vail, GA Whyatt, SK Wurstner. 1998. *Composite Analysis for Low-Level Waste Disposal in the 200-Area Plateau of the Hanford Site*. PNNL-11800, Pacific Northwest National Laboratory, Richland, WA.

Kipp KL and RD Mudd. 1973. *Collection and Analysis of Pump Test Data for Transmissivity Values.* BNWL-1709, Battelle Northwest, Richland, WA.

Kipp KL, AE Reisenauer, CR Cole, and LA Bryan. 1972. *Variable Thickness Transient Groundwater Flow Model: Theory and Numerical Implementation.* BNWL-1703, Battelle Northwest, Richland, WA.

Levenberg K. 1944. "A Method for the Solution of Certain Non-Linear Problems in Least Squares." *Quart. Appl. Math* Vol. 2, pp 164-168.

Liikala TL. 1994. Hydrogeology Along the Southern Boundary of the Hanford Site Between the Yakima and Columbia Rivers, Washington. PNL-10094, Pacific Northwest Laboratory, Richland, WA.

Liikala TL and RL Aaberg. 1988. *Geohydrologic Characterization of the Area Surrounding the 183-H Solar Evaporation Basins*. PNL-6728, Pacific Northwest Laboratory, Richland, WA.

Lindberg JW. 1993a. *Geology of the 100-B/C Area, Hanford Site, South-Central Washington.* WHC-SD-EN-TI-133, Westinghouse Hanford Company, Richland, WA.

Lindberg JW. 1993b. *Geology of the 100-K Area, Hanford Site, South-Central Washington.* WHC-SD-EN-TI-155, Westinghouse Hanford Company, Richland, WA.

Lindberg JW and FW Bond. 1979. *Geohydrology and Ground-Water Quality Beneath the 300 Area, Hanford Site, Washington.* PNL-2949, Pacific Northwest Laboratory, Richland, WA.

Lindsey KA. 1991. *Revised Stratigraphy for the Ringold Formation, Hanford Site, South-Central Washington.* WHC-SD-EN-EE-004 Rev. 0, Westinghouse Hanford Company, Richland, Washington.

Lindsey KA. 1992. *Geology of the Northern Part of the Hanford Site: An Outline of Data Sources and the Geologic Setting of the 100 Areas.* WHC-SD-EN-TI-011 Rev. 0, Westinghouse Hanford Company, Richland, WA.

Lindsey KA. 1995. *Miocene- to Pliocene-Aged Suprabasalt Sediments of the Hanford Site, South-Central Washington.* BHI-00184, Bechtel Hanford, Inc., Richland, WA.

Lindsey KA and GK Jaeger. 1993. *Geologic Setting of the 100-HR-3 Operable Unit, Hanford Site, South-Central Washington.* WHC-SD-EN-TI-132, Westinghouse Hanford Company, Richland, WA.

Lindsey KA, BN Bjornstad, and MP Connelly. 1991. *Geologic Setting of the 200 West Area: An Update.* WHC-SD-EN-TI- 008, Westinghouse Hanford Company, Richland, WA.

Lindsey KA, BN Bjornstad, JW Lindberg, and KM Hoffman. 1992. *Geologic Setting of the 200 East Area: An Update.* WHC-SD-EN-TI-012, Westinghouse Hanford Company, Richland, WA.

Loaiciga HA and MA Marino. 1986. "Estimation and inference in the inverse problem." *Proceedings of Water Forum '86, World Water Issues in Evolution,* pp. 973–980. ASCE, Long Beach, CA.

McDonald, JP, MA Chamness, and DR Newcomer. 1999. *Water-Level Monitoring Plan for the Hanford Groundwater Monitoring Project.* PNNL-13021, Pacific Northwest Laboratory, Richland, WA.

Marquardt DW. 1963. "An algorithm for least-squares estimation of nonlinear parameters." *J. Soc. Indust. Appl. Math.* 11(2):431-441.

Neuman SP. 1999. "Methodology to Identify and Evaluate Conceptual Models and Uncertainty Related to Groundwater Transport at Nuclear Facilities and Sites." Draft report for U.S. Nuclear Regulatory Commission presented at Research Symposium: Hydrologic Conceptual Model and Parameter Uncertainty, July 25-26, 2000, Rockville, MD.

Neuman SP and S Yakowitz. 1979. "A Statistical Approach to the Inverse Problem of Aquifer Hydrology, 1, Theory." *Water Resour. Res.* 15(4):845–860.

Nevulis R, S. Sorooshian, and D. R. Davis. 1987. *Effects of Surface Waste Disposal Activity on Ground-water Levels in the Saddle Mountain Basalt.* Department of Hydrology and Water Resources, University of Arizona, Tucson.

Peck A, S Gorelick, G de Marsily, S Foster, and V Kovalevsky. 1988. *Consequences of Spatial Variability in Aquifer Properties and Data Limitations for Groundwater Modeling Practice*. IAHS Publication No. 175, International Association of Hydrological Sciences, IAHS Press. Institute of Hydrology, Wallingford, Oxfordshire, UK.

Peterson RE. 1992. *Hydrologic and Geologic Data Available for the Region North of Gable Mountain, Hanford Site, Washington.* WHC-SD-EN-TI-006, Westinghouse Hanford Company, Richland, WA.

Poeter EP and MC Hill. 1996. "Unrealistic parameter estimates in inverse modeling: a problem or a benefit for model calibration." *Proceedings of the ModelCARE 96 Conference*. International Association of Hydrological Sciences Publication no. 237, Golden, CO, p. 277-285.

Poeter EP and MC Hill. 1998. *Documentation of UCODE, A Computer Code for Universal Inverse Modeling.* U.S. Geological Survey Water Resources Investigations Report 98-4080.

Puget Sound Power and Light (PSPL). 1982. *Skagit/Hanford Nuclear Project, Preliminary Safety Analysis Report.* Appendix 20, Amendment 23, Puget Sound Power and Light Company, Bellevue, WA.

Richmond MC, WA Perkins, and Y Chien. 2000a. *Numerical Model Analysis of System-Wide Dissolved Gas Abatement Alternatives.* Final Report, prepared for U.S. Army Corps of Engineers, Walla Walla District under Contract DACW68-96-D-0002, Battelle Pacific Northwest Division, Richland, WA.

Richmond MC, WA Perkins, and Y Chien. 2000b. *Numerical Model Analysis of System-Wide Dissolved Gas Abatement Alternatives.* Appendix B, Model Configuration and Optimization. Report prepared for U.S. Army Corps of Engineers, Walla Walla District. Battelle Pacific Northwest Division, Richland, WA.

Richmond MC, WA Perkins, and Y Chien. 2000c. *Numerical Model Analysis of System-Wide Dissolved Gas Abatement Alternatives.* Appendix F. Verification of MASS1 for Lower Columbia/Snake Temperature and Total Dissolved Gas Simulation. Report prepared for U.S. Army Corps of Engineers, Walla Walla District. Battelle Pacific Northwest Division, Richland, WA.

Seber GAF and CJ Wild. 1989. *Nonlinear Regression.* John Wiley & Sons, New York.

Simmons CS, CT Kincaid, and AE Reisenauer. 1986. *A Simplified Model for Radioactive Contaminant Transport: The TRANSS Code.* PNL-6029, Pacific Northwest Laboratory, Richland, WA.

Spane FA Jr and VR Vermeul. 1994. *Summary and Evaluation of Hydraulic Property Data Available for the Hanford Site Upper Basalt Confined Aquifer System*. PNL-10158, Pacific Northwest Laboratory, Richland, WA.

Spane FA Jr and RG. Raymond. 1993. *Preliminary Potentiometric Map and Flow Dynamic Characteristics for the Upper-Basalt Confined Aquifer System.* PNL-8869, Pacific Northwest Laboratory, Richland, WA.

Strait SR and FA Spane. 1983. *Preliminary Results of Hydrologic Testing the Umtanum Basalt Fracture Zone at Borehole RRL-2*. SD-BWI-TI-89 Rev. 0, Rockwell Hanford Operations, Richland, WA.

Sun NZ. 1994. *Inverse problems in groundwater modeling*. Kluwer Academic Publishers, Boston, p. 337.

Sun NZ, S Yang, and WW Yeh. 1998. "A proposed stepwise regression method for model structure identification." *Water Resources Research*, 34(10): 2561-2572.

Sun N, W Yeh, and F Tsai. December 2002. "Model structure identification: From the reliability of model prediction to the robustness of experimental design." Poster presented at the 2002 Fall Meeting of the American Geophysical Union, San Francisco.

Swanson LC. 1992. *Phase 1 Hydrogeologic Summary of the 300-FF-5 Operable Unit, 300 Area.* WHC-SD-EN-TI-052, Westinghouse Hanford Company, Richland, WA.

Swanson LC. 1994. *1994 Characterization Report for the State Approved Land Disposal Site.* WHC-SD-CO18H-RPT-003, Westinghouse Hanford Company, Richland, WA.

Theil H. 1963. "On the use of incomplete prior information in regression analysis." *Amer. Stat. Assoc. J.* 58(302):401-414.

Thiem A. 1906. *Hydrologische Methoden*. J.M Gephardt, Leipzig, Germany.

Thorne PD and MA Chamness. 1992. *Status Report on the Development of a Three-Dimensional Conceptual Model for the Hanford Site Unconfined Aquifer System*. PNL-8332, Pacific Northwest Laboratory, Richland, WA.

Thorne PD and DR Newcomer. 1992. *Summary and Evaluation of Available Hydraulic Property Data for the Hanford Site Unconfined Aquifer System.* PNL-8337, Pacific Northwest Laboratory, Richland, WA.

Thorne PD, MA Chamness, FA Spane Jr, VR Vermeul, and WD Webber. 1993. *Three-Dimensional Conceptual Model for the Hanford Site Unconfined Aquifer System, FY 93 Status Report.* PNL-8971, Pacific Northwest Laboratory, Richland, WA.

Thorne PD, MA Chamness, VR Vermeul, QC MacDonald, and SE Schubert. 1994. *Three-Dimensional Conceptual Model for the Hanford Site Unconfined Aquifer System, FY 1994 Status Report.* PNL-10195, Pacific Northwest Laboratory, Richland, WA.

U.S. Department of Energy (DOE). 1988. *Consultation Draft, Site Characterization Plan, Reference Repository Location, Hanford Site, Washington*. DOE/RW-0164, Vol. 1 and 2, DOE Richland Operations Office, Richland, WA.

U.S. Department of Energy (DOE). 1991. *Description of Codes and Models to be Used in Risk Assessment.* DOE/RW-9144, DOE Richland Operations Office, Richland, WA.

U.S. Department of Energy (DOE). 2000. *Selection and Review of a Site-Wide Groundwater Model at the Hanford Site.* DOE/RL-2000-11, DOE Richland Operations Office, Richland, WA.

U.S. Department of Energy (DOE). 2002. *Standardized Stratigraphic Nomenclature for the Post-Ringold-Formation Sediments Within the Central Pasco Basin.* DOE/RL-2002-39 Rev. 0, Richland Operations Office, Richland, WA.

Walters WH, MC Richmond, and BG Gilmore. 1994. *Reconstruction of Radionuclide Concentrations in the Columbia River from Hanford, Washington to Portland, Oregon, January 1950–January 1971.* BNWD-2225 HEDR, Battelle Pacific Northwest Division, Richland, WA.

Wigmosta MS, B Nijssen, and P Storck. 2002. "Mathematical Models of Small Watershed Hydrology and Applications." Chapter 2 in *The Distributed Hydrology Soil Vegetation Model* 7-42, Water Resources Publications LLC.

Wigmosta MS, LW Vail, and DP Lettenmaier. 1994. A distributed hydrology vegetation model for complex terrain. *Water Resources Research* (30):1665-1679.

Vermeul VR, CR Cole CR, MP Bergeron, PD Thorne, and SK Wurstner. 2001. Transient Inverse Calibration of Site-Wide Groundwater Model to Hanford Operational Impacts from 1943 to 1996--Alternative Conceptual Model Considering Interaction with Uppermost Basalt Confined Aquifer. PNNL-13623, Pacific Northwest National Laboratory, Richland, WA.

Washington State Department of Ecology, U.S. Department of Energy, and U.S. Environmental Protection Agency. 1989. *Hanford Federal Facility Agreement and Consent Order Between the U.S. Environmental Protection Agency, the U.S. Department of Energy, and the State of Washington Department of Ecology.* May 15, 1989, as amended. Ecology, DOE, and EPA, Olympia, Seattle, and Richland, WA.

Wurstner SK and JL Devary. 1993. *Hanford Site Ground-Water Model: Geographic Information System Linkages and Model Enhancements FY 1993.* PNL-8991, Pacific Northwest National Laboratory, Richland, WA.

Wurstner SK and MD Freshley. 1994. *Predicted Impacts of Future Water Level Decline on Monitoring Wells Using a Groundwater Model of the Hanford Site.* PNL-10196, Pacific Northwest Laboratory, Richland, WA.

Wurstner SK, PD Thorne, MA Chamness, MD Freshley, and MD Williams. 1995. *Development of a Three-Dimensional Groundwater Model of the Hanford Site Unconfined Aquifer System: FY 1995 Status Report*. PNL-10886, Pacific Northwest Laboratory, Richland, WA.

Appendix

Water Table Elevations and Head Residuals from Simulation of Hanford Wastewater Discharges (1943–2000) Using ACM-2

A.1 Simulated Water Table Elevations

1943–2000

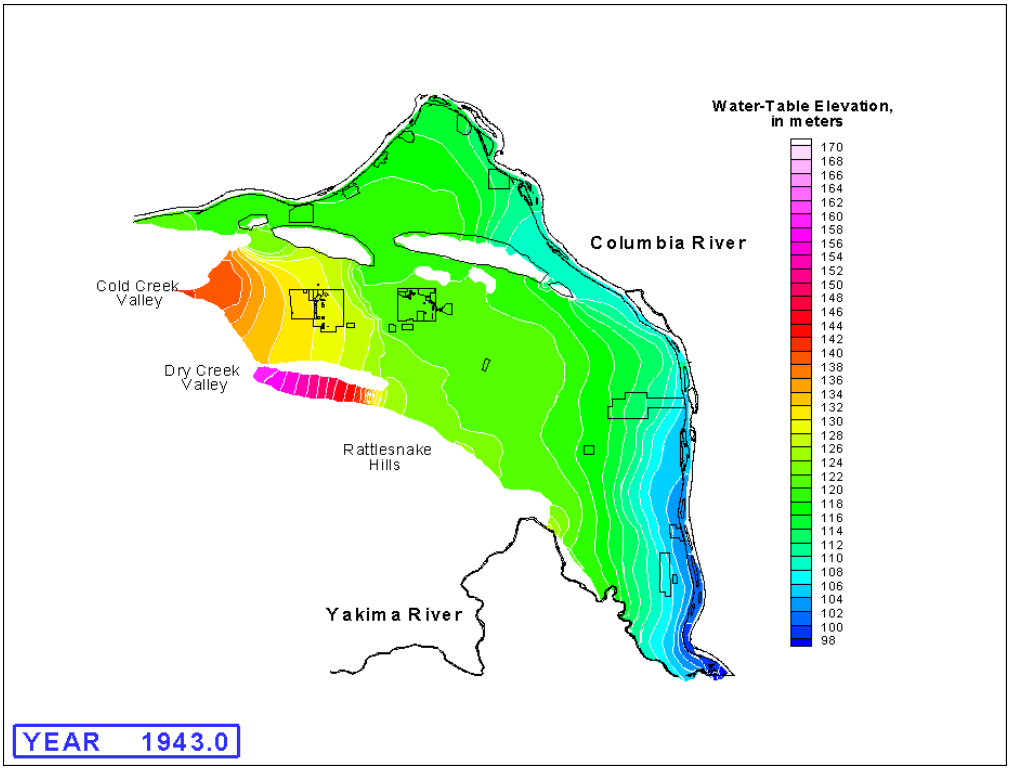

Figure A.1a. Simulated Water Table Elevations for 1943

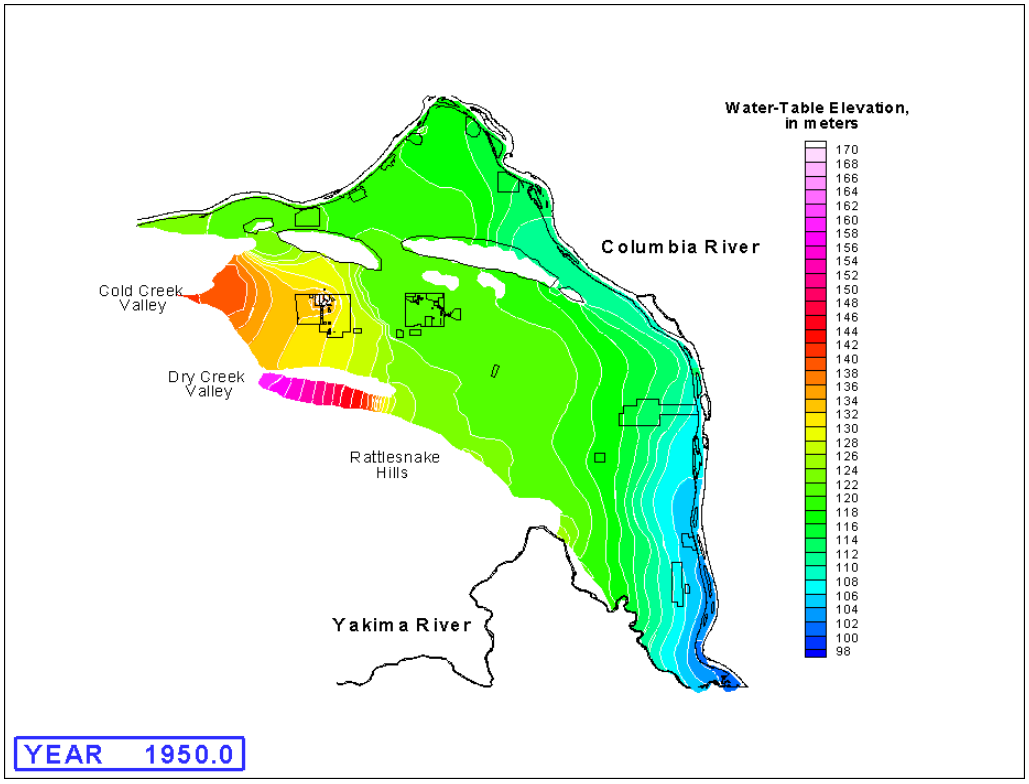

Figure A.1b. Simulated Water Table Elevations for 1950

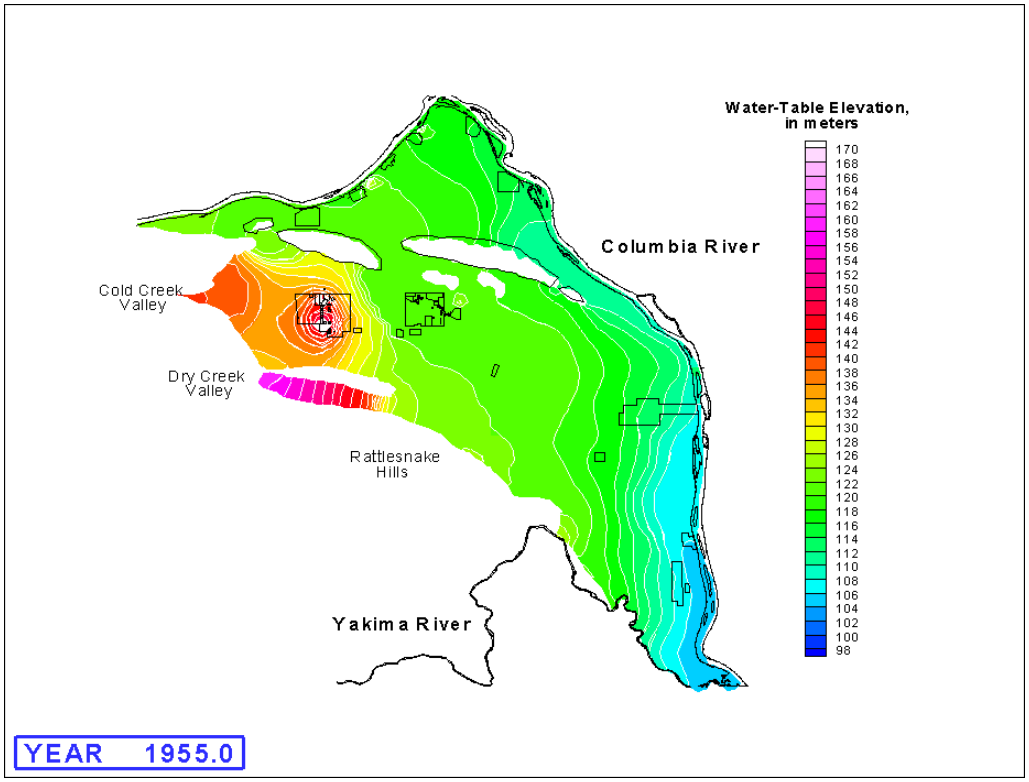

Figure A.1c. Simulated Water Table Elevations for 1955

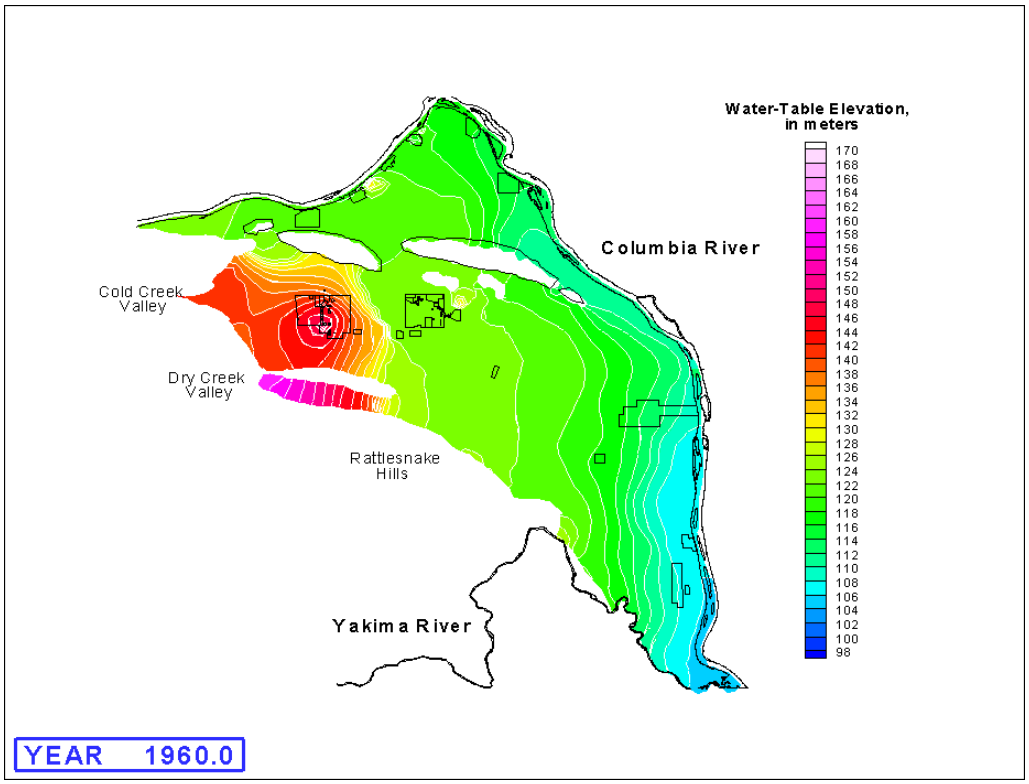

Figure A.1d. Simulated Water Table Elevations for 1960

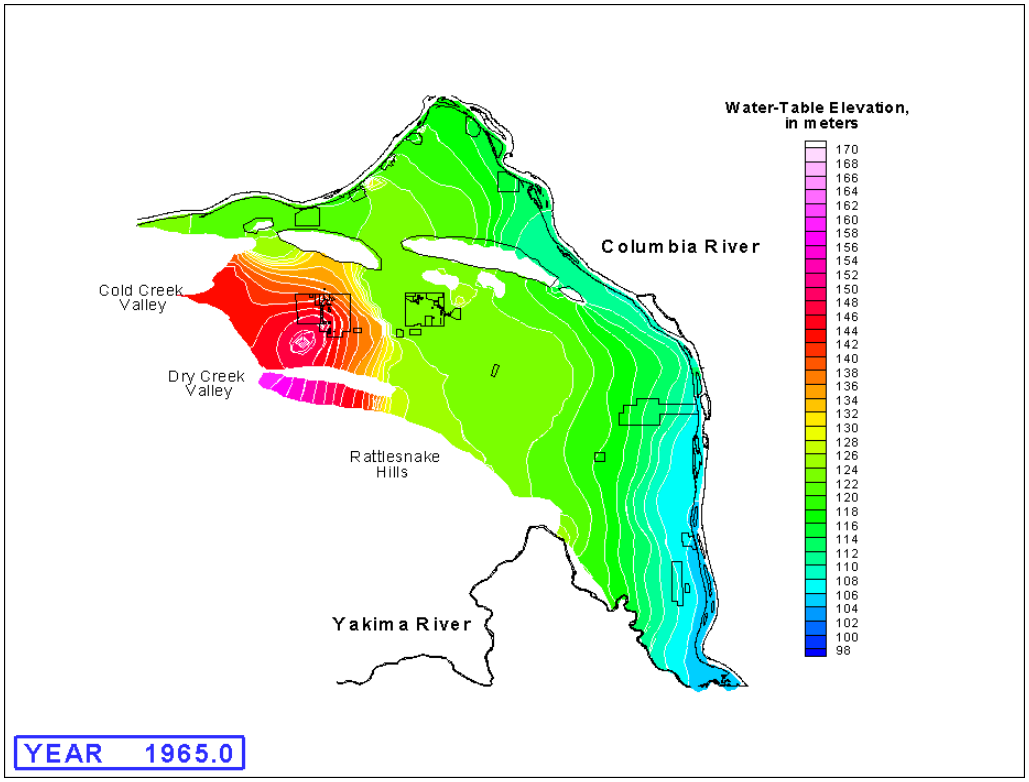

Figure A.1e. Simulated Water Table Elevations for 1965

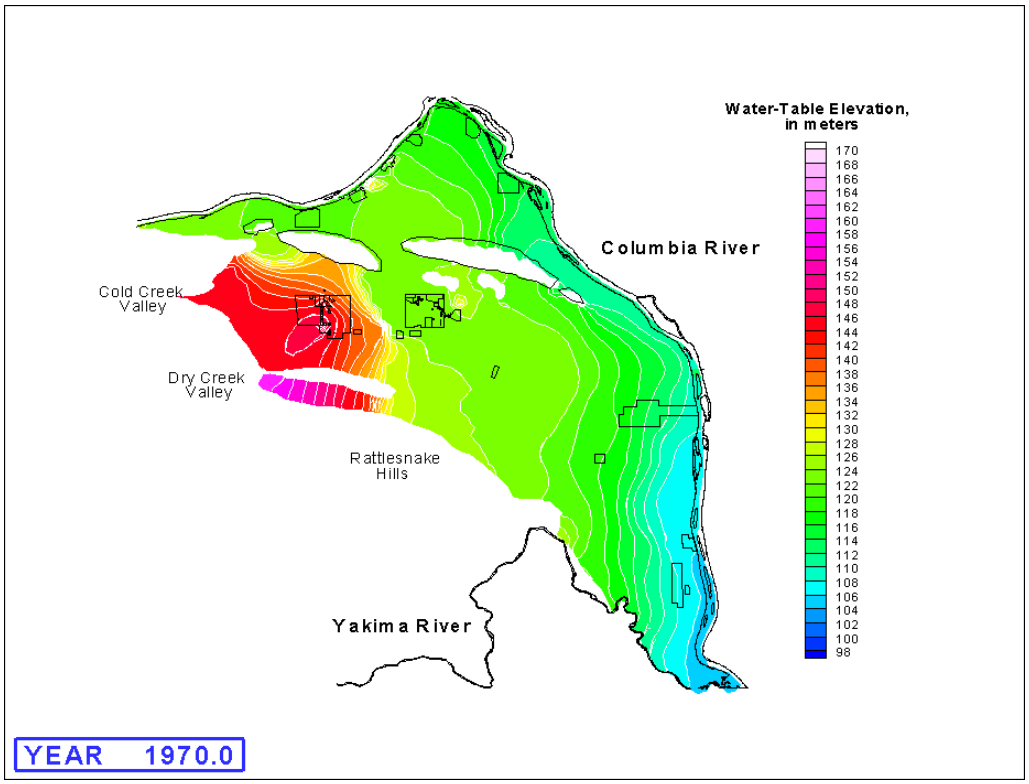

Figure A.1f. Simulated Water Table Elevations for 1970

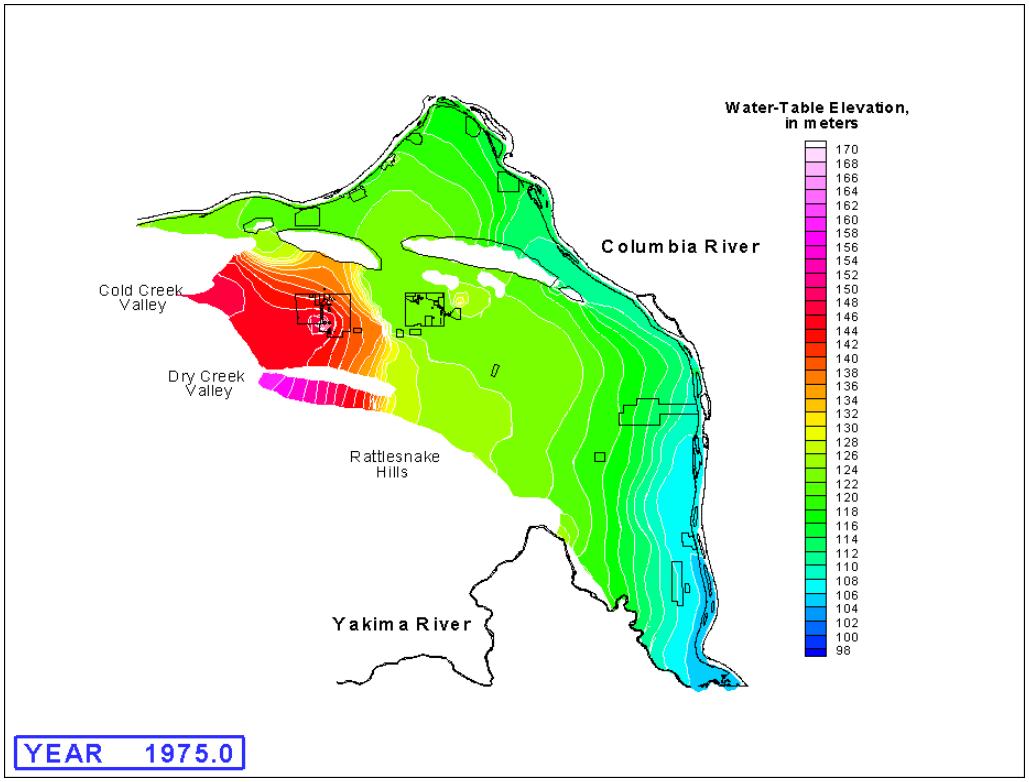

Figure A.1g. Simulated Water Table Elevations for 1975

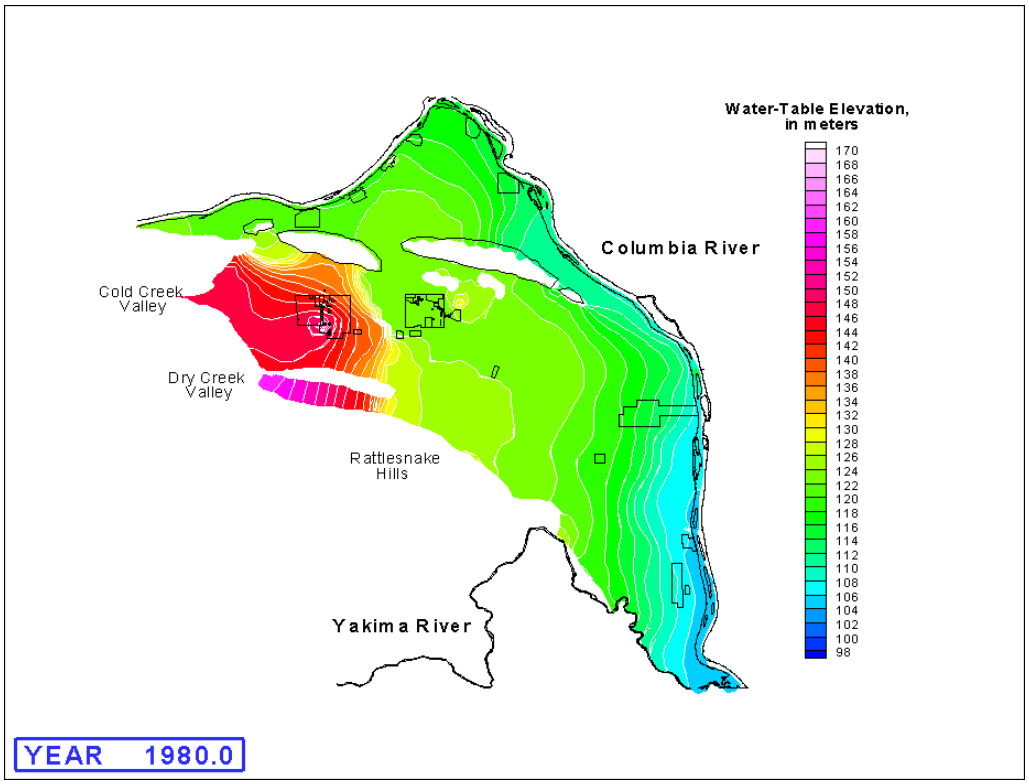

Figure A.1h. Simulated Water Table Elevations for 1980

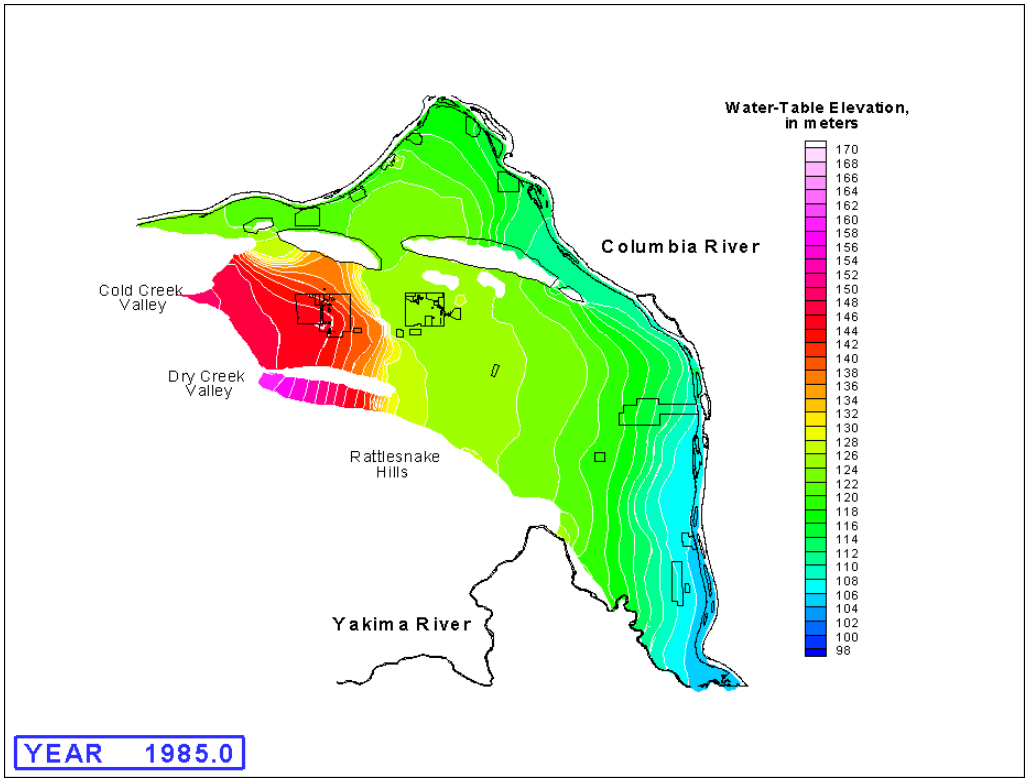

Figure A.1i. Simulated Water Table Elevations for 1985

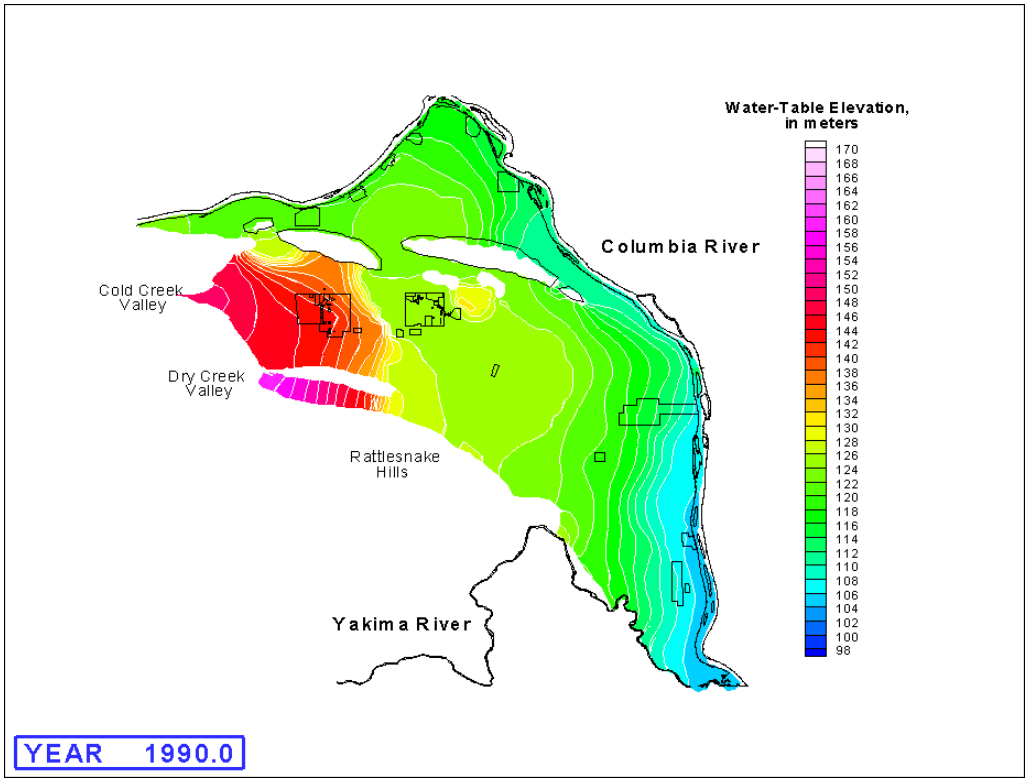

Figure A.1j. Simulated Water Table Elevations for 1990

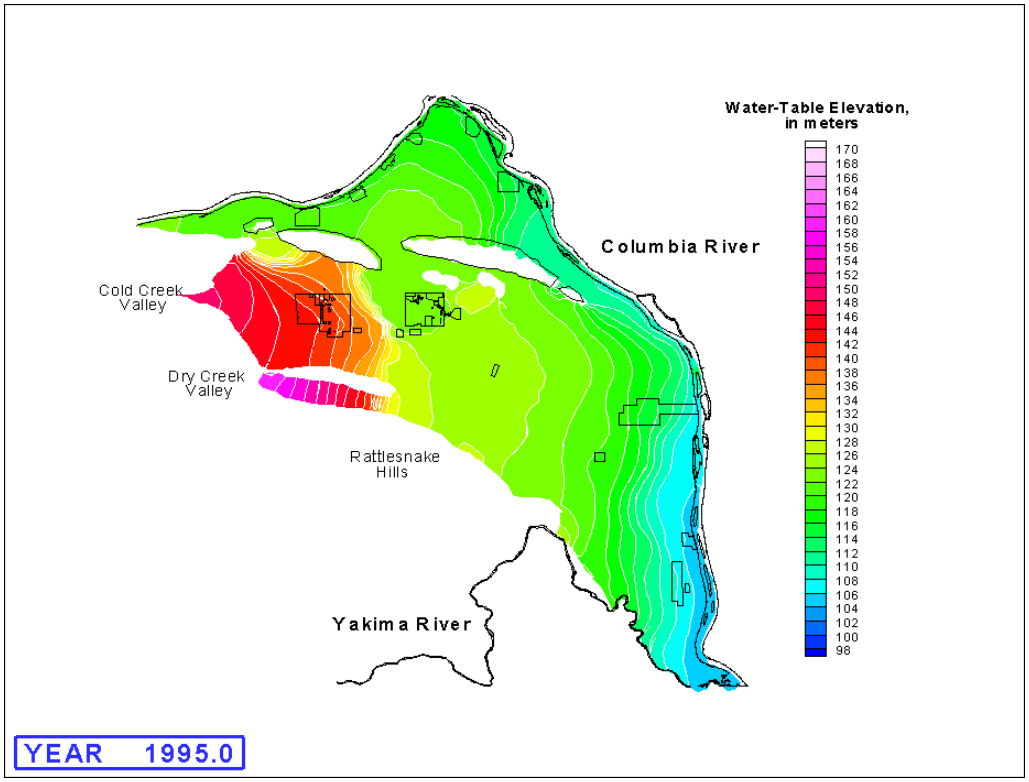

Figure A.1k. Simulated Water Table Elevations for 1995

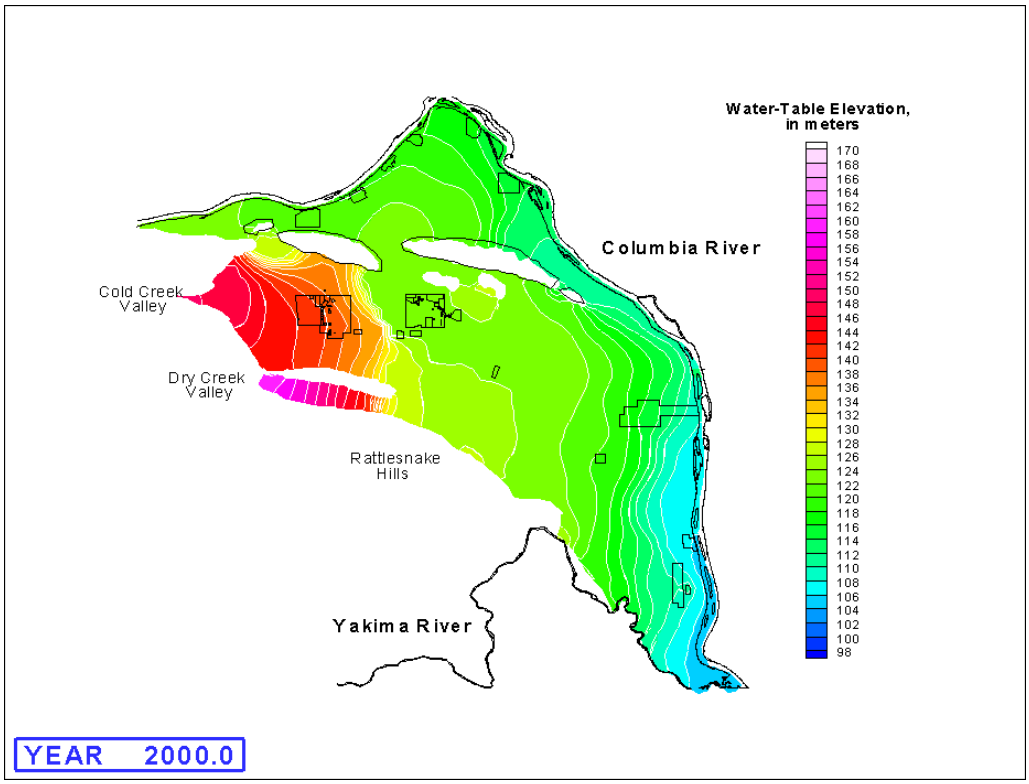

Figure A.1l. Simulated Water Table Elevations for 2000

A.2 Hydraulic Head Residuals

1943–2000

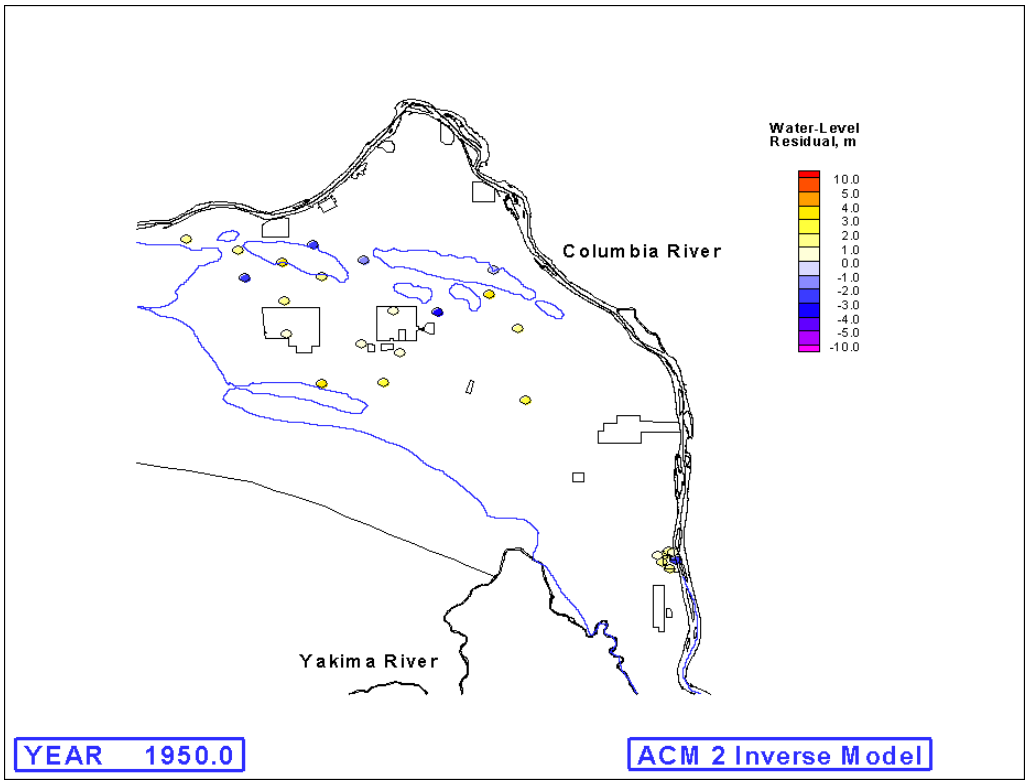

Figure A.2a. Hydraulic Head Residuals (simulated - measured water levels) for 1950

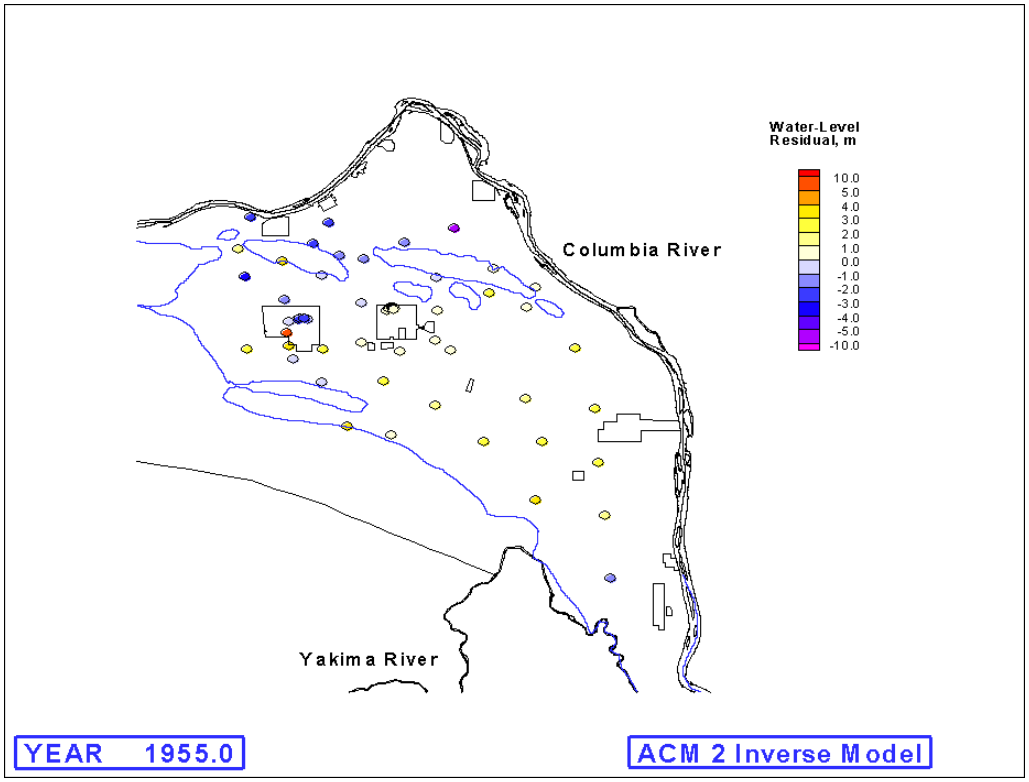

Figure A.2b. Hydraulic Head Residuals (simulated - measured water levels) for 1955

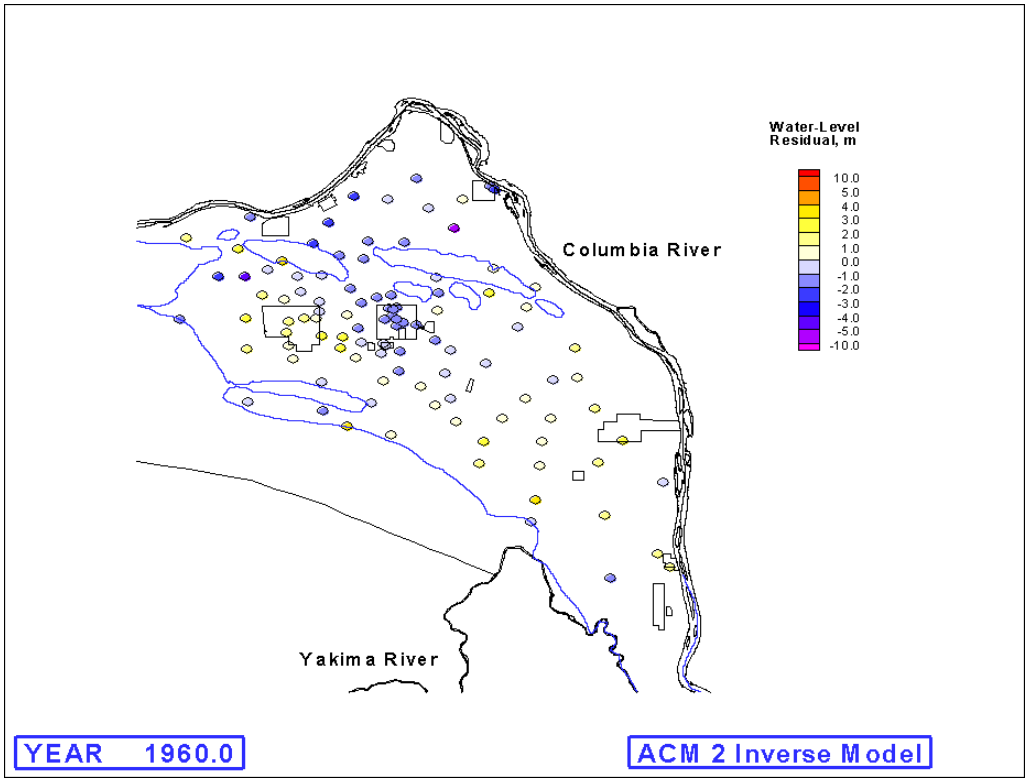

Figure A.2c. Hydraulic Head Residuals (simulated - measured water levels) for 1960

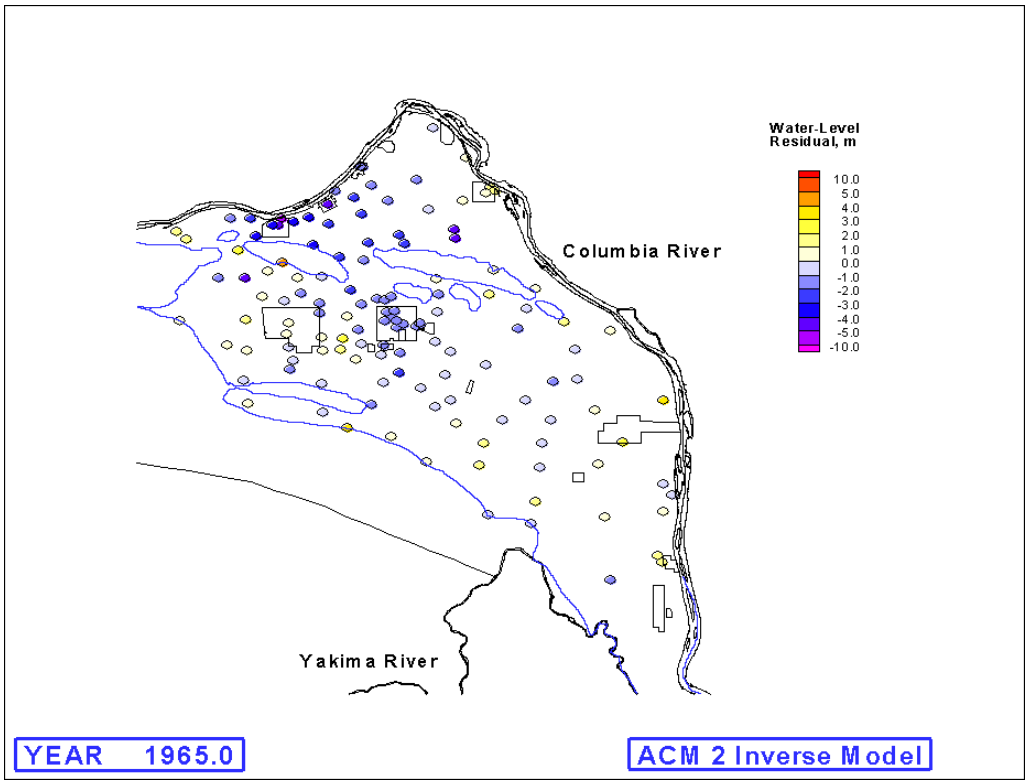

Figure A.2d. Hydraulic Head Residuals (simulated - measured water levels) for 1965

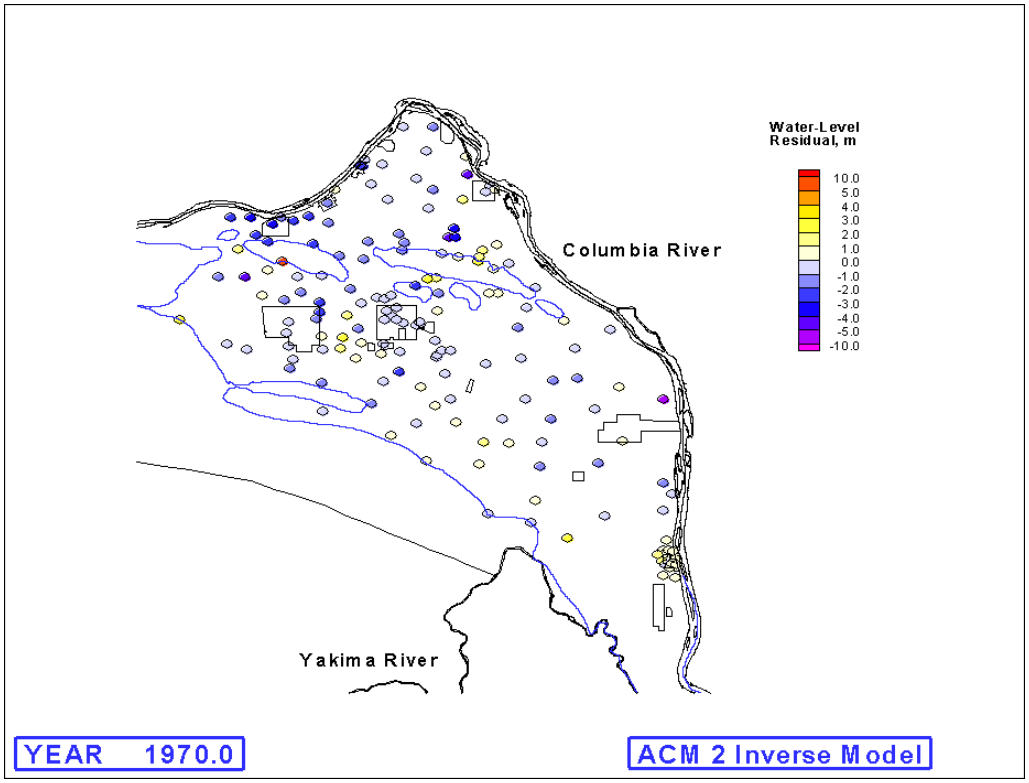

Figure A.2e. Hydraulic Head Residuals (simulated - measured water levels) for 1970

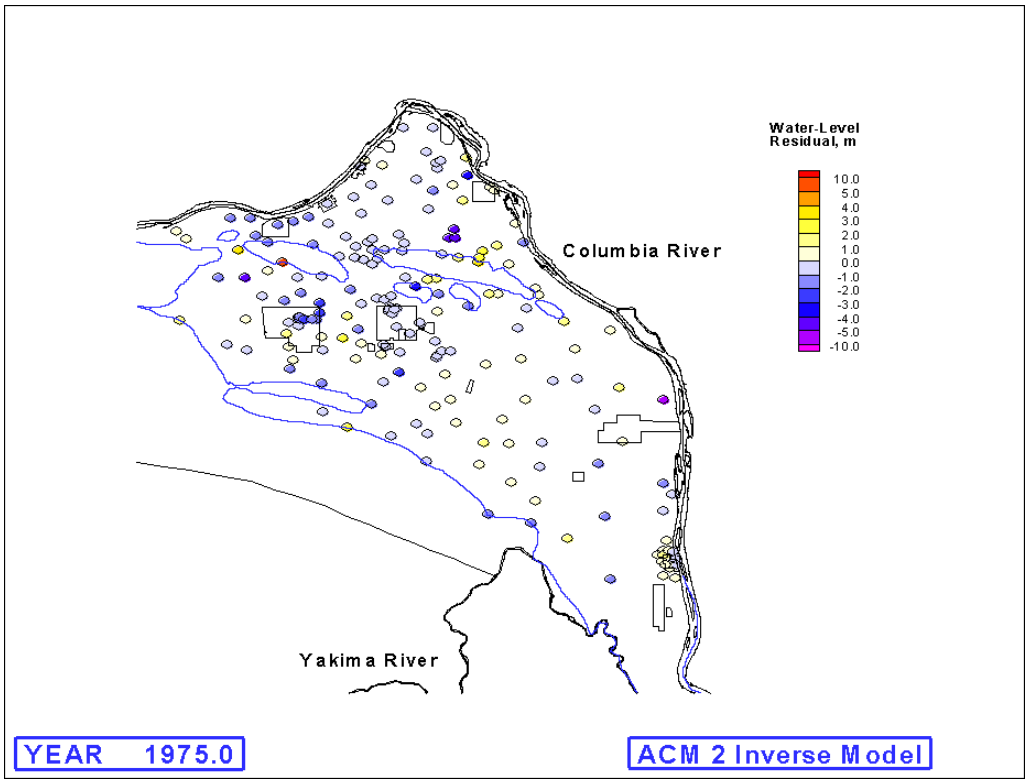

Figure A.2f. Hydraulic Head Residuals (simulated - measured water levels) for 1975

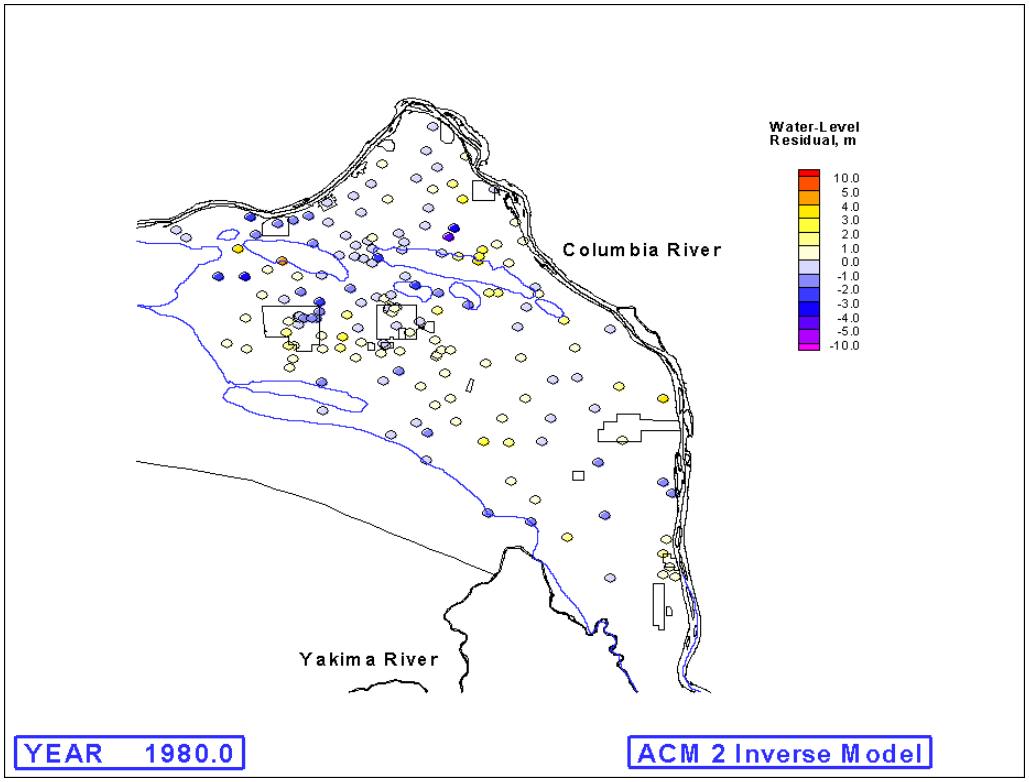

Figure A.2g. Hydraulic Head Residuals (simulated - measured water levels) for 1980

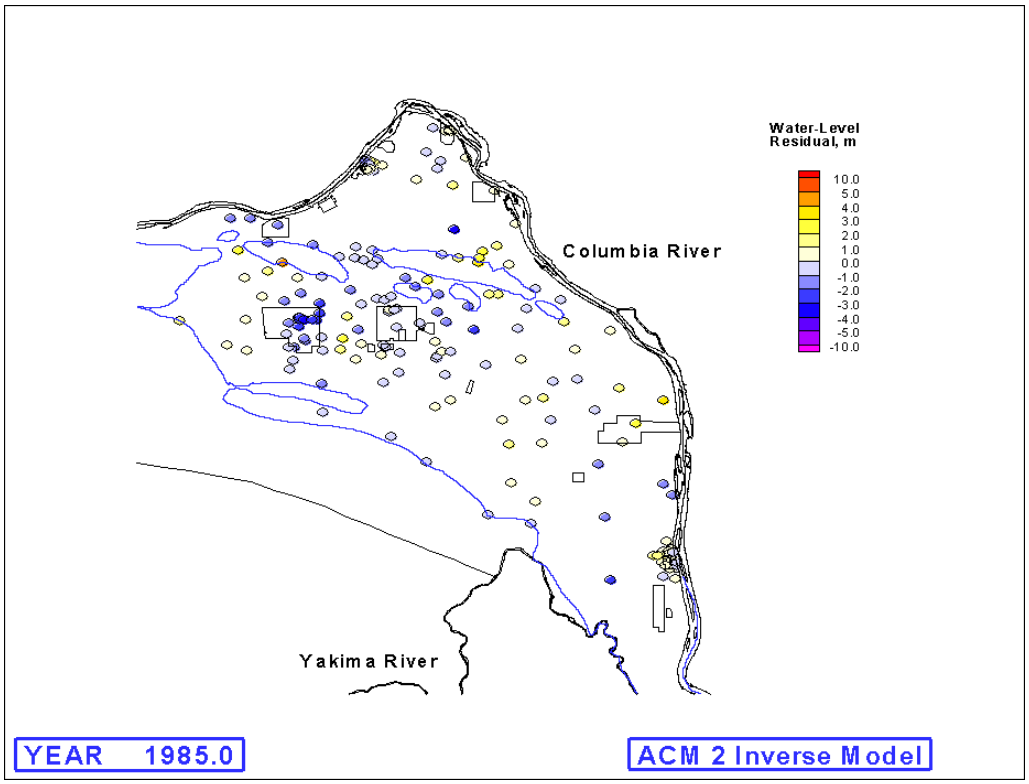

Figure A.2h. Hydraulic Head Residuals (simulated - measured water levels) for 1985

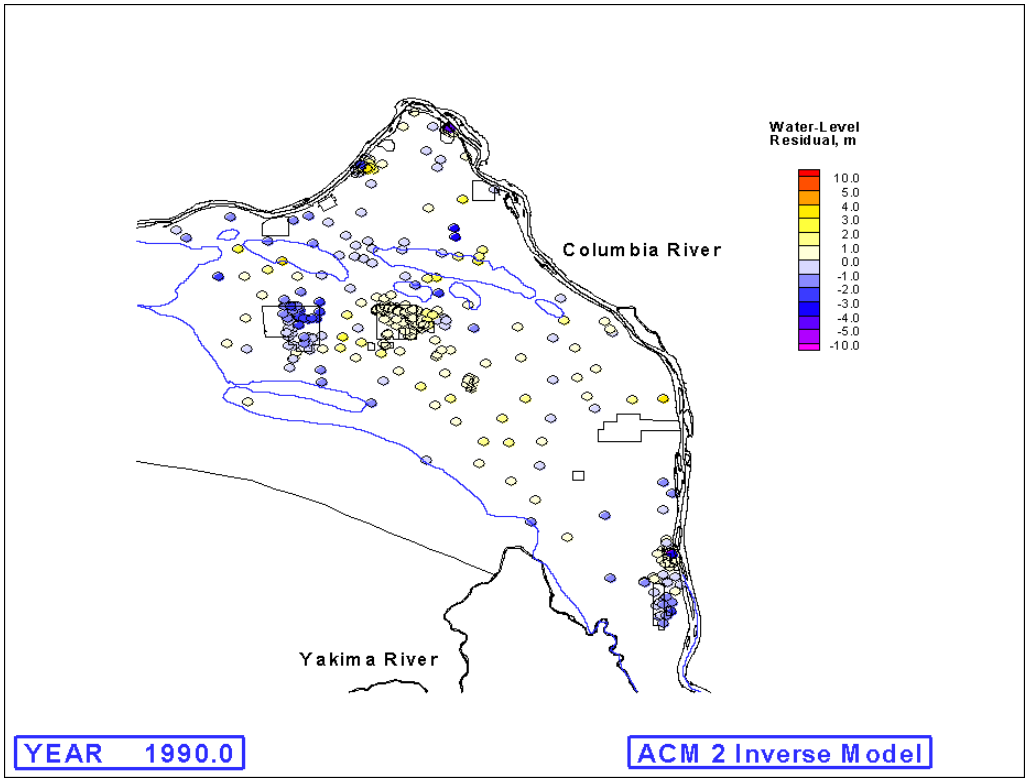

Figure A.2i. Hydraulic Head Residuals (simulated - measured water levels) for 1990

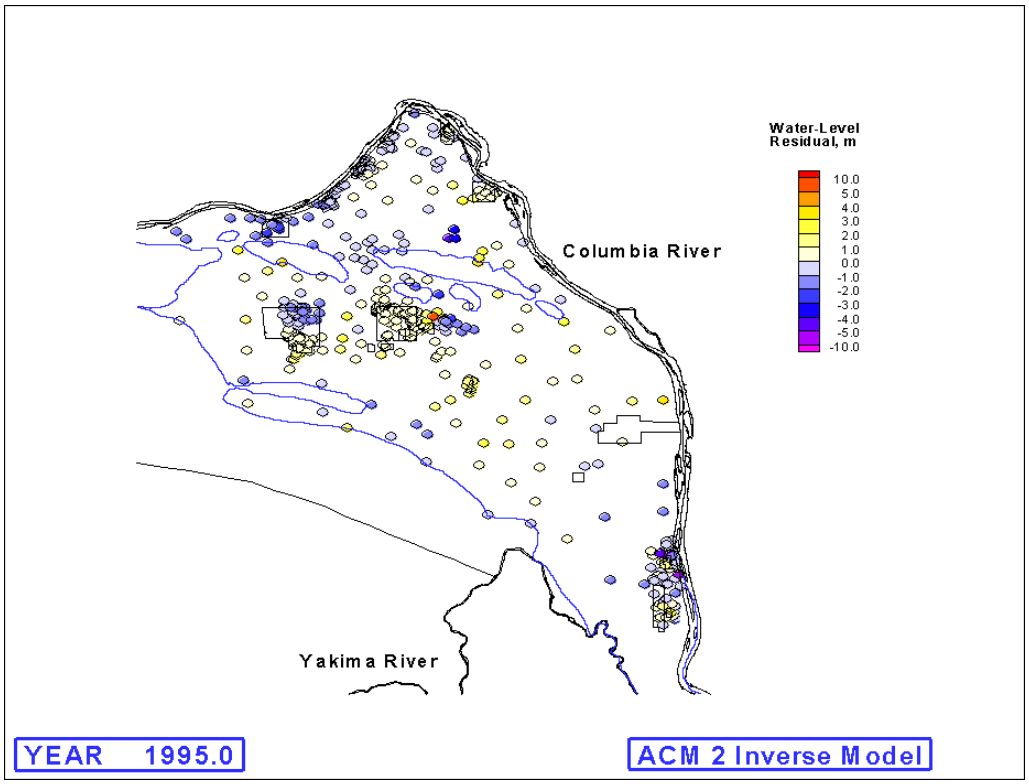

Figure A.2j. Hydraulic Head Residuals (simulated - measured water levels) for 1995

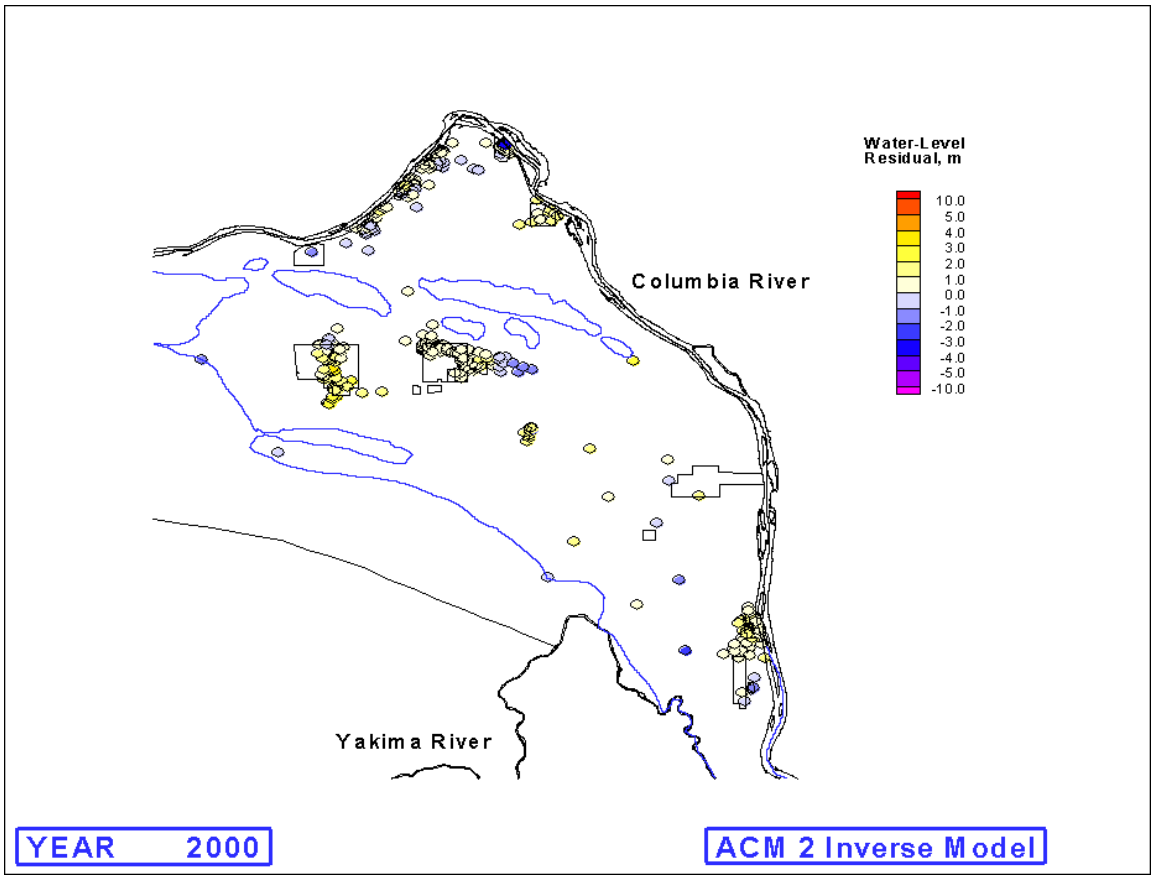

Figure A.2k. Hydraulic Head Residuals (simulated - measured water levels) for 2000

A.3 Simulated Versus Measured Water Levels

1943-2000

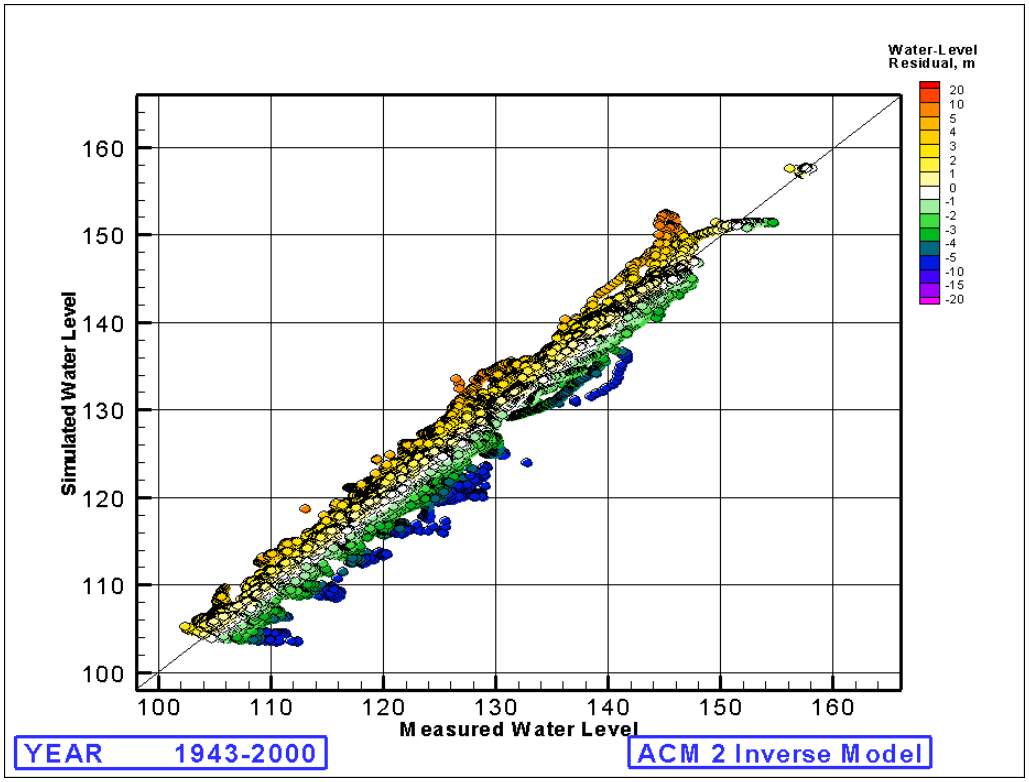

Figure A.3a. Comparison of Simulated Versus Measured Water Levels for 1943–2000

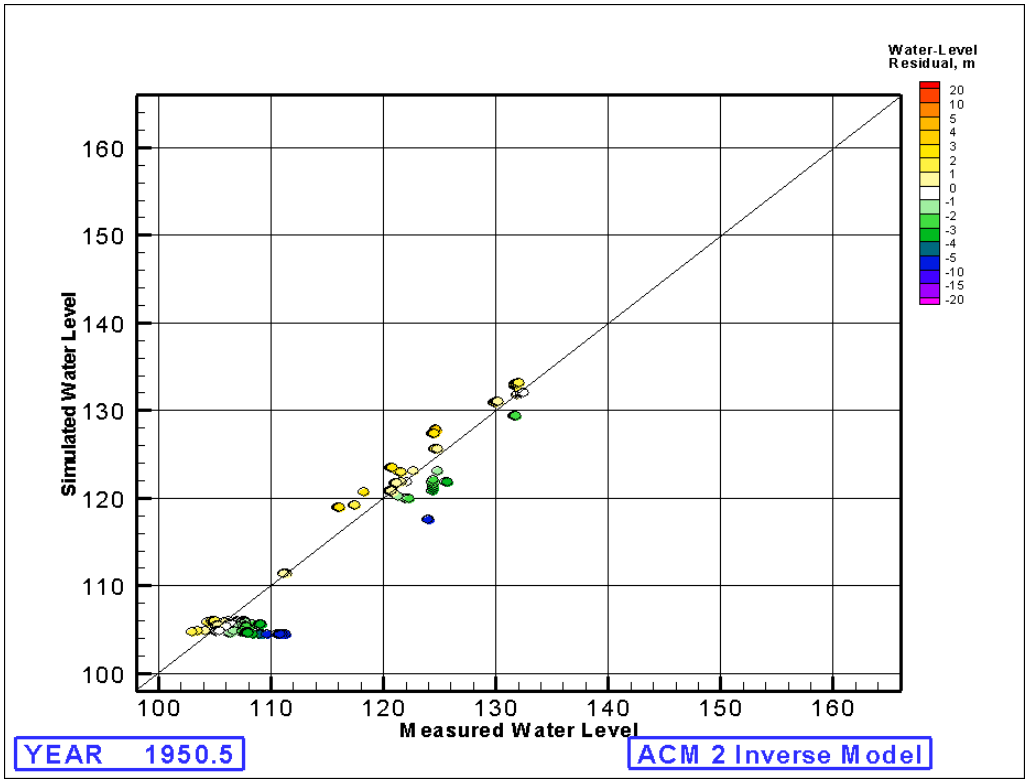

Figure A.3b. Comparison of Simulated Versus Measured Water Levels for 1950

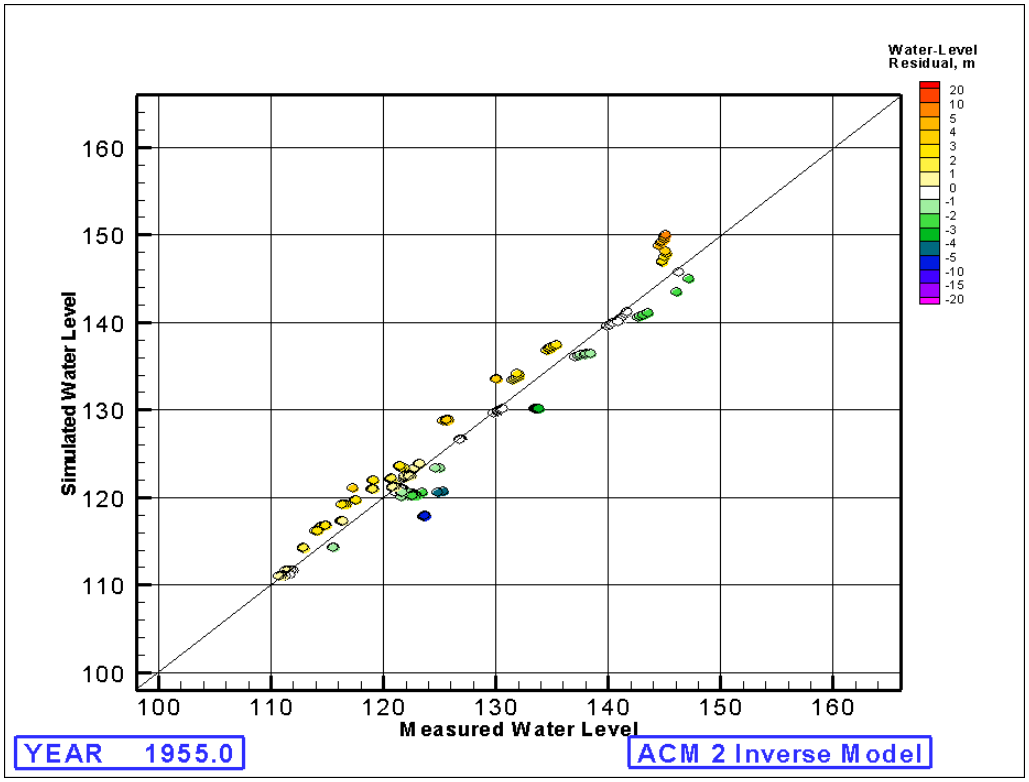

Figure A.3c. Comparison of Simulated Versus Measured Water Levels for 1955

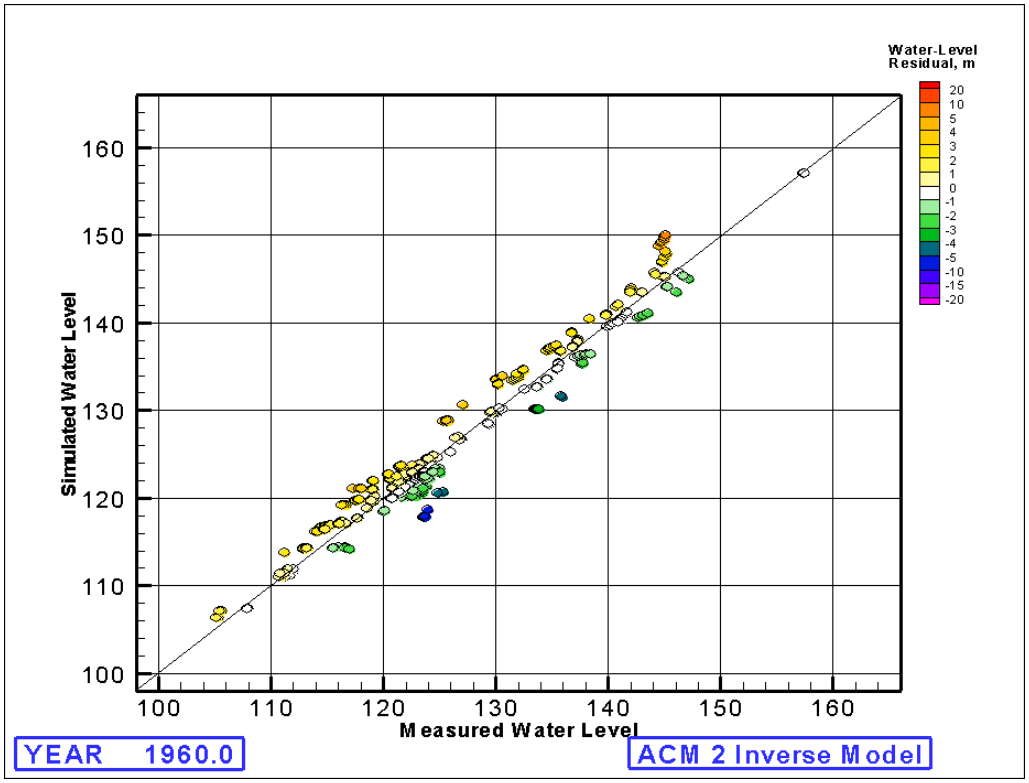

Figure A.3d. Comparison of Simulated Versus Measured Water Levels for 1960

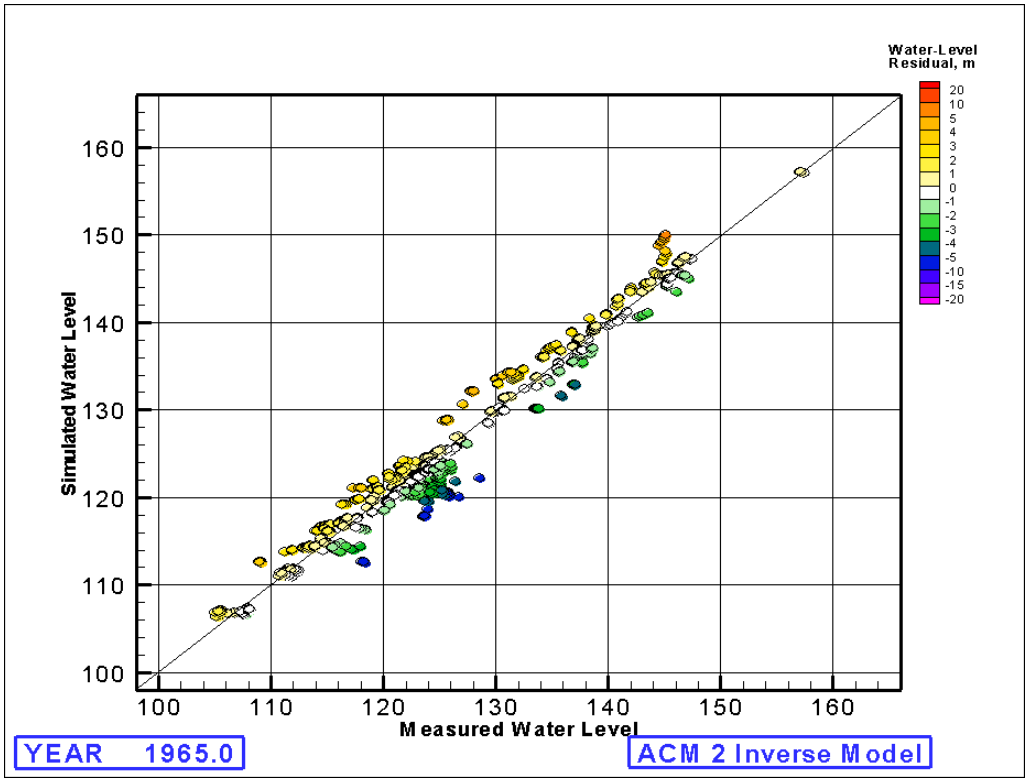

Figure A.3e. Comparison of Simulated versus Measured Water Levels for 1965

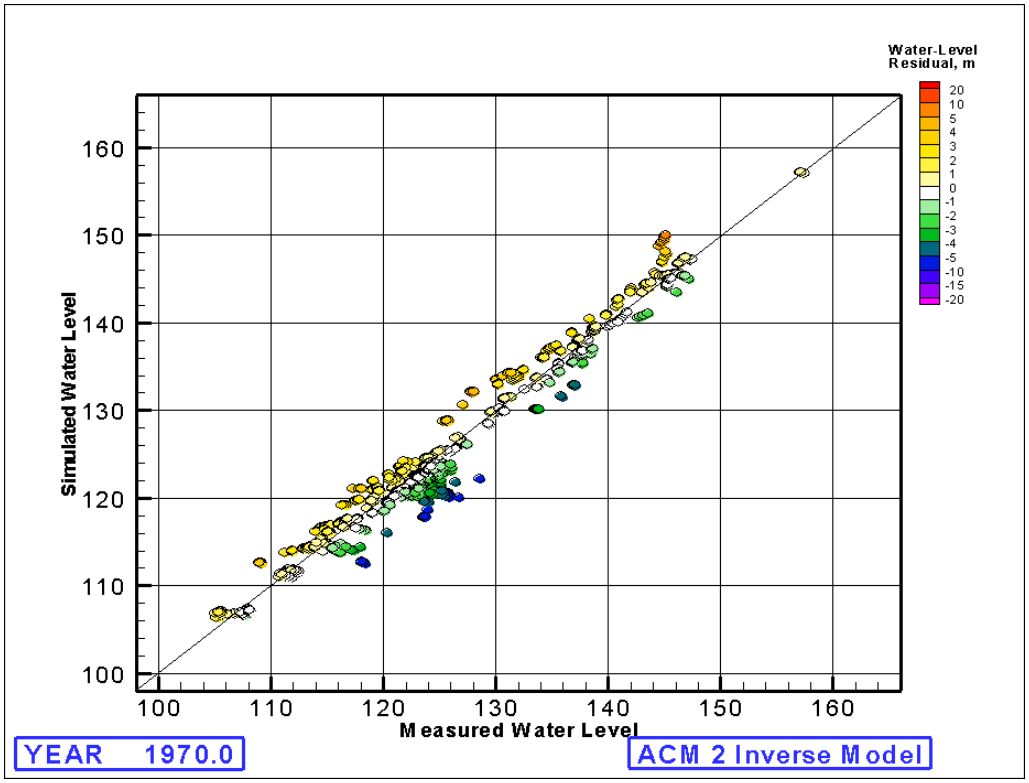

Figure A.3f. Comparison of Simulated Versus Measured Water Levels for 1970

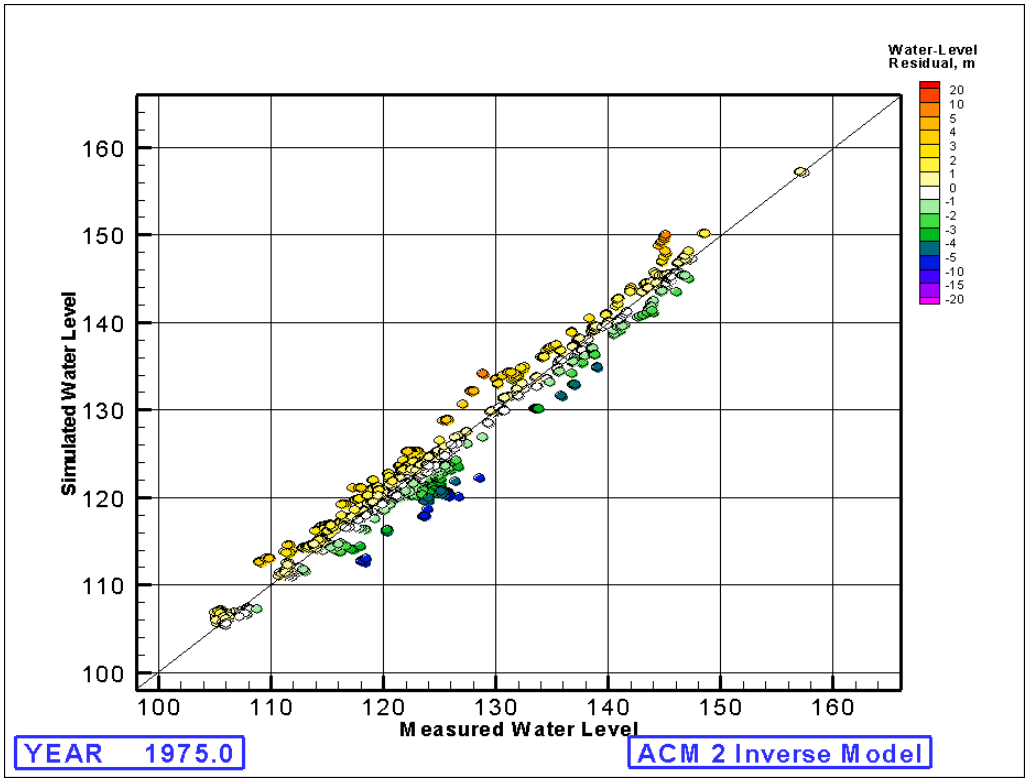

Figure A.3g. Comparison of Simulated Versus Measured Water Levels for 1975

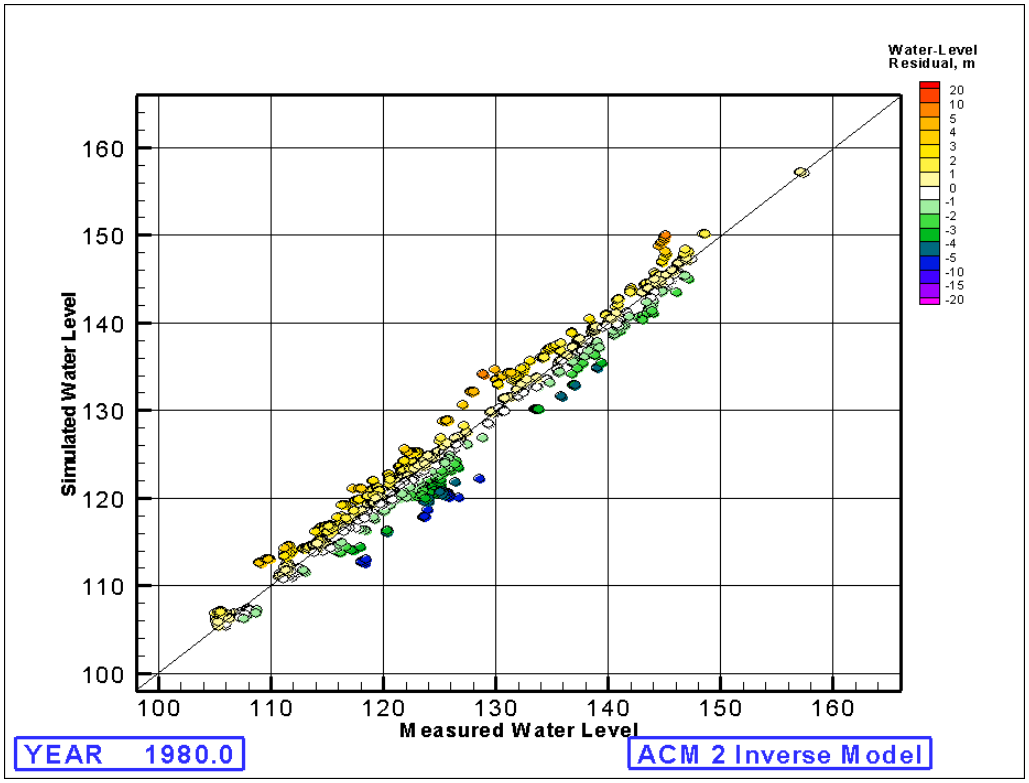

Figure A.3h. Comparison of Simulated Versus Measured Water Levels for 1980

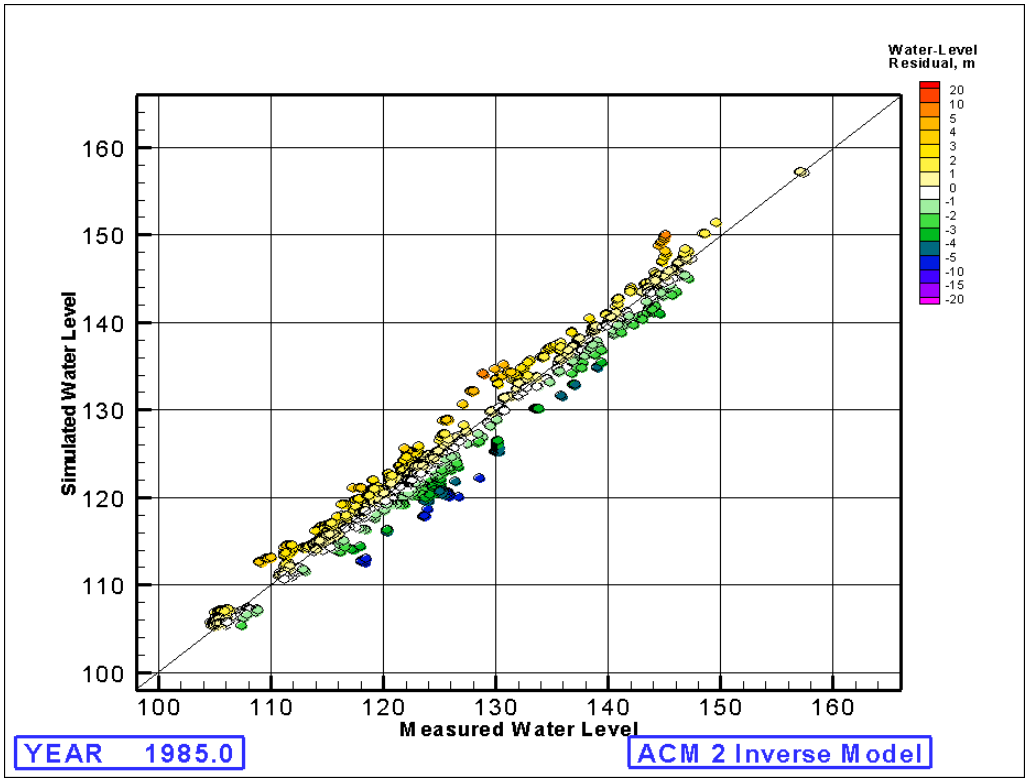

Figure A.3i. Comparison of Simulated Versus Measured Water Levels for 1985

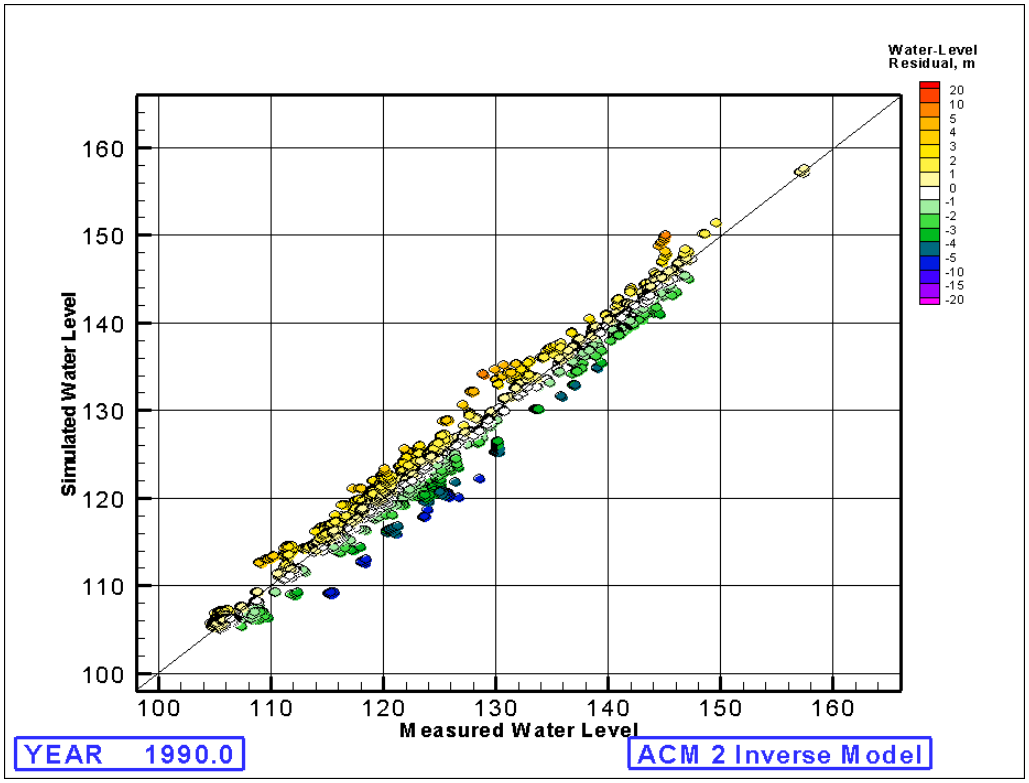

Figure A.3j. Comparison of Simulated Versus Measured Water Levels for 1990

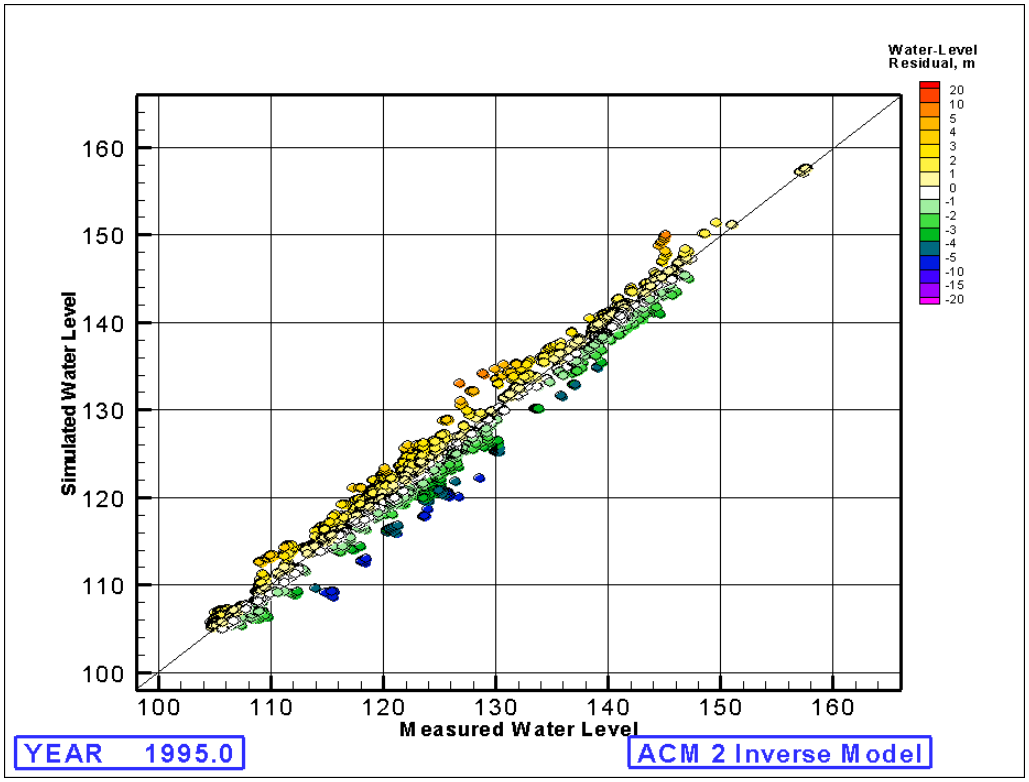

Figure A.3k. Comparison of Simulated Versus Measured Water Levels for 1995

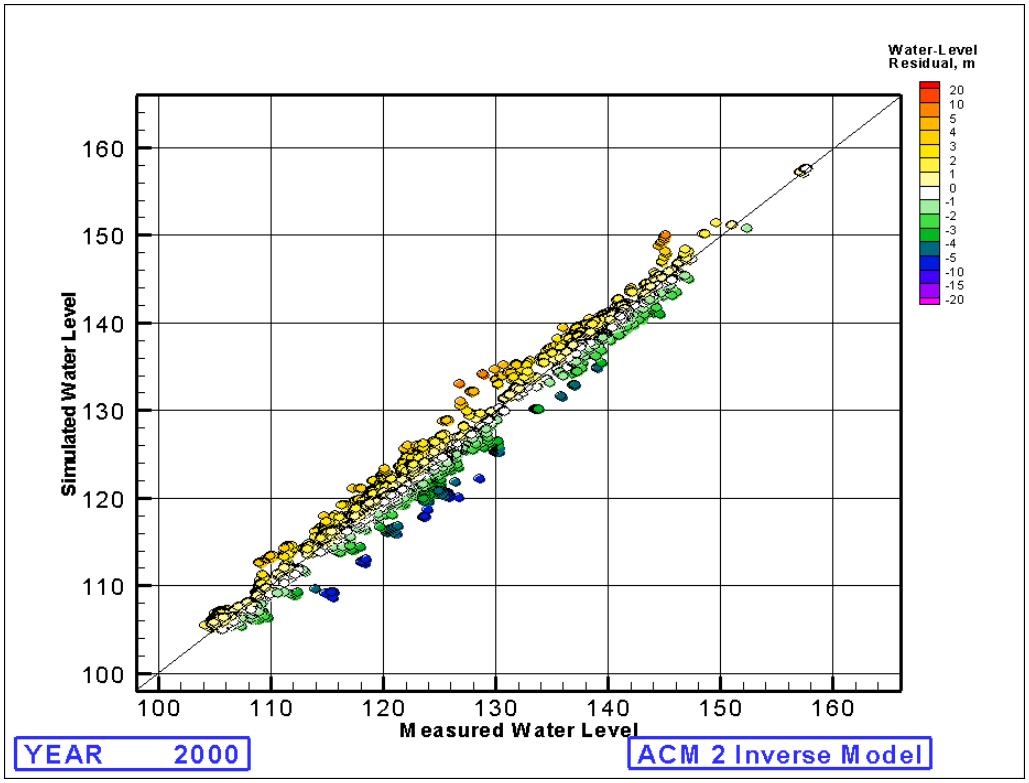

Figure A.3l. Comparison of Simulated Versus Measured Water Levels for 2000